Sequence-Controlled Synthesis of Soluble Oligo(p-benzamide)s

Dissertation zur Erlangung des Grades
„Doktor der Naturwissenschaften“
im Promotionsfach Chemie

am Fachbereich Chemie, Pharmazie und Geowissenschaften der
Johannes Gutenberg-Universität Mainz

Helga Seyler

geboren in Mar del Plata, Argentinien

Mainz 2009

Dekan:

1. Berichterstatter:
2. Berichterstatter:

Datum der mündlichen Prüfung: 24.Juni 2009

Hiermit versichere ich gemäß § 10 Abs. 3d der Promotionsordnung vom 24.07.2007, dass ich die als Dissertation vorgelegte Arbeit selbst angefertigt und alle benutzten Hilfsmittel (Literatur, Apparaturen, Material) in der Arbeit angegeben habe.

Danksagung

Contents

Abbreviations

4-NBC	4-nitro benzoic acid chloride
A	acceptor
BHT	butylhydroxytoluene
CHCA	α-cyano-4-hydroxycinnamic acid
conc.	concentrated
COSY	Correlation Spectroscopy
D	donor
DBU	1,8-diazabicyclo[5.4.0]undec-7-ene,
DCB	dichlorobenzene
DCM	dichloromethane
DEPT	Distortionless Enhanced Polarization Transfer
DLS	Dynamic Light Scattering
DMAc	dimethylacetamide
DMB	dimethoxybenzyl
DSC	Differential Scanning Calorimetry
e.g.	*exempli gratia,* for example
Fmoc	fluorenylmethoxycarbonyl
Fs (q,t)	amplitude correlation function
FT-IR	Fourier Transform Infrared Spectroscopy
GAM	general activation method
GM	general methode
GPC	Gel Permeation Chromathography
HABA	2-(4-hydroxyphenylazo) benzoic acid
HFIP	1,1,1,3,3,3-hexafluoro-2-propanol
HOBT	1-hydroxy benzotriazole
HR	hairy rod
JNR	Janus nanorod
MALDI-TOF	Matrix Assisted Laser Desorption Ionization Time of Flight
M_n	number average molecular weight
mp	melting point
M_w	weight average molecular weight
NMP	*N*-methyl-2-pyrrolidone
NMR	Nuclear Magnetic Resonance
NOE	Nuclear Overhauser Effect
NOESY	Nuclear Overhauser Effect Spectroscopy
NSO	*N*-sulfinylamino
OPBA	oligo(*p*-benzamide)
PAMBA	*p*-aminomethyl benzoic acid
PBA_5	penta(*p*-benzamide)
PDI	polydispersity index
PEG	polyethylene glycol
q	scattering vector
R_h	hydrodynamic radius
RP-HPLC	Reverse Phase High Pressure Chromathography
SPS	Solid Phase Synthesis

TBTU	2-(1-H-benzotriazole-1-yl)-1,1,3,3-tetramethyluronium tetrafluoroborate
t-Bu	*tert*.-butyl
TCM	trichloromethane
T_D	decomposition temperature
TEG	triethylene glycol
TFA	trifluoroacetic acid
TGA	Thermogravimetric Analysis
THF	tetrahydrofurane
TLC	Thin Layer Chromathography
TPP	triphenylphosphite
VT-NMR	Variable Temperature Nuclear Magnetic Resonance spectroscopy

Chapter 1

Introduction

1.1. Supramolecular Chemistry and Polymers

Supramolecular Chemistry is a popular, fast growing multi- and interdisciplinary science with the aim of developing highly complex and functional chemical systems through noncovalent intermolecular forces.[1,2] Beyond that, supramolecular systems undergo storage of information at the molecular level through molecular recognition and self organization processes. Numerous types of interactions and recognition units are used for the supramolecular preorganization of systems, involving e.g. robust hydrogen bonding and metal coordination or more sensitive van der Waals forces and π-stacking.[3] The modification of parameters such as concentration, stoichiometry of the components and the presence of foreign species, are mainly explored for the development of new architectures.[4,5]

Historically, the term "*Übermolekül*" is dated back to the mid 30's and was used to describe organized entities arising from the association of coordinatively saturated species.[6] The concept of "Supramolecular Chemistry" was introduced in 1978 and further developed by Jean-Marie Lehn.[7,8] In 1987 he was awarded the Nobel price for chemistry together with Charles J. Pedersen and Donald J. Cram for their pioneering work in this field. Supramolecular Chemistry has since become a very fast growing area of research and thus evolved into a wide-ranging science, giving rise to numerous developments of interdisciplinary nature at the interfaces with chemistry, biology and physics.

The generation of controlled and well defined functional supramolecular nanostructures is often inspired by nature as a method for mimicry and better understanding of biological processes.[9] Additionally it offers a powerful tool for the fabrication of optoelectronical systems or multiple applications in the field of catalysis.[10]

In nature, organization on the nanometer to micrometer scale is crucial for the remarkable properties and functional capabilities of biological systems. For example, biological ensembles like proteins, enzymes or DNA use complex, elegant and at the same time simple supramolecular principles for their essential roles in life.[11] Their functionalities, like molecular recognition, information storage and catalysis rely mainly on unique solution organization into stable supramolecular assemblies. Even though biological molecular recognition represents one of the most complex processes, it provides inspiration for the design of model systems or new functional materials. **Figure 1.1** shows an example of an enzyme (Coenzym B_{12}), which illustrates the significance of supramolecular chemistry in nature and its interdisciplinary aspect. This interesting

molecule highlights the biological, organometallic and chemical nature of the system, consisting of a tetrapyrrole macrocycle, that builds a cobalt-based host-guest complex **1** and associates specifically through noncovalent interaction to the substrate.

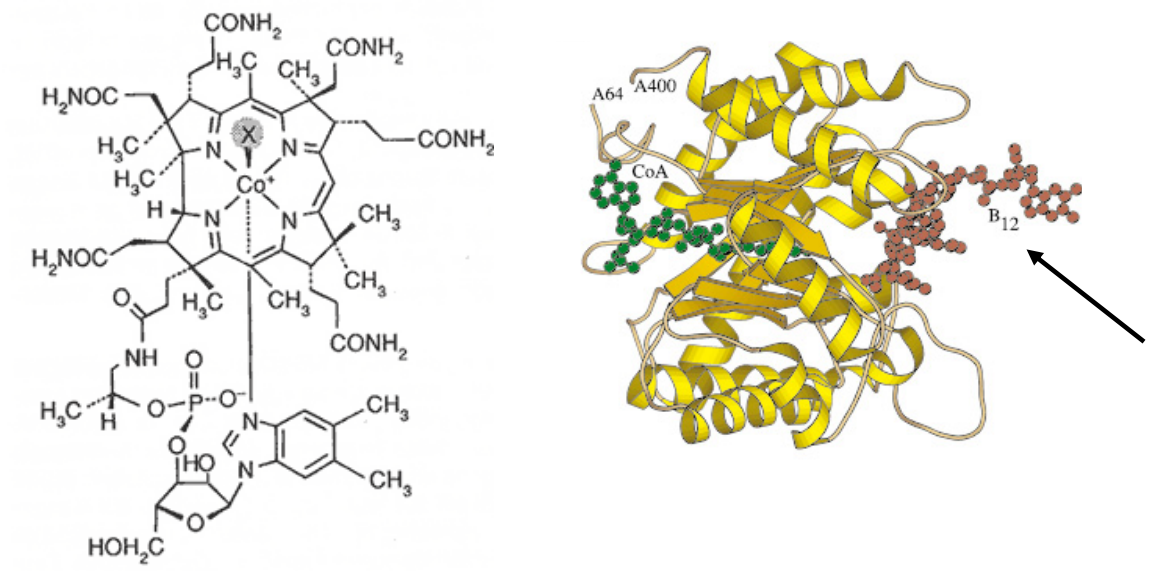

1

Figure 1.1. Coenzym B_{12} (X = 5'-Deoxyadenosyl) host-guest complex **1** (*left*) and enzyme-substrate association (*right*).[12]

The tobacco mosaic virus[13] is another biochemical example, whose self-assembly serves to illustrate many of the features present in self-assembling biological systems (see **figure 1.2**).[11] This system has a rod-like appearance and consists of a helical coat protein around the central RNA strand. It is particularly interesting that if the virus is decomposed into its component parts and these fragments are mixed again under physiological conditions, the virus particle is accurately self-assembled into these well defined aggregates and regains its functionality, requiring only a remarkably small amount of genetic information.[14]

In analogy to this structure-function relationship in biopolymers, self-assembly has become an important subfield of polymer science, where much efford has been made to control the solution organization of synthetic macromolecules.

Accordingly, many scientists have begun to replace traditional polymer synthesis with self-assembled processes in order to overcome a variety of synthetic hurdles and to exploit the dynamic nature of the noncovalent bond, new design principles and functionalization strategies.[15,16,17,18]

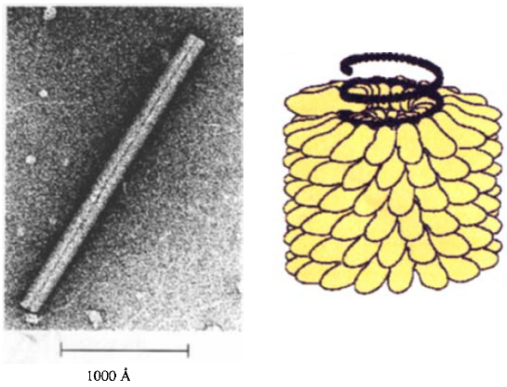

Figure 1.2. Electron micrograph image (*left*) and schematic representation (*right*) of the tobacco mosaic virus.[11]

Supramolecular polymers are typically divided in two major categories: main-chain and side-chain systems. Main-chain supramolecular polymers can be described as polymeric systems that are held together by directional noncovalent interactions at the molecule backbone, for example taking advantage of hydrogen bonding and metal coordination systems (see **figure 1.3**).[15] In contrast, side-chain supramolecular polymers are based on a covalently linked macromolecule backbone functionalized with side-chains, through which the self assembly process occurs (see **figure 1.4**).[19]

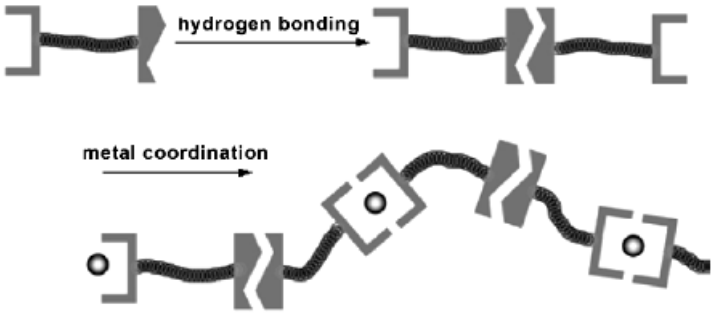

Figure 1.3. Representation of a supramolecular main-chain polymer with two types of non-covalent interactions (hydrogen bonding and metal complexation).[20]

For example, the formation of hierarchical peptide architectures such as α-helices or β-sheets are based on self-functionalization while the replication of DNA is based on a modular functionalization strategy.

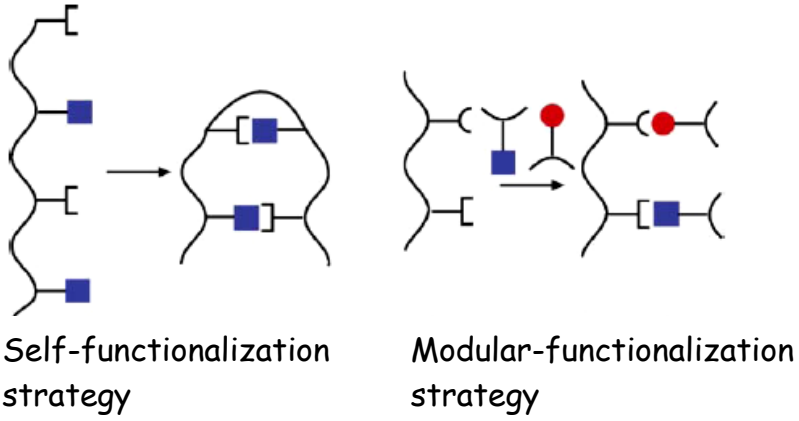

Figure 1.4. Side-chain supramolecular polymers. Comparison between intra- (or self-functionalization) and intermolecular (or modular functionalization) origin of the noncovalent interactions.

1.2. Foldamers

The innumerable variety of structures and functions in natural self-organized systems is mostly the result of specific information efficiently stored in surprisingly few structural units and by their appropriate combination. An example are proteins, whose structural and diverse functional properties are only determined by a set of 20 amino acids. To gain a deeper insight into the understanding of some of these processes, synthetic foldamers have attracted the interest of numerous scientists over the past decade.[21] The term foldamers (= *folding oligomers*) describes monodisperse non-natural oligomers that adopt well defined conformations through noncovalent interactions. The study of these oligomers bears particular significance for example in the prediction and design of secondary and tertiary structural motives and selective introduction or placement of functional groups.

Synthetic foldamers are also characterized by an easy synthetic accessibility and stable conformational states promoted by noncovalent bonds between remote intra- or interstrand monomeric units.[18,22] The various architectures that have been described recently in the literature by numerous researchers (see **figure 1.5**) are an evidence for the extent of the rapid development of this field.

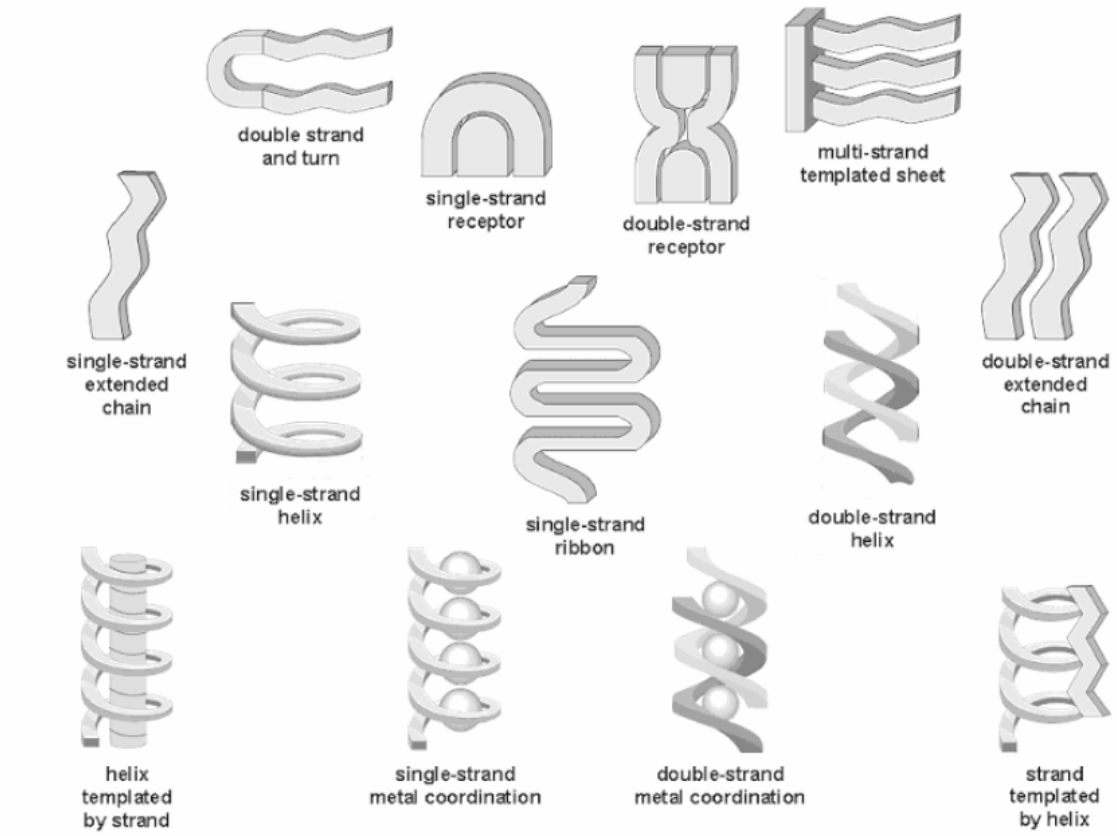

Figure 1.5. Illustration depicting the different types of foldamer secondary structures.[21]

1.3. Rod-like macromolecules

Today, the synthesis of rod-like molecules plays an important role in the production of chemically and thermomechanically stable materials. Polyamide, polyesters, π-conjugated and fully aromatic systems find versatile applications and are intensively explored.[23,24,25]

Even in nature a broad variety of examples of structurally stiff macromolecules are found, where the rod-like shape achieved through secondary structure is essential for their functionality (α-helices, β-sheets). This structural motif is frequently enforced or promoted by hydrogen bonds, solvophobic effects, van der Waals forces, electrostatic interactions or by their multiple combinations.

Rigid molecules can be principally categorized into two levels of organization. One sort is represented by rod-like macromolecules built from covalently spatially fixed monomeric units. The other class consists of polymers, whose rigid structures arrive from the organization into stable primary and secondary structures (see **figure 1.6**).[26]

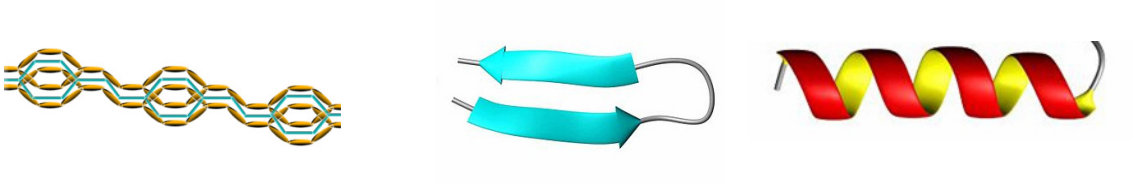

(a) (b)

Figure 1.6. Primary and secondary structures where chain rigidity is induced through π-*stacking* and π-electron conjugation (for example for (a) poly(*p*-phenylene vinylene)) or by hydrogen bonding and ionic forces such as in (b) β-sheets or α-helices.

The chain rigidity is usually achieved or reinforced through the following mechanisms:

- π-*Conjugation and* π-*stacking*. Electron delocalization along the polymer chain favors the straight conformation. Polyfluorenes, polythiophenes, poly(phenylene ethynylene)s and poly(phenylene)s are only few of an enormous variety found in the literature (see **figure 1.7**; **2-5**). Coplanarity in polyaromatic materials strongly contributes to the increase of chain stiffness. Flexible side chains have often been introduced for solubility enhancement.

- *Hydrogen bonding*. H-Donors and acceptors in the main or polymer side chain may fix the spatial arrangement of the macromolecule, whereas mostly stiff conformations are adopted. This stabilization can occur between next or remote monomer units but also intermolecularly. These kinds of macromolecules are found abundantly in nature, like peptides or polynucleotides. For example, the α-helical structure in peptides is stabilized by intramolecular interactions, while DNA forms intermolecular hydrogen bonds.

- *Coulomb interactions*. Ionic repulsions between like charges spatially close positioned along the molecule axis force the chain into a straight conformation as found in polyelectrolytes.

In the beginning, most of the developments on this class of polymers emerged from the research in liquid crystalline materials. Today polymers with rod-like shapes became a matter of particular interest in the scientific community, due to their possible application as thresholds for the precisely spatial arrangement of functional moieties.[27]

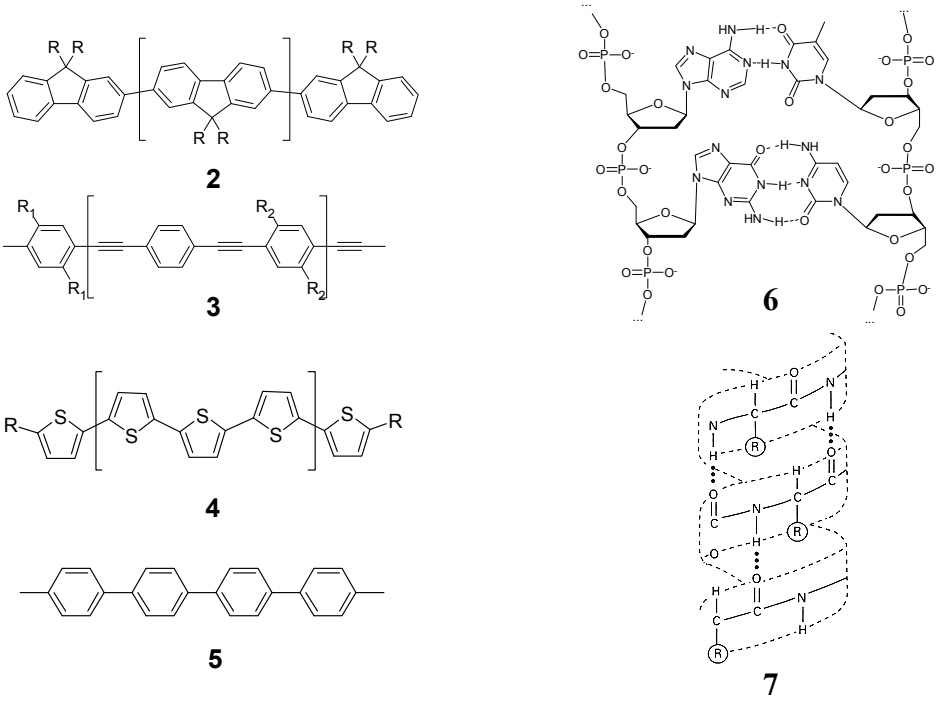

Figure 1.7. Selected examples illustrating the rigidity origin of various macromolecules: polyfluorene **2**, poly(phenylene ethynylene) **3**, polythiophene **4**, poly(phenylene) **5** and DNA-segment **6**, peptide **7**.

With the birth of supramolecular chemistry in the late 1970s, the major incentive in scientific research on stiff-chain polymers was the development and design of well defined, novel and functional superstructures and giant molecules for potential biomimetic and material science applications.[28]

When compared to flexible polymers, stiff-chain polymers, have received much less attention. The reason for that are properties like the exceedingly low solubility in common organic solvents as well as extremely high melting points (or even melting point absence), resulting in handling difficulties.

Flexible polymers mainly differ from rod-like macromolecules as they adopt a vast number of conformations in melt and solution. Hence, melting or dissolving a flexible coil is accompanied by a substantial gain in entropy. For the case of shape persistent molecules, numerous intermolecular contacts are cleaved, leading only to a minor gain in entropy.[23]

1.4. Aromatic Amide Foldamers

The combination of chain stiffness, ability of hydrogen bond formation, hydrophobicity, partial double bond character of the *trans*-amide bonds and π-interactions in aromatic backbones results in highly interesting multifunctional materials.[29]

Aryl amides (aramides) are also characterized by their excellent thermomechanical stability, anisotropy and their low solubility in organic solvents, as generalized previously for structurally stiff materials.[30] From this interplay of properties, materials based on *para*-linked aramides are only soluble in hydrogen bond-breaking solvents like dimethylacetamide (DMAc)/LiCl or conc. sulphuric acid, from which fibres can be spun.[31]

The most common approaches to enhance their solubility are depicted in **figure 1.8**. Flexible residues are often integrated into the stiff structures; *e.g.* as flexible spacers, as short flexible side chains attached to the rigid backbone[23,24,32] or in form of a block copolymer[24,33,34]. Other approaches concern the usage of temporary protecting groups, whose application was specially described for monodisperse oligomeric aramides to facilitate their synthesis, manipulation and purification,[35] as well as the introduction of bent units[23] which has also been exploited in this context.

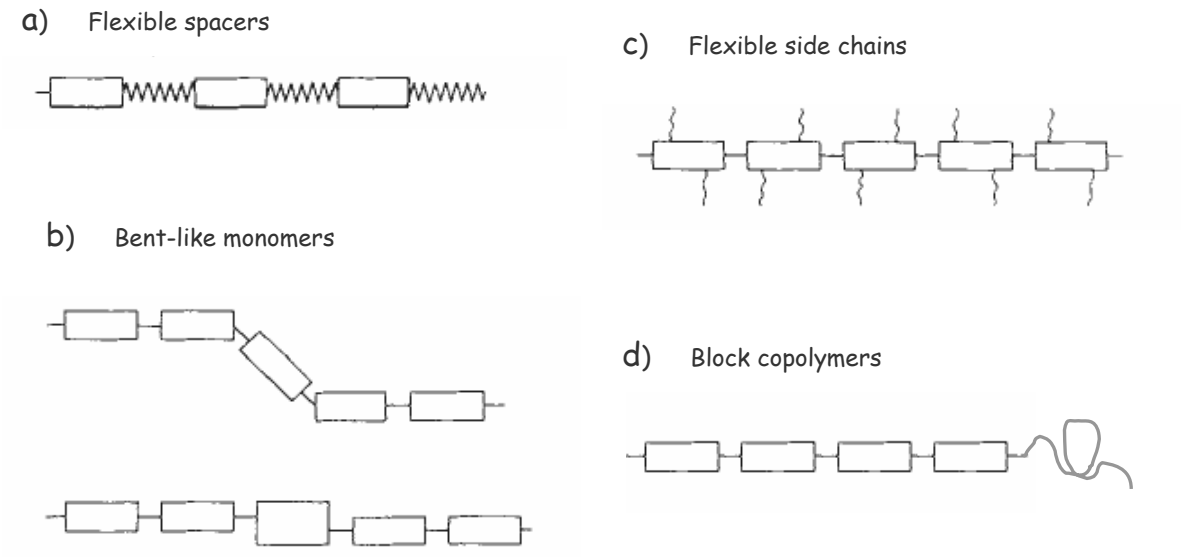

Figure 1.8. Concepts to improve the solubility and meltability of stiff-chain polymers: (a) insertion of flexible spacers between the rigid units, (b) insertion of bent monomers, (c) appending flexible side chains along the main chain or (d) at one terminus (block copolymers).

Aramides can be efficiently used for the design of foldamers, where hydrogen bonds, both of inter- or intramolecular origin, may be useful for their self-assembly and associate stabilization.[22]

Aramides are highly "tunable" referring to the design of structural motifs. The feasibility of designing a wide variety of structures is demonstrated by the numerous aromatic oligoamide-based architectures reported in the literature. Aromatic oligomers may serve as templates for the formation of strictly linear, branched, bent, cyclic oligomers and helices,[22] due to various conformational features as: coplanarity (or close to coplanarity) of the aryl and amide groups (partial conjugation);[36] preferred *trans*-conformation (for secondary amides);[37] or hydrogen bond-mediated conformational preferences through introduction of donors or acceptors on aryl rings adjacent to the amide functions.[22,38,39] **Figure 1.9** depicts the hydrogen bonding patterns commonly used for the restriction of the aryl amide bond rotation in benzamide oligomers to design novel scaffolds for the construction of supramolecular architectures.[38] Additional π-interactions play also an essential role in the formation of single and double helical structures, columnar aggregates (e.g. macrocycles) and less directional stacking of aramides.

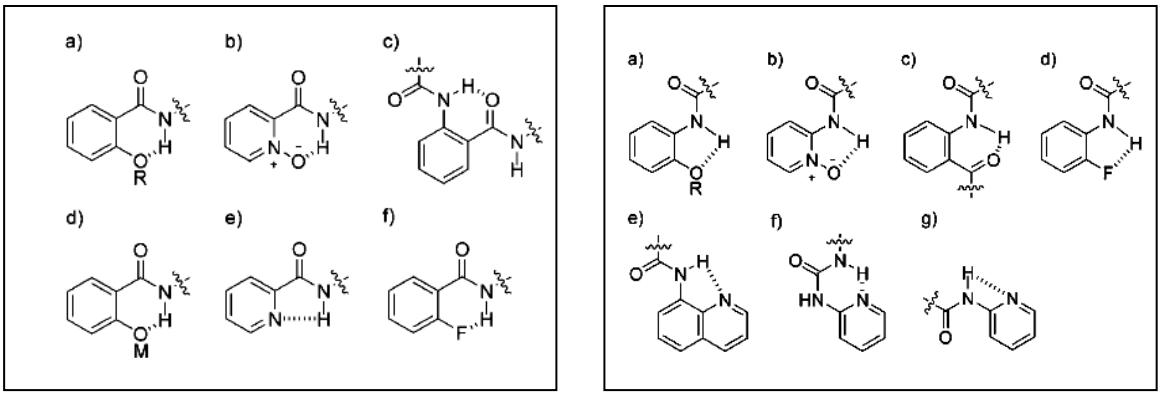

Figure 1.9. Various hydrogen bonding patterns for the rotational restriction of the Ar-CONH bond (*left*) and CO-NH-Ar (*right*).[38]

Particular progress has been made with a variety of non-natural oligomers that organize into helical conformations, thus mimicking α-helical structures and functions.[21,40] Another approach to mimic the molecular recognition properties of α-helical peptides is the positioning of substituents on an elongated stiff scaffold, while

matching the distance between the side chains of an α-helical secondary structure.[41] For the case of aromatic amides based on amino acid monomers utilizing hydrogen bonding interactions between adjacent monomer units, almost only helical structures were synthesized and just few examples of strictly linear stands were published. Hamilton and co-workers described a system based on *p*-aminobenzoic acid / acylurea derivatives, whose elongated pentameric rod carrying nine substituents could for example mimic 6.8 turns of an α-helix constituted of approximately 30 residues (see **figure 1.10**).[42]

Soluble linear structures consisting of *meta*-linked aryl amides were prepared for example from anthranilic acid scaffold units (see **figure 1.11**; **8**). The formation of a six-membered hydrogen bond-stabilized ring between adjacent units allows the preparation of extended molecular sheets. The viability of this approach to introduce different functional groups could also be successfully demonstrated on the basis of a tetramer.[43]

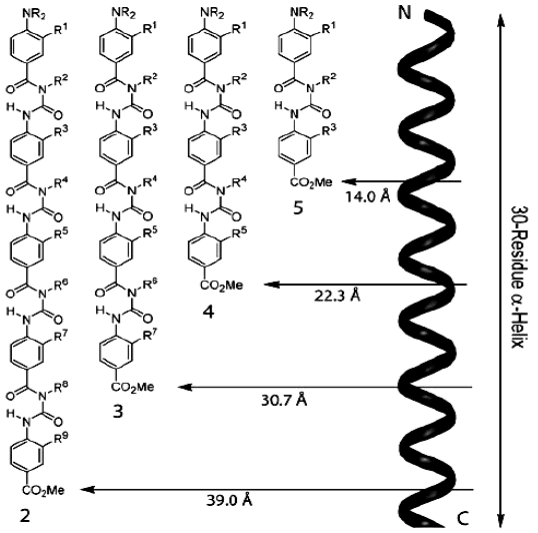

Figure 1.10. Dimensions of the benzoylurea structures compared to an ideal α-helix.

Oligoamides of substituted amino picolinic acid form also linear oligomers in which the amide proton hydrogen binds to both, the ether oxygen atom and the endocyclic pyridine nitrogen atom in a three centred coordination pattern (see **figure 1.11**; **9**). The trispyridylamide was the last soluble oligomer regarding the oligomerization degree. The preferred conformation allows the introduction of functional groups projected on the same face of the molecule.[44]

Oligobenzamide **10** and mixed oligopyridylamide / oligobenzamide trimers **12** and **13** (see **figure 1.11**) were also prepared and their structural properties analysed by

molecular modelling and crystallographic experiments. Compounds, in which hydrogen bonding takes place on both sides of the molecular strand adopt strictly linear conformations, while in those which exhibit a facial polarity a slight curvature is observed. It has to be mentioned, that this generalized trend may not apply for all systems. Structural analysis experiments of compounds **10-13** showed that the plain oligobenzamide **10** was less curved than the oligopyridylamide **11** and the co-oligomers **12** and **13** show a curvature extent in between.[45]

Synthesis of the oligomers **8**-**13** were all accomplished through a stepwise iterative solution synthesis: the activation of acid chlorides, unmasking of the amine terminus and subsequent coupling. Nowick and co-workers presented a new water soluble rod-like structure **14**, whose number of rotamers were diminished by the rotational restriction of the Ar-CO bonds applying the scaffold unit (a) (**figure 1.9**).[46] The synthesis was assembled manually on the solid support using standard solid phase peptide synthesis and could be performed up to the decamer. The remaining scaffold units depicted in **figure 1.9** have been prepared and combined with other monomers in bent structures, but linear homo-oligomers of this kind have not yet been reported.

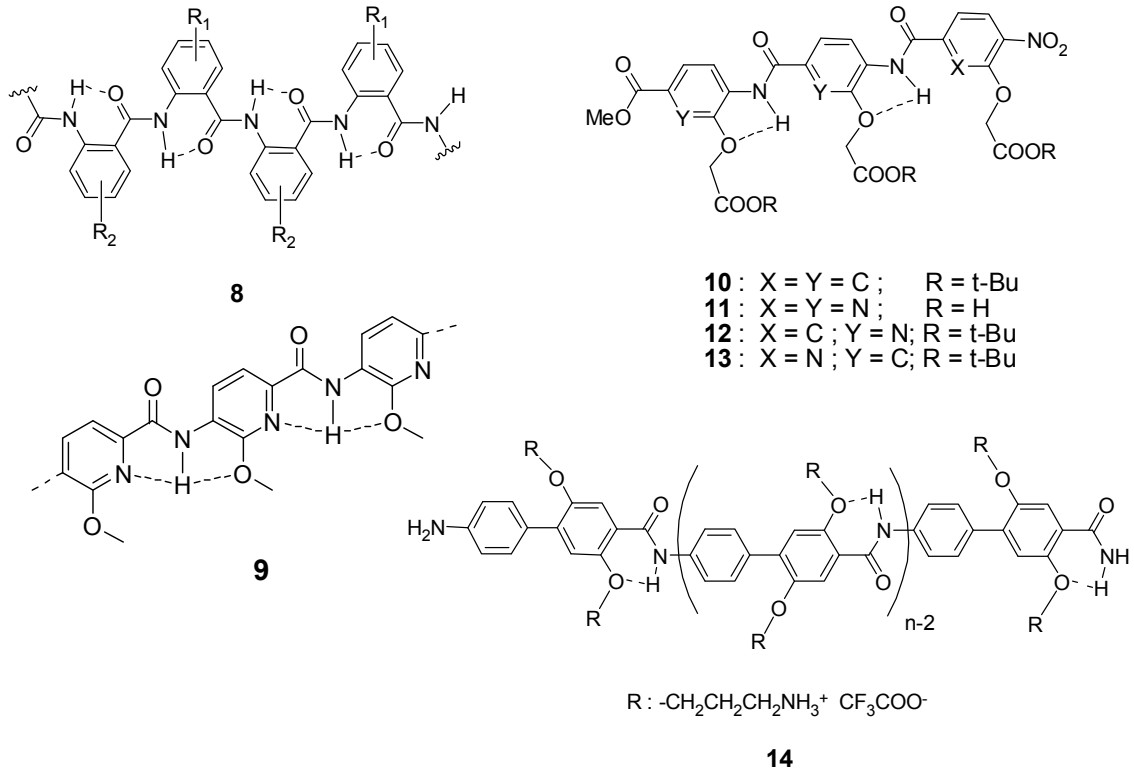

Figure 1.11. Intramolecular H-bonding patterns used in the creation of linear architectures based on aromatic amide backbones.

1.5 Oligo(*p*-benzamide)s (OPBAs)

Oligo(*p*-benzamide)s (OPBAs) are particularly interesting as they form shape-persistent linear rigid rods with hydrogen bond acceptors and donors pointing towards the edges of the flat oligomer and thereby mimicking peptide strands in β-sheets. The shape persistence, by means of the reduced conformational freedom of the linear oligomers, allows the prediction of the geometry and hence simplifies the correlation between molecular shape and superstructure.[47]

As a consequence of this perfect hydrogen bond motif, unsubstituted oligomers longer than the trimer are virtually insoluble in most organic solvents. Therefore, several synthetic strategies towards longer oligomers were developed in our group using soluble precursors and *N*-protected oligomers, either manual or automated solid phase synthesis. OPBA-PEG rod-coil block copolymers with various rod lengths were prepared via a stepwise attachment of imidoyl chlorides as OPBA precursors.[34a,35c]

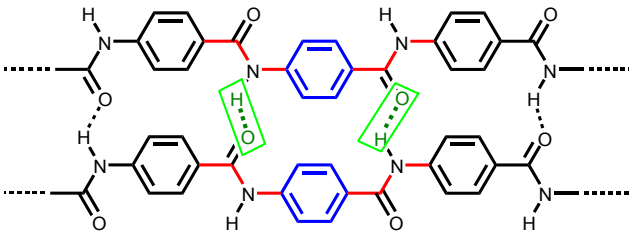

15

Figure 1.12. Chemical structure of the shape persistent linear OPBAs. The particular aspects of these oligomeric scaffolds are highlighted: hydrogen bonding pattern, partial π-conjugation and π-interaction between the phenyl units.

The preparation of OPBAs up to the octamer was also accomplished on the solid phase by subsequent PEG-attachment and cleavage from the resin. This approach showed to be successful with and without the introduction of orthogonal temporary protecting groups as well as manual or automated synthetic approach.[35d,35e,48]

Most recently, a fully automated solution synthesis was developed that allows the stepwise growth of OPBA at the chain end of a polymer by the alternating addition of 4-*N*-sulfinylaminobenzoyl chloride (NSO) and water to an amine-functionalized PEG.[34b]

All these synthetic strategies afforded materials with high aggregation tendency in non-polar solvents. Visualization of the self-assembled copolymer through imaging

techniques showed the formation of rigid rod-like micelles consisting of an aromatic core and a flexible polymer corona (see **figure 1.13**).

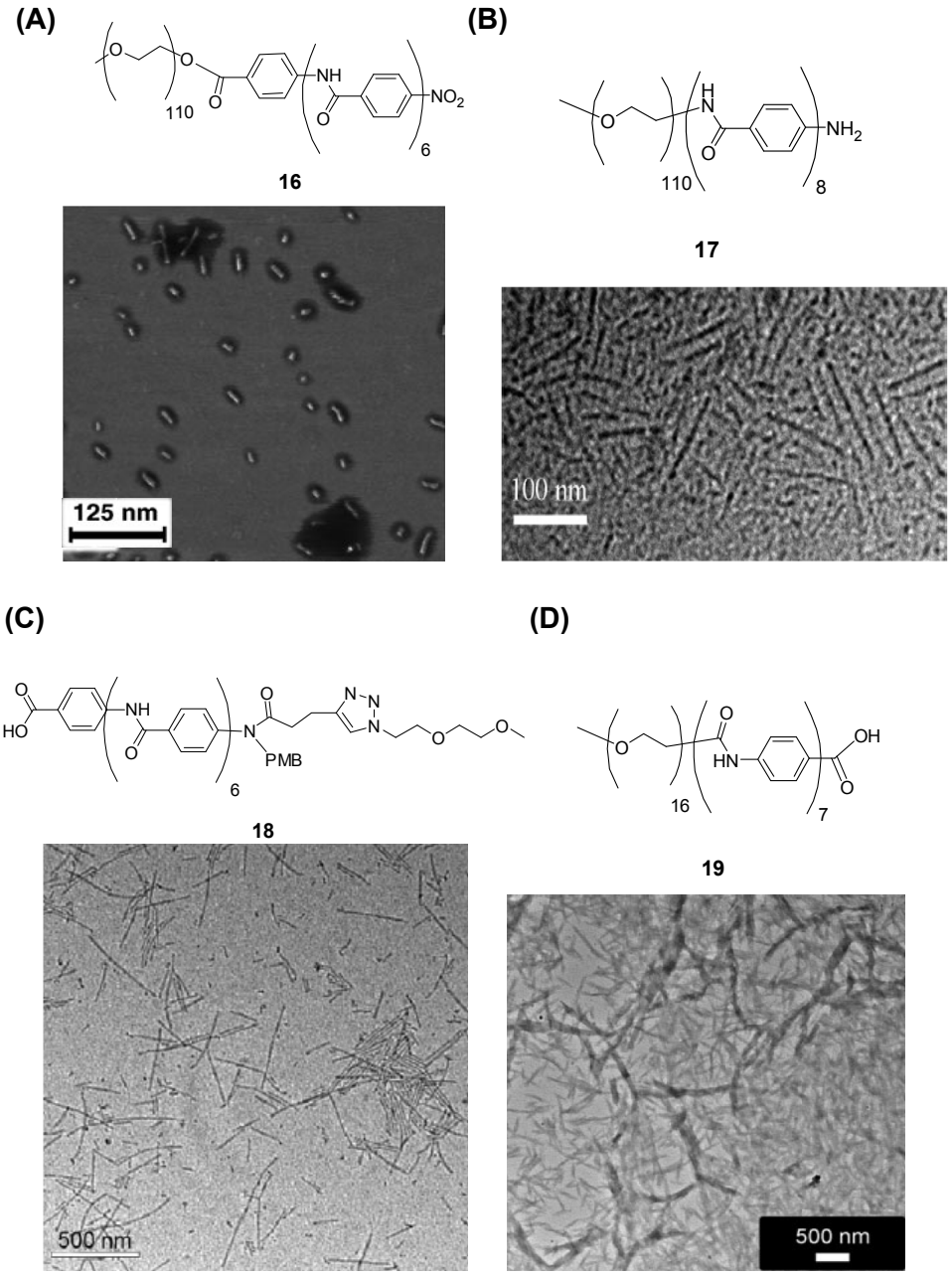

Figure 1.13. Images illustrating the solution structures of rod-like micelles obtained from PEG-OPBA block copolymers. **(A)**: AFM image of the copolymer obtained by the aramide precursor route in solution;[34c] **(B)**: TEM image of the copolymer obtained by the NSO coupling method;[34b] **(C)** and **(D)**: TEM images of a block copolymer obtained by automated solid phase synthesis[35e,48] (PMB = *p*-methoxybenzyl).

1.6. Motivation

This work focuses on the synthesis of molecular scaffolds of the OPBA family for the design of well defined supramolecular architectures. Therefore monodisperse and soluble oligomeric OPBAs should be prepared by different synthetic routes to overcome the insolubility problem. From the synthetic point of view, solution as well as solid phase approaches should be investigated and further developed. New monomers feasible for automatic peptide synthesis that also allow the incorporation of functionalities should be designed. The advantage of monomer sequence control in the automated aramide synthesis should be exploited for the preparation of shape persistent nanoscopic objects. Combining different monomeric scaffolds, may lead to a very simple way for the preparation of different functionalized strands stabilized by a network of intramolecular hydrogen bonds.

Several factors may be employed to facilitate their preparation and achieve stable folded conformations including: (a) intramolecular hydrogen bonding between adjacent subunits, (b) introduction of temporary protecting groups and (c) minimization of the conformational freedom to obtain strongly predictable structures. The aggregation strength of the materials may be characterized by standard analytical methods and the architectures visualized through imaging techniques.

This project will significantly contribute to the deeper understanding of the organization, control and preparation of more complex functional architectures based on OPBAs.

1.7. References

[1] Lehn, J.-M. *Supramolecular Chemistry: Concepts and Perspective*s (VCH, New York), **1995.**

[2] Atwood, J. L.; Davies, J. E. D.; MacNicol, D. D.; Vögtle, F.; Lehn, J.-M.; *Comprehensive Supramolecular Chemistry* (Pergamon, Oxford), **1996**.

[3] Schneider, H. J. *Angew. Chem.* **2009**, *121*, 3982-4036.

[4] Lehn, J.-M. *PNAS* **2002**, *99* (8), 4763-4768.

[5] Gloe, K.; Heßke, H.; Lindoy, L. F. *Wissenschaftliche Zeitschrift der Technischen Universität Dresden* **2007**, *56*, 32-38.

[6] (a) Wolf, K. L.; Frahm, H.; Harms, H. *Z. Phys. Chem.* **1937**, Abt. B *36*, 237; (b) Wolf, K. L.; Dunken, H.; Merkel, K. *Z. Phys. Chem.* **1940**, Abt. B *46*, 287; (c) Wolf, K. L.; Wolff, R. *Angew. Chem.* **1949**, *61*, 191.

[7] Lehn, J.-M. *Pure Appl. Chem.* **1978**, *50*, 871.

[8] Lehn, J. M., *Angew. Chem.* **1988**, *100*, 91; *Angew. Chem. Int. Ed.* **1988**, *27*, 89.

[9] Stoddart, J. F. *Nature Chem.* **2009**, *1*, 14-15.

[10] Malliaras, G.; Friend, R. *Phys. Today* **2005**, *58*, 53.

[11] Philip, D.; Stoddart, J. F. *Angew. Chem. Int. Ed.* **1996**, *35* (11), 1154-1196.

[12] Mancia, F.; Keep, N. H.; Nakagawa, A.; Leadlay, P. F.; McSweeney, S.; Rasmussen, B.; Bösecke, P.; Diat, O.; Evans, P. R. *Structure* **1996**, *4* (3), 339-350.

[13] Klug, A. *Angew. Chem.* **1983**, *95*, 579; *Angew. Chem. Int. Ed. Engl.* **1983**, *22*, 565.

[14] Steed, J. W.; Atwood, J. L. *Supramolecular Chemistry*, John Wiley & Sons, England, **2000**.

[15] Brunsveld, L.; Folmer, B. J. B.; Meijer, E. W.; Sijbesma, R. P. *Chem. Rev*. **2001**, *101*, 4071.

[16] Kato, T. *Science* **2002**, *295*, 2414.

[17] Ikkala, O.; ten Brinke, G. *Science* **2002**, *295*, 2407.

[18] Hecht, S.; Huc, I. *Foldamers: Structures, Properties and Applications*, Wiley-VCH GmbH & Co., Weinheim, **2007**.

[19] Pollino, J. M.; Weck, M. *Chem. Soc. Rev*. **2005**, *34*, 193-207.

[20] Hofmeier, H.; El-Ghayoury, A.*;* Schenning, A. P. H. J.; Schubert, U. S. *Chem. Commun.* **2004**, 318 – 319.

[21] Hill, D. J.; Mio, M. J.; Prince, R. B.; Hughes, T. S.; Moore, J. S. *Chem. Rev.* **2001**, *101*, 3893-4011.

[22] Huc, I. *Eur. J. Org. Chem.* **2004**, 17-29.

[23] Ballauf, M. *Angew. Chem. Int. Ed.* **1989**, *28*, 253-267.

[24] Neher, D. *Adv. Mater.* **1995**, *7* (8), 691-702.

[25] Takahashi, Y.; Ozaki, Y.; Takase, M.; Krigbaum, W. R. *J. Polym. Sci. Part B* **1993**, *31* (9), 1135-1143.

[26] (a) Schwab, P. F. H.; Levin, M. D.; Michl, J. *Chem. Rev.* **1999**, *99* (7), 1863-1934; (b) Schwab, P. F. H.; Smith, J. R.; Michl, J. *Chem. Rev.* **2005**, *105* (4), 1197-1280.

[27] (a) Gothard, C. M.; Rao, N. A.; Nowick, J. S. *J. Am. Chem. Soc.* **2007**, *129* (23), 7272-7273; (b) Kumin, M.; Sonntag, L.-S.; Wennemers, H. *J. Am. Chem. Soc.* **2007**, *129* (3), 466-467.

[28] (a) Lehn, J.-M. *Science* **1993**, *260*, 1762-1763; (b) Lehn, J.-M. *Angew. Chem. Int. Ed.* **1990**, *29* (11), 1304-1319.

[29] Kwolek, S. L.; Morgan, P. W.; Schaefgen, J. R.; Gulrich, L. W. *Macromolecules* **1977**, *10* (6), 1390-1396.

[30] (a) Herlinger, H.; Knoell, H.; Menzel, H.; Schlaefer, J. *Appl. Polym. Symp.* **1973**, *21*, 215-224; (b) Panar, M.; Beste, L. F. *Macromolecules* **1977**, *10* (6), 1401-1406; (c) Takahashi, Y.; Ozaki, Y.; Takase, M.; Krigbaum, W. R. *J. Polym. Sci. Part B* **1993**, *31* (9), 1135-1143.

[31] Herlinger, H.; Knoell, H.; Menzel, H.; Schlaefer, J. *Appl. Polym. Symp.* **1973**, *21*, 212-221.

[32] Ballauff, M. *Makromol. Chem.-Rapid* **1986**, *7*, 407-414; (b) Ballauff, M. *Makromol. Chem.-Rapid* **1987**, *8*, 93-97; (b) Wenzel, M.; Ballauff, M.; Wegner, G. *Makromol. Chem.* **1987**, *188*, 2865-2873; (c) Herrmann-Schönherr, O.; Wendorff, J. H.; Ringsdorf, H.; Tschirner, P. *Makromol. Chem.-Rapid* **1986**, *7*, 791-796.

[33] (a) Rivas, B. L.; Canessa, M. L.; Rabagliati, F. M.; Novi, M.; Preston, J. *Macromol. Chem. Phys.* **2001**, *202*, 1053-1059; (b) Cavalleri, P.; Ciferri, A.; Dell'Erba, C.; Gabellini, A.; Novi, M. *Macromol. Chem. Phys.* **1998**, *199*, 2087-2094; (c) Yokozawa, T.; Ogawa, M.; Sekino, A.; Sugi, R.; Yokoyama, A. *Macromol. Symp.* **2003**, *199*, 187-195; (d) Gabellini, A.; Novi, M.; Ciferri, A.; Dell'Erba, C. *Acta Polym.* **1999**, *50*, 127-134; (e) Rabagliati, F. M.; Aravena, M.; Lillo, I.; Ayal, H. A.; Rivas, B. L.; Canessa, G. S. *Polym. Bull.* **1996**, *37*, 345-351; (f) Chavan, N.; Ciferri, A.; Dell'Erba, C.; Novi, M.; Renamayor, C. S. *Macromol. Chem. Phys.* **1996**, *197*, 2415-2428; (g) Rivas, B. L.; Barria, B.; Canessa, G. S.; Rabagliati, F. M.; Preston, J. *Macromolecules* **1996**, *29*, 4449-4452; (h) Marsano, E.; Bianchi, E.; Conio, G.; Mariani, A.; Russo, S. *Polym. Commun.* **1991**, *32*, 45-46.

[34] (a) Abbel, R.; Schleuss, T. W.; Frey, H.; Kilbinger, A. F. M. *Macromol. Chem. Phys.* **2005**, *206*, 2067-2074; (b) Klos, J.; Wurm, F.; König, H. M.; Kilbinger, A. F. M. *Macromolecules* **2007**, *40*, 7827-7833; (c) Schleuss, T. W.; Abbel, R.; Gross, M.; Schollmeyer, D.; Frey, H.; Maskos, M.; Berger, R.; Kilbinger, A. F. M. *Angew. Chem. Int. Ed.* **2006**, *45*, 2969-2975.

[35] (a) Yokozawa, T.; Ogawa, M.; Sekino, A.; Sugi, R.; Yokoyama, A. *J. Am. Chem. Soc.* **2002**, *124*, 15158-15159; (b) Seyler, H.; Berger-Nicoletti, E.; Kilbinger, A. F. M. *J. Mater. Chem.* **2007**, *17*, 1954-1957; (c) Abbel, R.; Frey, H.; Schollmeyer, D.; Kilbinger, A. F. M. *Chem. Eur. J.* **2005**, *11*, 2170-2176; (d) Koenig, H. M.; Abbel, R.; Schollmeyer, D.; Kilbinger, A. F. M. *Org. Lett.*, **2006**, *8* (9), 1819-1822; (e) Koenig, H. M.; Gorelik, T.; Kolb, U.; Kilbinger, A. F. M. *J. Am. Chem. Soc.*, **2007**, *129* (3), 704-708.

[36] Malone, J. F.; Murray, C. M.; Dolan, G. M.; Docherty, R.; Lavery, A. *J. Chem. Mater.* **1997**, *9*, 2983-2989.

[37] Itai, A.; Toriumi, Y.; Tomioka, N.; Kagechika, H.; Azumaya, I.; Shudo, K.; *Tetrahedron Lett.*, **1989**, *30*, 6177.

[38] Li, Z.-T.; Hou, J.-L.; Yi, H.-P.; *Chem.–Asian J.*, **2006**, *1*, 766.

[39] Gong, B.; *Chem.–Eur. J.*, **2001**, *7*, 4336.

[40] Sanford, A. R.; Gong, B. *Curr. Org. Chem.*, **2003**, *7,* 1649-1659.

[41] (a) Rodriguez, J. M.; Hamilton, A. D. *Tetrahedron Lett*. **2006**, *47*, 7443 – 7446; (b) Davis, J. M.; Truong, A.; Hamilton, A. D. *Org. Lett.* **2005**, *7*, 5405 – 5408; (b) Yin, H.; Lee, G. I.; Park, H. S.; Payne, G. A.; Rodriguez, J. M.; Sebti, S. M.; Hamilton, A. D. *Angew. Chem*. **2005**, *117*, 2764 – 2767; *Angew. Chem. Int. Ed***. 2005**, *44*, 2704 – 2707; Yin, H.; Lee G. I.; Sedey, K. A.; Kutzki, O.; Park, H. S.; Omer, B. P.; Ernst, J. T.; Wang, H. G.; Sebti, S. M.; Hamilton, A. D. *J. Am. Chem. Soc*. **2005**, *127*, 10191 – 10196.

[42] Rodriguez, J. M.; Hamilton, A. D. *Angew. Chem*. **2007**, *119*, 8768 –8771.

[43] Hamuro, Y.; Geib, S. J.; Hamilton, A. D. *J. Am. Chem. Soc.* **1996**, *118*, 7529-7541.

[44] Ernst, J. T.; Becerril, J.; Park, H. S.; Yin, H.; Hamilton, A. D. *Angew. Chem. Int. Ed*. **2003**, *42* (5), 535-539.

[45] Saraogi, I.; Incarvito, C. D.; Hamilton, A. D. *Angew. Chem*. **2008**, *120*, 9837-9840.

[46] Gothard, C. M.; Rao, N. A.; Nowick, J. S. *J. Am. Chem. Soc.* **2007**, *129*, 7272-7273.

[47] Koenig, H. M.; Kilbinger, A. F. M. *Angew. Chem. Int. Ed*. **2007**, *46*, 8334-8340.

[48] Koenig, H. M.; Kilbinger, A. F. M. *Macromol. Rapid Commun*. **2008**, *29*, 1721-1725.

Chapter 2

Rod-Coil Copolymers

2.1. Rod-Coil Copolymers from Oligo(*p*-benzamide) Foldamers

*Helga Seyler, Elena Berger-Nicoletti, Andreas F.M. Kilbinger**

Published in *J. Mater. Chem.* **2007,** *17*, 1954.

Abstract

Rod-coil copolymers with shape persistent and precisely defined oligo(*p*-benzamide) (OPBA)-blocks offer the possibility of creating nanoscale objects in block-selective solvents. However, the preparation and characterization of these oligomers as monodisperse rods present difficulties due to their strong aggregation and low solubility.
Based on the synthetic strategy developed during the prior diploma thesis, a new route to soluble OPBAs up to the octamer was developed using an iterative coupling protocol (dimer-tetramer-octamer). The introduction of the acid labile and bulky 2,4-dimethoxybenzyl (DMB) amide protective group prevents intermolecular hydrogen bond formation, thus increasing the solubility and allowing the preparation of OPBAs in solution.

Kurzfassung

Stab-Knäuel Copolymere mit formtreuen und monodispersen Oligo(*p*-benzamid) (OPBA)-Blöcken sind für die Herstellung von gut definierten Aggregaten im Nanometerbereich von besonderem Interesse. Jedoch stellt sich die Herstellung und Charakterisierung der OPBA-Blöcke als große Herausforderung dar, wenn längere Oligomere als das Trimer erwünscht sind, was auf deren starkes Aggregationsverhalten und ihre geringe Löslichkeit zurückzuführen ist.
Basierend auf der synthetischen Strategie, die während der Diplomarbeit entwickelt worden ist, konnten OPBAs bis zum Octamer synthetisiert werden. Die Oligomere wurden in einer iterativen Syntheseroute (Dimer-Tetramer-Octamer) unter Verwendung der säuren-labilen 2,4-Dimethoxybenzyl-(DMB) Amidschutzgruppe hergestellt. Der Schutz jeder zweiten Amidfunktion erwies sich als ausreichend um die Bildung von intermolekularen Wasserstoffbrückenbindungen zu unterdrücken und somit die Lösungssynthese längerer Oligomere zu ermöglichen.

2.1.1. Introduction

Rod-like molecules with nanometer dimensions have recently attracted increased attention.[1] Most of these shape persistent molecules gain rigidity from either helix formation[2] or π-conjugation.[3] Molecular rods offer the possibility to position reactive centres at known distances from each other which is for example important for the study of electron and energy transfer. On the other hand they are useful nano-scaffolds used in the construction of larger shape persistent molecules as well as in supramolecular chemistry.[4] Oligo(*p*-benzamide)s (OPBA) are particularly interesting molecular rods as they combine chain stiffness with the ability to form multiple hydrogen bonds. This combination of shape persistence and directionality in noncovalent bond formation makes them interesting building blocks for the construction of supramolecular objects such as rod-coil copolymers. These supramolecular polymers offer the possibility of creating defined nano-structures in solution or the solid state on length scales much smaller than typically accessible using coil-coil block copolymers.[5] We recently described the synthesis and aggregation behaviour of rod-coil copolymers in which the rod-segments are based on shape persistent OPBA.[6,7]

The greatest challenge in synthesizing OPBA for use in supramolecular chemistry is their strong aggregation and hence low solubility in most organic solvents.[8] We previously reported a precursor route[9] as well as a solid supported synthesis protocol[10,11] that overcomes these limitations. Here we describe a new synthetic route to OPBA up to the octamer using *N*-2,4-dimethoxybenzyl (*N*-DMB) protection on every second amide group.

2.1.2. Results and discussion

As shown in **scheme 2.1.1**, *p*-aminobenzoic acid **1** was reductively alkylated using 2,4-dimethoxy benzaldehyde **2** and sodium borohydride to give the secondary amine **4** (50% over two steps). Acylation of **4** with *p*-nitrobenzoyl chloride gave the *N*-DMB protected dimer **5** (82%). The nitro group of **5** could be reduced to the amine using Pd/C and ammonium formate to give amino acid **7** (90%). The nitro reduction at rt was found to be slow and completion of reaction was monitored by RP-HPLC (see supporting information, **chapter 2.1.6**). Using an activation protocol described by Zollinger and co-workers[12] and more recently by Ueda and co-workers,[13] **5** could be transformed into the

acid chloride **6** using thionyl chloride in NMP without any detectable loss of the DMB-protective group. Acylation of **7** with **6** gave the tetramer **8** (68%).

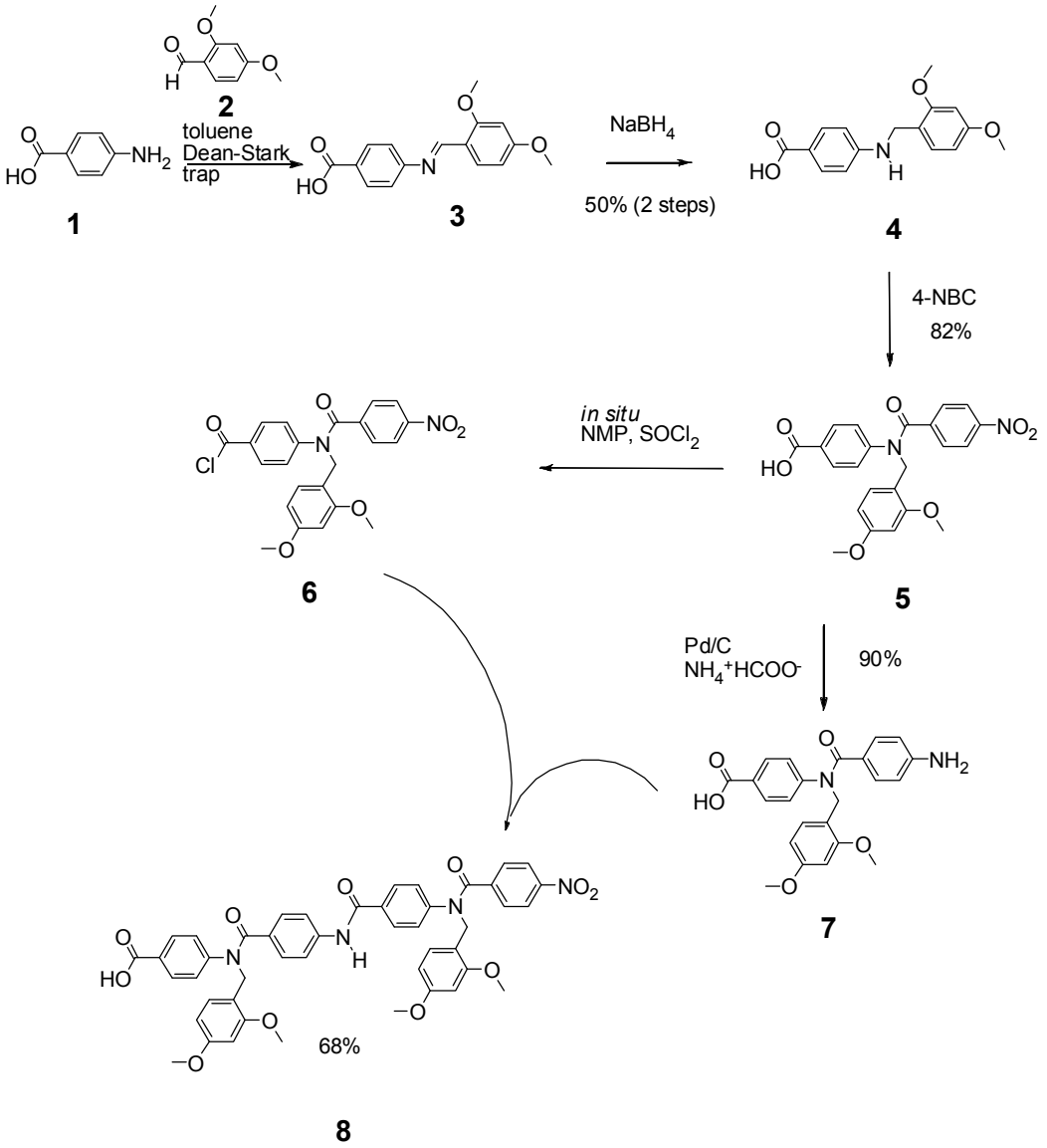

Scheme 2.1.1. Synthesis of the OPBA dimers **5**, **7** and tetramer **8**.

We were fortunate to grow single crystals of **8** from ethanol / water mixture which allowed X-ray crystallographic analysis (see crystal data[14]). Of particular interest was the conformation of the three amide bonds in **8**. It has been well established that secondary aromatic amides (Ar-CONH-Ar) exist predominantly in the *trans* conformation while the tertiary aromatic amides of the type Ar-CONR-Ar (R = alkyl) prefer *cis* conformation (with respect to the phenyl rings).[15] In a previous report we could show that this was also true for OPBA dimers in solution as well as in the solid state.[10]

Of the three amide bonds present in **8** only the centre one exists in the *trans* conformation while the outer ones are in the *cis* conformation. This confirms the

previous assumption that this conformational preference persists in longer OPBAs. COSY and NOESY-NMR spectroscopy of solutions of **8** allowed the complete peak assignment of the ^{1}H-NMR spectroscopic data and showed that at least one tertiary amide existed exclusively in the *cis* conformation (the conformation of the other amide group could not be assigned due to overlapping peaks; see supporting information).

Continuing with the iterative strategy, **8** could be reduced to the amine **9** using Pd/C and ammonium formate (90%, **scheme 2.1.2**). *In situ* activation of **8** with thionyl chloride in NMP gave the acid chloride **10**, which was coupled with **9** to give the octamer **11** (52%). **11** could be converted into an acid chloride *in situ* ($SOCl_2$-NMP) and coupled with propargylamine to install a terminal alkyne in **13** (95%). Poly(ethylene glycol) mono-methyl ether mono-azide[16] could be reacted with **13** in a [2+3]-cycloaddition under Cu(I)-catalysis[17] to give the block copolymer **14** (40%) in which both blocks are 1,4-linked via a 1,2,3-triazole unit.

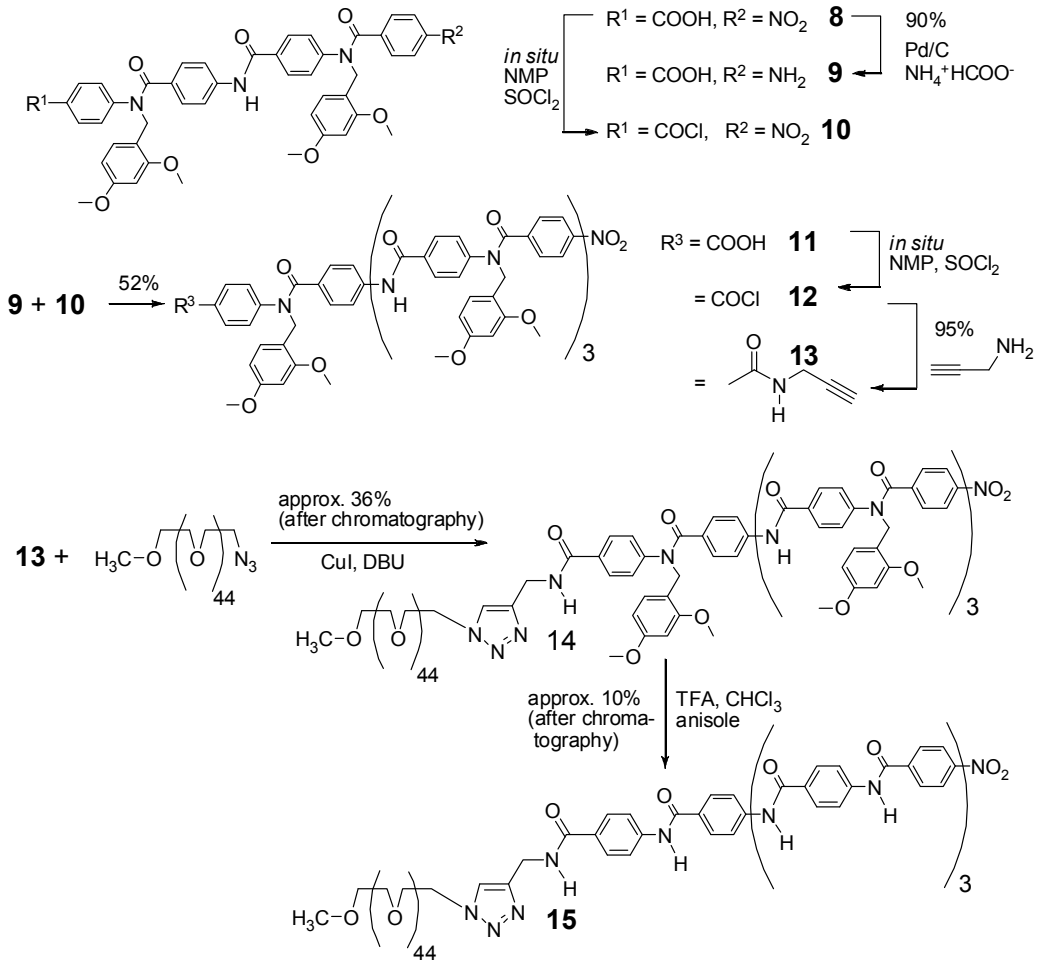

Scheme 2.1.2. Synthesis of an OPBA octamer **11** and conjugation with poly(ethylene glycol) to yield a coil-coil copolymer **14** or rod-coil copolymer **15** after DMB-deprotection.

Block copolymer **14** which most likely adopts a coil-coil like conformation showed no aggregation in chloroform. The presence of DMB-*N*-protective groups on every second amide effectively disrupted the aggregation process. It is important to note that a virtually identical synthetic strategy using a dimer analogous to **7** carrying a *p*-methoxy benzyl group was unsuccessful when carried out on solid support. We attributed this to backbone aggregation of the oligomers on the solid phase. For this reason we previously reported that complete *N*-protection is necessary for successful solid supported synthesis of such oligomers.[10] In the case described here, the bulky polymer chain of **14** possibly helps in reducing the aggregation strength via steric shielding. **14** could be analyzed by MALDI-TOF mass spectroscopy (**figure 2.1.1**, *top*). The mass spectrum shows only the fully protected block copolymer as the sodium, potassium and lithium adduct.

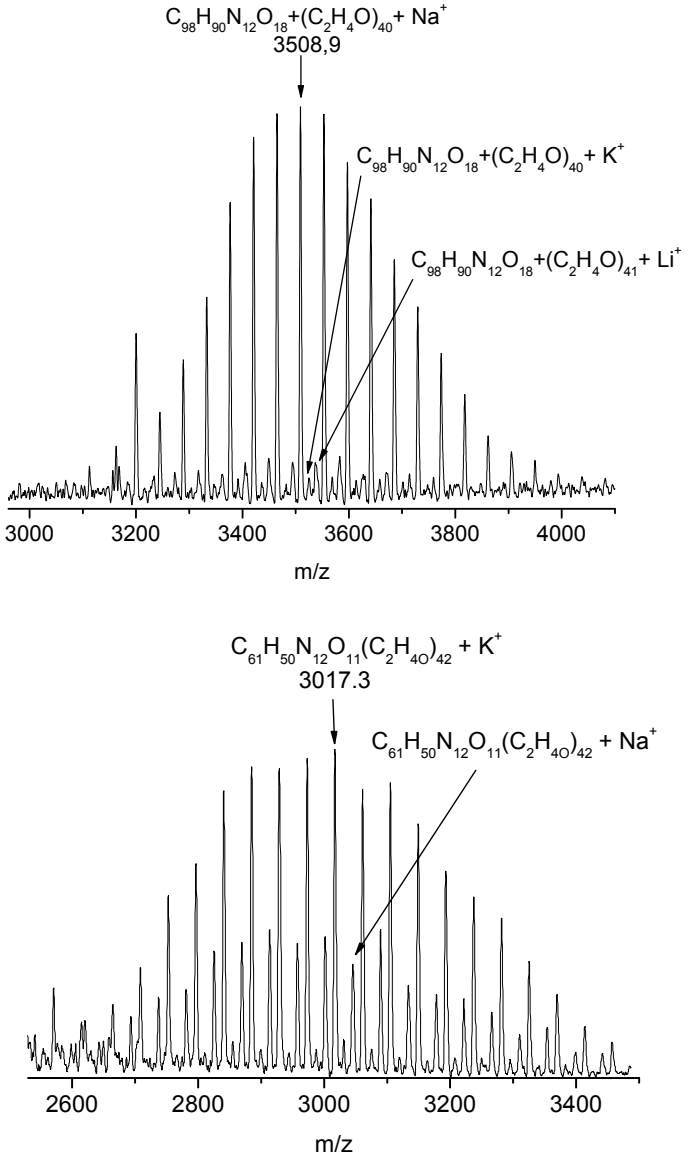

Figure 2.1.1. MALDI-TOF mass spectrum of protected **14** (*top*) and unprotected **15** (*bottom*).

The DMB-protective group was removed by dissolving **14** in a mixture of trifluoroacetic acid (TFA), chloroform and anisole at rt for 15 h. The ease of protective group removal could be demonstrated by addition of polymer **14** to neat TFA. This immediately gave a purple coloured solution, indicative of the successfully cleaved DMB cation. Polymer **15**, in which all aromatic amides are assumed to exist exclusively in all-*trans* conformation was further purified by silica gel chromatography in THF and DMF. **Figure 2.1.1** (*bottom*) shows the MALDI-TOF mass spectrum of **15**. Two mass distributions, one for the potassium and one for the sodium adduct of **15** can be observed.

Figure 2.1.2 (*top, middle*) shows the chloroform GPC traces for **14**, **15** as well as for the parent PEG-azide (PEG-N_3). A shift to higher mass is clearly visible going from PEG-N_3 to the DMB-protected block copolymer **14**. The elugram of **14** showed the molecularly dissolved polymer eluting at the poly(styrene) equivalent hydrodynamic radius (M_n = 3500 g mol^{-1}, M_w = 3800 g mol^{-1}; PDI = 1.07).

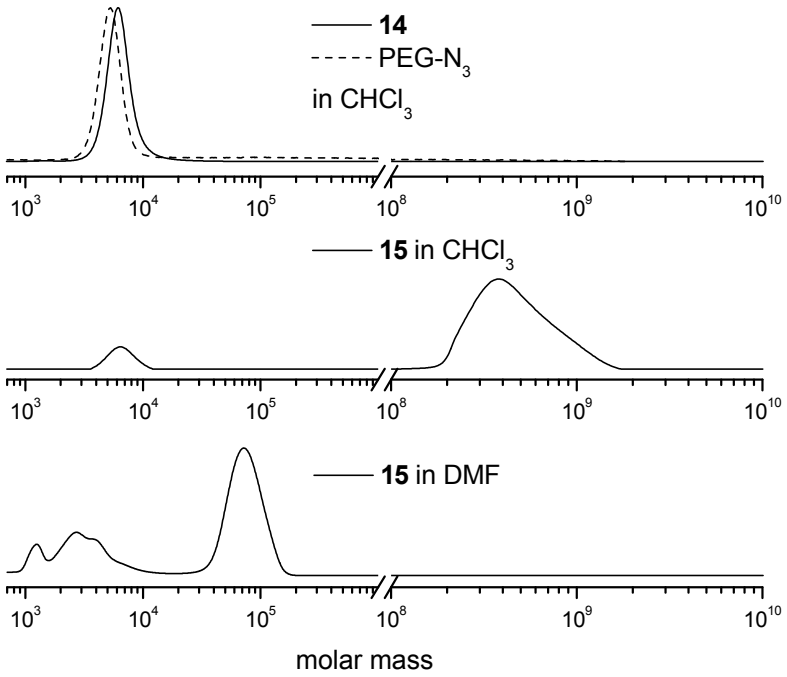

Figure 2.1.2. GPC traces. *Top*: PEG-N_3 (dashed line) and **14** (straight line) in $CHCl_3$; *middle*: **15** in $CHCl_3$; *bottom*: **15** in DMF.

The GPC trace of **15** in chloroform showed the presence of molecularly dissolved polymer as well as high molecular weight aggregates. The noncovalent aggregates

elute at very high molecular weight (> 2 x 10^6 g mol^{-1}) outside the calibration limit of the GPC setup. Similar behaviour has previously been observed by us for other rod-coil copolymers in chloroform solution.[9] The GPC elugram of the same sample of **15** in DMF (**figure 2.1.2**, *bottom*) also showed the presence of aggregates as well as molecularly dissolved polymer. The aggregates of **15** in DMF appear as a multi modal mass distribution, which was unexpected and had not been observed by us previously.

However, the prior reported rod-coil copolymers differed from the ones shown here.[6,7,9] Detailed investigations in the past had been carried out on a hepta(*p*-benzamide) carrying six amide groups. The octamer shown here carries eight amide groups and it is likely that this causes the increased aggregation strength. By comparing the very different aggregate masses and mass distributions in the elugrams of **15** in $CHCl_3$ and DMF it could safely be concluded that all aggregation phenomena were due to noncovalent interactions rather than covalent cross-linking.

The non-aggregating *N*-DMB-protected copolymer **14** could be analysed by ^{1}H-NMR spectroscopy in DMSO-d_6 and all peaks of the spectrum could be assigned. A ^{1}H-NMR spectrum of **15** was recorded in DMSO-d_6. The polymer appeared to aggregate in this solvent, as the aromatic signals of the OPBA block integrated to only 15% of the expected value when compared to the integral of the PEG methylene protons. This can be explained, considering the observed aggregation of **15** in DMF (see GPC results above). The solvent (DMSO-d_6) was then removed under vacuum and the residue dissolved in deuterated sulphuric acid, which is known to be a strong hydrogen bond disrupting solvent.[18] The ^{1}H-NMR spectrum of **15** in D_2SO_4 shows a significant increase in intensity of the aromatic protons in the range δ = 7.0 - 8.5 compared to the spectrum recorded in DMSO-d_6. This marked difference in intensity is further evidence for the strong aggregation of **15** in DMSO (see NMR-data in the supporting information).

In order to further study the aggregation phenomena, chloroform solutions of **15** were investigated by transmission electron microscopy (TEM). **Figure 2.1.3** shows a representative TEM image of aggregates of **15**. Elongated, rod-like micelles can be observed similar to those reported previously.[7] The anisotropic aggregation is most likely driven by highly directional intermolecular hydrogen bonds.

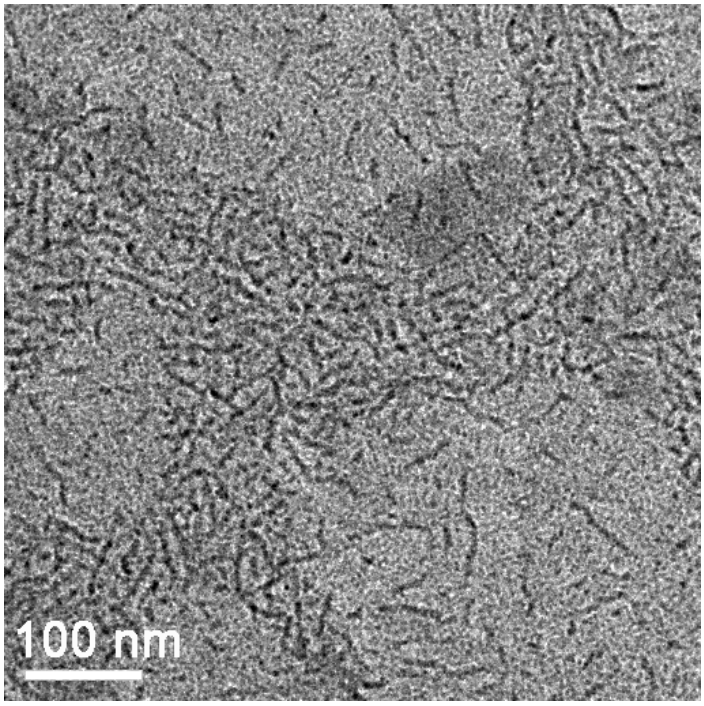

Figure 2.1.3. TEM image of aggregates of **15** drop cast (3 x) from chloroform solution (0.5 mg mL^{-1}) onto carbon coated copper grids. The sample was stained with OsO_4.

2.1.3. Conclusions

In conclusion, we have successfully employed the 2,4-dimethoxybenzyl protective group for the protection of oligo(*p*-benzamide)s up to the octamer. Protection of every second amide group was sufficient to suppress aggregation during synthesis. The more acid labile DMB-protective group was cleaved faster than the previously employed 4-methoxybenzyl group, yet tolerates the activation of the amino acid as an acid chloride without any detectable cleavage. An alkyne derivatized octa(*p*-benzamide) could be linked to a polymer chain *via* Cu(I)-catalyzed [2+3]-cycloaddition. The *N*-DMB-protected amphiphilic block copolymer showed no aggregation in nonpolar solvents while the de-protected polymer aggregated strongly in chloroform. Both polymers could be analyzed by MALDI-TOF mass spectroscopy. TEM imaging showed rod-like micelles for the DMB-deprotected polymer in chloroform solution. Further investigations will focus on the variation of the polymer block and the effect on superstructure formation in solution.

2.1.4. Experimental Section

Materials

Technical solvents were purchased from Acros Organics, solvents of p. a. quality from Fisher Scientific. All chemical reagents including compounds **1** and **2** were obtained from Acros Organics and were used as received. *N*-Methylpyrrolidinone was dried over calcium hydride followed by distillation and storage over molecular sieve (4 Å). Deuterated solvents (DMSO-d_6, $CDCl_3$ and D_2SO_4) were purchased from Deutero GmbH and used as received.

Techniques

Standard ^1H and ^{13}C nuclear magnetic resonance spectra were recorded at a frequency of 300 MHz (75 MHz for ^{13}C) on a Bruker AC 300. For two dimensional COSY and NOESY experiments a Bruker AMX 400 was used working at 400 MHz. Infrared spectra were recorded on a Nicolet 5 DXC FT-IR spectrometer. X-ray crystal structures were obtained on a Turbo CAD 4. The RP-HPLC analysis was performed on a HP 1090 Liquid Chromatograph of Hewlett Packard by using a PerfectSil column (MZ Analysentechnik, Mainz, Germany, 250 x 4.0 mm; 120 ODS-2 5 μm). The samples were eluted with an acetonitrile/water gradient that started from 10 % acetonitrile rising to 90 % over a period of 35 min. Both solvents were buffered with 0.1 % TFA. UV-detection was performed at 254 nm. Melting points were recorded on a FP 62 Mettler Toledo in a capillary tube and are uncorrected. Field desorption mass spectra were measured on a Finnigan MAT 95 and ESI mass spectra on a Micromass Q-TOF Ultima 3. Gel permeation chromatography with chloroform was performed on an instrument consisting of a Waters 717 plus auto sampler, a TSP Spectra Series P 100 pump and a set of three PSS SDV columns ($10^6/10^5/10^4$ g/mol for high molecular masses, $10^4/10^3/10^2$ g/mol for low molecular masses). Signal detection occurred by use of a TSP Spectra System UV 2000 (UV 254 nm) and a Wyatt Optilab DSP (refractive index). For measurements in DMF containing 1 g/L of lithium bromide, an Agilent 1100 Series was used as an integrated instrument including a PSS Gral column ($10^6/10^5/10^4$ g/mol), a UV (254 nm) and RI detector. Calibration was done using poly(styrene) standards provided by Polymer Standards Service. MALDI-TOF mass spectra were recorded on a Kratos Axima CFR in linear, positive mode using dithranol or CHCA as matrix.

A Philips EM 420 transmission electron microscope using a LaB_6 cathode at an acceleration voltage of 120 kV was used to obtain TEM-images. TEM grids (carbon film

on copper, 300 mesh) were obtained from Electron Microscopy Sciences, Hatfield, PA, USA. For cryo-TEM Quantifoil R1.2/1.3 copper grids were used.

Synthesis of 4-(2,4-Dimethoxybenzylamino)benzoic acid **4**[1]

4-Aminobenzoic acid **1** (80 g; 0.583 mol) and 2,4-dimethoxybenzaldehyde **2** (97 g; 0.584 mol) were suspended in toluene (1 L) and refluxed under Dean-Stark conditions until ca. 11 ml of water had been removed. The solvent was removed under reduced pressure and the yellow solid (**3**) dissolved in THF (ca. 4 L). Sodium borohydride (48 g; 1.27 mol) was added in small portions while stirring and cooling with an ice-bath. The colour of the reaction mixture changed from yellow to colourless over a period of 72h. Water was added until hydrogen formation could no longer be observed and all $NaBH_4$ was quenched. THF was removed under reduced pressure and the aqueous phase neutralized with HCl (1 M). The colourless precipitate was recovered by filtration and dried under vacuum at 40°C to yield 4-(2,4-dimethoxybenzylamino)benzoic acid **4** (83.32 g; 50 %).

mp: 185-187 ºC.

^{1}H-NMR: δ (300 MHz, DMSO-d_6) 3.73 (s, 3 H); 3.81 (s, 3 H); 4.18 (d, J = 5.52 Hz, 2 H); 6.46 (dd, J_1 = 8.09 Hz, J_2 = 2.39 Hz, 1 H); 6.54 – 6.57 (m, 3 H); 6.76 (t, 1 H); 7.10 (d, J = 8.09 Hz, 1 H); 7.63 (d, J = 8.82 Hz, 2 H).

^{13}C-NMR and DEPT: δ (300 MHz, DMSO-d_6) 40.6 (-); 55.18 (+); 55.43 (+); 98.38 (+); 104.38 (+); 111.01 (+); 116.93; 118.65; 128.81 (+); 131.14 (+); 152.59; 157.95; 159.78; 167.58.

IR ν (cm^{-1}): 3403 (N-H), 1672 (C=O), 1604 (C=C Ar), 1507 (C=C Ar), 1295 (Ar-O-C).

RP-HPLC (min.): 4.45.

Synthesis of N-(2,4–Dimethoxybenzyl)-4-(4-nitrobenzamido)benzoic acid **5**

A solution of 4-nitrobenzoyl chloride (39 g; 0.21 mol) in dry NMP (500 ml) was added to a solution of **4** (48.6 g; 0.169 mol) in dry NMP (1 L) while stirring and cooling with an ice-bath. The reaction mixture was stirred for 1h and left at rt for 2 days. The yellow solid was recovered by vacuum filtration, washed neutral with water and re-crystallized from ethanol to give *N*-(2,4–dimethoxybenzyl)-4-(4-nitrobenzamido)benzoic acid **5** (60.5 g; 82 %).

[1] Brest, F.; Holmes, A.B.; Ladlow, M. *Org. Biomol. Chem*. **2003**, *1*, 1711-1719.

mp: 228 ºC.

^{1}H- NMR (400 MHz, DMSO-d_6): δ 3.63 (s, 3 H); 3.70 (s, 3 H); 5.03 (s, 2 H); 6.45 (dd, J_1 = 2.20 Hz, J_2 = 8.25 Hz, 1 H); 6.47 (d, J = 2.20 Hz, 2 H); 7.18-7.22 (m, 3 H); 7.58 (d, J = 8.44 Hz, 2 H); 7,72 (d, J = 8.44 Hz, 2 H); 8.10 (d, J = 8.80 Hz, 2 H), 12.94 (br. s, 1 H).

^{13}C NMR and DEPT (300 MHz, DMSO-d_6): δ 47.60 (-); 55.12 (+); 55.30 (+); 98.25 (+); 104.59 (+); 116.24; 123.24 (+); 127.85 (+); 128.88; 129.42 (+); 129.92 (+); 130.08 (+); 142.50; 145.93; 147.59; 158.01; 160.05; 166.55; 167.76.

IR ν (cm^{-1}): 3424, 2931, 2632, 1708, 1594, 1508, 1272, 1031, 862.

RP-HPLC (min.): 22.63.

M (FD): *m/z* (%) = 436.2 (100); 437.2 (23.4); 438.2 (4.1). calc.[$C_{23}H_{22}N_2O_5$] = 436.13.

General activation method for the in situ preparation of acid chlorides **6**, **10** *and* **12**

A Schlenk-flask was equipped with the compound carrying a carboxylic acid dissolved in dry NMP. The solution was evacuated and refilled with dry nitrogen gas. This procedure was repeated three times. One equivalent (with respect to the carboxylic acid) of thionyl chloride was added dropwise to the solution while stirring and cooling with an ice-bath. The reaction mixture was stirred for an additional 2h at rt. The activated carboxylic acid was used in the next reaction step without characterization.

Synthesis of N-(2,4–Dimethoxybenzyl)-4-(4-aminobenzamido)benzoic acid **7**

A solution of ammonium formate (21.7g; 0.344 mol) in methanol (400 ml) was added dropwise to a solution of **5** (15 g; 34.4 mmol) in NMP (150 ml) while stirring and cooling with an ice-bath. Pd/C (10%, 0.8 g) was added in small portions to the cold solution while maintaining a slight flow of nitrogen gas over the reaction mixture. After stirring for 36h at rt the suspension was filtered through Celite and the methanol removed under reduced pressure. Water was added to the residue to give a colourless precipitate which was isolated via vacuum filtration. The crude solid was washed with water and dried under vacuum at 60°C to give *N*-(2,4–dimethoxybenzyl)-4-(4-aminobenzamido)benzoic acid **7** (12.5 g; 90 %).

mp: 207 ºC.

^{1}H-NMR (300 MHz, DMSO-d_6) δ: 3.66 (s, 3 H); 3.71 (s, 3 H); 4.97 (s, 2 H); 6.35 (d, J = 8.46 Hz, 2 H); 6.47 – 6.49 (m, 2 H); 7.04 (d, J = 8.46 Hz, 2 H); 7.11 (d, J = 8.83 Hz, 2 H); 7.20 (d, J = 7.72 Hz, 1 H); 7.74 (d, J = 8.46 Hz, 2 H).

^{13}C-NMR und DEPT (300 MHz, DMSO-d_6) δ: 47.55 (-); 55.12 (+); 55.31 (+); 98.22 (+); 104.60 (+); 112.30 (+); 117.54; 121.71; 126.43 (+); 127.25; 128.96 (+); 129.84 (+); 130.86 (+); 148.80; 150.88; 157.70; 159.68; 166.79; 169.94.

IR ν (cm^{-1}): 3363 (N-H), 2937, 2823, 1662, 1600, 1403, 1299, 1027.

RP-HPLC (min): 15.26.

M (FD): *m/z* (%) = 406.1 (100); 407.2 (24.8); 408.1 (2.7). calc.[$C_{23}H_{22}N_2O_5$] = 406.15.

Synthesis of 4-(N-(2,4-Dimethoxybenzyl)-4-(4-(N-(2,4-dimethoxybenzyl)-4-nitrobenzamido)benzamido)benzamido)benzoic acid **8**

Thionyl chloride (1.60 ml; 22.14 mmol) was added to a solution of **6** (9.66 g; 22.14 mmol) in dry NMP (150 ml) according to the general activation method (GAM). The reaction mixture was stirred for 90 minutes at rt. A solution of **7** (4.66 g; 11.46 mmol) in dry NMP (30 ml) was added dropwise to the mixture while cooling the reaction flask with an ice bath. After stirring for 12h at rt under a N_2-atmosphere the reaction product was precipitated from solution by adding water to the reaction mixture (300 ml). The precipitate was isolated by vacuum filtration, washed with water and dried. The solid was suspended in ethanol (1 L) and stirred for 5 h. The white insoluble solid was isolated by filtration and dried under vacuum at 40°C to give 4-(*N*-(2,4-dimethoxybenzyl)-4-(4-(*N*-(2,4-dimethoxybenzyl)-4-nitrobenzamido)benzamido) benzamido)benzoic acid **8** (12.35 g; 68 %).

mp: 223-225 ºC.

^{1}H-NMR (400 MHz, DMSO-d_6) δ: 3.63 (s, 3 H); 3.65 (s, 3 H); 3.71 (s, 6 H); 5.01 (s, 2 H); 5.04 (s, 2 H); 6.44 – 6.48 (m, 4 H); 7.14 (d, *J* = 8.41 Hz, 2 H); 7.20 – 7.25 (m, 4 H); 7.28 (d, *J* = 8.80 Hz, 2 H); 7.57 – 7.62 (m, 4 H); 7.72 (d, *J* = 8.80 Hz, 2 H); 7.73 (d, *J* = 8.41 Hz, 2 H); 8.11 (d, *J* = 8.22 Hz, 2 H); 10.23 (s, 1 H).

^{13}C-NMR (400 MHz, DMSO-d_6) δ: 47.57; 55.12; 55.36; 98.24; 98.27; 104.60; 116.23; 116.92; 119.15; 123.27; 127.26; 127.73; 128.07; 128.44; 129.29; 129.46; 129.84; 130.06; 130.89; 132.64; 140.33; 142.64; 144.92; 147.47; 147.58; 157.83; 158.03; 159.83; 160.03; 164.71; 166.68; 167.87; 169.23.

IR ν (cm^{-1}): 3295 (, 2937, 1654, 1598, 1506, 1407, 1313, 1255, 1207, 1120, 1031, 848, 707.

RP-HLPC (min.): 27.51.

M (ESI-MS): *m/z* (%) = $[M + Na]^+$ 847.32 (100); 848.32 (41.5); 849.32 (1.7). calc. [$C_{46}H_{40}N_4O_{11}Na^+$] = 847.26.

Crystallographic data: molecular weight = 842.84; crystal dimensions = 0.064 x 0.128 x 0.128 mm^3; space group = P $na2_1$ (orthorhombic); Z = 4; lattice constants: a = 14.0604(5) Å, b = 10.721(2) Å, c = 27.612(3) Å; V = 4162.1(9) $Å^3$; density: $\rho_{x\text{-}ray}$= 1.345 gcm^{-3}; R1 = 8.78 %.

Synthesis of 4-(N-(2,4-Dimethoxybenzyl)-4-(4-(N-(2,4-dimethoxybenzyl)-4-aminobenzamido)benzamido)benzamido)benzoic acid **9**

A solution of **8** (5 g; 6.06 mmol) in NMP (60 ml) was added to a solution of ammonium formate (3.82 g; 60.6 mmol) in methanol (160 ml). Pd/C (10%; 0.32 g) was added to the reaction mixture under a gentle flow of nitrogen gas while cooling the reaction vessel with an ice-bath. After stirring the reaction for 48 h, 96 h and 118 h more Pd/C (0.5 g) was added to the reaction mixture in the manner described above. 12h after the last addition of Pd/C the reaction mixture was filtered through Celite and the methanol evaporated under reduced pressure. Water was added to the remaining solution. The white precipitate was recovered by filtration and dried under vacuum to give **9** (4.4 g; 90 %).

mp: 197-198 °C

^{1}H-NMR (300 MHz, DMSO-d_6) δ: 3.64 (s, 3 H); 3.66 (s, 3 H); 3.71 (s, 3 H); 3.72 (s, 3H); 4.97 (s, 2 H); 5.01 (s, 2 H); 6.33 (d, *J* = 8.46 Hz, 2 H); 6.45-6.48 (m, 4 H); 7.03 (d, *J* = 8.82 Hz, 2 H); 7.12 – 7.23 (m, 6 H); 7.29 (d, *J* = 8.82 Hz, 2 H); 7.60 (d, *J* = 8.82 Hz, 2 H); 7.70-7.74 (m, 4 H); 10.24 (s, 1 H).

IR ν (cm^{-1}): 3355, 2935, 1596, 1506, 1401, 1284, 1207, 1176, 1031, 835.

RP-HPLC (min.): 22.09

M (ESI-MS): *m/z* (%) = $[M + Na]^+$ 817.30 (100); 818.30 (41.6); 819.30 (3.9). calc.[$C_{46}H_{42}N_4O_9\,Na^+$] = 817.29.

Synthesis of Octamer-(DMB)$_4$ **11**

Thionyl chloride (364 µl; 5.03 mmol) was added to a solution of **8** (4.14 g; 5.02 mmol) in dry NMP (35 ml) according to the general activation method (GAM). The reaction mixture was stirred for 2 h before a solution of **9** (4 g; 5.02 mmol) in dry NMP (35 ml) was added. After further stirring for 94 h at rt the reaction mixture was cooled with an ice-bath and water (600 ml) was added to the mixture. An off-white solid precipitated and was recovered by filtration. The solid was stirred in either isopropanol or methanol at rt for 3 h and then recovered by filtration to give **11** (4.19-4.92 g; 52-61 %).

^{1}H-NMR (300 MHz, DMSO-d_6) δ: 3.64 (s, 12 H); 3.70 – 3.71 (m, 12 H); 5.00 – 5.03 (m, 8 H); 6.43 – 6.47 (m, 8 H); 7.12 – 7.31 (m, 18 H); 7.56 – 7.61 (m, 8 H); 7.68 – 7.74 (m, 8 H); 8.10 (d, *J* = 8.46 Hz, 2 H); 10.21 – 10.23 (m, 3 H); 12. 93 (s, 1 H). ^{13}C-NMR (300 MHz, DMSO-d_6) δ: 47.58; 55.10; 55.28; 55.31; 98.22; 104.59; 116.21; 116.90; 119.09; 119.15; 123.22; 127.13; 127.20; 127.71; 128.01; 128.31; 128.37; 129.26; 129.39; 129.44; 129.47; 129.81; 130.04; 130.77; 130.90; 130.98; 131.89; 132.58; 140.26; 140.37; 140.43; 142.63; 146.45; 147.45; 147.54; 157.82; 157.85; 158.01; 159;80; 159.83; 160.01; 164.68; 164.86; 166.64; 167.84; 169.20; 169.28.

IR ν (cm^{-1}): 3303, 2940, 1637, 1598, 1504, 1403, 1263, 1207, 1157, 1118, 1031, 835, 759.

RP-HPLC (min.): 32.04.

M (MALDI-TOF): *m/z* = 1640 $[M + K]^+$. calc.[$C_{92}H_{80}N_8O_{19}K^+$] = 1640.

GPC (DMF + 1 g/L LiBr): M_n = 510, M_w = 540 g/mol; PDI = 1.04.

Synthesis of alkyne functionalized octamer-(DMB)$_4$ **13**

Thionyl chloride (0.97 ml; 13.4 mmol) was added to a solution of **11** (3.07 g; 1.91 mmol) in dry NMP (50 ml). Propargylamine (0.58 ml; 10.7 mmol) was added to the reaction mixture after stirring for 10 min. at rt. After that the reaction mixture was stirred at rt for further 36 h. Addition of cold water (500 ml) resulted in the precipitation of a brown resin-like compound which was stirred under cooling for further 3h resulting in a brown solid which was dried under vacuum at 40 °C (3 g; 1.83 mmol; 95 %).

^{1}H-NMR (300 MHz, DMSO-d_6) δ: 3.07 (t, 1 H); 3.64 (s, 12 H); 3.70 – 3.71 (m, 12 H), 3.97 – 3.99 (m, 2 H); 5.01 – 5.03 (m, 8 H); 6.43 – 6.48 (m, 8 H); 7.11 – 7.32 (m, 18 H); 7.59 – 7.76 (m, 16 H); 8.10 (d, *J* = 8,46 Hz, 2 H); 8.91 (t, 1 H); 10.30 – 10.32 (m, 3 H).

IR ν (cm^{-1}): 3293, 2927, 1643, 1598, 1502, 1403, 1286, 1207, 1155, 1110, 1029, 829, 759.

RP-HPLC (Min.): 32.25

M (MALDI-TOF): *m/z* = 1645 $[M + Li]^+$. calc.[$C_{95}H_{83}N_9O_{18}Li^+$] = 1645.

GPC (DMF + 1g/L LiBr): M_n = 1500, M_w = 1550 g/mol; PDI = 1.04.

Synthesis of octamer-(DMB)$_4$ block copolymer, **14**

A solution of **13** (2.9 g; 1.8 mmol) in NMP (20 ml) was added to a solution of PEG-N_3 ($M_{n\ PEG}$ = 2000 g/mol; 1.67 g; 0.82 mmol) in NMP (10 ml). This was followed by the

addition of solid CuI (60 mg, 0.31 mmol) and DBU (4.5 ml, 30 mmol). After stirring the reaction mixture at rt for 2 days, diethyl ether (300 ml) was added upon which a brown oil separated from the ether phase. The crude product was dried under vacuum to yield 2.5 g of a mixture of **14** and **13**. The crude product mixture (1.2 g) was dissolved in tetrahydrofuran and purified by column chromatography. Eluting with THF, the excess of **13** could be removed. Elution with DMF gave the block copolymer **14** (500 mg).

^{1}H-NMR (400 MHz, DMSO-d_6) δ: 3.23 (s, 3 H); 3.35 (s, 162 H); 3.63 – 3.66 (m, 12 H); 3.69 – 3.71 (m, 12 H); 3.75 (t, 2 H); 3.41 – 3.44 (m, 4 H); 4.98 – 5.01 (m, 8 H); 6.43 - 6.47 (m, 8 H); 7.11 – 7. 30 (m, 18 H); 7.55 – 7.59 (m, 16 H); 7.87 (s, 1 H); 8.09 (d, *J* = 8.51 Hz, 2 H); 8.91 (t, 1 H); 10.17 – 10.20 (m, 3 H).
RP-HPLC (min.): 28.14
M (MALDI-TOF): *m/z* = 3508 $[M + Li]^+$; repeat unit 44. calc.$[C_{98}H_{90}N_{12}O_{19}(C_2H_4O)_{40}\ Li^+]$ = 3508.
GPC (TCM): M_n = 6000, M_w = 6600 g/mol; PDI = 1.08.

Synthesis of octamer-PEG block copolymer **15**
14 (500 mg; 0.13 mmol) was dissolved in a mixture of TFA (12 ml), chloroform (5ml) and anisole (4ml) and stirred at rt for 15h. After that, the volatiles were removed under reduced pressure. The crude product was dried under vacuum, dissolved in tetrahydrofuran and purified by column chromatography. With THF the cleaved off protective groups could be removed. Elution with DMF gave the block copolymer **15**. Several product containing fractions were collected, the purest one contained 40 mg of **15**.

^{1}H-NMR (400 MHz, DMSO-d_6) δ: 3.5 (s, 180 H), 4.49 (t, 2H), 6.5 – 8.5 (m, 5 H); 9 (s, NH), 10.45 – 11 (m, NH).
^{1}H-NMR (400 MHz, D_2SO_4) δ: 3.57 (s, 180 H), 4.35 (s, N-C$\underline{H_2}$-CH_2-O-), 6.8-8.1 (m, 20 H), 16-18 (m, NH).

2.1.5. References

[1] (a) Schwab, P.F.H.; Levin, M.D.; Michl, J. *Chem. Rev.* **1999**, *99*, 1863-1933; (b) Schwab, P.F.H.; Smith, J.R.; Michl. J. *Chem. Rev.* **2005**, *105*, 1197-1280.

[2] see for example (a) Vernino, D.; Tirrell, D.; Tirrell, M. *Polym. Mater. Sci. Eng*. **1994**, *71*, 496 – 497; (b) Chen, J.T.; Thomas, E.L.; Ober, C.K.; Mao, G.-P. *Science* **1996**, *273*, 343 –346.

[3] (a) Nelson, J.C.; Young, J.K.; Moore, J.S. *J. Org. Chem.* **1996**, *61,* 8160-8168.; (b) Young, J.K.; Nelson, J.C.; Moore, J.S. *J. Am. Chem. Soc*. **1994**, *116*, 10841-10842; (c) Huang, S.; Tour, J.M. *J. Org. Chem.* **1999**, *64*, 8898-8906; (d) Huang, S.; Tour, J.M. *J. Am. Chem. Soc*. **1999**, *121*, 4908-4909; (e) Jones, L.; Schumm, J.S.; Tour, J.M. *J. Org. Chem.* **1997**, *62*, 1388-1410.

[4] Lee, M.; Cho, B.-K.; Zin, W.-C. *Chem. Rev.* **2001**, *101*, 3869-3892.

[5] Klok, H.-A.; Lecommandoux, S. *Adv. Mater.* **2001**, *13*, 1217-1229.

[6] Abbel, R.; Schleuss, T.W.; Frey, H.; Kilbinger, A.F.M. *Macromol. Chem. Phys.* **2005**, *206*, 2067-2074.

[7] Schleuss, T.W:; Abbel, R.; Gross, M.; Schollmeyer, D.; Frey, H.; Maskos, M.; Berger, R.; Kilbinger, A.F.M. *Angew. Chem. Int. Ed.* **2006**, *45*, 2969-2975.

[8] Bredereck, H.; von Schuh, H. *Chem. Ber*. **1948**, *81*, 215-221.

[9] Abbel, R.; Frey, H.; Schollmeyer, D.; Kilbinger, A.F.M. *Chem. Eur. J.* **2005**, *11*, 2170-2176.

[10] König, H.M.; Abbel, R.; Schollmeyer, D.; Kilbinger, A.F.M. *Org. Lett.* **2006**, *8*, 1819-1822.

[11] König, H.M.; Gorelik, T.; Kolb, U.; Kilbinger, A.F.M. *J. Am. Chem. Soc.* **2007**, *129*, 704.

[12] Bosshard, H.H.; Mory, R.; Schmid, M.; Zollinger, H. *Helv. Chim. Acta* **1959**, *176*, 1653-1658.

[13] Washio, I.; Shibasaki, Y.; Ueda, M. *Org. Lett.* **2003**, *5*, 4159-4161.

[14] **Crystal data**. $C_{46}H_{42}N_4O_{12}$, M = 842.84, orthorhombic, *a* = 14.0604(5), *b* = 10.7206(19), *c* = 27.612(3) Å, U = 4162.1(9) $Å^3$, T = 193 K, space group Pna21, Z = 4, F(000) = 1768, μ(Cu-Kα) = 0.817 mm^{-1}, 7534 reflections measured, 7379 unique (R_{int} = 0.0679) which were used in all calculations. The final *wR(F2)* was 0.2513 (all data).

[15] (a) Tanatani, A.; Yokoyama, A.; Azumaya, I.; Takakura, Y.; Mitsui, C.; Shiro, M.; Uchiyama, M.; Muranaka, A.; Kobayashi, N.; Yokozawa, T. *J. Am. Chem. Soc.* **2005**,

127, 8553-8561; (b) Itai, A.; Toriumi, Y.; Saito, S.; Kagechika, H.; Shudo, K. *J. Am. Chem. Soc.* **1992**, *114*, 10649-10650; (c) Masu, H.; Sakai, M.; Kishikawa, K.; Yamamoto, M.; Yamaguchi, K.; Kohmoto, S. *J. Org. Chem*. **2005**, *70*, 1423-1431; (d) Nishimura, T.; Maeda, K.; Yashima, E. *Chirality*, **2004**, *16*, 12-22; (e) Tanatani, A.; Kagechika, H.; Azumaya, I.; Fukutomi, R.; Ito, Y.; Yamaguchi, K.; Shudo, K. *Tet. Lett*. **1997**, *38*, 4425-4428; (f) Azumaya, I.; Kagechika, H.; Yamaguchi, K.; Shudo, K. *Tetrahedron*, **1995**, *51*, 5277-5290; (g) Forbes, C.C.; Beatty, A.M.; Smith, B.D. *Org. Lett.* **2001**, *3*, 3595-3598.

[16] Opsteen, J.A.; van Hest, J.C.M. *Chem. Commun*. **2005**, 57-59.

[17] Rostovtsev, V.V.; Green, L.G.; Fokin, V.V.; Sharpless, K.B. *Angew. Chem. Int. Ed.* **2002**, *41*, 2596-2599.

[18] Cavalleri, P.; Ciferri, A.; Dell'Erba, C.; Gabellino, A.; Novi, M. *Macromol. Rapid. Commun.* **1998**, *199*, 2097-2094.

2.1.6. Supporting Information for "Rod-Coil Copolymers from Oligo(*p*-benzamide) Foldamers"

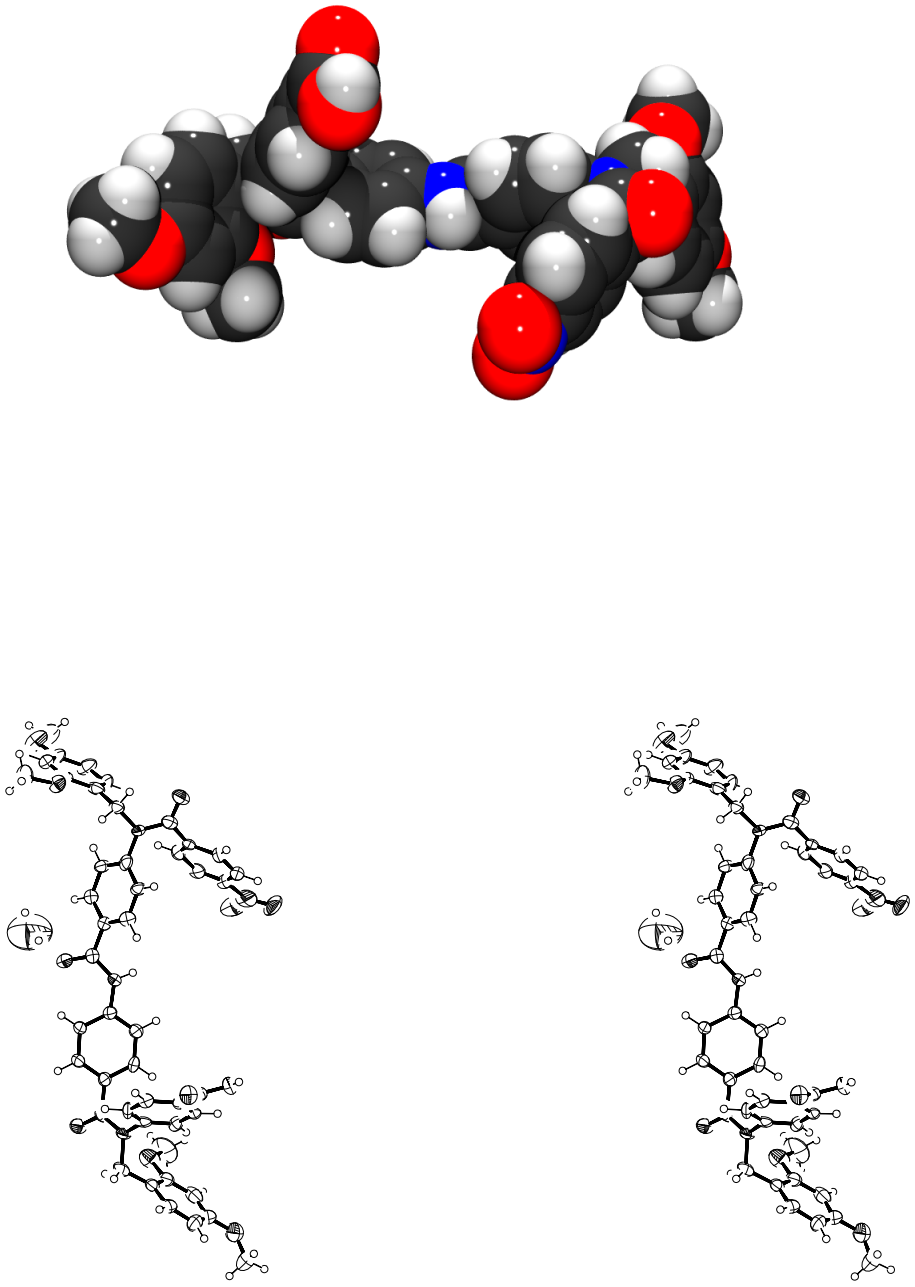

Figure SI-2.1.1. X-ray single crystal structure of **8**. *Top*: CPK model, *bottom*: shown as a stereo image with displacement ellipsoids drawn at the 50 % probability level. The bottom phenyl ring of the tetramer points towards, the top phenyl ring away from the viewer.

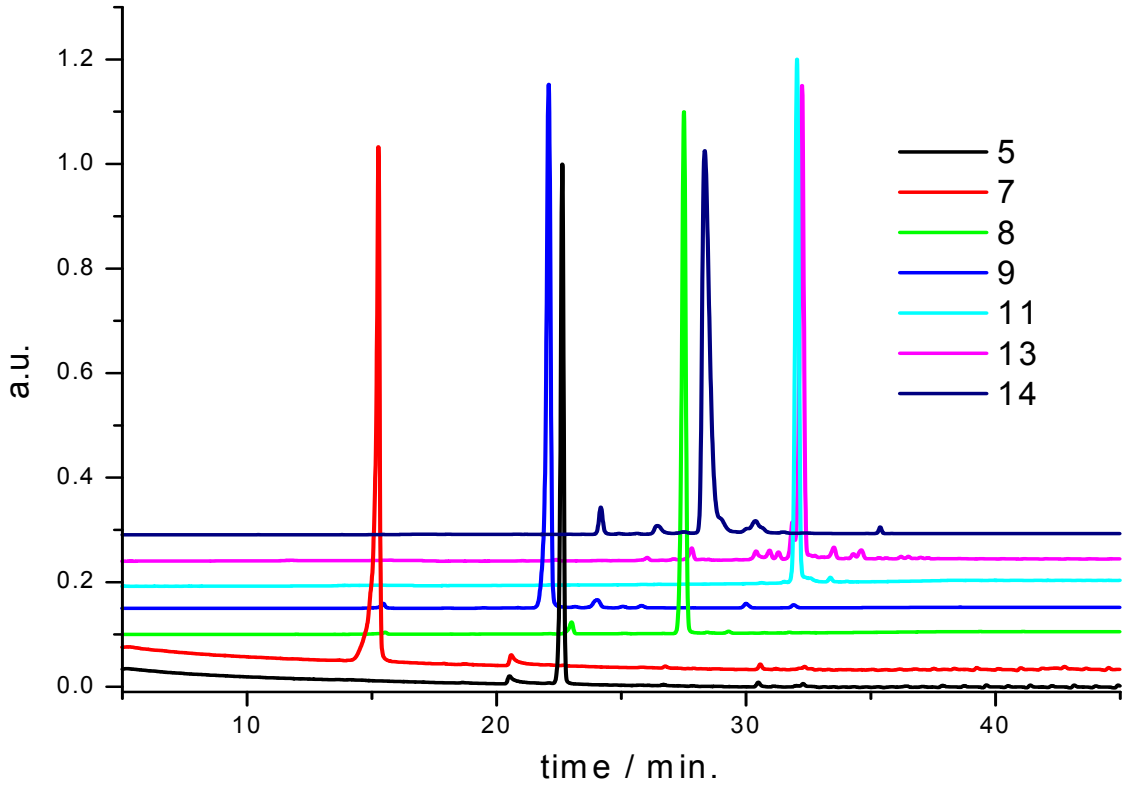

Figure SI-2.1.2. RP-HPLC traces of compounds **5**,**7**,**8**,**9**,**11**,**13** and **14**.

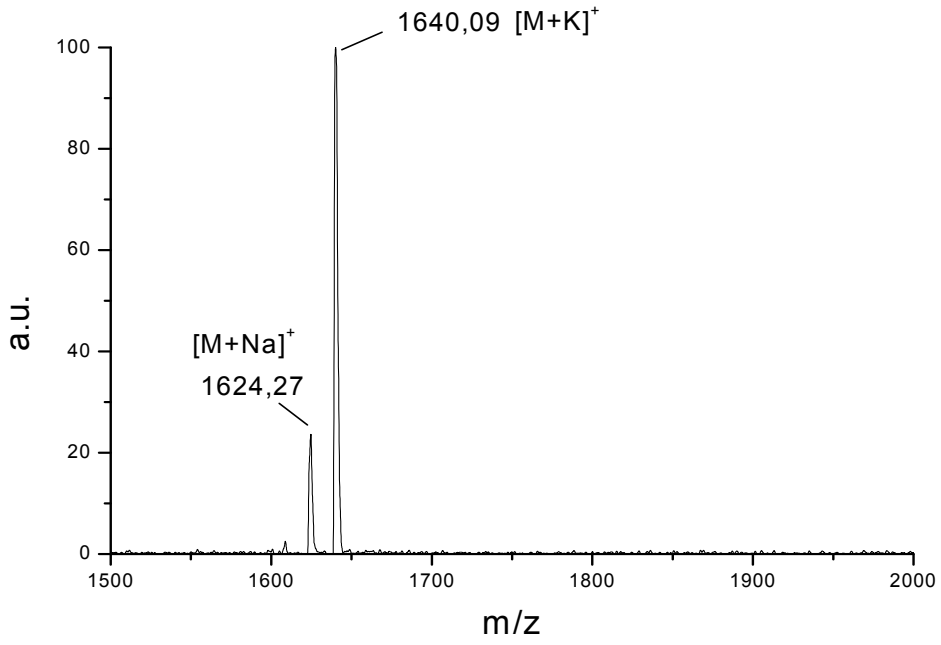

Figure SI-2.1.3. MALDI-TOF mass spectrum of **11**.

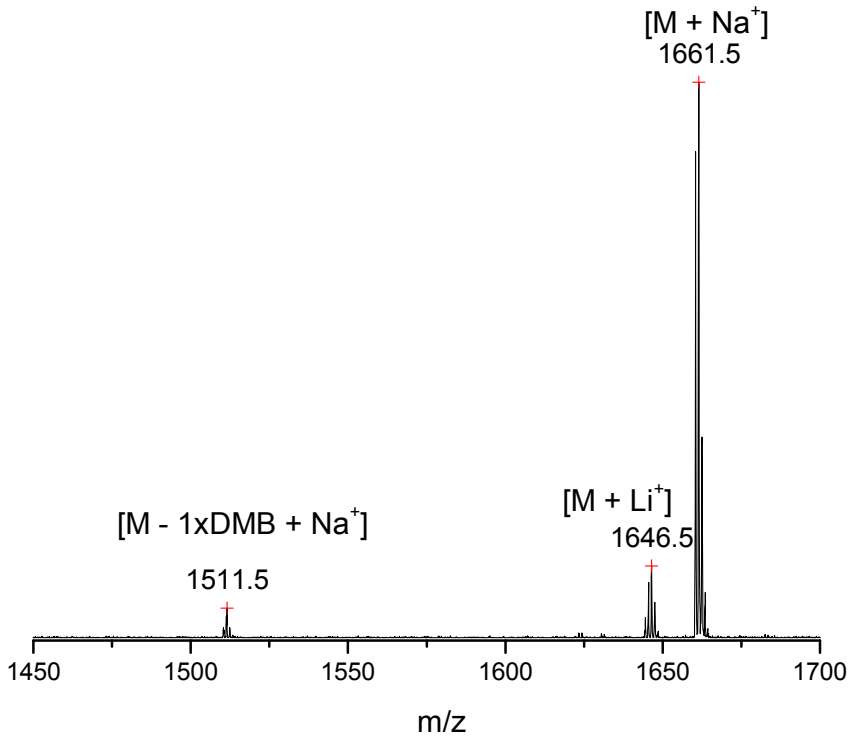

Figure SI-2.1.4. MALDI-TOF mass spectrum of **13**.

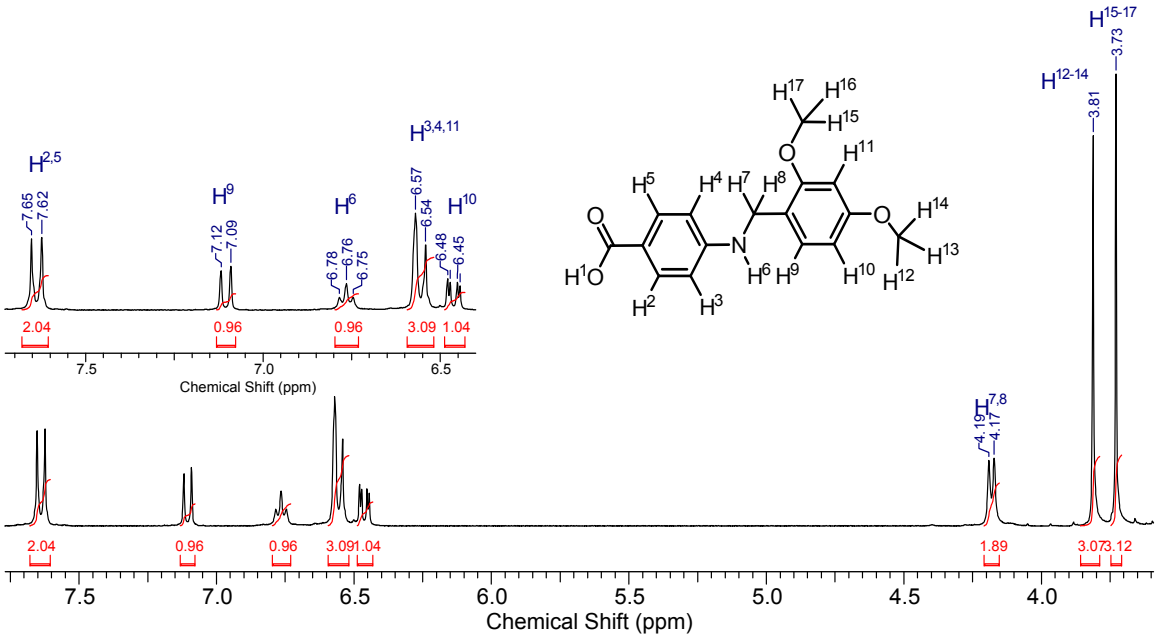

Figure SI-2.1.5. ^{1}H-NMR spectrum (DMSO-d_6) of **4**.

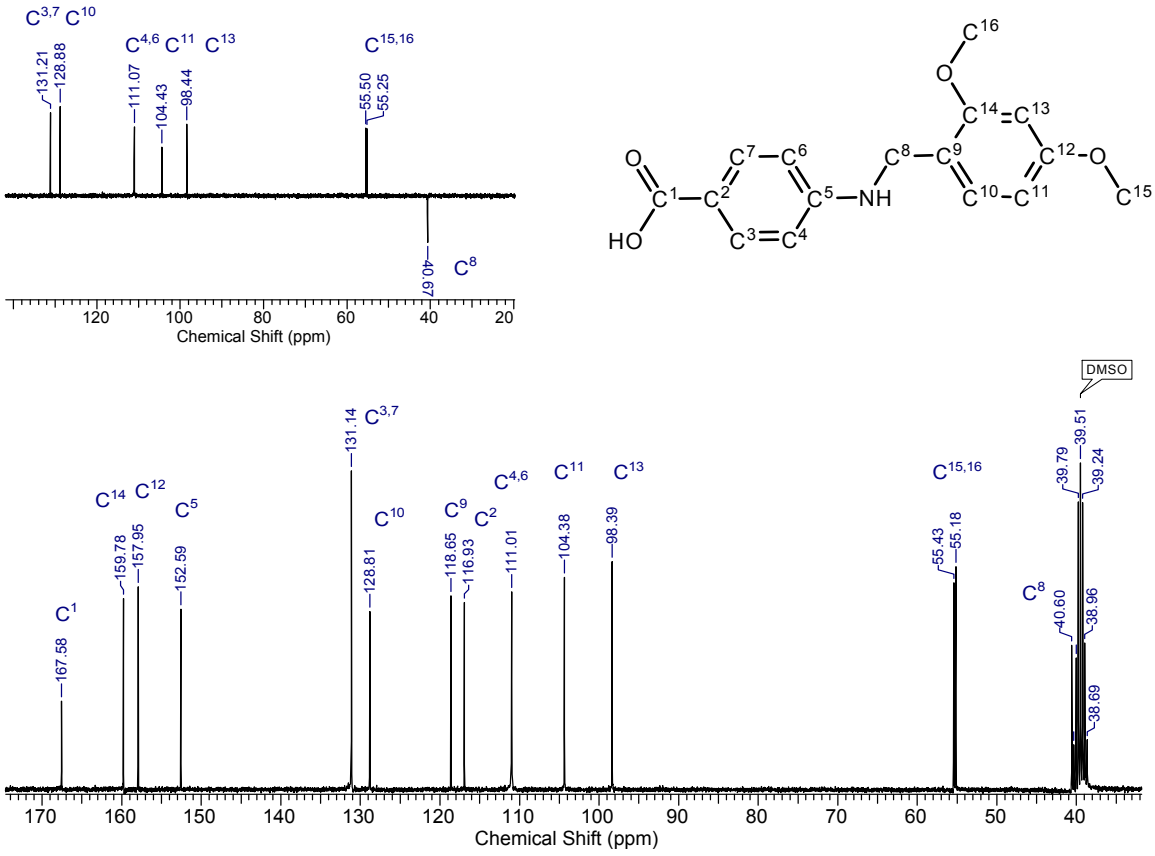

Figure SI-2.1.6. ^{13}C-NMR spectrum (DMSO-d_6) of **4**.

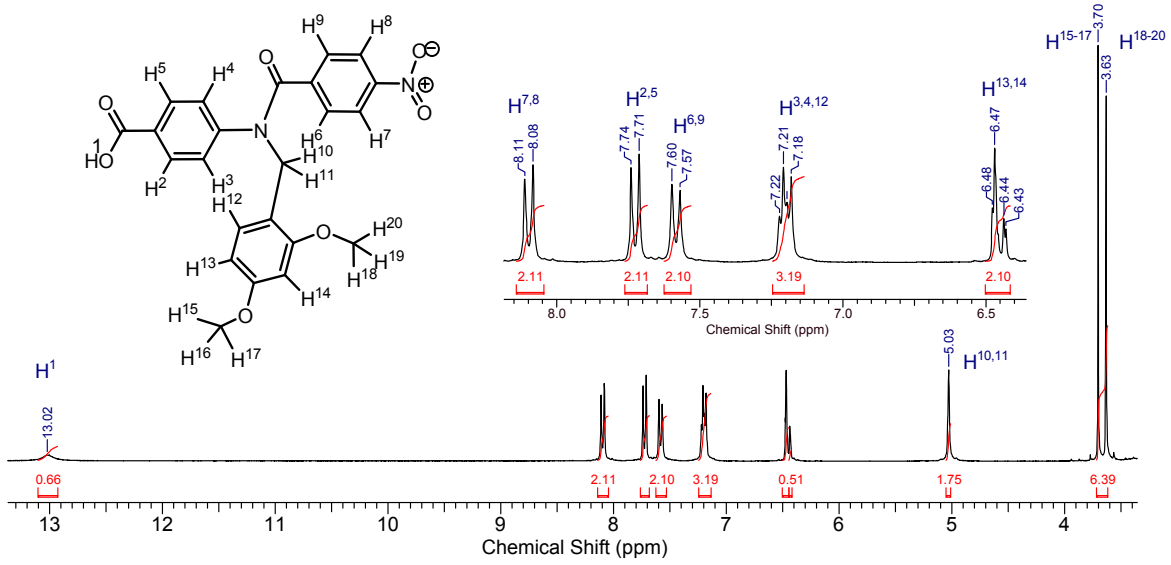

Figure SI-2.1.7. ^{1}H-NMR spectrum (DMSO-d_6) of **5**.

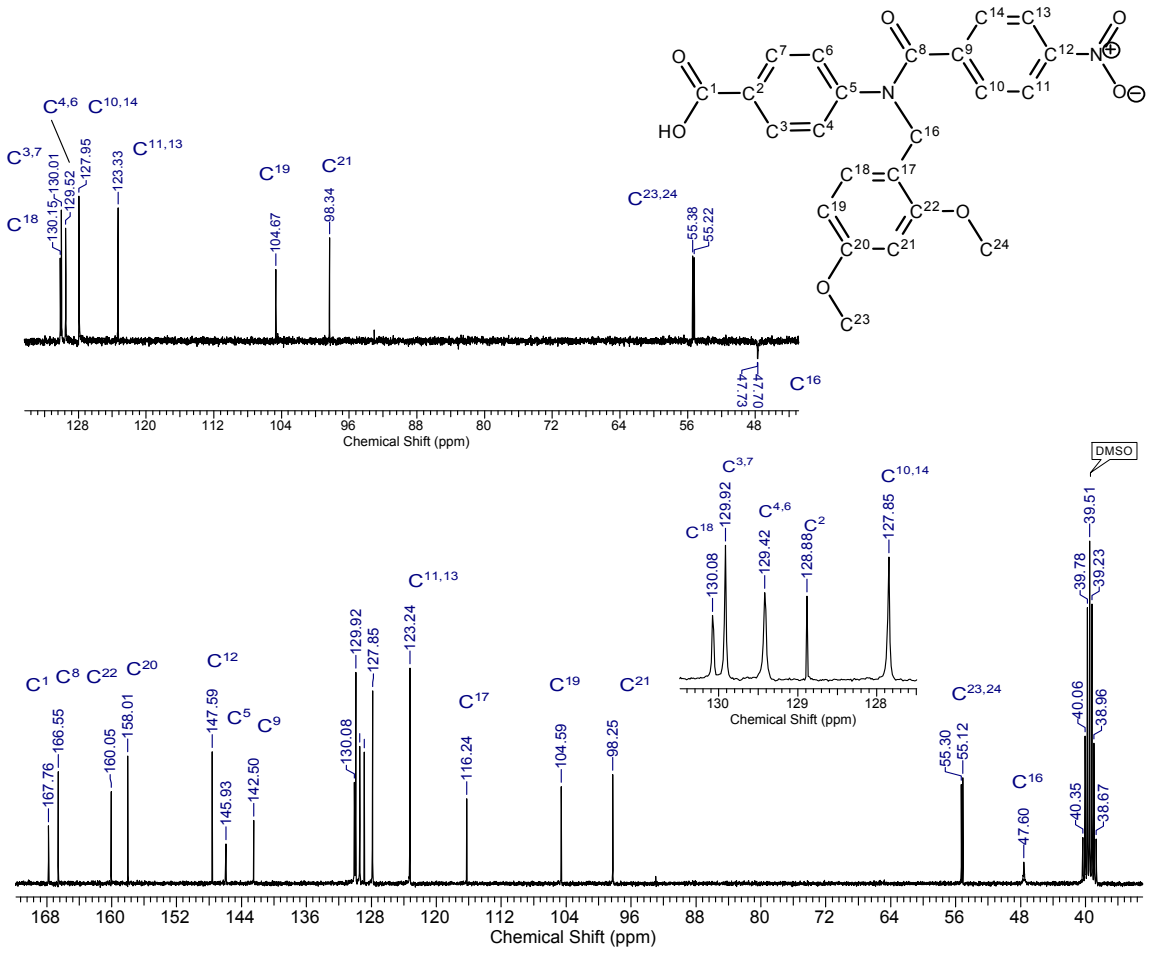

Figure SI-2.1.8. ^{13}C-NMR spectrum (DMSO-d_6) of **5**.

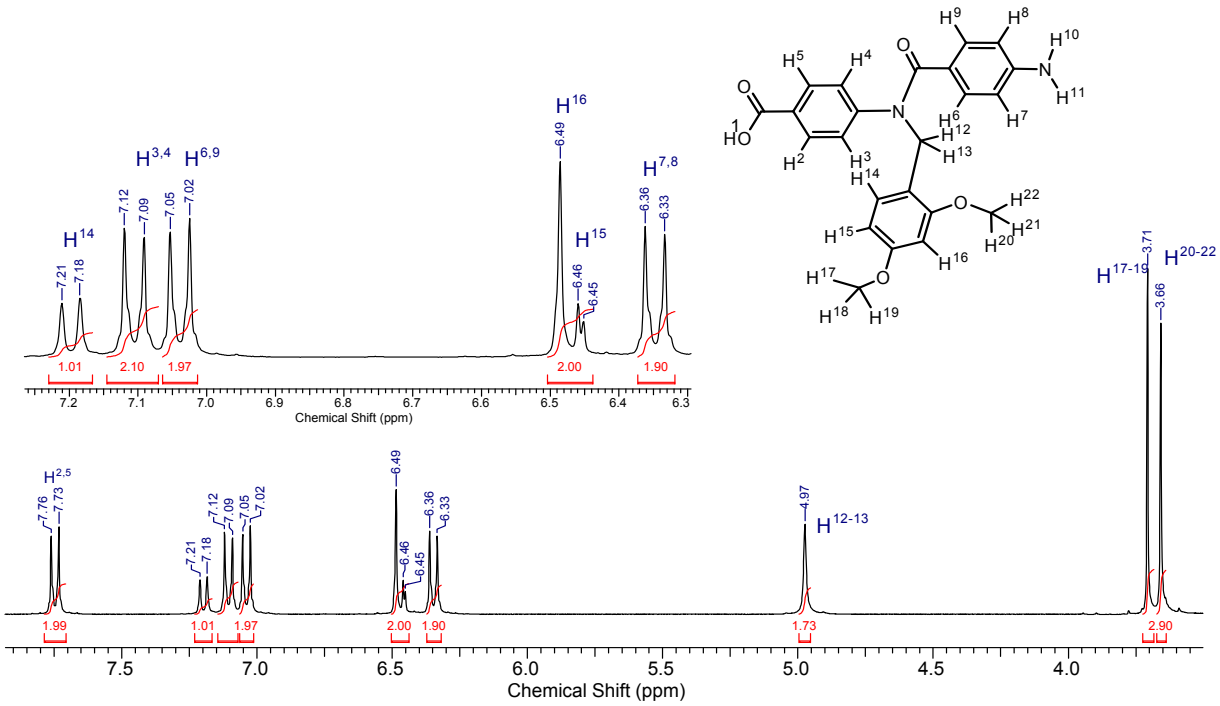

Figure SI-2.1.9. ^{1}H-NMR spectrum (DMSO-d_6) of **7**.

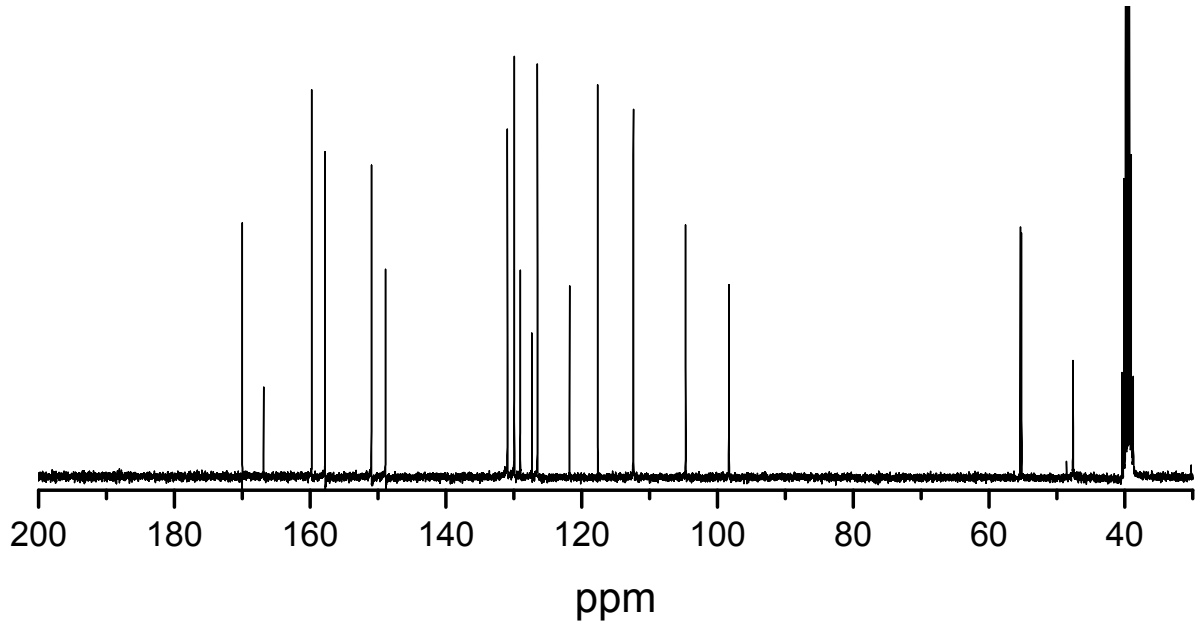

Figure SI-2.1.10. ^{13}C-NMR spectrum (DMSO-d_6) of **7**.

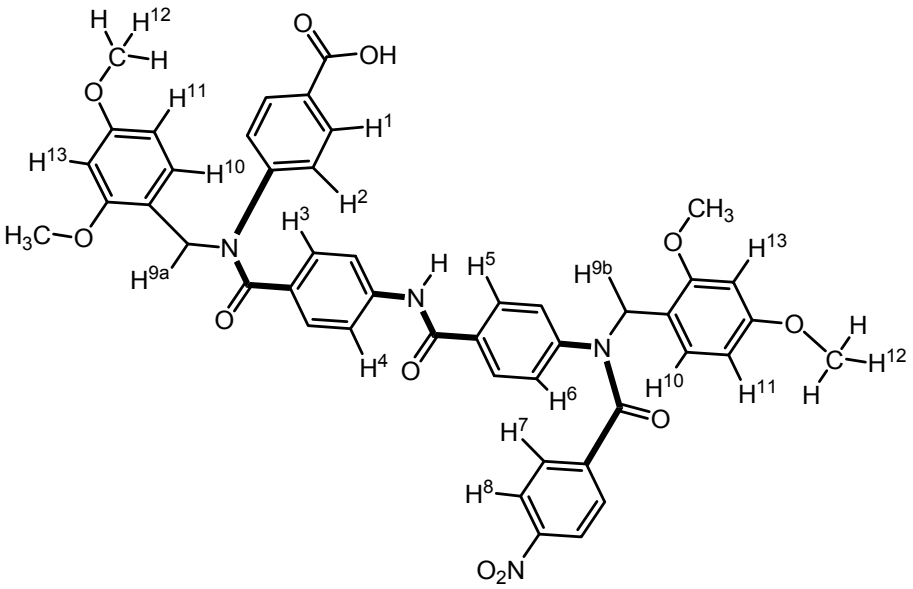

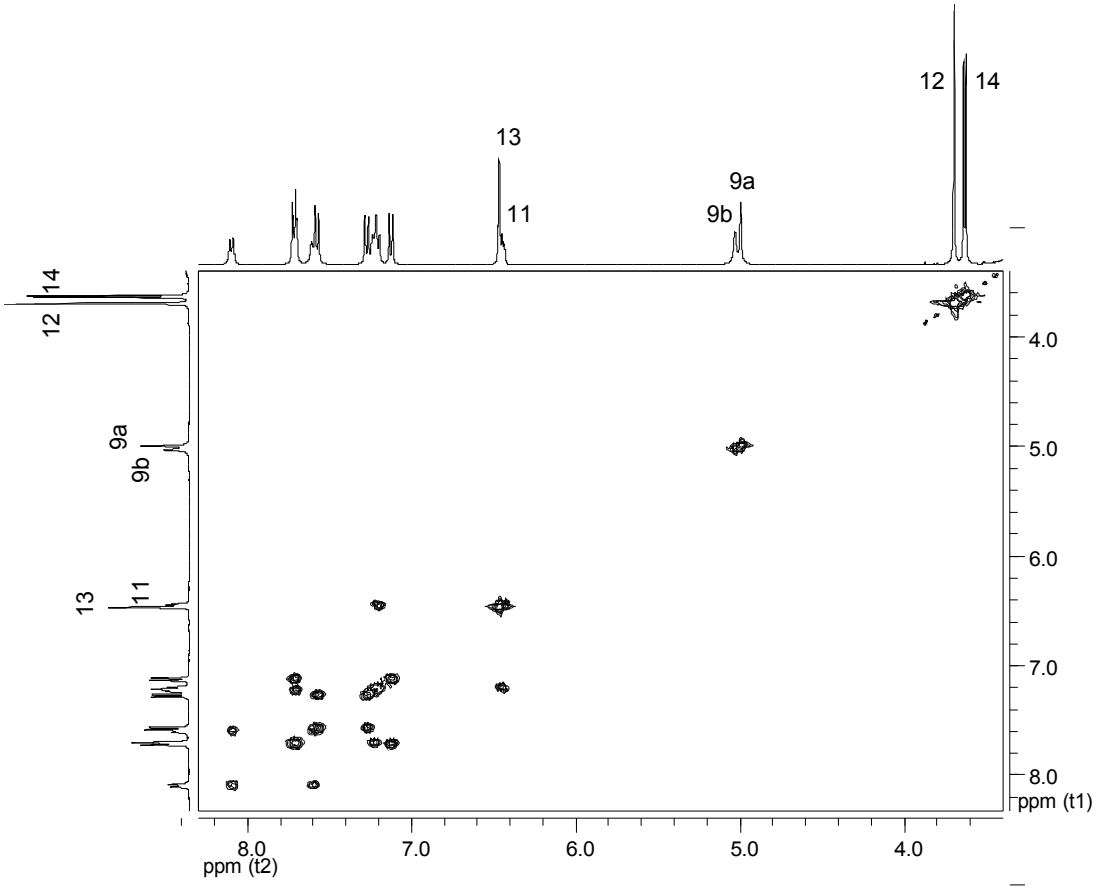

Figure SI-2.1.11. ^{1}H-COSY (DMSO-d_6) of **8** (full spectrum).

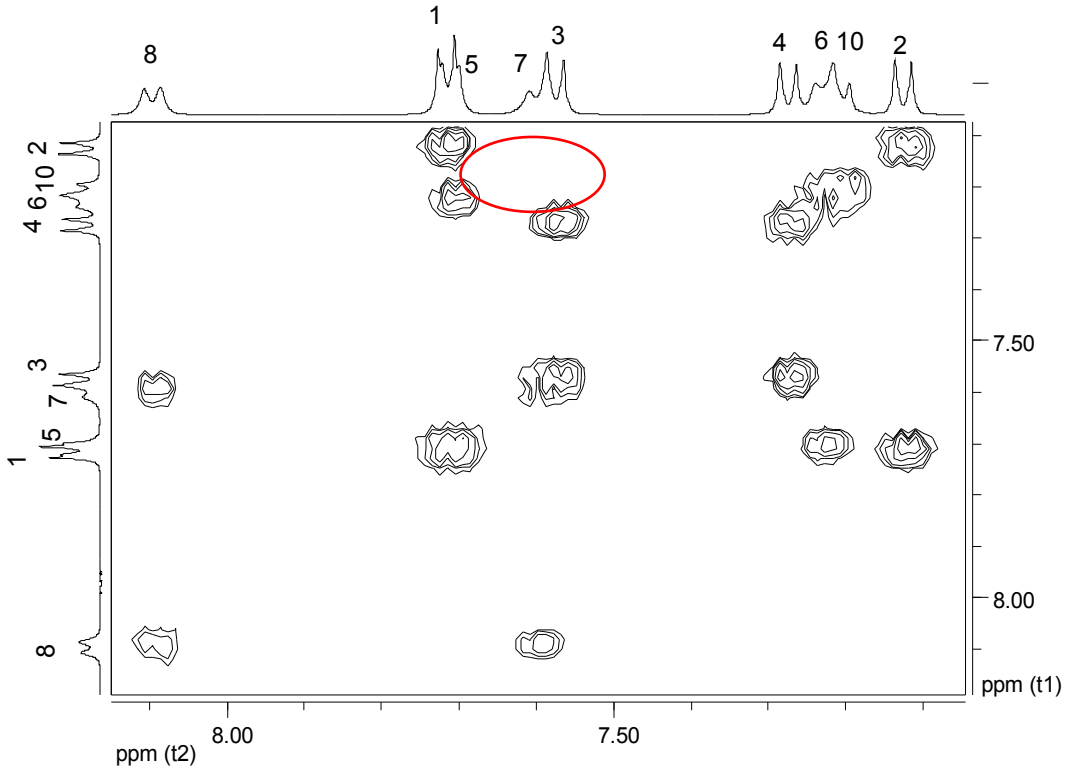

Figure SI-2.1.12. ^{1}H-COSY spectrum (DMSO-d_6) of **8** (aromatic region). (Protons H2 and H3 do not show a cross-peak, see NOESY spectrum **fig. SI-2.1.14**)

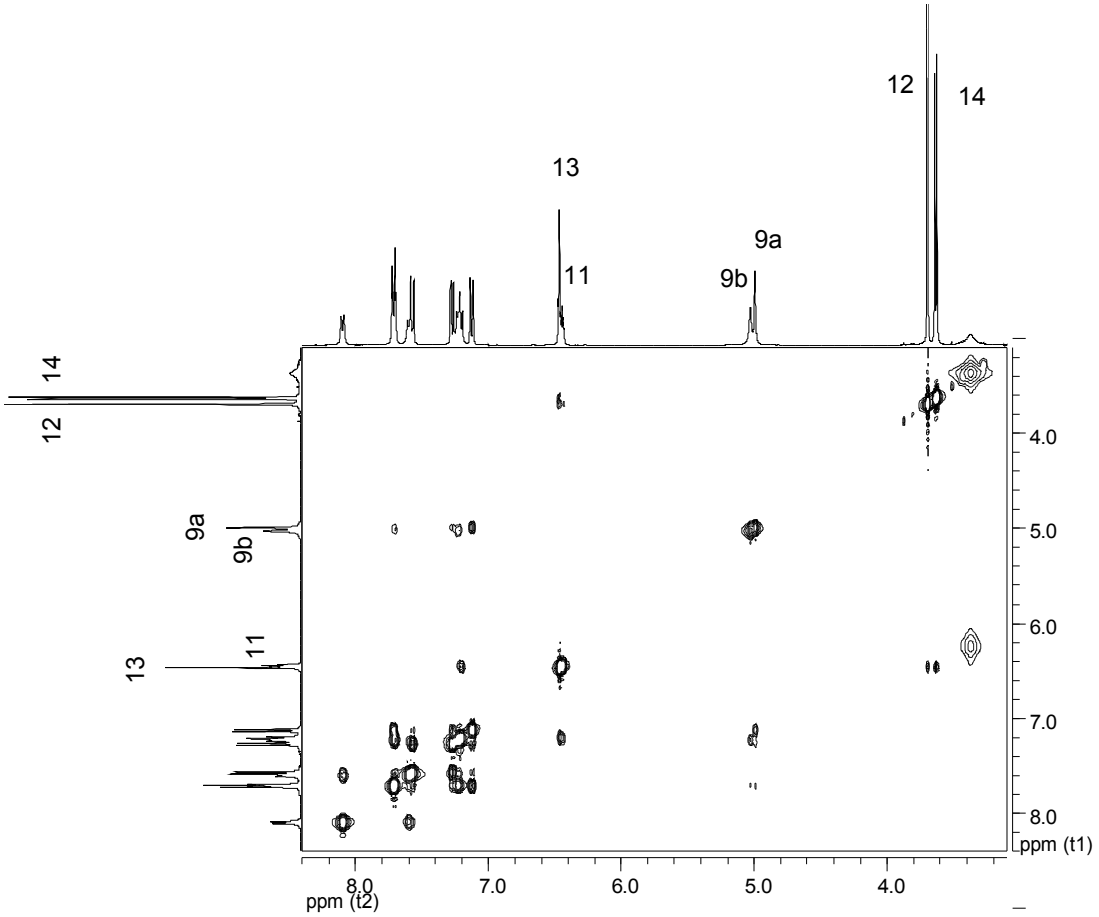

Figure SI-2.1.13. ^{1}H-NOESY spectrum (DMSO-d_6) of **8** (full spectrum).

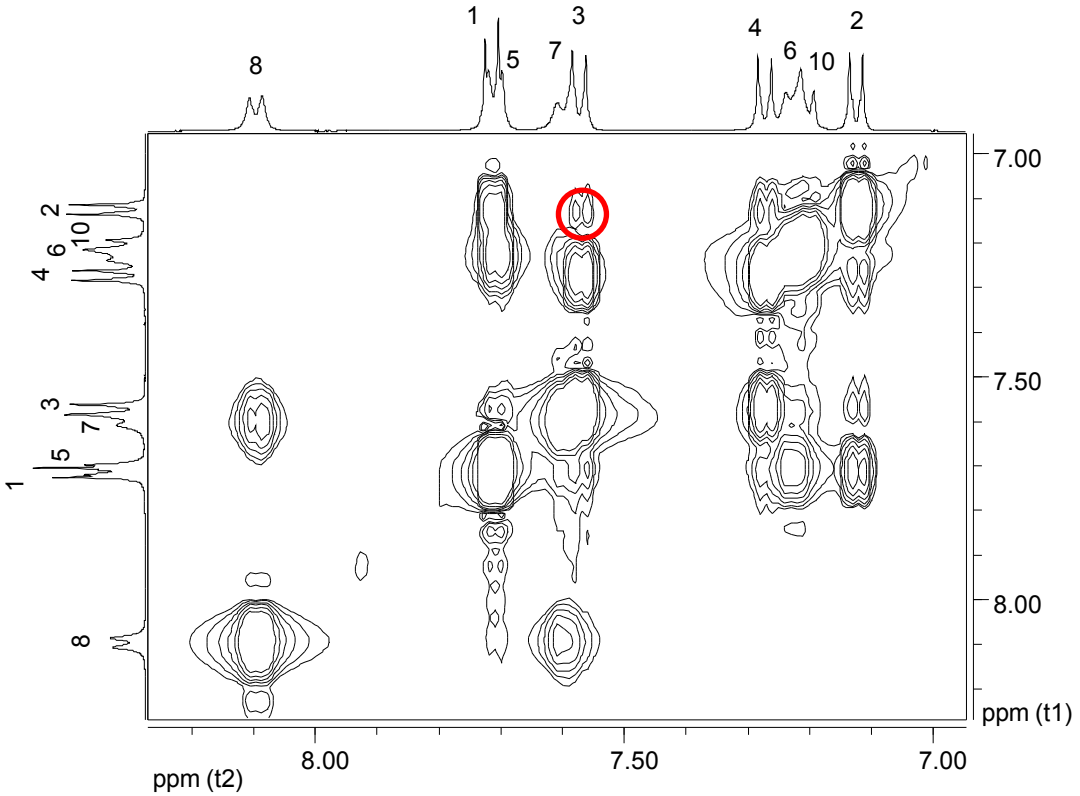

Figure SI-2.1.14. ^{1}H-NOESY spectrum (DMSO-d_6) of **8** (aromatic region). The cross-peak between protons H2 and H3 is circled in red.

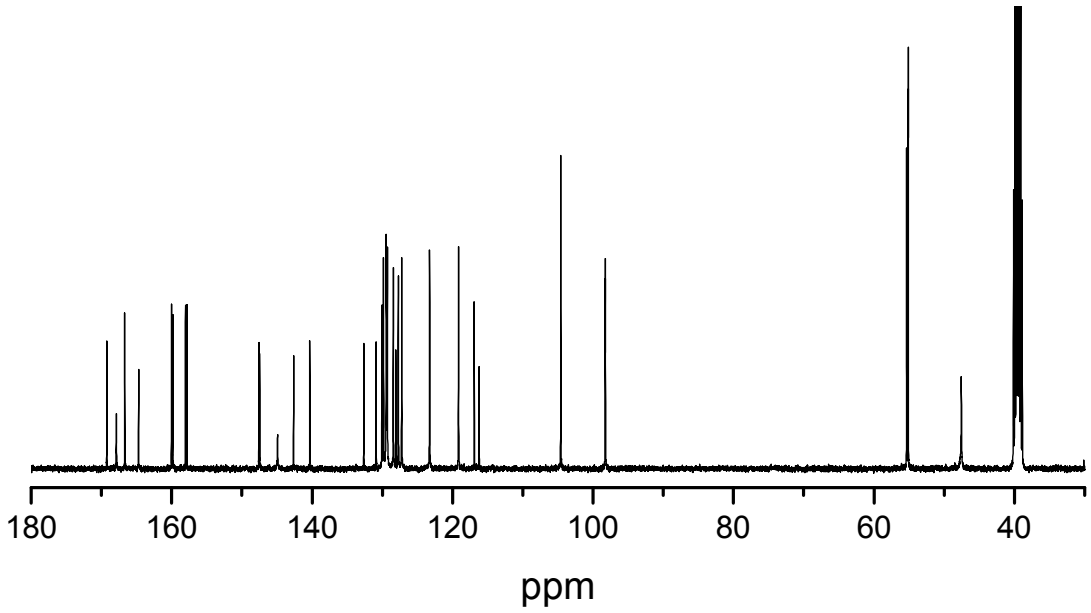

Figure SI-2.1.15. ^{13}C-NMR spectrum (DMSO-d_6) of **8**.

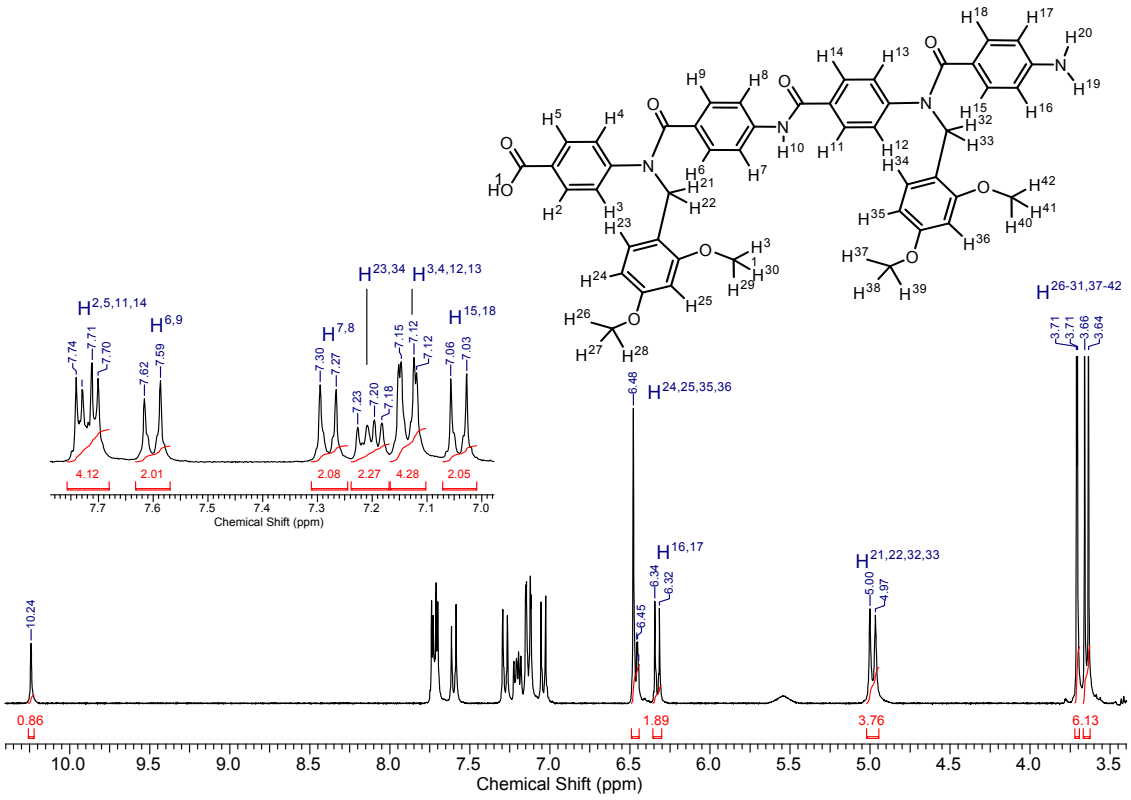

Figure SI-2.1.16. ^{1}H-NMR spectrum (DMSO-d_6) of **9**.

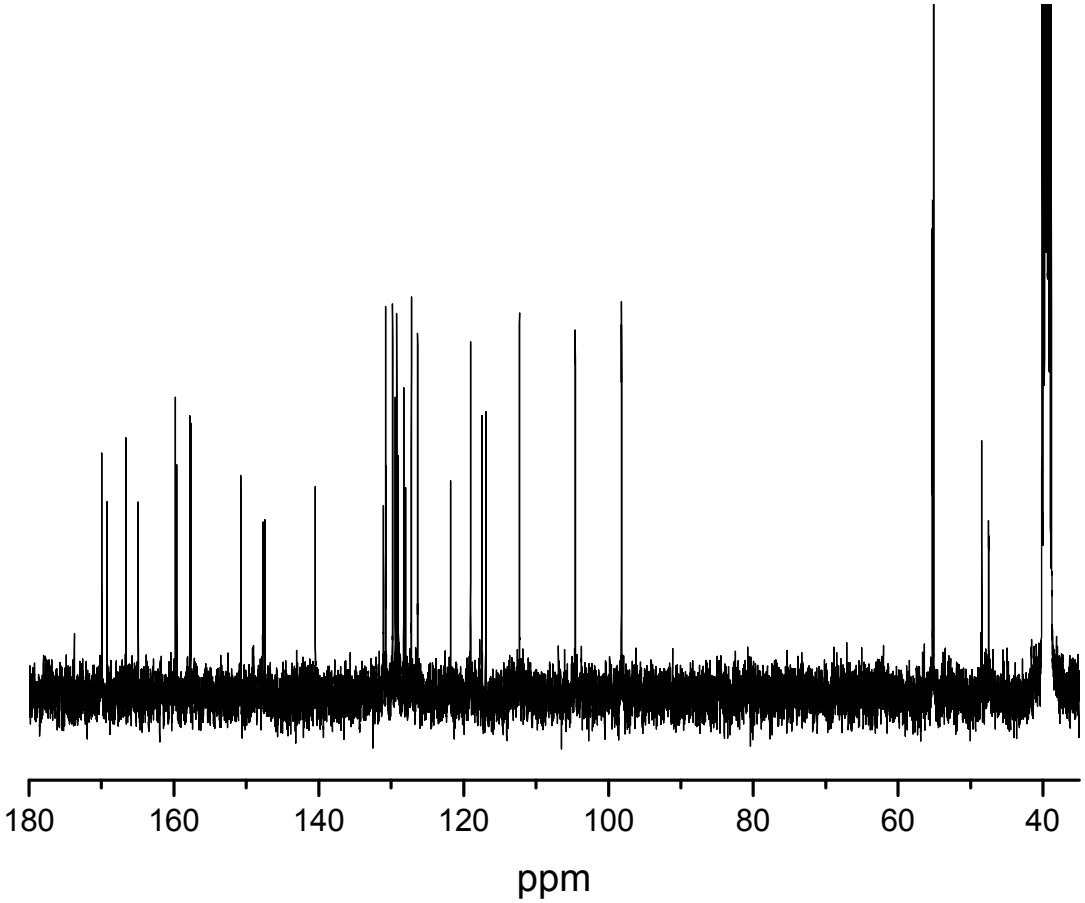

Figure SI-2.1.17. ^{13}C-NMR spectrum (DMSO-d_6) of **9**.

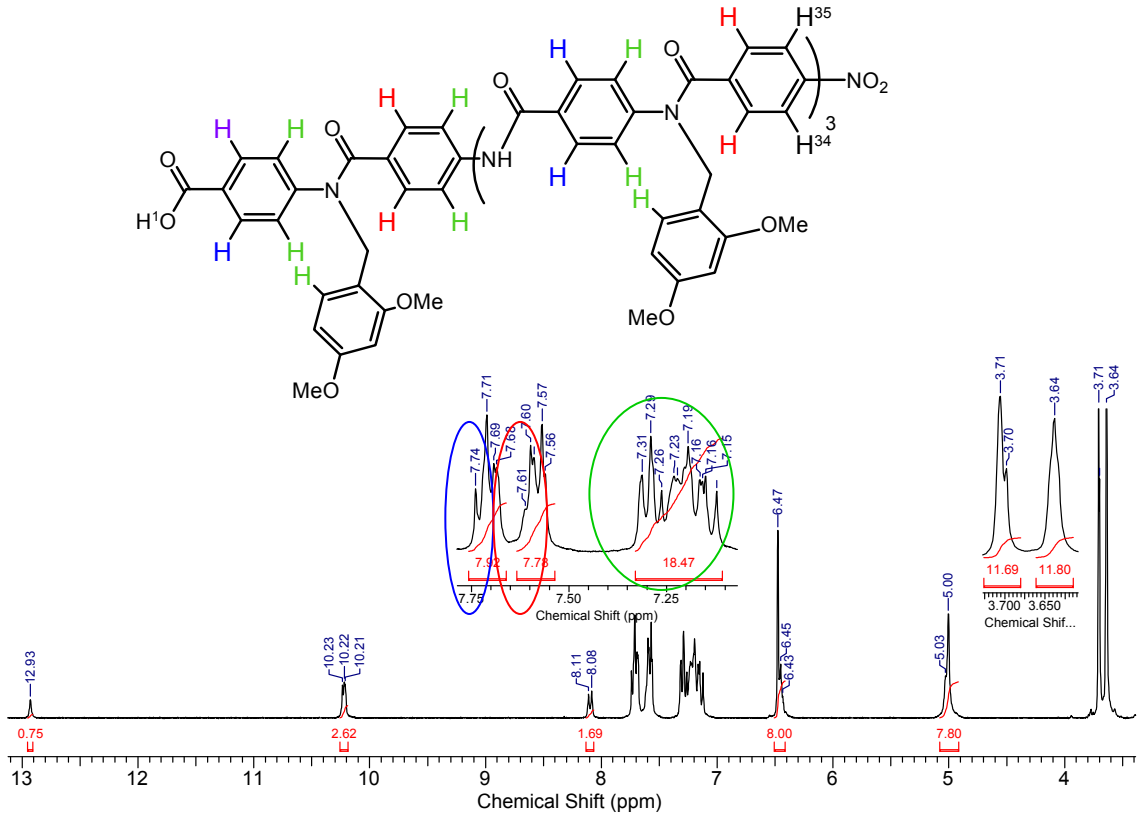

Figure SI-2.1.18. ^{1}H-NMR spectrum (DMSO-d_6) of **11**.

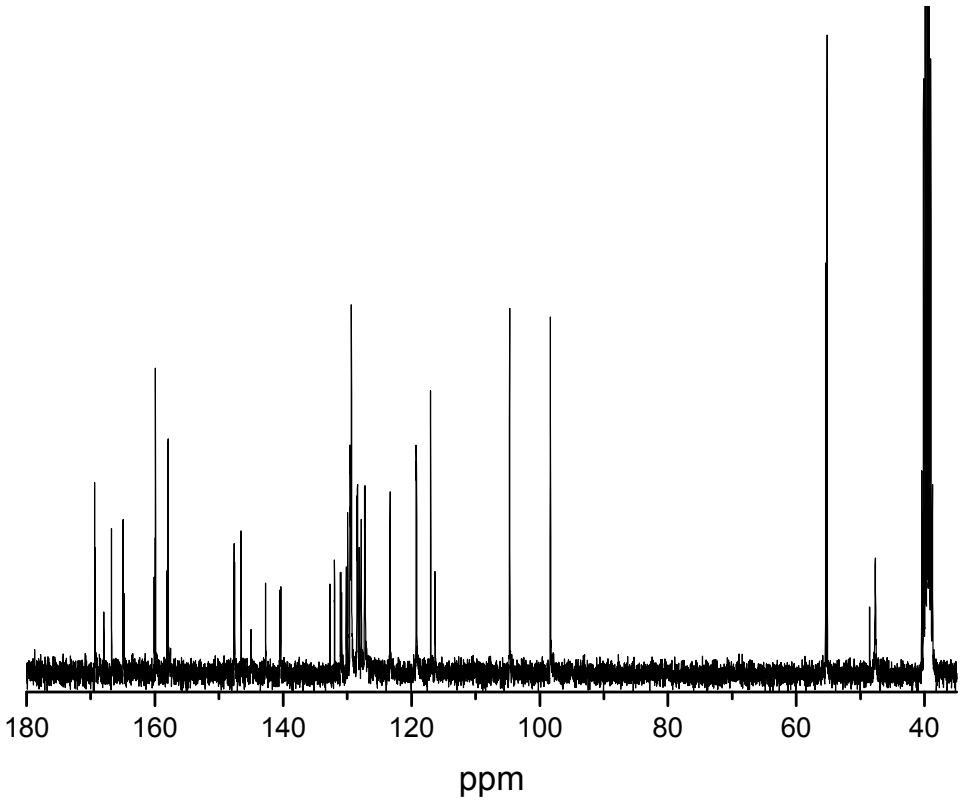

Figure SI-2.1.19. ^{13}C-NMR spectrum (DMSO-d_6) of **11**.

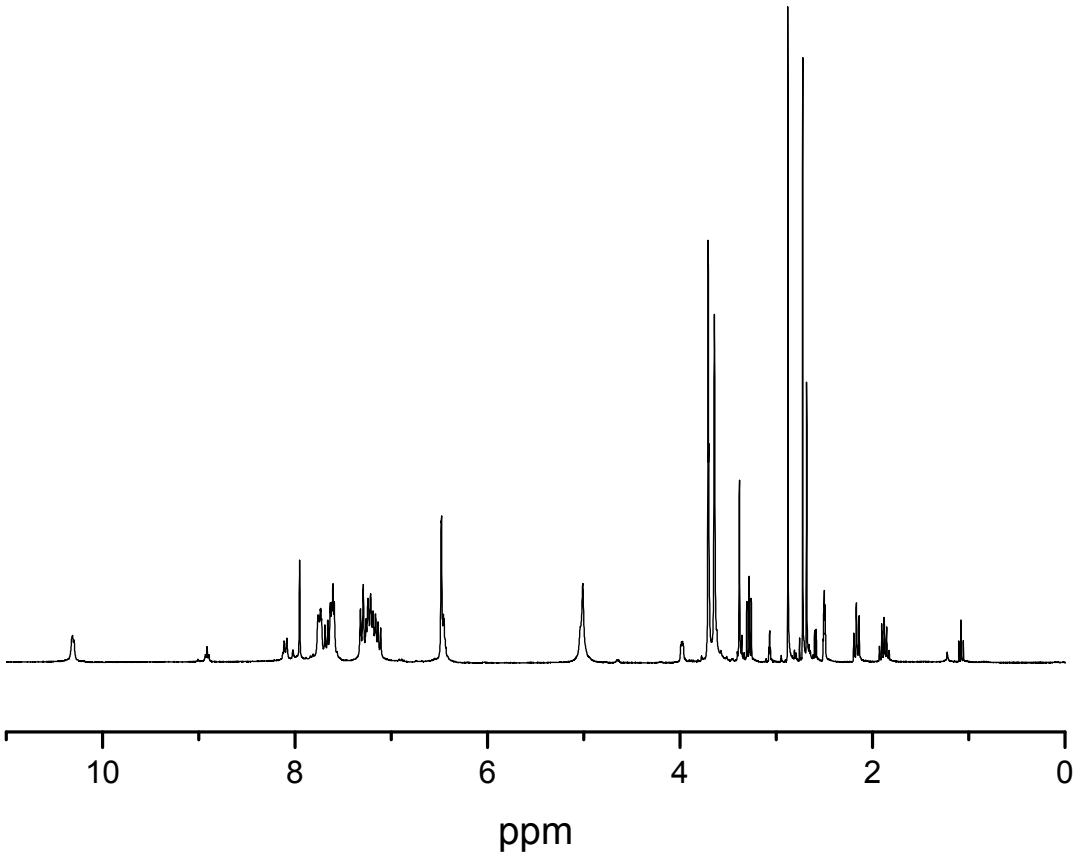

Figure SI-2.1.20. ^{1}H-NMR spectrum (DMSO-d_6) of **13**.

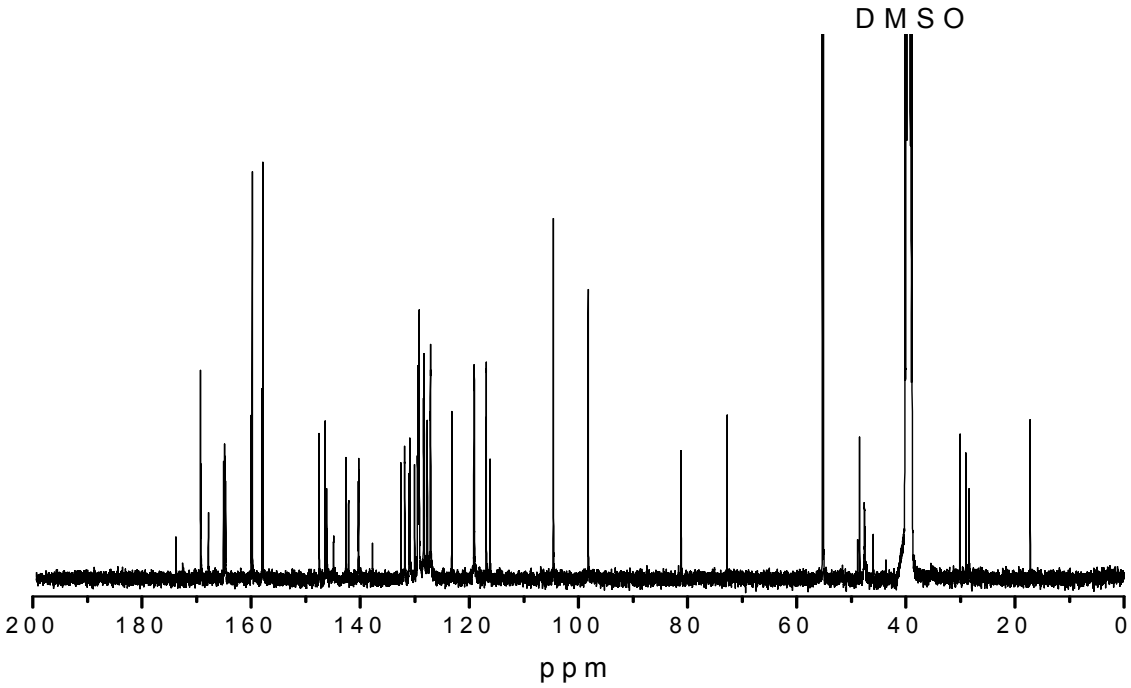

Figure SI-2.1.21. ^{13}C-NMR spectrum (DMSO-d_6) of **13**.

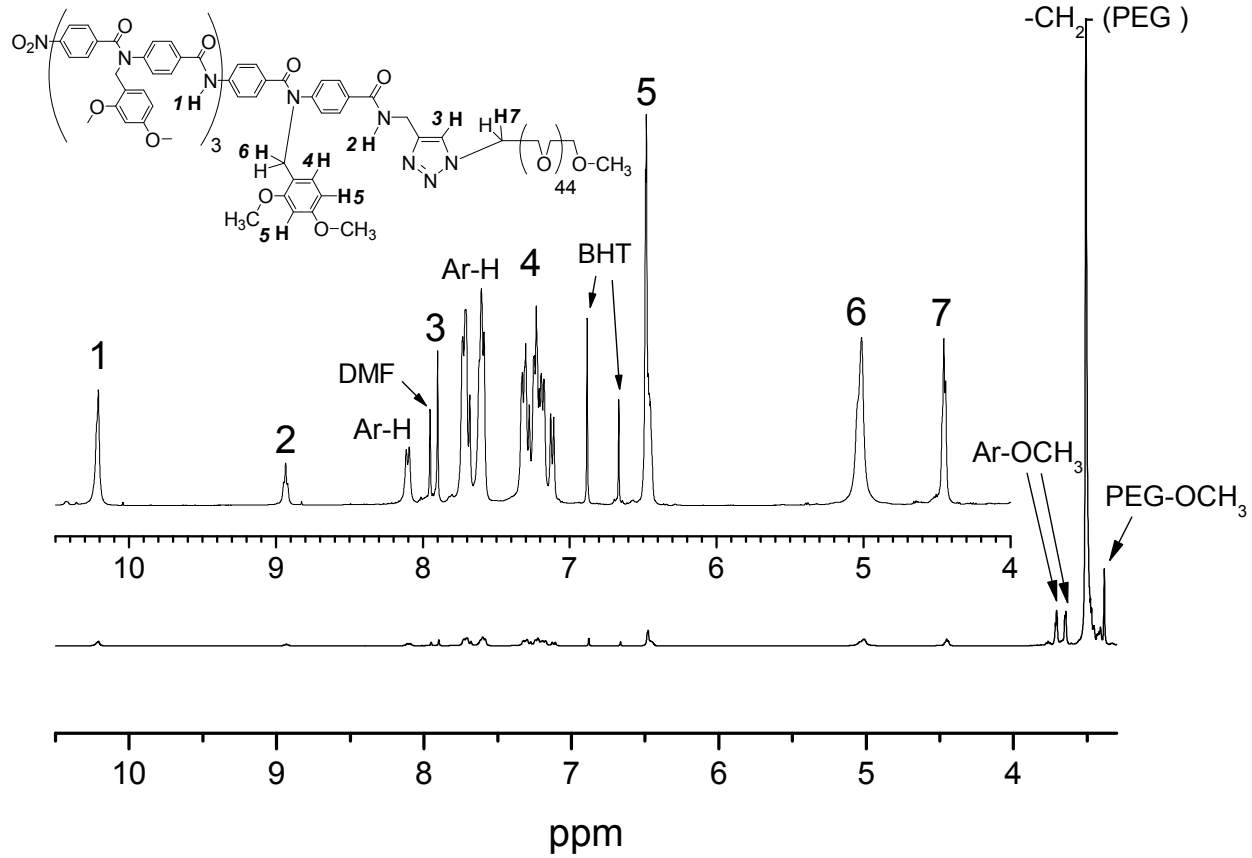

Figure SI-2.1.22. ^{1}H-NMR spectrum (DMSO-d_6) of **14**. The spectrum also shows residual peaks for DMF and BHT. This is due to the chromatographic purification in DMF and THF (which was stabilized with BHT).

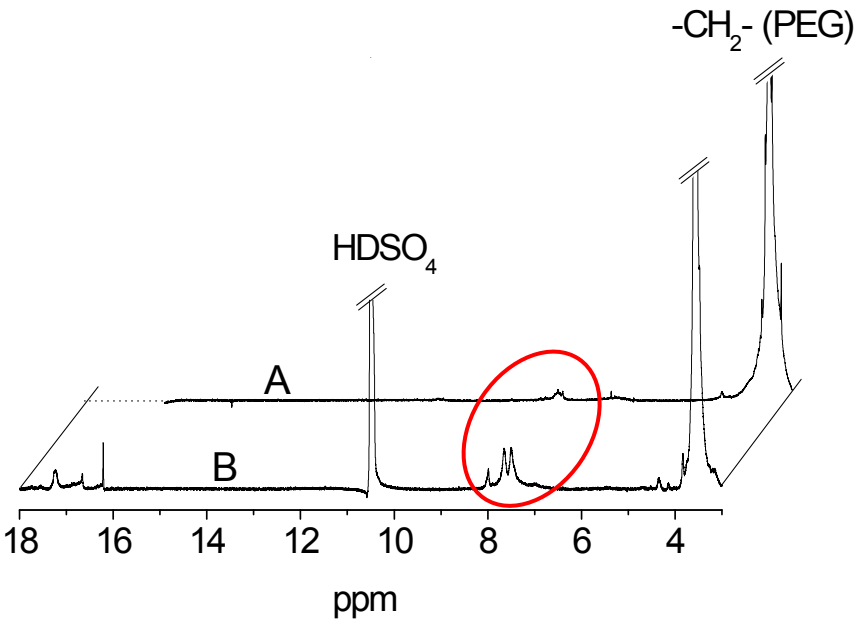

Figure SI-2.1.23. ^{1}H-NMR spectra of **15** in (A) DMSO-d_6 and (B) D_2SO_4.

Chapter 3

Comb- and Rod-like Macromolecules

3.1. Tuning Oligo(*p*-benzamide) Aggregation via Heterosequences

*Helga Seyler and Andreas F.M. Kilbinger**

Abstract

The automated synthesis of hepta(*p*-benzamide) heterosequences on solid support using a modified peptide synthesizer is reported. The oligomers are synthesized from 4-aminobenzoic acid and 4-amino-2-(hexyloxy)benzoic acid, the latter carrying a solubilizing hexyl side chain. While it was known from previous studies that the unsubstituted hepta(*p*-benzamide) is insoluble in all organic solvents, the complete insolubility of the hepta(2-hexyloxy-benzamide) carrying seven hexyl side chains was first counterintuitive to us. *Ab inito* calculations of model compounds revealed that the formation of intramolecular hydrogen bonds to the hexylether gives a perfectly flat oligobenzamide. The reduced conformational freedom of the oligomer backbone cannot be compensated by the entropic gain of the flexible side chains and leads to insolubility. To investigate whether we could fine tune this rigidifying effect, we prepared the two possible hetero-heptamers in which 4-aminobenzoic acid and 4-amino-2-(hexyloxy)benzoic acid alternate. One of the heptamers carried three, the other four hexyloxy side chains. Both exhibit good solubility in DMSO but form organogels upon standing at rt for several hours. The 1:1 mixture of both hetero-heptamers does not form a gel probably due to a selective hetero-dimer formation. We demonstrate here that designed hetero sequences in non-natural oligoamides can lead to materials with distinctly different conformations which directly affects the intermolecular interactions and hence the supramolecular organization.

Kurzfassung

Die automatisierte festphasengeträgerte Synthese von Hepta(p-benzamid) Heterosequenzen mittels eines Peptid-Syntheseautomaten wird vorgestellt. Die Co-Oligomere wurden ausgehend von 4-Aminobenzoesäure und 4-Amino-2-(hexyloxy)benzoesäure hergestellt. Das Hepta(2-hexyloxy-benzamid) mit höchst möglicher Anzahl an Substituenten erwies sich als unlöslich in organischen Lösungsmitteln. Ab initio Rechnungen von Modelverbindungen ließen erkennen, dass durch intramolekulare Wasserstoffbrückenbindungen zwischen den Amidprotonen und Ethersauerstoffen alle Phenyle in eine Ebene gezwungen werden, wodurch sich komplett planare Moleküle ergeben. Der Entropiegewinn durch Einführung flexibler Alkylketten kann den Energieverlust durch Einschränkung der Rotationsfreiheit um die Carbonyl-Phenyl Bindungen nicht kompensieren, wodurch das Molekül unlöslich wird.

Alternierende Co-Oligomere aus 4-Aminobenzoesäure und 4-Amino-2-(hexyloxy)benzoesäure wurden mit dem Ziel dargestellt, lösliche selbst-organisierende Oligomere zu erhalten. Beide möglichen Heterosequenzen zeigten gute Löslichkeit in DMSO und dienen bei geringen Konzentrationen als niedermolekularen Organogelatoren. Stöchiometrische Mischungen bilden, eventuell durch Heterodimerbildung, keine Gele in DMSO.

Nicht natürliche Oligoamid-Heterosequenzen wurden auf diese Weise für deren Konformations- und gleichzeitig Aggregationskontrolle modifiziert und für das Design von supramolekularen Materialien eingesetzt.

3.1.1. Introduction

Molecular rods built from lower molecular weight building blocks that allow precise length control have been attracting interest over the last two decades.[1,2] Of particular interest are synthetic approaches that allow a precise control over the building block sequence. Solid supported synthesis, similar to that commonly employed in peptide chemistry, allows facile sequence control while offering the possibility of automation. Molecular rods have been employed as beam-like building blocks in supramolecular assemblies[3] or as molecular spacers that place two active residues at precise distances from each other.[4,5] Rod-like aromatic oligoamides with pendant carboxylic acid groups have been employed to modify the crystallization of calcium carbonate.[6] Molecular rods have also been used in protein binding, for example mimicking the α-amino acid residue arrangements in peptide helices[7] or to prevent protein binding by inhibiting a substrate as shown in the case of rigid arylamide oligomers binding to low-molecular weight heparin.[8] They have also been extensively used in the shape of conjugated electro- and photoactive materials.[9,10]

We recently reported several synthetic routes to rigid rod-like oligo(*p*-benzamide)s employing modified peptide coupling protocols on commercially available peptide synthesizers.[11,12] Oligo(*p*-benzamide)s (OPBA) are particularly rigid aromatic amides which suffer from poor solubility due to their linearly aligned hydrogen bond donors and acceptors. In order to solubilize these oligomers, we previously conjugated them with polyethylene glycol chains, resulting in supramolecular rod-coil block copolymers, which self-assemble into rod-like micelles in nonpolar solvents.[13,14,15,16]

The most common strategy to improve solubility in rigid rod-like molecules is the attachment of flexible side chains to the stiff oligomer/polymer backbone. It is believed that such side chains act like covalently attached solvent, allowing a gain in entropy upon dissolution of the oligomer or polymer.[17,18,19,20,21]

Here we report the synthesis of hepta(*p*-benzamide) heterosequences, varying in the number and pattern of hexyloxy substituents. Using automated solid supported synthesis allowed the facile and rapid access to precisely defined heterosequences. We present evidence that the number and position of hexyloxy substituents strongly affects oligomer rigidity, solubility and aggregation/gelation behavior.

3.1.2. Results and Discussion

Our initial aim was to increase the solubility of oligo(*p*-benzamide)s by introducing hexyloxy side chains *ortho* to the carboxylic acid, using *i.e.* 4-amino-2-(hexyloxy)benzoic acid as the monomer. We rationalized that in an oligomer formed from this monomer the amide N-H protons should form an intramolecular hydrogen bond to the neighboring hexylether oxygen thus preventing intermolecular aggregation via H-bonds. In addition, the presence of hexyl side chains was believed to increase solubility as has been reported previously.[17,18,19,20,21]

4-Amino-2-(hexyloxy)benzoic acid (**3**) was prepared as shown in **scheme 3.1.1**. 4-Aminosalicylic acid was *N*-acetylated using one equivalent of acetyl chloride to give **1** in 85% yield. The subsequent reaction with hexyl bromide produced the corresponding hexyl ether and ester **2** in 82% yield. Alkaline hydrolysis with KOH resulted in ester as well as amide cleavage to give 4-amino-2-(hexyloxy)benzoic acid **3** in 85% yield. *N*-Fluorenylmethyloxycarbonyl (Fmoc) protection was achieved using 9-fluorenylmethylchloroformate (Fmoc-Cl) to give **4** in 89% yield. Activation of **4** as an acid chloride was carried out *in situ* without further work-up of the activated species **5** using $SOCl_2$ and *N*-methylpyrrolidone (NMP).[22]

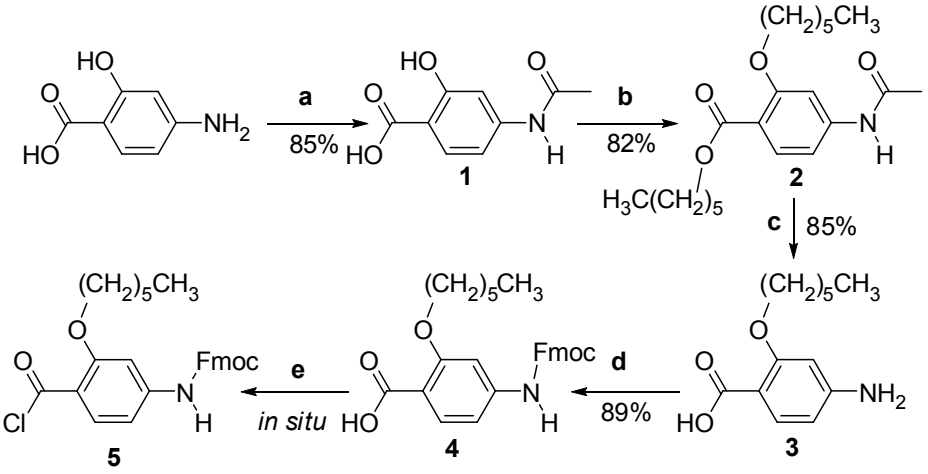

Scheme 3.1.1. Synthesis and activation of 4-amino-2-(hexyloxy)benzoic acid. a) acetyl chloride, b) hexyl bromide, c)KOH, d) Fmoc-Cl, e) $SOCl_2$ and NMP

Using activated monomer **5** we prepared a homo-heptamer on solid support using a previously reported coupling protocol on a commercial peptide synthesizer (**scheme 3.1.2**).[11,12]

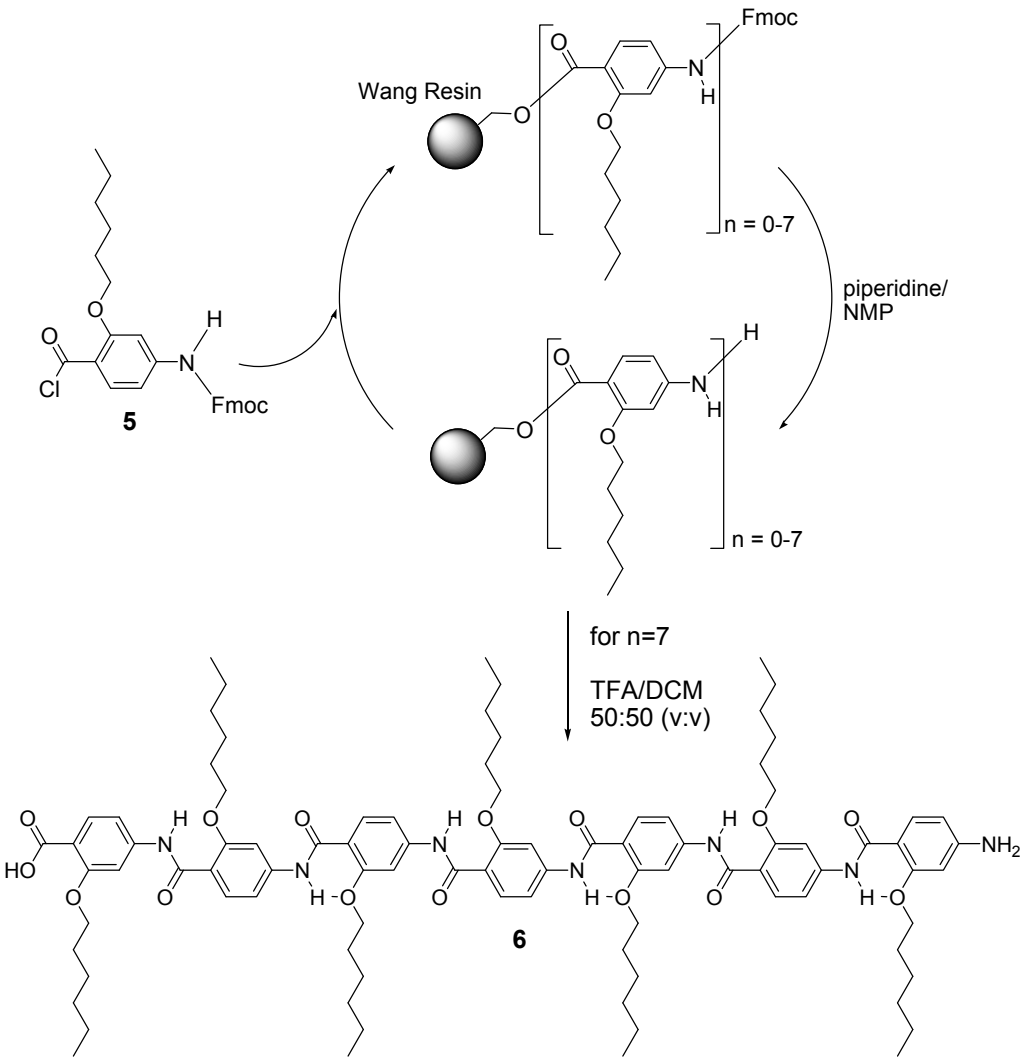

Scheme 3.1.2. Hepta(2-(hexyloxy)benzamide) **6**. Every phenyl ring carries one hexyloxy side-chain.

The Fmoc cleavage elugram for the seven automated reaction steps showed a slight decrease in coupling efficiency with increasing oligomer length (see supporting information) but indicated the overall success of the reaction. However, cleavage of oligomer **6** from the solid support produced a precipitate that was insoluble in all common organic solvents (TCM, THF, DMSO, DMF and others).

We could previously show that the site isolation and dilution effect of the solid support allows the preparation of insoluble oligomers in good yields that could otherwise not be synthesized using classic solution chemistry.[12]

In order to explain the unexpected lack of solubility of the heptamer **6** we carried out *ab initio* geometry optimizations (DFT, 6-31G*)[23] on a model heptamer, carrying methoxy instead of hexyloxy side chains (see supporting information for details). The model showed that the amide N-H proton formed a hydrogen bond to the methoxy side chain as described earlier.[24,25] This resulted in the coplanarity of all phenyl rings (0°) giving a flat, ribbon-like oligomer. We previously reported that the angle between phenyl planes in unsubstituted oligo(*p*-benzamide)s is ca. 30°.[26]

Consequently, the introduction of the alkyloxy side chains leads to a flattening of the oligomer. Fewer conformations accessible to the oligomer backbone and an almost perfectly flat π-face leads to an increased tendency for the oligomers to stack and aggregate. The rigidification of the backbone cannot be compensated by an entropical gain of the solvated hexyl side chains. Therefore the oligomer remains insoluble.

To prove our assumptions concerning the conformational restraints of hexyloxy substituted oligo(*p*-benzamide)s, we prepared tri(*p*-benzamide) **7** (**figure 3.1.1**) on solid support according to previously reported procedures (see supporting information for Fmoc cleavage elugrams).[11,12] While tri(*p*-benzamide)s carrying no hexyloxy groups are only soluble in hydrogen bond breaking solvents such as DMSO and DMF,[13] trimer **7** showed very good solubility in DMSO as well as in TCM. This improved solubility could therefore clearly be attributed to the presence of the solubilizing hexyl side chains. ^{1}H-NMR spectra, COSY and NOESY spectra of **7** were recorded in $CDCl_3$ and DMSO-d_6 (see supporting information for details). The data confirmed that the amide N-H_d (**figure 3.1.1**) was H-bonded to the hexyloxy ether oxygen in both solvents as no rotation of the *N*-terminal phenyl ring was observed (no H_d-H_c coupling was observed in either solvent). This behavior is in good agreement with the conformational restrains found in similar oligoamides.[7]

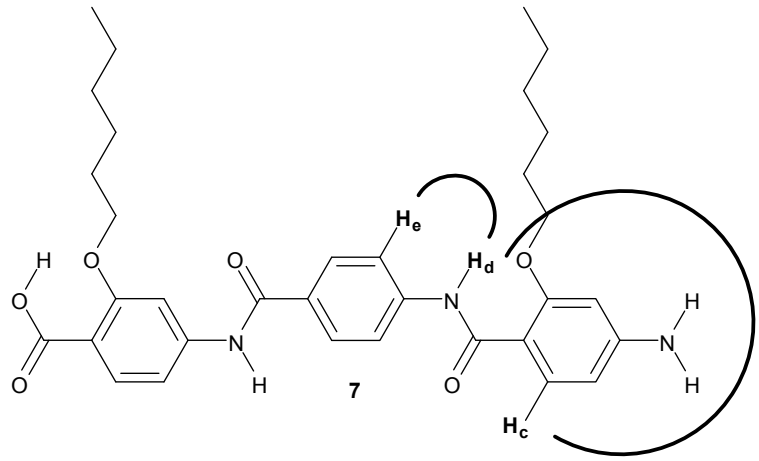

Figure 3.1.1. Model trimer **7** for evaluation of solution conformation. NOE NMR experiments show that the amide N-H_d is H-bonded to the hexyloxy ether in $CDCl_3$ as well as in DMSO-d_6.

In agreement with literature precedence,[24,25] our NMR-experiments showed that the six-membered ring formed via hydrogen bonding of H_d to the alkyloxy ether oxygen is energetically more favorable than forming a hydrogen bond to the solvent, i.e. DMSO.
The automated synthesis of oligomers on solid support allows for a the quick and facile variation of the monomer sequence. We were curious to see whether the synthesis of heterosequences from *p*-aminobenzoic acid and 4-amino-2-(hexyloxy)benzoic acid would allow for a fine-tuning of the oligomer rigidity and hence its aggregation behavior. We therefore synthesized both heterosequence heptamers **8** and **9** on solid support according to reported procedures (**figure 3.1.2** *top*).[11,12] Fmoc cleavage elugrams for both heptamers **8** and **9** as well as their corresponding MALDI-TOF mass spectra are reported in the supporting information section. Despite carrying three and four hexyloxy side chains, the oligomers **8** and **9** are insoluble in TCM, THF or dichloromethane (DCM) but show good solubility in DMSO. As reported previously, hepta(*p*-benzamide)s not carrying alkyloxy side chains are insoluble in all organic solvents. The increased solubility for **8** and **9** in DMSO must therefore be a direct result of the attached hexyloxy side chains. Compounds **8** and **9** dissolve readily in DMSO-d_6 and appear to be molecularly dissolved, as evidenced by the well resolved ^{1}H-NMR spectra shown in **figure 3.1.2** (*bottom*). However, the DMSO-d_6 solutions of **8** and **9** turn into gels when left at room temperature for ca. 12h. Oligomer **8** forms a clear gel, while oligomer **9**, just carrying one more hexyloxy side chain, forms an opaque gel (see **figure 3.1.3**).

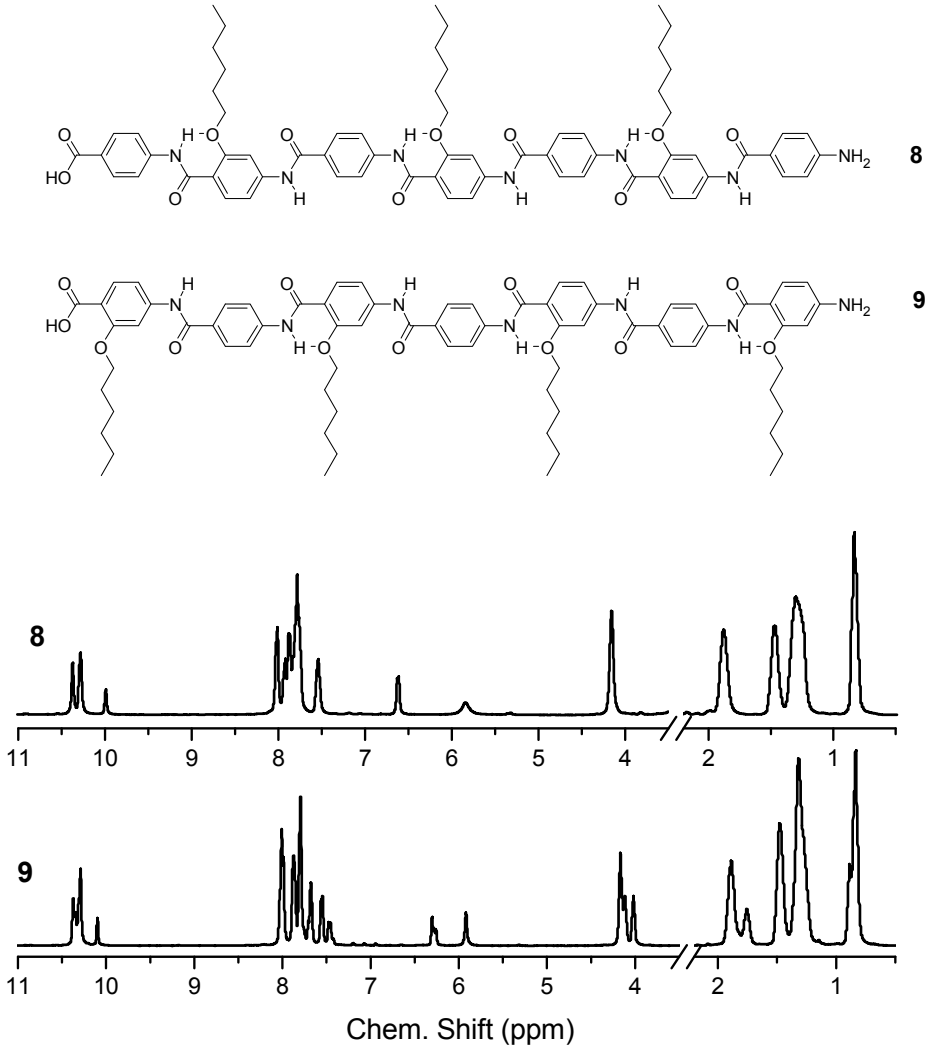

Figure 3.1.2. *Top*: Molecular structures of hepta(*p*-benzamide) heterosequences **8** and **9**. *Bottom*: Corresponding ^{1}H-NMR (DMSO-d_6, 300 MHz) spectra.

This behavior fits well into our previous prediction that the hexyloxy side chains rigidify the oligomer structure and thus lead to an increased aggregation tendency. In the partially hexyloxy substituted oligomers **8** and **9**, there appears to be a delicate interplay between the solubility increase due to the hexyl side chains and at the same time the rigidification due to intramolecular hydrogen bonding to the hexyloxy ether. This balance between solubility and aggregation tendency leads to the formation of gels.

The DMSO gels of **8** and **9** were investigated by transmission electron microscopy (TEM). As can be seen in **figure 3.1.3**, both oligomers form multi-micrometer long fibers in DMSO, which entangle to give a gel-like macroscopic appearance. It is worth noting, that the TEM image of oligomer **9**, carrying four hexyloxy side chains, shows a denser, more entangled fiber network than oligomer **8**, carrying three hexyloxy side chains. The bundles of fibers that can be observed in the TEM images (**figure 3.1.3**) also differ in

size. The one for oligomer **9** are typically around 4-5 μm long, while oligomer **8** shows bundles of average size 1-2 μm. This data confirms once more that while the hexyloxy side chains improve the solubility of the hepta(*p*-benzamide)s **8** and **9** in the first place, they are also clearly involved in their supramolecular aggregation, i.e. fiber and gel formation (see above).

The solubility trend observed before, with **8** forming a clear gel, **9** forming an opaque gel and **6** being insoluble in DMSO is directly related the number of hexyloxy side chains increasing and oligomer becoming flatter going from **8** to **9** to **6.**

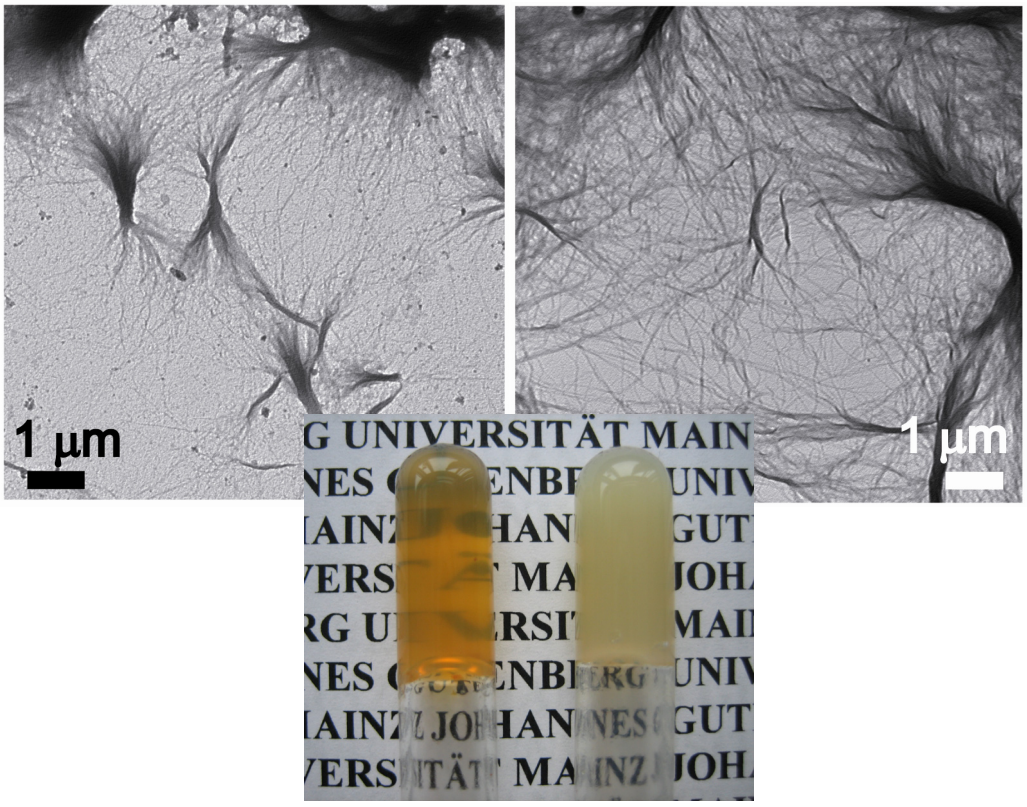

Figure 3.1.3. *Left*: TEM image of a gel of oligomer **8** in DMSO (c = 7.6 mM). *Right* TEM image of a gel of oligomer **9** in DMSO (c = 7.6 mM).

Both gels of **8** and **9** formed in DMSO are thermoreversible and were investigated with regard to their melting points using the dropping ball method.[27] The gel formed from **8** in DMSO shows a melting point of 70°C, the gel formed from **9** in DMSO a melting point of 84°C. This is in good agreement with our assumption that oligomer **8**, carrying fewer "flattening" hexyloxy side chains forms a weaker aggregate than oligomer

9 carrying four hexyloxy side chains. The thermal and solubility characteristics of compounds **6**, **8** and **9** are summarized in **table 3.1.1**.

Table 3.1.1. Physical properties of DMSO solutions of oligomers **6**, **8** and **9**.

oligomer	**appearance**	**m.p. gel / °C**
8	clear gel	84.1
9	opaque gel	70.1
6	Insoluble	
8+9 (1:1)	precipitates	

In a previous report we described the single crystal X-ray structure of an oligo(*p*-benzamide) trimer.[15] There, the oligoamide strands form infinite parallel sheets bridged by hydrogen bonds. In addition, the carbonyl groups of the amide strictly alternate their orientation, most likely in order to minimize the net dipole moment of the individual molecules.

Assuming parallel sheet formation and alternation of the carbonyl dipole along the oligomer chain are indeed preserved in solution, one could devise suitable alkyloxy substitution patterns that would result in all alkyl groups facing towards the same edge of the oligomer (**figure 3.1.4**). This could be achieved by the formation of an intramolecular hydrogen bond of the amide N-H to the alkyloxy-ether. This way, the alkyl chain would always be *trans* to the carbonyl group.

Moreover, placement of such alkyloxy groups on only the even phenyl rings (**8**, **figure 3.1.4** *top*; counted from C-terminus to N-terminus) would selectively prevent one edge of the oligomer from further intermolecular stacking via hydrogen bonds, as all hydrogen bond donors would be intramolecularly saturated. Placement of alkyloxy groups on all odd phenyl rings (**9**, **figure 3.1.4** *bottom*; counted from C-terminus to N-terminus) would selectively prevent further intermolecular hydrogen bonds on the opposite edge of the oligomer. Hence, in both oligomeric heterosequences opposite edges would be selectively blocked while the others could allow hetero-dimerisation via hydrogen bonds (**figure 3.1.4**, dashed bonds between top and bottom oligomer).

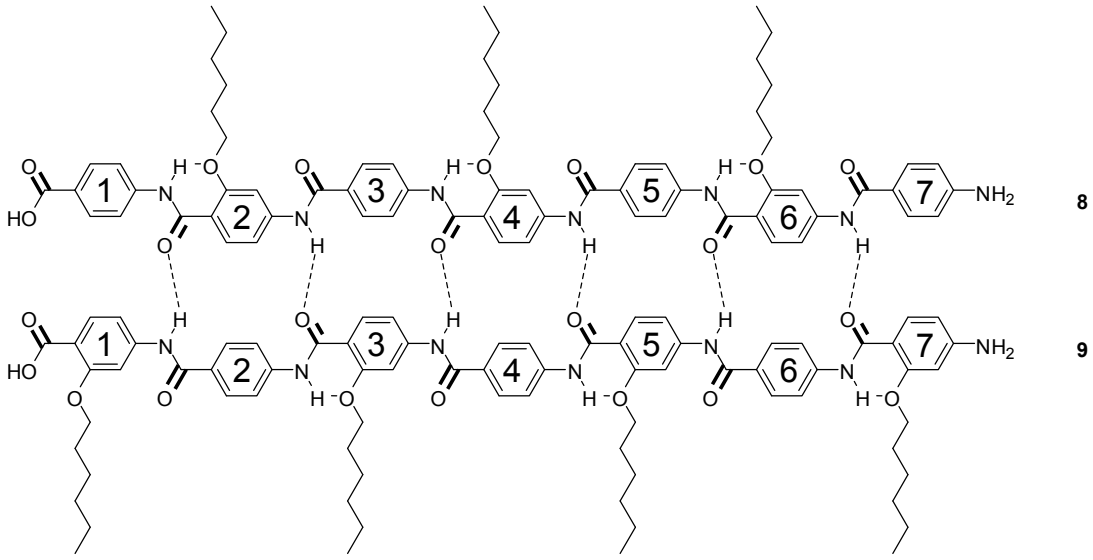

Figure 3.1.4. Proposed hetero-dimer formation of two differently hexyloxy substituted heptamers.

To investigate whether our assumption of dimer formation between **8** and **9** in solution would hold (see **figure 3.1.4**), we carried out ^{1}H-NMR titration experiments in DMSO-d_6, adding **8** to a solution of **9** and *vice versa*. No shifts of peaks could be observed and the resulting spectra appeared as mere additions of the individual compound spectra.

We further investigated whether a 1:1 mixture of **8** and **9** in DMSO would have any effect on the gelation of the oligomers. However, the 1:1 mixture of **8** and **9** starts to precipitate from DMSO after 0.5 h and does not gel the DMSO solution at all. To investigate this process by TEM, we prepared a fresh 1:1 mixture of **8** and **9** in DMSO and deposited a small drop of the warm (40 °C) solution onto a carbon coated TEM copper grid. After precipitation, excess solvent was removed and the grid examined under the microscope. **Figure 3.1.5** shows a representative image observed for the precipitate from the 1:1 mixture of **8** and **9** in DMSO. Similar to the TEM images observed for the individual compounds **8** and **9** (**figure 3.1.3**), long fibers are formed. In contrast to the images in **figure 3.1.3**, no significant bundling of the fibers can be observed. This suggests that the supramolecular fiber formation of oligomers **8** and **9** is significantly influenced by the presence of the corresponding complementary oligomer.

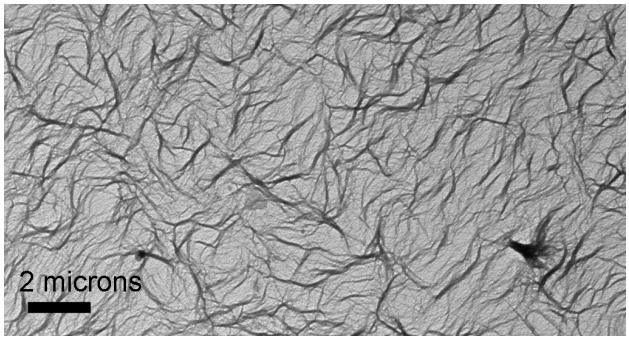

Figure 3.1.5. TEM image of a 1:1 (mol:mol) mixture of oligomer **8** and oligomer **9** in DMSO (c = 7.6 mM).

3.1.3. Conclusions

In conclusion, we have presented evidence that oligo(*p*-benzamide)s carrying alkyloxy substituents in the 2-position show an improved organo-solubility compared to their non-substituted analogues. Nonetheless, the two possible hepta(*p*-benzamide)s in which 4-amino benzoic acid and 4-amino-2-(hexyloxy)benzoic acid alternate form gels in DMSO. TEM investigations of the gels reveal that long flexible fibers are formed that entangle to form the macroscopic gel. We believe that the 2-alkyloxy substituent forms a hydrogen bond to the adjacent amide N-H-amide donor resulting in coplanar neighboring phenyl rings. This prevents the amide bond to form intermolecular hydrogen bonds. The perfectly flat coplanar phenyl rings on the other hand favor non-directional π-stacking among the oligomers. Hence, a change in noncovalent aggregation mechanism is induced by introducing 2-alkyloxy substituents. We believe that this synthetic feature will play an important role in the design and understanding of noncovalent interactions and hierarchical structure formation.

3.1.4. Experimental Section

General.

Technical and most of the p. a. quality solvents were purchased from Acros Organics. DCM and DMSO were purchased from Fisher Scientific. *N*-Methylpyrrolidone (NMP) was

kindly donated by BASF and stored over molecular sieve (4 Å). 9-Flourenylmethoxycarbonyl-chloride (Fmoc-Cl) and Wang resin were obtained by Iris Biotech GmbH, all other chemical reagents were purchased from Acros Organics and were used without further purification. Deuterated solvents (DMSO-d_6 and $CDCl_3$) were purchased from Deutero GmbH.

Instrumentation.

Standard ^1H and ^{13}C nuclear magnetic resonance spectra were recorded on a Bruker AC (300 MHz) or on a Bruker AMX 400 (400 MHz). 2D COSY and NOESY experiments were acquired on a Bruker AMX 400. Infrared spectra were recorded on a Nicolet 5 DXC FT-IR spectrometer. RP-HPLC analysis was performed on a Hewlett Packard HP 1090 Liquid Chromatograph equipped with PerfectSil column (MZ Analysentechnik, Mainz, Germany, 250 x 4.0 mm; 120 ODS-2 5 μm). The samples were eluted with an acetonitrile/water gradient that started from 10 % acetonitrile rising to 90 % over a period of 35 min and maintained constant for additional 10 min. Both solvents were buffered with 0.1 % TFA. UV-detection was performed at 254 nm. Melting points were recorded on a FP 62 Mettler Toledo in a capillary tube and are uncorrected. Field desorption mass spectra were measured on a Finnigan MAT 95 and ESI mass spectra on a Micromass Q-TOF Ultima 3. Matrix-assisted laser desorption and ionization time-of-flight (MALDI-TOF) measurements were performed on a Shimadzu Axima CFR MALDI-TOF mass spectrometer equipped with a nitrogen laser delivering 3 ns laser pulses at 337 nm. 2-(4-hydroxyphenylazo) benzoic acid (HABA) was used as matrix. A Philips EM 420 transmission electron microscope using a LaB_6 cathode at an acceleration voltage of 120 kV was used to obtain TEM-images. TEM grids (carbon film on copper, 300 mesh) were obtained from Electron Microscopy Sciences, Hatfield, PA, USA. The synthesis of the oligomers was performed on an Applied Biosystems ABI 431a automated peptide synthesizer using standard Fmoc chemistry protocols. Modules A, G and E were modified as described in detail before.[11,12]

4-Acetamidosalicylic acid **(1).** Acetyl chloride (23.2 ml, 1 eq.) was added dropwise into a cold solution of 4-aminosalicylic acid (50 g, 0.33 mol, 1 eq.) in pyridine (250 ml) under an inert atmosphere. The solution was further refluxed for 2 hrs. The cold reaction

mixture was poured to a mixture of 800 ml ice and 400 ml 6N hydrochloric acid. The solid was filtered, washed with water and dried to give **1** (54g, 85%).

mp: 222 ºC.
^{1}H-NMR: δ (300 MHz, DMSO-d_6) 2.06 (s, 3 H); 7.04 (d, ^{3}J = 8.46 Hz, 1 H); 7.34 (s, 1 H); 7.70 (d, ^{3}J = 8.46 Hz, 1H); 10.21 (s, 1H).
^{13}C-NMR and DEPT: δ (300 MHz, DMSO-d_6) 24.29 (+); 105.77 (+); 107.48; 110.11 (+); 131.05 (+); 145.7; 162.21; 169.2; 171.69.
IR ν (cm^{-1}): 3350, 2872, 1676, 1599, 1535, 1383, 1282, 1222, 1162.
RP-HPLC (min): 9.9
M (FD): *m/z* (%) = 195.6 (100); 196.6 (9.3); 197.6 (0.49); calc.[$C_9H_9NO_4$] = 195.1

4-Acetamido-2-hexyloxy-benzoic acid hexyl ester **(2). 1** (37.1 g, 0.19 mol), dry acetone (700 ml), 153 ml 1-bromohexane (153 ml, 1.1 mol), 18-crown-6 (1,5 g), anhydrous K_2CO_3 (229.8 g) and KI were heated for 50 hrs under reflux and inert atmosphere. The solvent was removed under reduced pressure, water (460 ml) was added to the residue, the resulting solution extracted with DCM, dried over magnesium sulfate and the solvent removed on a rotary evaporator. The residue was cooled over night at -18 ºC, the precipitate was collected by suction filtration, washed with cold petroleum ether and dried in vacuum to give **2** as a beige solid (56.7 g, 82 %).

mp: 66 ºC.
^{1}H-NMR: δ (300 MHz, DMSO-d_6) 0.84-0.89 (m, 6 H); 1.25-1.49 (m, 12 H); 1.59-1.76 (m, 4 H); 2.06 (s, 3H); 3.94 (t, ^{3}J = 6.25 Hz, 2 H); 4.15 (t, ^{3}J = 6.4 Hz, 2 H); 7.16 (dd, ^{4}J = 1.7 Hz, ^{3}J = 8.6 Hz, 1 H); 7.47 (d, ^{4}J = 1.47 Hz, 1 H); 7.64 (d, ^{3}J = 8.46 Hz, 1 H); 10.18 (s, 1 H).
^{13}C-NMR and DEPT: δ (300 MHz, DMSO-d_6) 13.87 (+); 22.08 (+); 22.14 (+); 24.2 (+); 25.21 (-); 25.3 (-); 28.31 (-); 28.68 (-); 31.03 (-); 31.08 (-).
IR ν (cm^{-1}): 3306, 3272, 2955, 2932, 2856, 1679, 1662, 1595, 1543, 1409, 1274, 1261, 1191, 1138, 831.
RP-HPLC (min.): 35.6
M (FD): *m/z* (%) = 363.4 (100); 364.4 (19); calc.[$C_{21}H_{33}NO_4$] = 363.2

4-Amino-2-hexyloxy-benzoic acid **(3).** A solution of **2** (55.3 g, 0.15 mol), KOH (35 g) and ethanol (550 ml) was heated under reflux for 50 hrs. The solvent was then removed under reduced pressure, the residue dissolved in water (550 ml) and neutralized with 6N HCl. The precipitate was collected, washed well with water and dried under vacuum at 60 ºC to give **3** (30.3 g, 85%).

mp: 122 ºC.
^{1}H-NMR: δ (300 MHz, DMSO-d_6) 0.87 (t, ^{3}J = 6.99 Hz, 3 H); 1.26-1.31 (m, 4 H); 1.43 (m, 2 H); 1.71 (tt, 2 H); 3.93 (t, ^{3}J = 6.4 Hz, 2 H); 5.86 (s, 2H); 6.14 (dd, ^{4}J = 1.84 Hz, ^{3}J = 8.46 Hz, 1 H); 6.2 (d, ^{4}J = 2.21 Hz, 1 H); 7.50 (d, ^{3}J = 8.82 Hz, 1 H); 11.31 (s, 1 H).
^{13}C-NMR and DEPT: δ (300 MHz, DMSO-d_6) 13.88 (+); 22.08 (-); 25.09 (-); 28.58 (-); 30.94 (-); 67.98 (-); 97.22 (+); 105.82 (+); 106.06; 133.79 (+); 154.49; 160.42; 166.34.
IR ν (cm^{-1}): 3428, 3345, 3232, 2930, 1685, 1586, 1456, 1401, 1339, 1267, 1191, 998, 831.
RP-HPLC (min.): 21.9
M (FD): *m/z* (%) = 237.8 (100); 238.8 (17); 239.8 (1.4); calc.[$C_{13}H_{19}NO_3$] = 237.1

N-Fmoc-4-amino-2-(hexyloxy) benzoic acid **(4). 3** (19.9 g, 84 mmol) was dissolved in dry NMP (140 ml) under an inert atmosphere followed by the dropwise addition of Fmoc-Cl (21.67 g, 83.8 mmol) in dry NMP (55 ml). After 24 hrs, the reaction mixture was poured slowly into 280 ml water. The beige precipitate was collected by filtration, washed with water, petroleum ether and recrystallized from toluene to afford **4** (38.6 g, 89%).

mp: 159 ºC.
^{1}H-NMR: δ (300 MHz, DMSO-d_6) 0.86 (t, ^{3}J = 6.62 Hz, 3 H); 1.27-1.30 (m, 4 H); 1.43 (m, 2 H); 1.71 (tt, 2 H); 3.95 (t, ^{3}J = 6.25 Hz, 2 H); 4.32 (t, ^{3}J = 6.62 Hz, 1 H); 4.52 (d, ^{3}J = 6.62 Hz, 2 H); 7.08 (d, ^{3}J = 8.09 Hz, 1H); 7.33-7.45 (m, 5 H); 7.65 (d, ^{3}J = 8.46 Hz, 1H); 7.76 (d, ^{3}J = 6.99 Hz, 2 H); 7.91 (d, ^{3}J = 7.35 Hz, 2 H), 9.98 (s, 1H).
^{13}C-NMR and DEPT: δ (300 MHz, DMSO-d_6) 13.87 (+); 22.06 (-); 25.01 (-); 28.5 (-); 30.9 (-); 46.56 (+); 65.8 (-); 68.15 (-); 102.63 (+); 109.34 (+); 114.43; 120.19 (+); 125.11 (+); 127.13 (+); 127.71 (+); 132.34 (+); 140.82; 143.69; 143.87; 153.24; 158.94; 166.57.
IR ν (cm^{-1}): 3302, 3218, 2952, 2932, 2856, 1738, 1710, 1608, 1528, 1414, 1309, 1196, 1103, 736.

RP-HPLC (min.): 34.9
M (FD): *m/z* (%) = 459.5 (100); 460.6 (16.7); calc.[$C_{28}H_{29}NO_5$] = 459.2

*N-Fmoc-p-amino benzoic acid***.** *p*-Aminobenzoic acid (10 g, 73 mmol) was dissolved in dry NMP (50 ml) under an inert atmosphere followed by the dropwise addition of Fmoc-Cl (18.9 g, 73 mmol) in dry NMP (50 ml). After 24 hrs, the reaction mixture was poured slowly into 400 ml water. The colorless precipitate was collected by filtration, washed with water and dried in vacuum at 120 ºC (yield: 24.8 g, 94%).

mp: 215 ºC (dec.)
^{1}H-NMR: δ (300 MHz, DMSO-d_6) 4.33 (t, ^3J = 6.25 Hz, 1 H); 4.54 (d, ^3J = 6.25 Hz, 2 H); 7.33-7.45 (m, 4 H); 7.57 (d, ^3J = 7.35 Hz, 2 H); 7.76 (d, ^3J = 7.35 Hz, 2 H); 7.89 (m, 4 H), 10.08 (s, 1H); 12.69 (s, 1H).
^{13}C-NMR and DEPT: δ (300 MHz, DMSO-d_6) 46.61 (+); 65.83 (-); 117.5 (+); 120.22 (+); 124.48; 125.14 (+); 127.17 (+); 127.74 (+); 130.48 (+); 140.86; 143.31; 143.74; 153.31; 167.03.
IR ν (cm^{-1}): 3344, 2970, 2887, 2660, 2544, 1709, 1673, 1610, 1592, 1526, 1511, 1411, 1311, 1282, 1221, 1052, 850, 736.
RP-HPLC (min.): 26.6
M (FD): *m/z* (%) = 359.1 (100); 360.1 (17.4); calc.[$C_{22}H_{17}NO_4$] = 359.1

General method for resin functionalization **(GM 1).** Wang resin (417 mg, 0.25 mmol) was swollen in a minimum amount of dry NMP. Amino acid **4** or *N-Fmoc-p-amino benzoic acid* (2 mmol) was dissolved in NMP (2 ml) and thionyl chloride (0.22 ml, 3 mmol) was added. After 2 hrs, the solution was evacuated for 30 min and poured to the Wang resin. After 24 hrs the resin was drained and washed 4 times with NMP. Unreacted functional groups on the resin were capped with a solution of 4-nitrobenzoyl chloride (0.46 g, 2.5 mmol) in NMP (1.5 ml).

General method for the preparation of acid chlorides for the automated solid phase synthesis **(GM 2).** The corresponding acid was dissolved in thionyl chloride and a catalytic amount of dry NMP was added. After stirring for 2 hrs, thionyl chloride was removed under reduced pressure. The acid chloride was dissolved in dry NMP (to

obtain a final concentration of 0.5 mmol/ml) and the solution filtered through a 400 micron syringe filter into the cartridges of the peptide synthesizer (1 mmol per cartridge).

General method for the automated oligomer synthesis on a peptide synthesizer **(n-mer) (GM 3).** The functionalized resin (prepared as described in **GM 1**) was *N*-deprotected, reacted with 4 eq. acid chloride **5** or *N-Fmoc-p-amino benzoic acid chloride* (2x, prepared as described in **GM 2**), followed by the reaction with 4 eq. 4-nitrobenzoyl chloride as capping reagent. This sequence was repeated n-1 times to afford the n-mer.

STEP	**Rpt.**	**Name**	**Modules (ABI 431A)**
1	n-1	Middle cycle with capping	GgBdefffGgdefffGgeff
2	1	Deprotection and NMP wash	gBd
3	1	Rinse cycle	E

The efficiency of the monomer coupling steps was monitored during the synthesis by UV-detection of the deprotected Fmoc groups.

The desired oligomer was cleaved off the solid support by stirring in TFA-DCM (50%) solution for 12 hrs. The solvent was evaporated to obtain the crude product.

Trimer **(7). 7** was prepared as described in **GM 3**, starting with a *N*-Fmoc-4-amino-2-hexyloxy benzoic acid- functionalized resin. Step 1 was repeated 2 times. The resin was filtered off from the TFA/DCM solution, the product was precipitated in diethyl ether and then lyophilized to afford a beige product (70 mg, 49%).

^{1}H-NMR: δ (300 MHz, DMSO-d_6) 0.82-0.9 (m, 6 H); 1.23-1.35 (m, 8 H); 1.46 (m, 4 H); 1.75 (tt, 2 H); 1.90 (tt, 2H); 4.01 (t, ^3J = 6.46 Hz, 2 H); 4.11 (t, ^3J = 6.26 Hz, 2 H); 6.27 (dd, ^4J = 1.96 Hz, ^3J = 8.61 Hz, 1 H); 6.30 (d, ^4J = 1.96 Hz, 1 H); 7.46 (dd, ^4J = 1.86 Hz, ^3J = 8.51 Hz, 1 H); 7.66-7.70 (m, 3 H); 7.79 (d, ^3J = 9 Hz, 1H); 7.97 (d, ^3J = 8.8 Hz, 2 H); 10.09 (s, 1H); 10.3 (s, 1 H).
RP-HPLC (min.): 33.4

M (ESI): *m/z* (%) = 598.3 (100); 599.3 (14.7); calc.$(M+Li)^+$ $[C_{34}H_{45}N_3O_6]$ = 598.3
IR ν (cm^{-1}): 3345, 2929, 2859, 1670, 1591, 1509, 1405, 1315, 1246, 1183, 1133, 1010, 883, 763, 669.

*Heptamer **(8)***. **8** was prepared as described in **GM 3**, starting with a *N*-Fmoc-4-amino benzoic acid- functionalized resin. Step 1 was repeated 6 times. The heptamer was dissolved in hot DMSO (100 °C), precipitated into methanol, centrifugated and dried in vacuum at 100 ºC (80% yield).

^{1}H-NMR: δ (300 MHz, DMSO-d_6) 0.79-0.85 (m, 9 H); 1.21-1.49 (m, 18 H); 1.86-1.89 (m, 6 H); 4.15-4.17 (m, 6 H); 6.63 (d, ^3J = 8.51 Hz, 2 H); 7.5 -8.03 (m, 23 H); 10.0 (s, 1 H); 10.27-10.37 (m, 5H).
M (MALDI-TOF): *m/z* = 1229 $[M(K\text{-salt}) + K]^+$; calc.$[C_{67}H_{72}N_7O_{11}K_2]^+$ = 1228.5.
IR ν (cm^{-1}): 3334, 2930, 2859, 1654, 1585, 1500, 1408, 1238, 1175, 1013, 846, 757, 660.

Heptamer **(9). 9** was prepared as described in **GM 3**, starting with a *N*-Fmoc-4-amino-2-hexyloxy benzoic acid- functionalized resin. Step 1 was repeated 6 times. The heptamer was dissolved in hot DMSO, precipitated into methanol, centrifugated and dried in vacuum at 100 ºC (67% yield).

^{1}H-NMR: δ (300 MHz, DMSO-d_6) 0.82-0.9 (m, 12 H); 1.24-1.49 (m, 24 H); 1.72-1.93 (m, 8 H); 4.02 (t, ^3J = 6.3 Hz, 2 H); 4.10-4.18 (m, 6 H); 5.92 (s br.; NH_2); 6.27 (d, 1H); 6.30 (s, 1H); 7.46-8.03 (m, 22 H); 10.1 (s, 1 H); 10.29-10.37 (m, 5H).
M (MALDI-TOF): *m/z* = 1296 $[M(Na\text{-salt}) + Na]^+$; calc.$[C_{73}H_{84}N_7O_{12}Na_2]^+$ = 1296.6
IR ν (cm^{-1}): 3333, 2928, 2858, 1663, 1586, 1507, 1405, 1239, 1180, 1013, 832, 757.

3.1.5 References

[1] Schwab, P.F.H.; Levin, M.D:; Michl, J. *Chem. Rev*. **1999**, *99*, 1863-1933.

[2] Schwab, P.F.H.; Smith, J.R.; Michl, J. *Chem. Rev*. **2005**, *105*, 1197-1279.

[3] Ryu, J.-H.; Hong, D.-J.; Lee, M. *Chem. Commun*. **2008**, 1043-1054.

[4] Gothard, C.M.; Nosheen, A.R.; Nowick, J.S. *J. Am. Chem. Soc*. **2007**, *129*, 7272-7273.

[5] Kümin, M.; Sonntag, L.-S.; Wennemers, H. *J. Am. Chem. Soc*. **2007**, *129*, 466-467.

[6] Estroff, L.A.; Incarvito, C.D.; Hamilton, A.D. *J. Am. Chem. Soc*. **2004**, *126*, 2-3.

[7] Ernst, J.T.; Becerril, J.; Park, H.S.; Yin, H.; Hamilton, A.D. *Angew. Chem. Int. Ed.* **2003**, *42*, 535-539.

[8] Choi, S.; Clements, D.J.; Pophristic, V.; Ivanov, I.; Vemparala, S.; Bennett, J.S.; Klein, M.L.; Winkler, J.D.; DeGrado, W.F. *Angew. Chem. Int. Ed.* **2005**, *44*, 6685 –6689.

[9] Samori, P.; Francke, V.; Müllen, K.; Rabe, J.P. *Chem. Eur. J.* **1999**, *5*, 2312-2317.

[10] Neher, D.; *Adv. Mater*. **1995**, *7*, 691-702.

[11] Koenig, M. H.; Gorelik, T.; Kolb, U.; Kilbinger, A.F.M *J. Am. Chem. Soc.* **2007**, *129*, 704-708.

[12] König, H.M.; Kilbinger, A.F.M. *Macromol. Rapid Commun.* **2008**, *29*,1721-1725.

[13] Abbel, R.; Frey, H.; Schollmeyer, D.; Kilbinger, A.F.M. *Chem. Eur. J.* **2005**, *11*, 2170-2176.

[14] Abbel, R.; Schleuß, T.W.; Frey, H.; Kilbinger, A.F.M. *Macromol. Chem. Phys.* **2005**, *206*, 2067-2074.

[15] Schleuss, T.W.; Abbel, R.; Gross, M.; Schollmeyer, D.; Frey, H.; Maskos, M.; Berger, R.; Kilbinger, A.F.M. *Angew. Chem. Int. Ed.* **2006**, *45,* 2969-2975.

[16] Seyler, H.; Berger-Nicoletti, E.; Kilbinger, A.F.M. *J. Mater. Chem.* **2007**, *17*, 1954-1957.

[17] Ballauff, M. *Makromol. Chem., Rapid. Commun*. **1986**, *7*, 407-414.

[18] Ballauff, M. *Makromol. Chem., Rapid. Commun*. **1987**, *8*, 93-97.

[19] Wenzel, M.; Ballauff, M.; Wegner, G. *Makromol. Chem*. **1987**, *188*, 2865-2873.

[20] Herrmann-Schönherr, O.; Wendorff, J.H.; Ringsdorf, H.; Tschirner, P. *Makromol. Chem., Rapid Commun*. **1986**, *7*, 791-796.

[21] Ballauff, M. *Angew. Chem. Int. Ed*. **1989**, *28*, 253-267.

[22] Bosshard, H.H.; Mory, R.; Schmid, M.; Zollinger, H. *Helv. Chim. Acta* **1959**, *176*, 1653-1658.

[23] using the software ***Spartan '06***, Wavefunction, Inc. Irvine, CA

[24] Parra, R.D.; Zeng, H.; Zhu, J.; Zheng, C.; Zeng, X.C.; Gong, B. *Chem. Eur. J*. **2001**, *7*, 4352-4357.

[25] Gong, B.; Zeng, H.; Zhu, J.; Yuan, L.; Han, Y.; Cheng, S.; Furukawa, M.; Parra, R.D.; Kovalevsky, A.Y.; Mills, J.L.; Skrzypczak-Jankun, E.; Matrinovic, S.; Smith, R.D.; Zheng, C.; Szyperski, T.; Zeng, X.C. *Proc. Nat. Acad. Sci*. **2002**, *99*, 11583-11588.

[26] See Cambridge Crystallographic Data Centre compound CCDC-283302. Crystallographic data can be obtained free of charge from The Cambridge Crystallographic Data Centre via www.ccdc.cam.ac.uk/data_request/cif.

[27] Takahashi, A.; Sakai, M.; Kato, T. *Polymer J*., **1980**, *12*, 335-341.

3.1.6. Supporting Information for "Tuning Oligo(*p*-benzamide) Aggregation via Heterosequences"

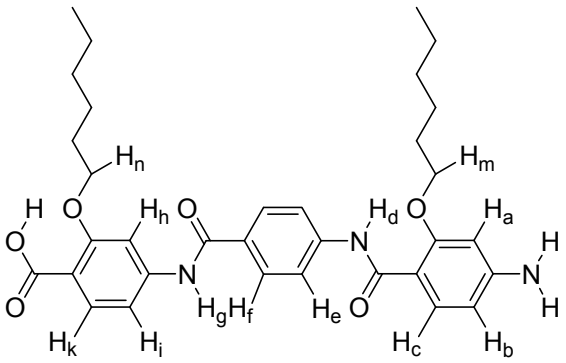

Figure SI-3.1.1. Structure and proton assignment for model compound **7**.

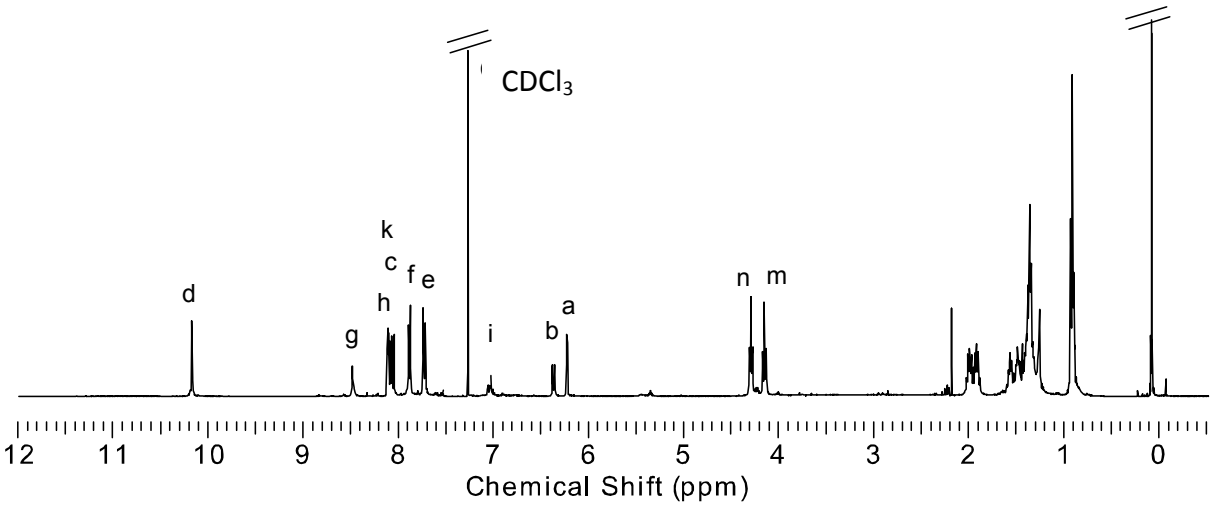

Figure SI-3.1.2. ^{1}H-NMR spectrum (300 MHz) of **7** in chloroform-*d*.

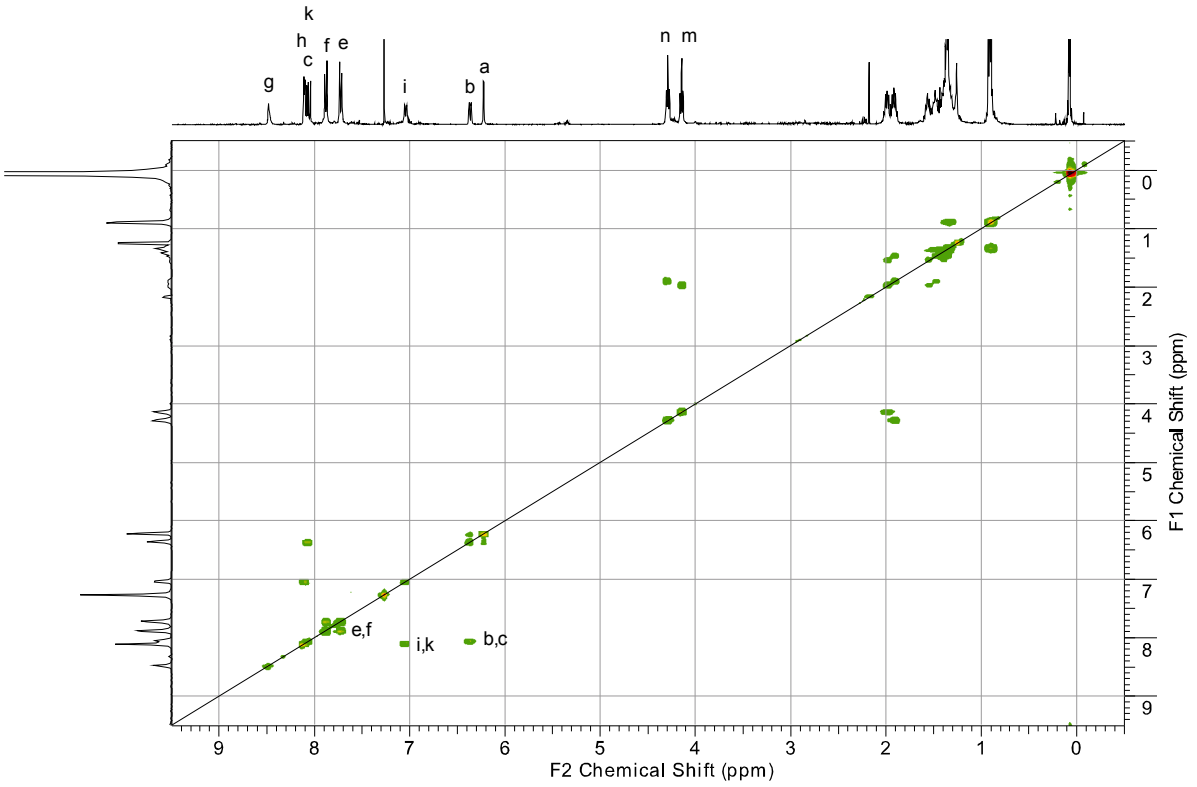

Figure SI-3.1.3. COSY-NMR spectrum (300 MHz) of **7** in chloroform-*d*.

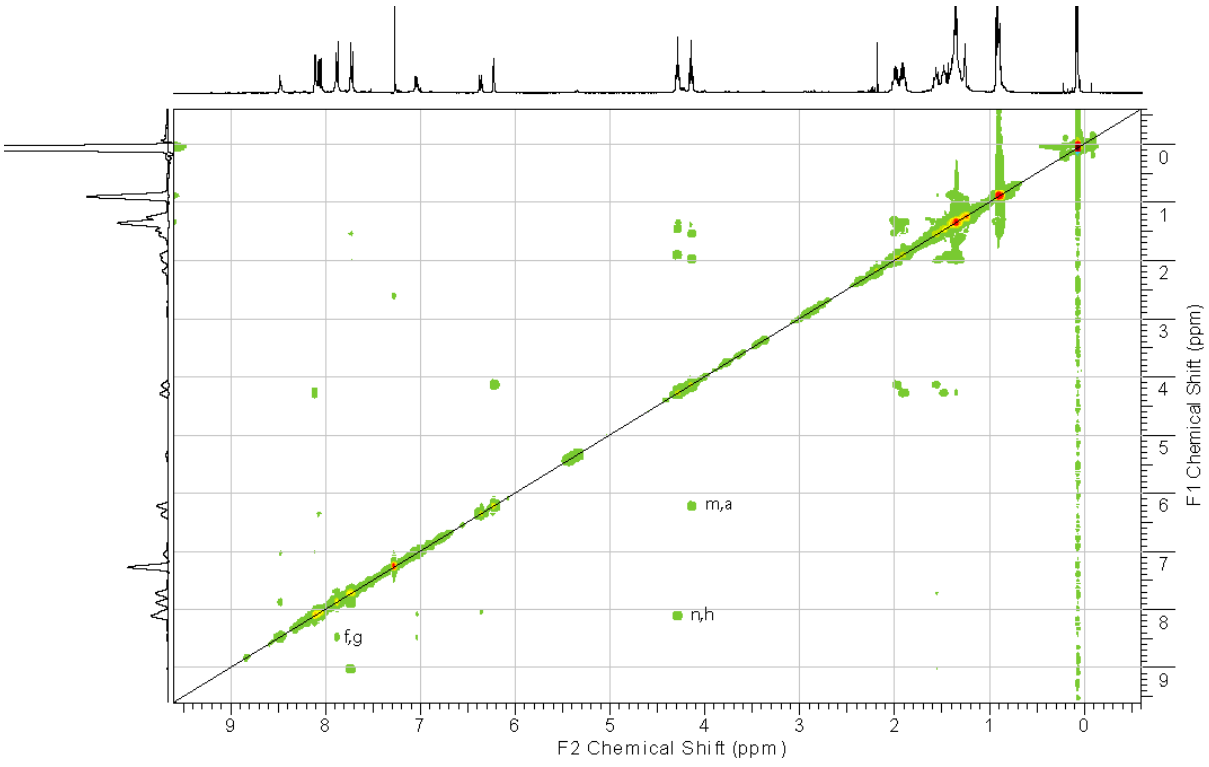

Figure SI-3.1.4. NOESY-NMR spectrum (300 MHz) of **7** in chloroform-*d*.

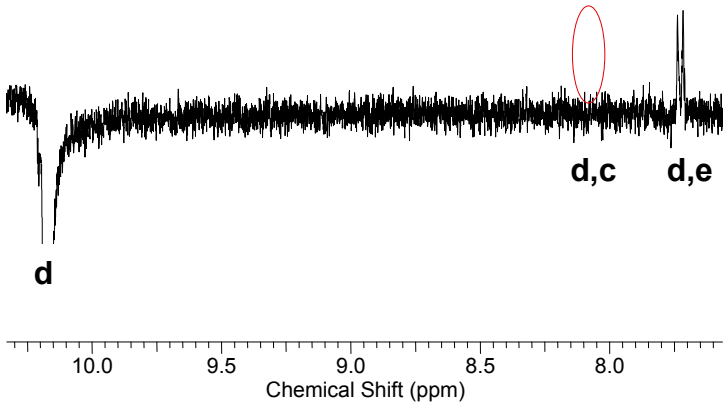

Figure SI-3.1.5. NOE NMR spectrum (300 MHz) of **7** in $CDCl_3$.

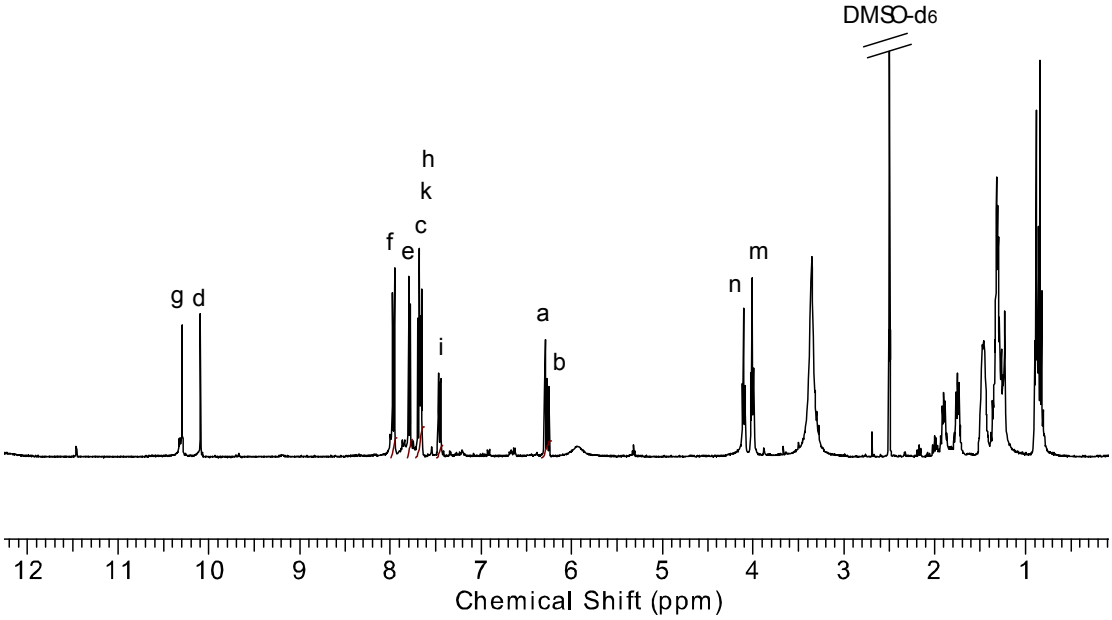

Figure SI-3.1.6. ^{1}H-NMR spectrum (300 MHz) of **7** in DMSO-d_6.

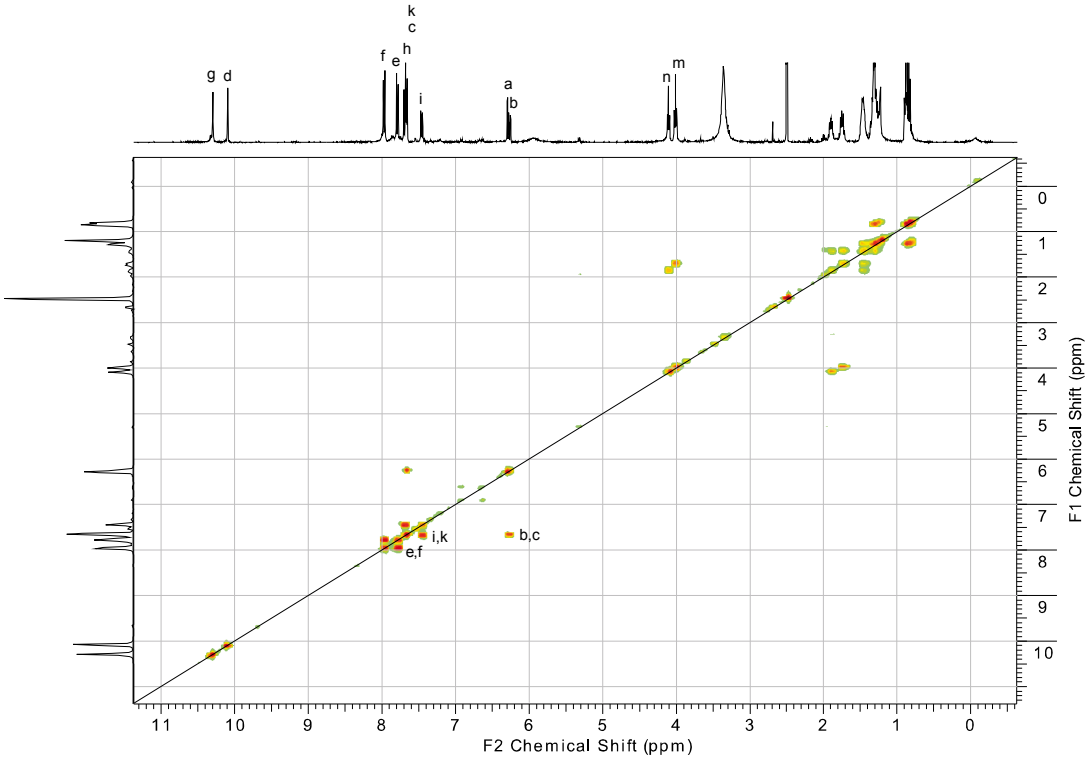

Figure SI-3.1.7. COSY-NMR spectrum (300 MHz) of **7** in DMSO-d_6.

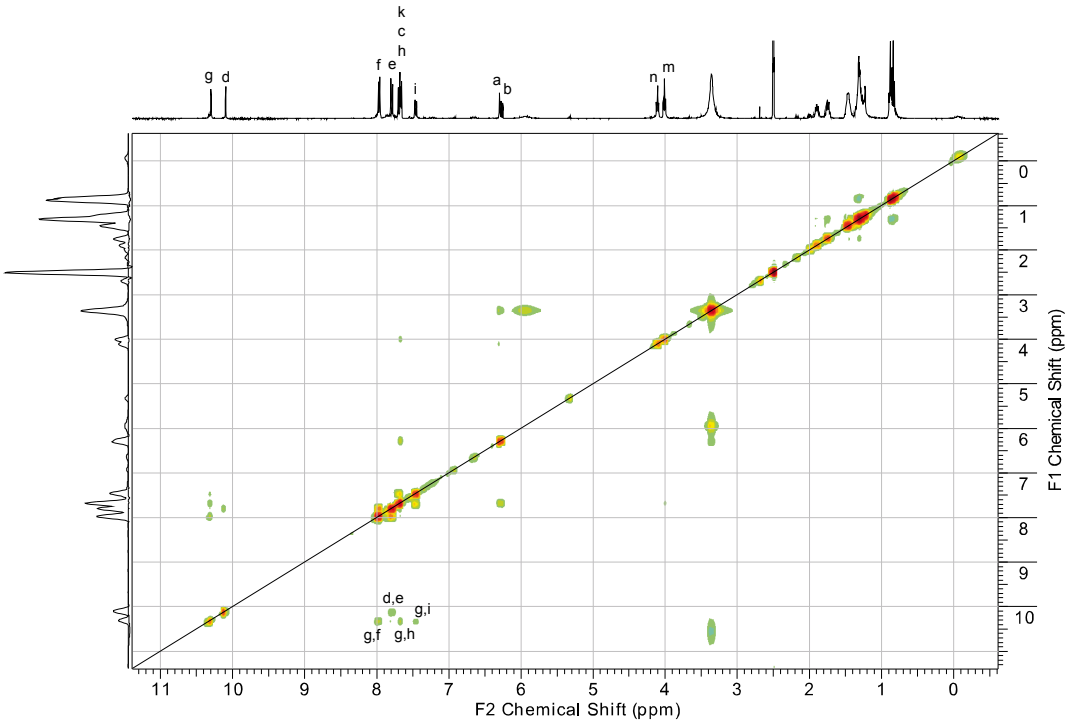

Figure SI-3.1.8. NOESY-NMR spectrum (300 MHz) of **7** in DMSO-d_6.

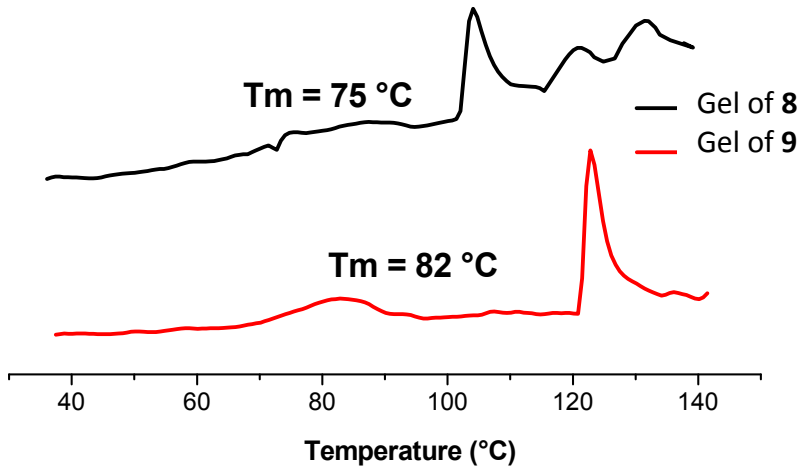

Figure SI-3.1.9. Melting temperatures of the gels determined by DSC (heating rate 40°C min^{-1}).

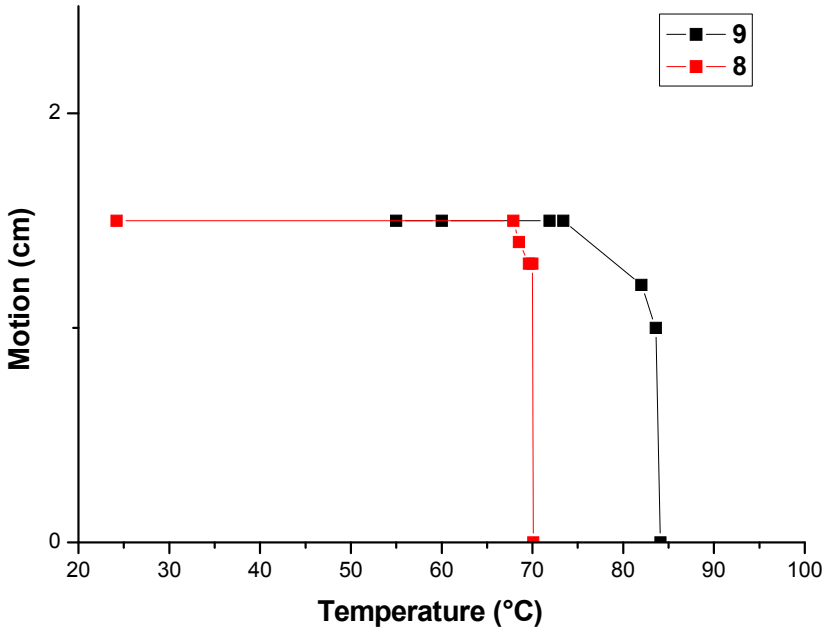

Figure SI-3.1.10. Melting temperatures of the gels **8** and **9**, determined by the dropping ball method.

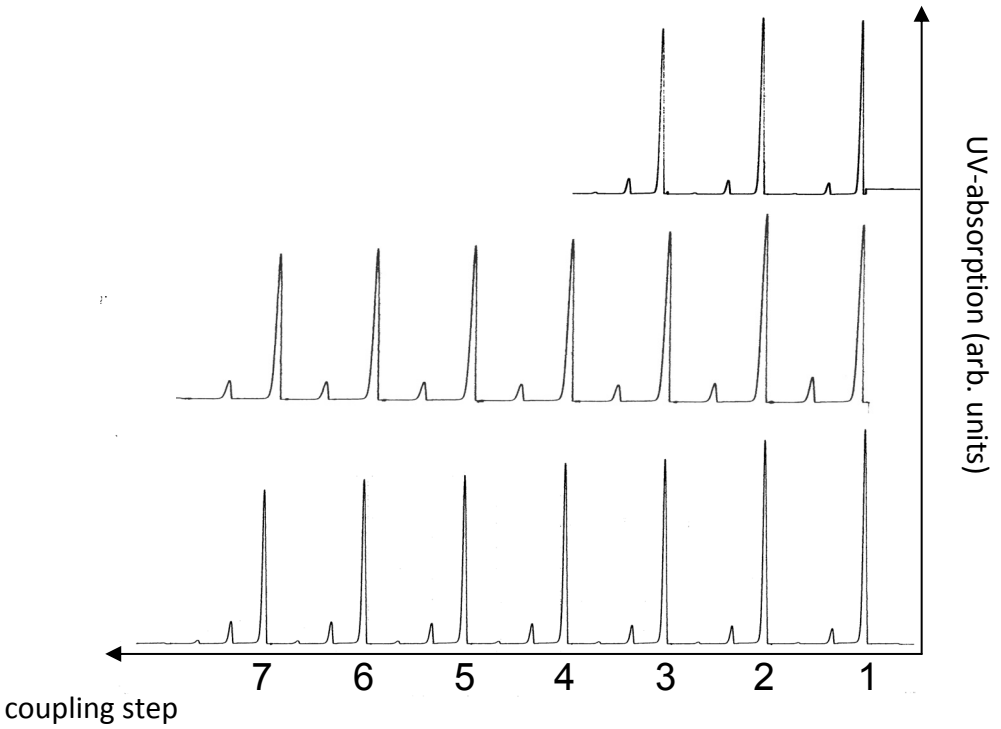

Figure SI-3.1.11. Fmoc-UV detection for hetero- trimer **7** (*top*), -heptamers **8** (*middle*) and **9** (*bottom*).

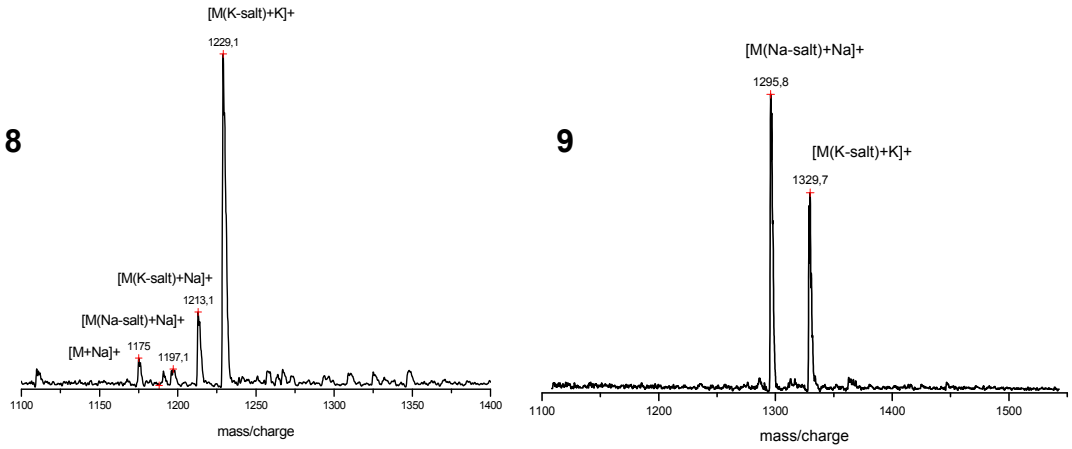

Figure SI-3.1.12. MALDI-TOF mass spectra of oligomers **8** (*left*) and **9** (*right*).

3.2. Molecular Zippers

*Helga Seyler and Andreas Kilbinger**

Abstract

The focus of the research presented in this chapter is the evaluation of the ability of the heterosequences **1** and **2** to form a double stranded hetero-complex.
The introduction of hydrogen bond acceptors in *ortho* position to the amide group allows the conformational control of the OPBA-rotamers based on specific interactions between remote sites in the oligomeric structure. An alternating substitution pattern of the side chains saturates in a selective way all H-bonding donors on one edge of the rigid rod, promoting the conformational restriction of the oligomers. Investigations on the ability of these materials to form defined hybridized strands allow the greater understanding of the aggregation behavior of the OPBAs.

Kurzfassung

Die automatische sequenzkontrollierte Synthese von Oligo(*p*-benzamiden) an der Festphase wurde für die Herstellung von hexyloxy-funktionalisierten Benzamiden eingesetzt. Die Alkyloxysubstituenten in *ortho*-Position zu den Amid-Carbonylen erhöhen die Löslichkeit der stabförmigen Moleküle und dienen als Wasserstoffbrückenakzeptoren zur Konformationskontrolle der Rotamere. Ein alternierendes Substitutionsmuster erlaubt die selektive Absättigung der Amid-wasserstoffe und die Hydrophobisierung einer Molekülseite. Die Fähigkeit dieser formtreuen Moleküle doppelsträngige Komplexe in Lösung zu bilden, wurde im Rahmen dieser Arbeit untersucht.

3.2.1 Introduction

Multiple hydrogen bonding motifs have been designed for the development of complexes with high stability and selectivity for the better understanding of strand pairing interactions in biology, the preparation of new materials and self-assembly tools at the nanometer scale.[1] In recent years, much effort has been devoted to the design and characterization of artificial oligomers capable of pairing into duplexes stabilized by (self)-complementary hydrogen bond arrays based on alternating arrays of hydrogen-bond donors and acceptors.[2]

Association strength between multiple hydrogen bonding units depends on the nature of donor and acceptor, the number of hydrogen bonds and is influenced by solvent interactions. The arrangement of the donor (D) and acceptor (A) sites within the molecule has also been shown to play an important role in the complexation strength. The AAA-DDD motif of linear arrays of three hydrogen bonding sites was shown to be the most efficient pattern,[3] with association constants exceeding 10^5 M^{-1}.[4] Other very stable complexes were obtained when arrays of 4,[1(g)] 6^5 or 8^6 hydrogen bonding units were employed.

Aromatic oligoamides have been designed to assemble in linear dimers using complementary hydrogen bonding patterns, where two strands are supposed to adopt a ladder (or zipper) like conformation.[5,7,8,9]

To achieve high binding stability and selectivity, predictable preorganization and rigidity of the backbones is often required. This feature can be realized by a consecutive arrangement of intramolecular hydrogen bonds.[10]

3.2.2. Results and Discussion

This chapter was dedicated to the evaluation of the ability of the heterosequences **8** and **9** to form a double stranded hetero-complex **8:9** (**figure 3.2.1**). Aramides were synthesized and fully characterized as reported previously (see **chapter 3.1**). These amphiphilic oligomers were shown to be capable to gelate organic solvents. The proposed gelation mechanism of the oligomers relies on aromatic stacking interactions, as well as inter- and intramolecular hydrogen bonding.

Hence, we wanted to evaluate whether their alternated array of hydrogen bond donors and acceptors is suitable for the formation of stable heterodimers in polar solvents.

The concentration and temperature influence on aggregation strength of the individual heterosequences was first analyzed experimentally by NMR-spectroscopy. In order to differentiate the intra- from the intermolecular hydrogen bonded N*H*s,[1]H-NMR spectra of the heptameric strand solutions were measured at different concentrations. Decreasing the concentration was expected to influence primarily the

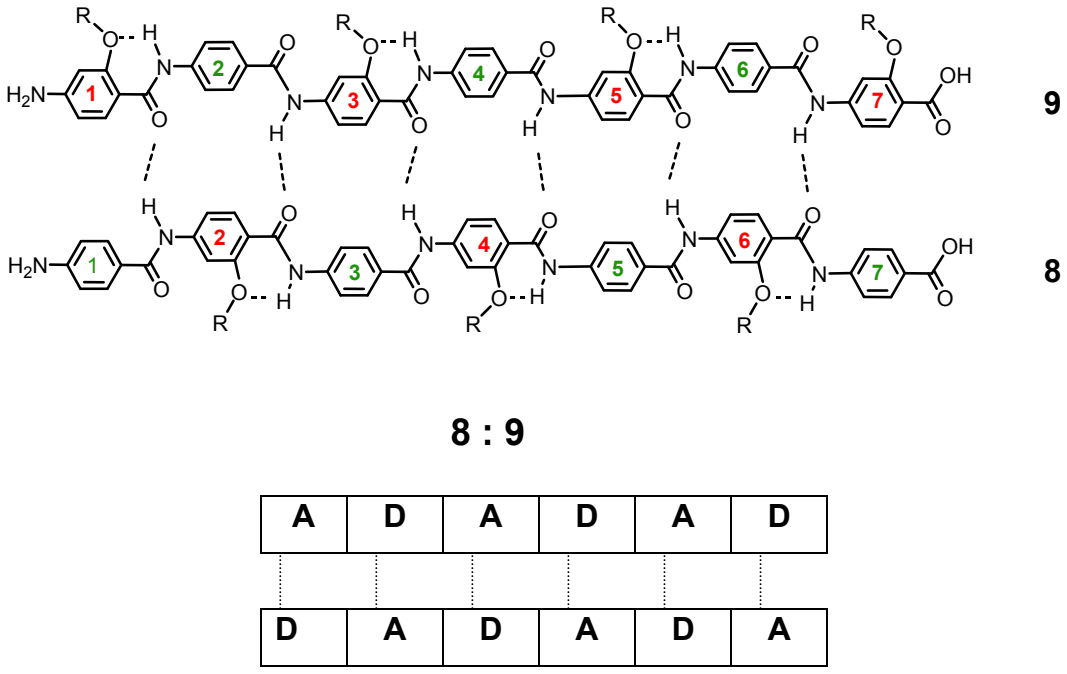

Figure 3.2.1. Proposed hetero-complex from oligomers with 2,4,6-(**8**) and 1,3,5,7-(**9**) substitution patterns (the numbers refer to the position of the monomer within the oligomer, R = hexyl) with alternating donor (D) and acceptor (A) array.

environment and thus the chemical shift of the intermolecular noncovalent bonded N*H*s. The obtained spectra are shown in the supporting information. The amide region of the proton spectra shows the differentiation of the last N*H*-amide at the *N*-terminus and two sets of protons shifted downfield. The signals at lower ppm (~ 10.28 ppm, see **figure 3.2.2**) are most probably attributed to the protons involved in the intramolecular hydrogen bonds (in analogy to the proton spectra of the model compounds shown in the supporting information). Although, no substantial shift of the amide proton signals could be observed over the concentration rage from 33 to 4.4 mg/ml. This might be due to the

high stability of the aggregates upon dilution. On the other hand, if the interstrand hydrogen bonds are broken upon dilution, as a consequence DMSO can easily interact as new *H*-bond acceptor, resulting in no substantial chemical shift. It can be emphasized, that despite dilution of the sample the two sets of protons remain present, indicating at least the high stability of the intramolecular interactions.

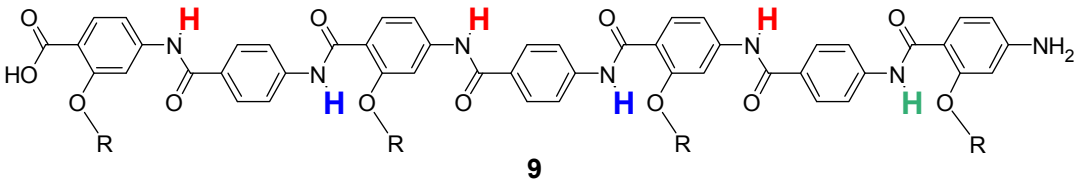

9

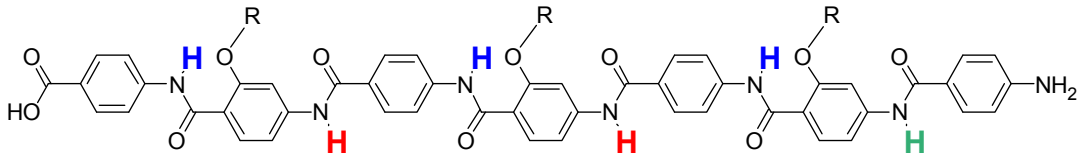

8

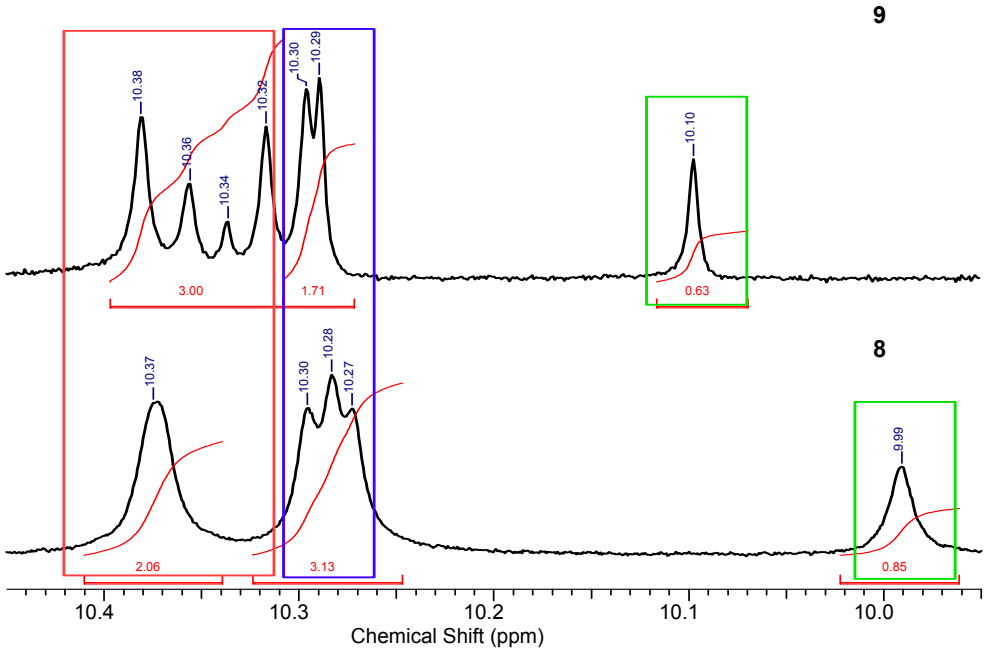

Figure 3.2.2. *NH*-Amide region of the ^{1}H-NMR spectra of compounds **8** and **9**. The N*H* –protons involved in the intramolecular H-bonds (*blue*) are shifted downfield compared to the signals of the “free” amides (*red and green*).

Regarding the sequence specific association of the complementary sequences into the hetero-duplex further titration experiments were performed. The ^{1}H- NMR spectra obtained upon addition of **9** to a solution of **8** in DMSO-d_6 at room temperature showed no chemical shifts of the proton signals from **8** due to the chemical environment changes. Stoichiometric mixture of compound **8** and **9** resulted in the same spectrum as the one obtained by addition of both individual spectra (see supporting information, **figure SI-3.2.3**).

IR-Spectroscopy was applied as a method to investigate hydrogen bond interactions in the solid state.[11] Formation of hydrogen bonds affects the vibrational modes of the groups involved in several ways.[12] The frequency of the donor N-H stretching vibration ($\nu_{N\text{-}H}$) is commonly analyzed, where red-shift of the absorption band, band broadening or intensification may occur due to hydrogen bond interactions. A direct effect of the hydrogen bond formation can often be observed also on the acceptor side. In NH--O=C bonds for example, the O=C bond is weakened, leading to a lowering of the stretching vibration frequency.

FT-IR measurements of the heterosequences and 1:1 mixture were analyzed, although no significant change of the absorption bands could be detected (see supporting info, **figure SI-3.2.4**). This can be explained by the fact, that H-bonding interactions (of intra- and intermolecular origin) are present in all samples and the structural difference between aggregates of the same strands and the hetero-duplex is too small to detect.

Photochemical investigation of the individual heterosequences and stoichiometry mixture was performed first by UV-vis experiments in DMSO. If hybridization is favored and no other self-assembly mechanism takes place, the aggregation tendency of the compounds should be reduced and only the formation of dimers should be observed. This effect was expected to be detected by changes in the absorption spectra (e.g by a bathochromic shift or the appearance of a new band). It was impossible to make any statement in this context, since the absorptions spectra of the three samples showed no detectable differences (see supporting information, **figure SI-3.2.5**).

Excimer fluorescence can be used to monitor close interactions between molecules. The most popular fluorophore is pyrene[13] and innumerable examples of inter- and intramolecular excimer formation involving pyrene residues have been reported.[14]

Pyrene was employed here as the fluorophore to take advantage of its intense fluorescence and well-studied photochemistry[15] to examine the relative spatial

orientation of the single and mixed rod solutions. For this purpose, both heterosequences were labeled using pyrene butyric acid.

The emission spectrum of pyrene is known to be sensitive to changes in solute concentration or environment polarity. The solvent polarity influences its vibronic structure; the ratio of the fluorescence intensity of the first to the third vibronic peaks (Ham bands) ranges from ~0.6 in hydrocarbon media to ~2 in DMSO.[16]

The pyrene spectral properties are dependent upon its relative proximity to other neighboring pyrene molecules. Excitation (348 nm) of ground-state pyrene monomers gives rise to excited-state monomers with typical emission maxima between 370 and 420 nm. An excited-state monomer can interact with a spatially proximal ground state pyrene moiety to form an excited-state dimer or "excimer", with characteristic emission bands at 460 nm. Excimer emission arises only from stacked pyrenes in close proximity (in the excimer of pure pyrene the distance between the pyrenes has been estimated to be 3.4 Å).[16]

Thus pyrene butyric acid was converted *in situ* into the corresponding acid chloride by treatment with oxalyl chloride, as shown in **scheme 3.2.1**. The pyrene butyroyl chloride **11** was then coupled to the heptamers **8** and **9** in moderate yields. The products **12** and **13** were characterized by NMR- (see supporting information **figures SI-3.2.6** and **3.2.7** and fluorescence spectroscopy techniques (see below).

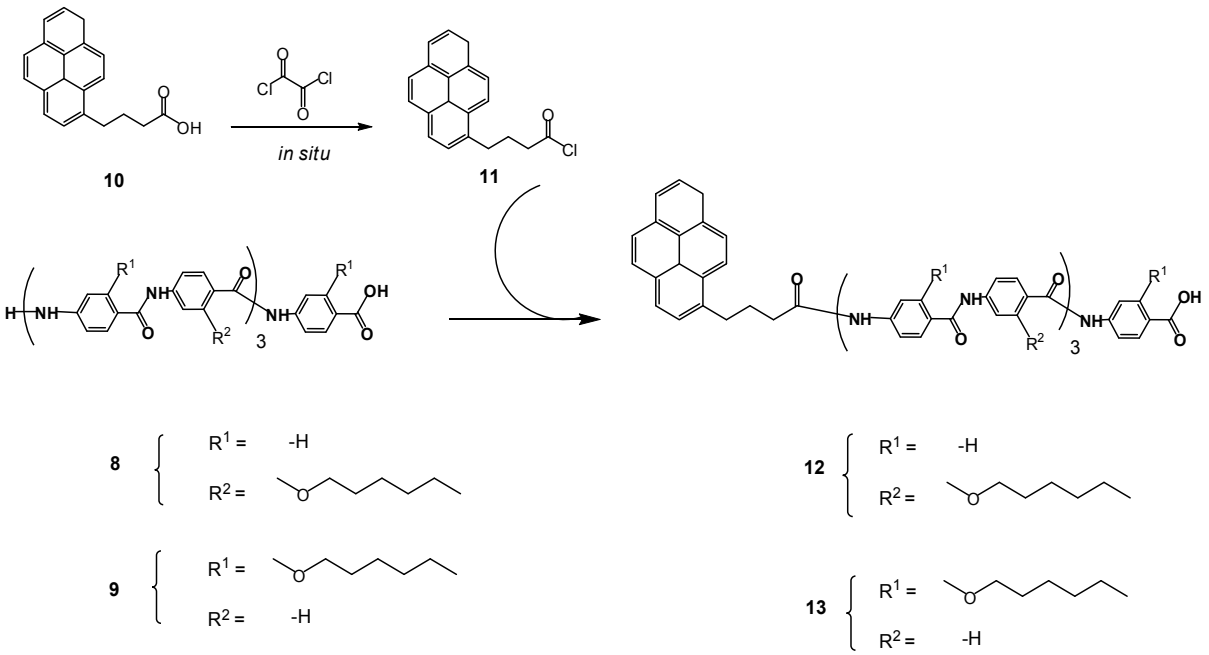

Scheme 3.2.1. Synthetic scheme for the preparation of the pyrene-labeled heptamers.

Fluorescence spectra recorded for diluted solutions of **12** and **13** are shown in **figure 3.2.3**. For the case of compound **12** there was an absence of excimer fluorescence in the region around 460 nm (**figure 3.2.3**, *black* curve). For compound **13** and the stoichiometric (1:1) mixture, the fluorescence spectra show both monomer and excimer formation, although the excimer band is not as intense as may be expected for perfectly stacked pyrenes (**figure 3.2.3**, *red* and *green* curves).

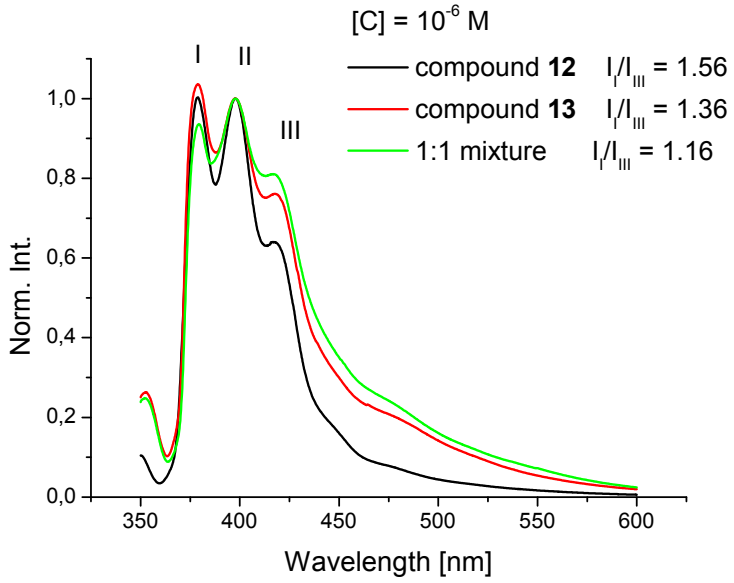

Figure 3.2.3. Fluorescence emission spectra of the individual pyrene-labeled heptamers **12** and **13** and stoichiometric (1:1) solutions in DMSO ([c] = 1μM).

Analysis of the intensity ratio of the bands I_I/I_{III} shows the polarity decrease of the pyrene environment when increasing the numbers of hexyl substituents on the aramide block. The 1:1 mixture shows the lowest polarity around the pyrene moiety. From this observation, the assembly driven by hydrogen bond interactions for the 1:1 mixture could be similar to the one proposed in **figure 3.2.4**.

This model is only true for a head to head arrangement of the rods, where the slide of the strands relative to each other could differ from the arrangement proposed below (see **figure 3.2.4**). This aggregation mechanism does not allow the superposition of the fluorescent dye, other than by interstrand π-π stacking. The fact that no excimer fluorescence is observed could be most probably attributed to alkyl chain-pyrene interaction induced by the molecule amphiphilicity.

It has to be mentioned, that this method presents two major disadvantages. Very dilute concentrations (<10^{-4} mM) must be used for excimer interpretation, hence disfavouring intermolecular interactions. Another problem could be the fluorescence quenching by residual molecular oxygen in the samples.

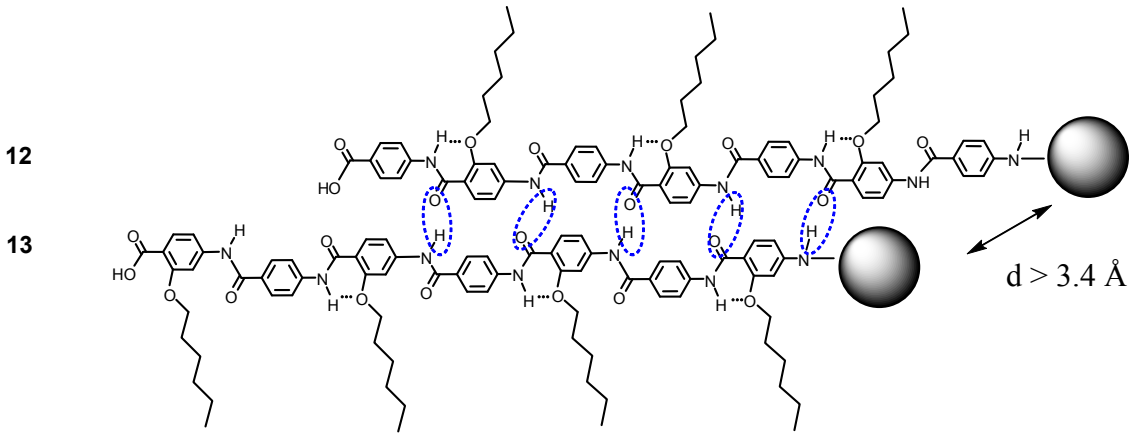

Figure 3.2.4. "*Head to head*" arrangement proposed from the fluorescence experiments. The fluorophore is represented by the grey spheres. Pyrene-pyrene interaction becomes unlikely, due to the relative spatial shift of one rod.

3.2.3. Conclusion

Various studies were performed on the dimerization of alkoxy-substituted hepta(*p*-benzamide) heterosequences **8** and **9**. The introduction of the hexyloxy substituents enhances the solubility of the aramides compared to the unsubstituted *p*-benzamides, allowing their characterization in DMSO solutions. Attempts have been made to verify the hypothesis of the hetero-dimer complex formation using a variety of analytical methods, including nuclear magnetic resonance, FT-IR and UV-vis techniques. Analyses were performed for each heterosequence as well as for the stoichiometric mixture. The oligomers were successfully functionalized with pyrene butyric acid for fluorescence characterization.

However the polarity and the hydrogen bond accepting ability of this solvent hinder the evidences of the hetero-duplex motif formation. On the other hand, the self-assembly mechanisms of the individual strands and the hetero-dimer are of the same

nature. As a consequence they are difficult to be differentiated by techniques like NMR, IR and photochemical measurements.

3.2.4. Experimental Section

General.

DCM and NMP were dried over P_2O_5 and CaH_2, respectively. Both solvents were freshly destilled prior to use. All other reagents were used as received. Deuterated solvents (DMSO-d_6 and $CDCl_3$) were purchased from Deutero GmbH. The heterosequences were synthesized as described in chapter **3.1**.

Instrumentation.

Standard ^1H nuclear magnetic resonance spectra were recorded on a Bruker AMX 400 (400 MHz). Infrared spectra were performed on a Nicolet 5 DXC FT-IR spectrometer. UV-vis measurements were accomplished on a V-630 UV-VIS Spectrophotometer. Pure solvent was used as a reference. Fluorescence emission spectra were obtained on an apparatus composed of a Spex 1681 Minimate excitation monochromator, a Spex Florolog 2 spectrofluorometer, a Spex 1680 Double Spectrometer emission monochromator and a photomultiplier. For fluorescence measurements, commercial DMSO stored over molecular sieves (purchased from Fluka) was filtered prior use through a syringe filter (400 μm) and purged with argon for 15 min. The measurements were carried out at room temperature.

Compound **(13)**: Pyrene butyric acid (25 mg, 86 μmol) was suspended in dry DCM (0.5 ml) under inert atmosphere, followed by the addition of oxalyl chloride (0.5 ml). The reaction mixture was stirred for 1 h at rt. The solvent and the excess of oxalyl chloride were removed under reduced pressure. The residual solid was dissolved in dry NMP (1 ml) under argon atmosphere, added to a solution of **9** (10 mg, 7.9 μmol) in 0.5 ml dry NMP and stirred for 3 days at room temperature. The reaction mixture was then poured into 20 ml of cold diethyl ether and the resulting precipitate centrifuged, washed again with diethyl ether, DCM and acetone to obtain **13** (5.1 mg, 42 %). The absence of pyrene butyric acid was confirmed by TLC using methanol as a solvent.

^{1}H-NMR: δ (400 MHz, DMSO-d_6) 0.82-0.89 (m, 12 H); 1.20-1.53 (m, 26 H); 1.72-1.93 (m, 8 H); 2.12-2.20 (m, 2 H); 3.39-3.44 (m, 2 H); 3.98-4.21 (m, 8 H); 7.24-8.44 (m, 33 H); 10.18-10.40 (m, 7 H).

Compound **(12)**: **12** was synthesized following the same procedure as described for **13**, starting with 15.9 mg (18.8 μmol) to obtain 12 mg of product (8.4 mmol, 61 %).

^{1}H-NMR: δ (400 MHz, DMSO-d_6) 0.79-0.85 (m, 9 H); 1.25-1.48 (m, 22 H); 1.83-1.93 (m, 6 H); 4.15-4.17 (m, 6 H); 7.54-8.45 (m, 34 H); 10.25-10.37 (m, 7 H).

3.2.5. References

[1] (a) Djurdjevic, S.; Leigh, D. A.; McNab, H.; Parsons, S.; Teobaldi, G.; Zerbetto, F. *J. Am. Chem. Soc.* **2007**, *129*, 476-477, (b) Zimmerman, S. C.; Corbin, P. S. *Struct. Bonding (Berlin)* **2000**, *96*, 63-94, (c) Brunsveld, L.; Folmer, B. J. B.; Meijer, E. W.; Sijbesma, R. P. *Chem. Rev.* **2001**, *101*, 4071-4097, (d) Prins, L. J.; Reinhoudt, D. N.; Timmerman, P. *Angew. Chem., Int. Ed.* **2001**, *40*, 2383-2426, (e) Schmuck, C.; Wienand, W. *Angew. Chem., Int. Ed.* **2001**, *40*, 4363-4369, (f) Sherrington, D. C.; Taskinen, K. A. *Chem. Soc. Rev.* **2001**, *30*, 83-93, (g) Sijbesma, R. P.; Meijer, E. W. *Chem. Commun*. **2003**, 5-16, (h) Zimmerman, S. C.; Park, T. *Polym. Prepr.* **2005**, *42*, 1159-1160.

[2] Hill, D. J.; Mio, M. J.; Price , R. B.; Hughes, T. S.; Moore, J. S. *Chem. Rev.* **2001**, *101*, 3893-4011.

[3] (a) Jorgensen, W. L.; Pranata, J. *J. Am. Chem. Soc.* **1990**, *112*, 2008-2010, (b) Pranata, J.; Wierschke, S. G.; Jorgensen, W. L. *J. Am. Chem. Soc.* **1991**, *113*, 2810-2819.

[4] (a) Murray, T. J.; Zimmerman, S. C. *J. Am. Chem. Soc.* **1992**, *114*, 4010-4011, (b) Zimmerman, S. C.; Murray, T. J. *Tetrahedron Lett.* **1994**, *35*, 4077-4080.

[5] Zeng, H.; Miller, R. S.; Flowers, R. A.; Gong, B. *J. Am. Chem. Soc.* **2000**, *122*, 2635-2644,

[6] Folmer, B. J. B.; Sijbesma, R. P.; Kooijman, H.; Spek, A. L.; Meijer, E. W. *J. Am. Chem. Soc.,* **1999**, *121*, 2001-2007.

[7] (a) Huc, I. *Eur. J. Org. Chem*. **2004**, 17-29, (b) Gong, B.; Yan, Y.; Zeng, H.; Skrzypczak-Jankunn, E.; Wah Kim, Y.; Zhu, J.; Ickes, H. *J. Am. Chem. Soc.* **1999**, *121,* 5607-5608, (c) Zeng, H.; Ickes, H.; Flowers, R. A.; Gong, B. *J. Org. Chem.* **2001**, *66*, 3574-3583, (d) Zeng, H.; Yang, X.; Flowers, R. A.; Gong, B. *J. Am. Chem. Soc.* **2002**, *124*, 2903-2910, (e) Yang, X.; Martinovic, S.; Smith, R. D.; Gong, B. *J. Am. Chem. Soc.* **2003**, *125*, 9932-9933, (f) Li, M.; Yamato, K.; Ferguson, J. S.; Gong, B. *J. Am. Chem. Soc.*, **2006**, *128* (39), 12628–12629.

[8] (a) Zeng, H.; Yang, X.; Flowers, R. A.; Gong, B. *J. Am. Chem. Soc*. **2002**, *124*, 2903, (b) Yang, X. W.; Gong, B. *Angew. Chem. Int. Ed.* **2005**, *44*, 1352.

[9] (a) Nowick, J. S.; Chung, D. M. *Angew. Chem., Int. Ed.* **2003**, *42*, 1765, (b) Chung, D. M.; Nowick, J. S. *J. Am. Chem. Soc.* **2004**, *126*, 3062.

[10] Zhu, J.; Lin, J. B.; Xu, Y. X.; Shao, X. B.; Jiang, X. K.; Li, Z. T. *J. Am. Chem. Soc.* **2006**, *128*, 12307-12313.

[11] Jeffrey, G. A. *An Introduction to Hydrogen Bonding*, Oxford University Press, Oxford, **1997**.

[12] Steiner, T. *Angew. Chem. Int. Ed.* **2002**, 41, 48-76.

[13] Birks, J. B.; Dyson, D. J.; Munro, I. H. *Proc. R. Soc. London, Ser A* **1963**, *275*, 575-588.

[14] (a) Shazmann, B.; Alhashimy, N.; Diamond, D. *J. Am. Chem. Soc.* **2006**, *128*, 8607-8614, (b) Kim, S. H.; Kim, J. S.; Park, S. M.; Chang,S.-K. *Org. Lett.* **2006**, *8*, 371 – 374, (c) Xiao, X.; Xu, W.; Zhang, D.; Xu, H.; Liu, L.; Zhu, D. *New J. Chem.* **2005**, *29*, 1291-1294, (d) Yuasa, H.; Miyagawa, N.; Izumi, T.; Nakatani, M.; Izumi, M.; Hashimoto, H. *Org. Lett.* **2004**, *6*, 1489-1492, (e) Yuasa, H.; Miyagawa, N.; Nakatani, M.; Izumi, M.; Hashimoto, H. *Org. Biomol. Chem.* **2004**, *2*, 3548-3556.

[15] (a) Birks, J. B. *Organic Molecular Photophysics*; John Wiley and Sons, New York, **1973**; (b) Murov, S. L.; Carmichael, I.; Hug, G. L. *Handbook of Photochemistry,* 2nd Ed.; Marce Dekker: New York, **1993**.

[16] Birks, J. B. *In Photophysics of Aromatic Molecules*; John-Wiley and Sons, New York, **1970**.

3.2.6. Supporting Information for "Molecular Zippers"

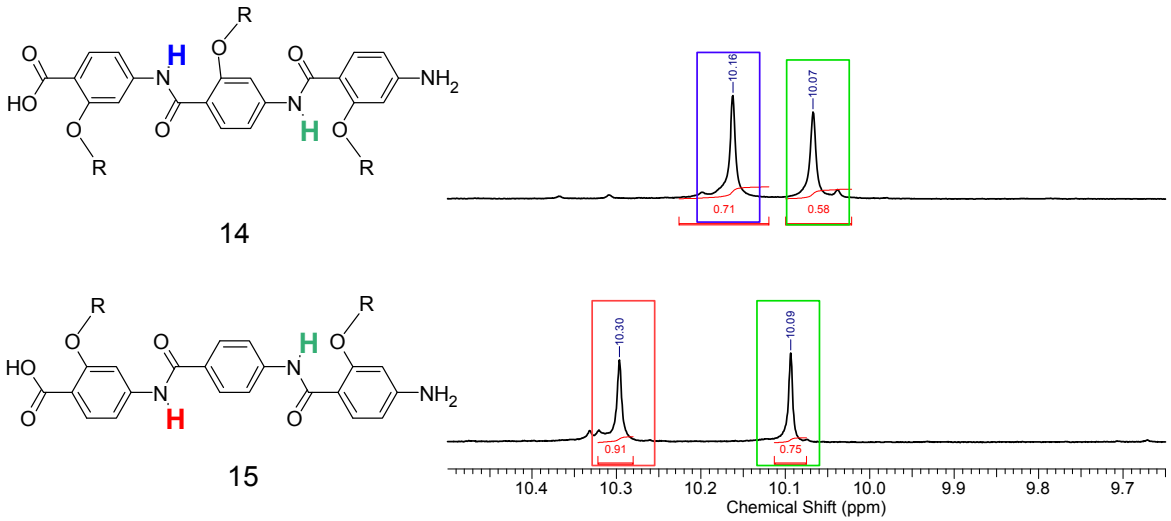

Figure SI-3.2.1. Part of the ^{1}H-NMR (400 MHz) spectra of trimer **14** (*upper line*) and trimer **15** (*lower line*) in DMSO-d_6. The N*H* –proton involved in the intramolecular H-bond in trimer **14** is shifted to higher fields compared to the "free" N*H* –proton in **15**. This shift results from the higher electron density in the central aromatic ring.

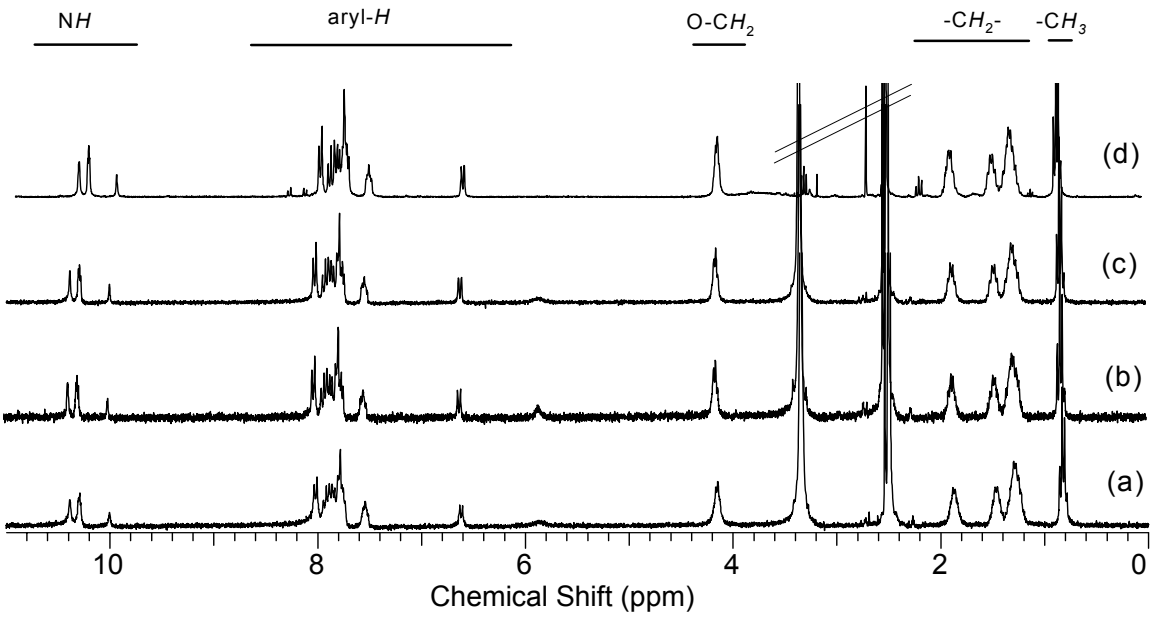

Figure SI-3.2.2. ^{1}H-NMR spectra (400 MHz) of **8** in DMSO-d_6 at different concentrations: (a) gel (7.6 mM), (b) 4.4 mM, (c) 7.6 mM and (d) 28 mM.

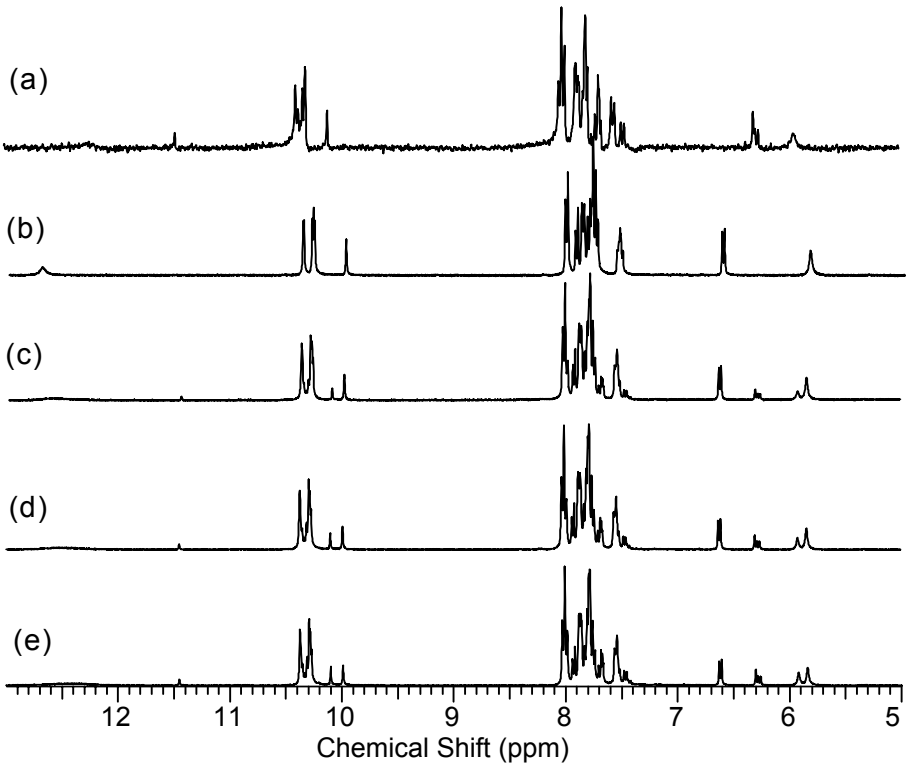

Figure SI-3.2.3. Part of the ^{1}H-NMR (400 MHz, 298 K) spectra of **9** (a) and **8** in the absence (b) and in the presence of 0.3 eq. (c), 0.7 eq. (d) and 1 eq. of **1** (e).

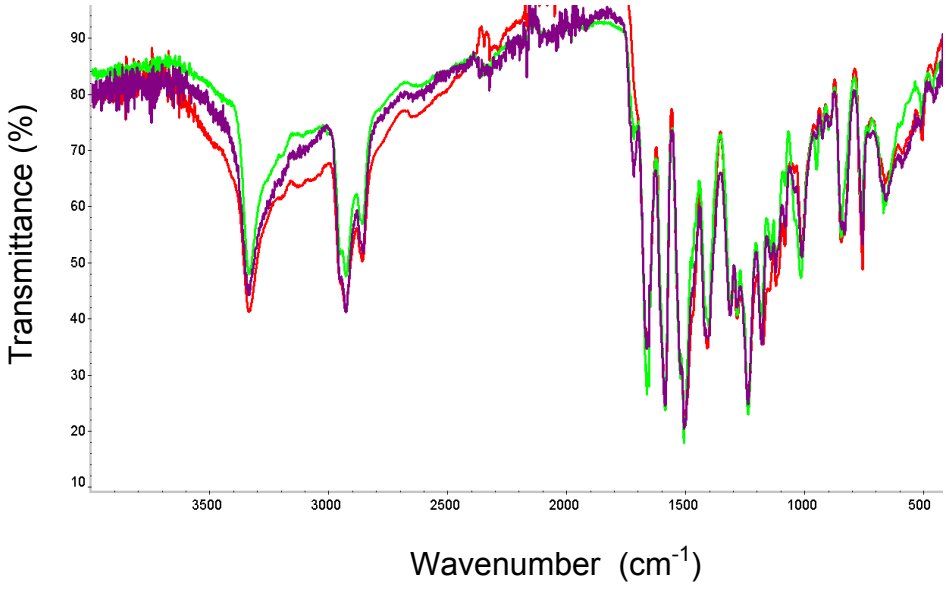

Figure SI-3.2.4. FT-IR Spectra of **8** (*red*), **9** (*orange*), and 1:1 mixture (*green*). No shift or broadening of the amide or carbonyl absorption bands are observed in the spectrum of the mixture. The later was prepared by heating a 1:1 stoichiometric solution in DMSO (393 K), followed by removal of the solvent under reduced pressure.

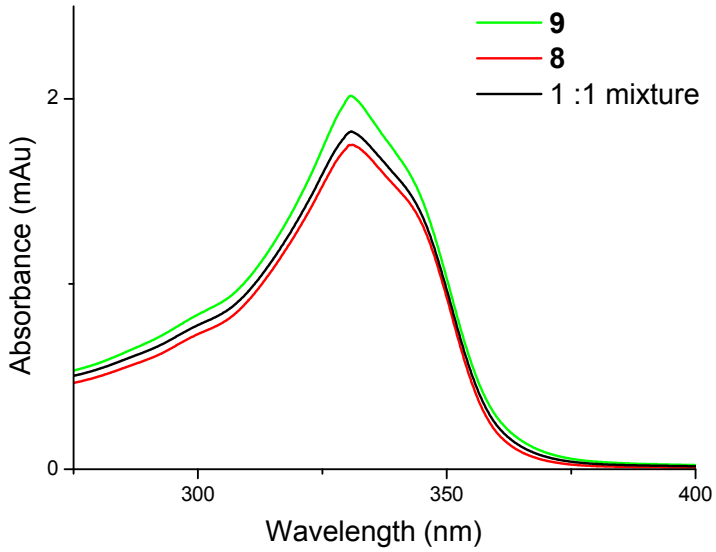

Figure SI-3.2.5. UV-vis spectra of the heterosequences **8** and **9** and 1:1 mixture in DMSO ([c] = 0.01 mM). No detectable differences in the absorption spectra are observed.

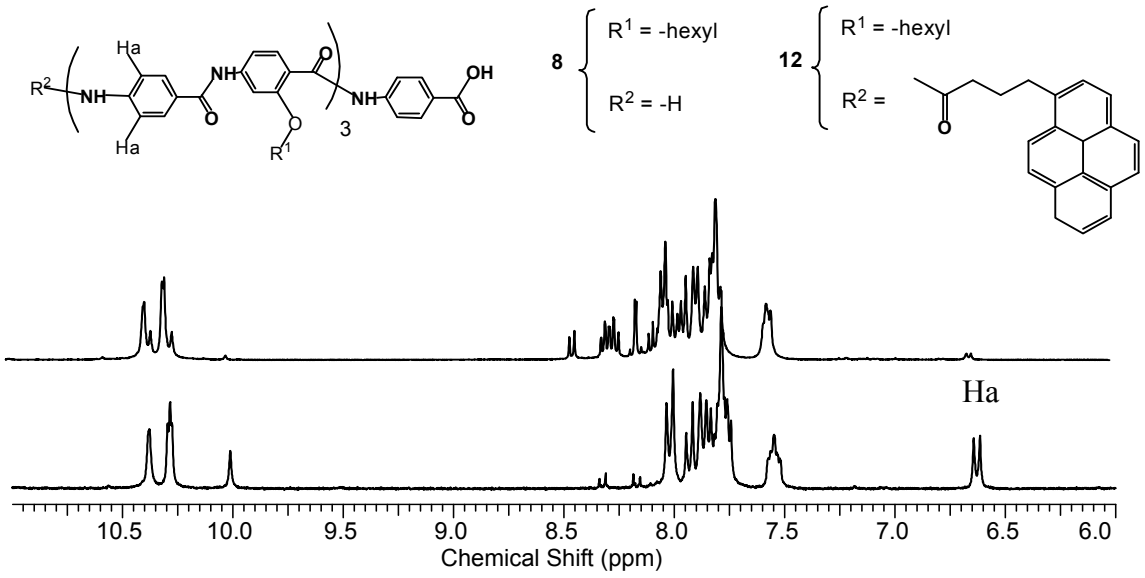

Figure SI-3.2.6. Part of the ^{1}H-NMR spectra of **8** (*bottom*) and **12** (*top*) and in DMSO-d_6 (400 MHz, 298 K). The functionalization can be monitored by the upfield shift of the proton signals at 6.6 and 10 ppm.

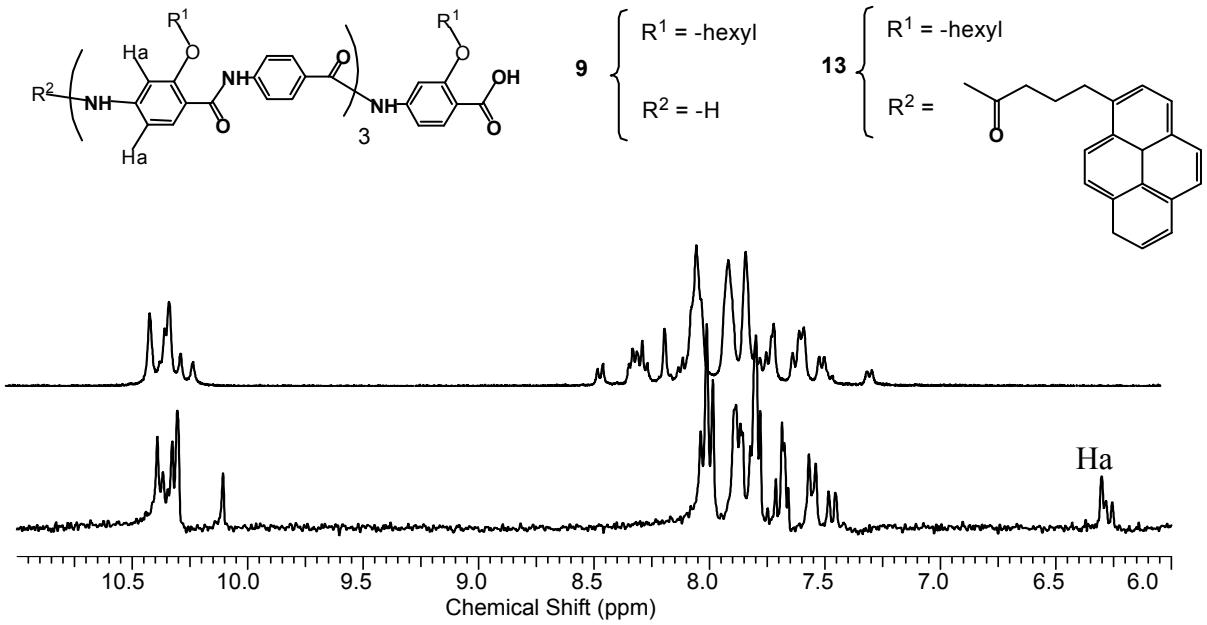

Figure SI-3.2.7. Part of the ^{1}H-NMR spectra of **9** (*bottom*) and **13** (*top*) in DMSO-d_6 (400 MHz, 298 K). The functionalization can be monitored by the upfield shift of the proton signals at 6.3 and 10.2 ppm.

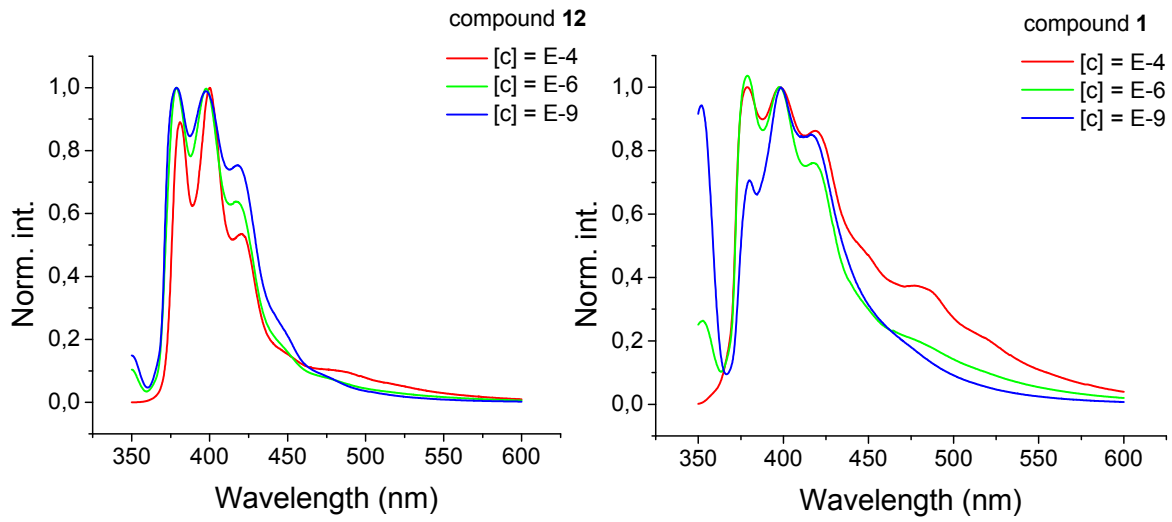

Figure SI-3.2.8. Concentration dependence of the fluorescence emission spectra of **12** and **13** in DMSO. Excitation was performed at 348 nm and emission was monitored between 350 and 600 nm. From the comparison of the spectra in **figure SI-3.2.8**, 1 μM solution concentrations were chosen for the measurements of 1:1 stoichiometry. It is known that at this concentration, solutions of pure pyrene do not exhibit excimer formation.

3.3. Comb-like Rod-Coil Copolymers

*Helga Seyler and Andreas F.M. Kilbinger**

Abstract

Rod-Coil block copolymers composed from comb-like monodisperse oligo(*p*-benzamide)s carrying pedant alkyl chains were synthesized and their self-assembly properties were investigated. The abiotic oligopeptide block was prepared automatically on solid support using a commercial peptide synthesizer. This synthetic strategy allowed the complete sequence control for the precise array of H-bond donors and acceptors. Subsequent reaction with a PEG polymer block was performed manually. Cleavage from the solid support yielded amphiphilic polymers, which self-organized into supramolecular fibrous structures in TCM / DMSO mixtures. Well defined tape-like nanometer sized structures are thus formed due to the anisotropic nature of the aramide block as well as hydrophobic interactions of the alkyl chains.

Kurzfassung

Stab-Knäuel Copolymere aus kammartigen monodispersen Oligo(*p*-benzamiden) mit Alkyloxy-Substituenten wurden an der Festphase synthetisiert und deren Überstrukturbildung untersucht. Die Synthese der abiotischen Oligopeptide erfolgte automatisiert mit Hilfe eines Peptid-Syntheseautomaten, durch den die Monomersequenz gesteuert wurde. Der gut lösliche PEG-Block wurde anschließend manuell an die geträgerte Oligomere gebunden.
Das amphiphile Blockcopolymer bildet durch Selbstorganisation in TCM / DMSO Mischungen supramolekulare bänderähnliche Aggregate. Das vorgeschlagene Modell für die Bildung der Nanofasern umfasst die Anisotropie des Aramid-Blocks sowie die hydrophoben Wechselwirkungen zwischen den Alkyl-Substituenten.

.

3.3.1. Introduction

The principles of self-assembly based on noncovalent interactions are used to design novel polymers and conjugates with desired properties such as controlled structures and defined morphologies.[1] Rod-coil block copolymers with discrete oligomeric rod-block offer the possibility to obtain defined nanostructures with smaller domain sizes than the ones usually obtained by coil-coil copolymers. The precise control of the nano- and microstructures in synthetic polymer materials is important as it is a key-factor to achieve advanced functional control.

Amphiphiles, gel-forming molecules and anisotropic compounds can all generate fibrous structures through self-organization, having potential as building blocks for molecular engineering or as novel elements for molecular devices.[2] Amphiphilic structures can be facile used for constructing fibers of different sizes and shapes on the nanometer scale.[3] However the practical application of these nanostructures is sometimes limited by their lack of stability, due to the weakness of the hydrophobic interactions that hold the amphiphiles together. Enhancement of the stability and robustness of these self-organized structures may rely on the combination of different intermolecular interactions.[4]

Self-assembly of natural and artificial oligopeptides through hydrogen bonding patterns and robust β-sheets formation has received increased attention to design novel peptides and peptide conjugates with desired properties such as controlled fibril morphology, enhanced stability, responsive gelation, or functionalization of bio-inorganic hybrids.[5] β-Sheets are of particular interest because of their great stability and critical role in nature, for example in protein folding or in many diseases, including AIDS[6] or Alzheimer.[7] Numerous examples can be found in the literature, in which this scaffold was used for the aggregation of peptidomimetic molecules[8] and PEG-conjugates,[9] multiblock copolymers inspired by spider silk,[10] as well as the use of self-assembled oligopeptides in the manufacture of gold nanowires.[11] The conjugation of these β-sheet forming peptides to synthetic polymers such as PEG, was observed to improved solubility, enhanced stability against dilution and reduced toxicity and immuno-genicity.[12]

The self-assembly of bioinspired β-sheet forming peptide-polymer hybrids (carrying precisely defined peptide blocks) into stable fibers, tapes or helical aggregates have so far received great attention. But also non-biological compounds mimicking the

organizational motif of natural β-sheet peptides, like oligo(*p*-benzamide)s, provide an attractive alternative to stable tape-like aggregates.[13]

3.3.2. Results and Discussion

Solid-phase synthesis offers a practical synthetic route to peptide-polymer hybrids, because excess reagents and reaction by-products can be washed away, while the desired molecule remains attached to a solid support. This procedure allows also complete sequence control and automatization. Recently, we developed an iterative method for synthesizing OPBA homo-, heterosequences and their corresponding polymer-OPBA hybrids on the solid support.[14]

The automated synthesis of heterosequences of hepta(*p*-benzamide)s was previously shown in **chapter 3.1**. The introduction of hexyloxy-substituents on every second aromatic unit reduces the rotational freedom of the amide bonds due to non-covalent intramolecular interactions. X-ray crystal structure analysis of the plain trimeric *p*-benzamide[15] showed that the carbonyl functions are oriented in opposite directions to minimize the net dipole moment of the molecules. Assuming that this alternation of the carbonyls along the oligomer chain is preserved in the hexyloxy-functionalized hetero-sequences, substitution of every second aromatic unit will lead to comb-like molecules, with alkyl groups facing towards the same edge of the oligomer (see **figure 3.3.1**).

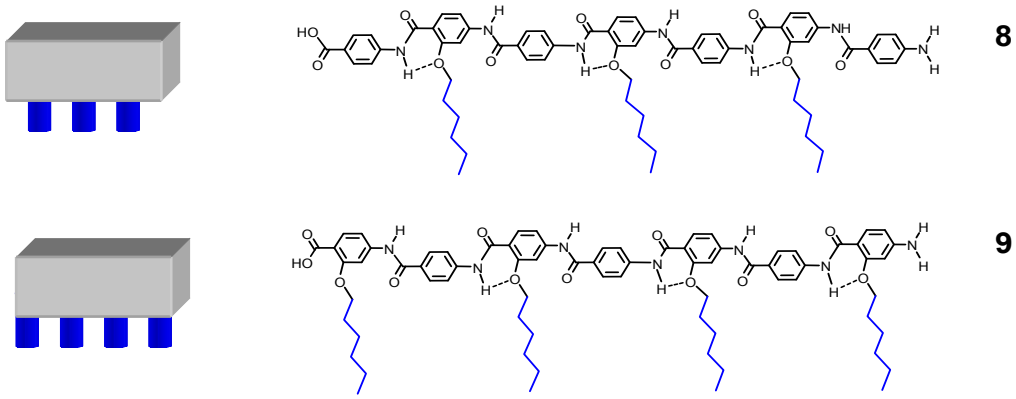

8

9

Figure 3.3.1. Chemical structure and schematic representation of comb-like hepta(*p*-benzamide) with pendant hexyl groups.

The introduction of 3 or 4 hexyloxy substitutents in heptameric *p*-benzamides showed enhanced solubility compared to the unsubstituted analogues. Dilute solutions of these

compounds in DMSO self-assemble into fibrillar networks, acting as low molecular mass organic gelators.[16]

For further analysis in solvents of lower polarity, PEG-blocks with 2000 g/mol average molecular weight were attached to the aramides **8** and **9**. For this purpose, PEG-carboxylic acid was prepared by direct oxidation of PEG-monomethyl ether using chromium trioxide.[17] Activation of the carboxylic acid into the acid chloride and further reaction with the *N*-terminus of the heptamers on the Wang resin afforded the desired PEG-functionalized heterosequences (**scheme 3.3.1**).

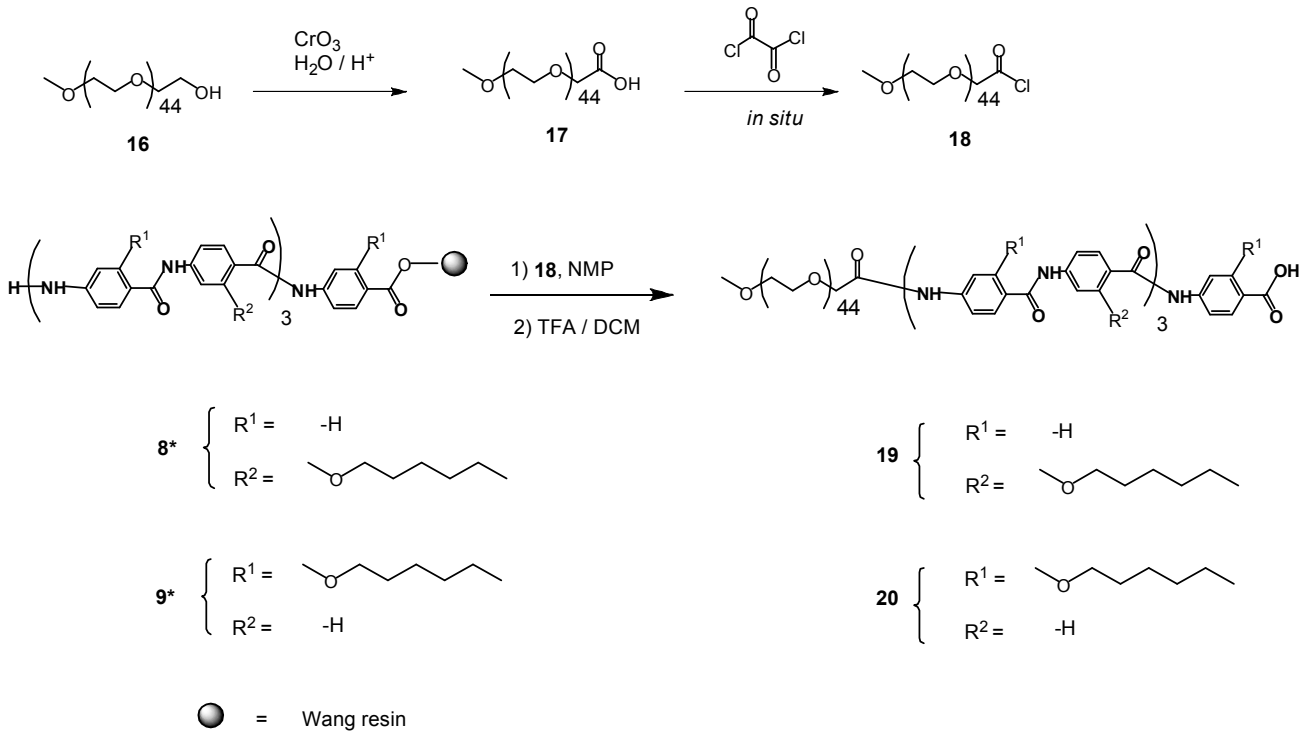

Scheme 3.3.1. PEG-functionalization of the heterosequences on the solid support (* = attached to the resin).

Cleavage from the solid support using TFA gave the final block copolymers **19** and **20**. The attachment of the soluble polymer segment improved the solubility in nonpolar solvents, however only at relatively low concentrations. The limited solubility is attributed to the high aggregation tendency of the block copolymers in such solvents. Aggregation is associated with the loss or broadening of NMR-signals, as it is observed for example for compound **20** in TCM, where the aromatic signals are not resolved at all and the aliphatic signals lost their fine structure (see **figure SI-3.3.1**). The polymers

were analyzed by NMR-spectroscopy in a polar solvent (DMSO), where all proton signals can be resolved and assigned (see **figure 3.3.2**).

Polymer **20**, carrying four hexyl groups could also be successfully characterized by MALDI-TOF mass spectrometry (see **figure 3.3.3**). The mass spectrum shows the singly charged mass distribution of the copolymer (K^+-adduct), where only one repeat unit observed, attributed to the polydisperse PEG-block. The experimental mass of the single charge species is for example 3036.4 g/mol (for 38 repeating units of ethylene glycol). The experimental value of 3036.5 agrees very well with the expected value, with only a small deviation of 0.1 units.

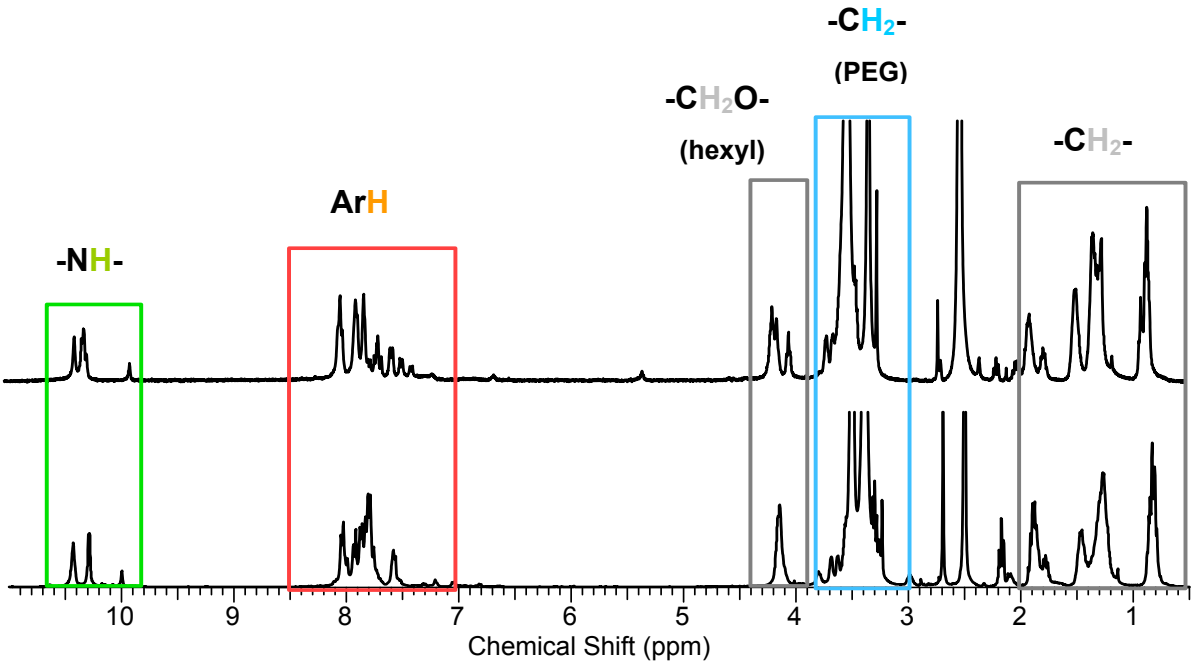

Figure 3.3.2. ^{1}H-NMR spectra (400 MHz) of **19** (*bottom*) and **20** (*top*) in DMSO-d_6 (the lower intensity signals between 2 and 3 ppm correspond to residual NMP).

Characterization of the compounds by GPC measurements elucidates their aggregation in nonpolar solvents like TCM (see **figure 3.3.4**). In order to analyse, whether the formation of the hetero-duplex (for detailed discussion see **chapter 3.2**) is more favorable for the block copolymers in solvents of lower polarity, a stoichiometric solution of both block copolymers was also analyzed. If the complex formation was the only assembly process, then only dimeric aggregates should be observed in the GPC trace.

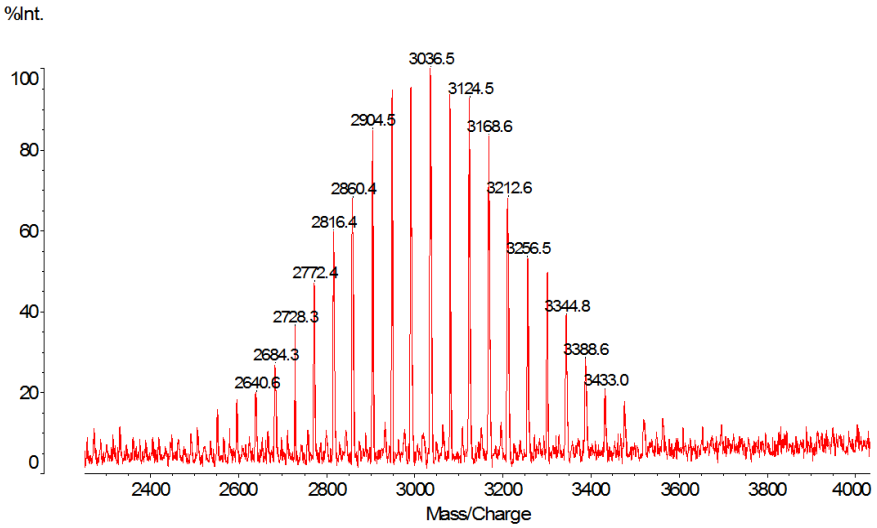

Figure 3.3.3. MALDI-TOF spectrum of block copolymer **20** as potassium adduct.

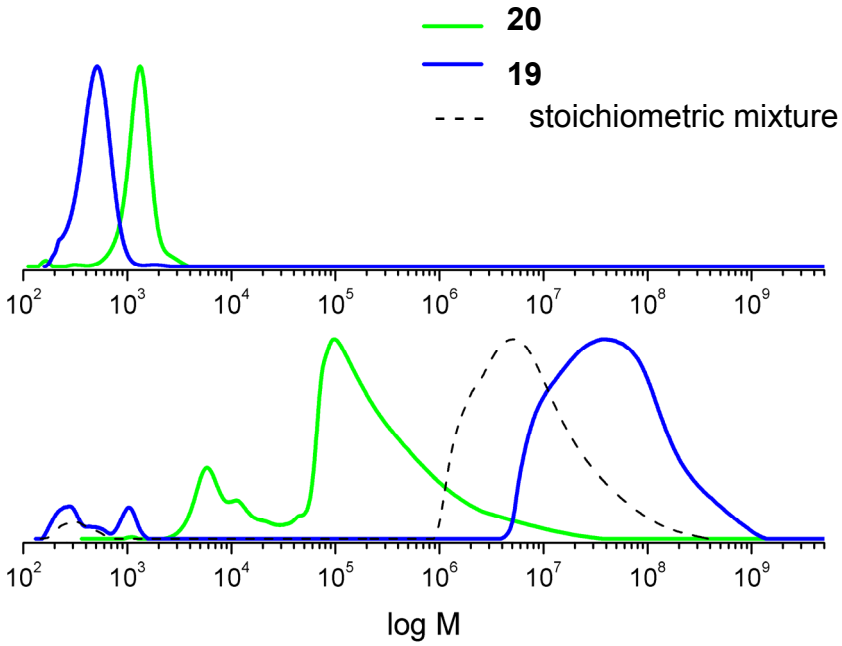

Figure 3.3.4. GPC traces of the amphiphilic polymers **19** and **20** in DMF (*top*) and TCM (*bottom*). The GPC traces in TCM confirmed their high aggregation tendency in nonpolar solvents, previously elucidated by spectroscopic measurements (see **figure SI-3.3.1**).

The GPC chromatograms show higher molecular weight aggregates, with mean values of hydrodynamic radii compared to the ones observed for the single polymer solutions.

The appearance of only one high molecular weight signal can also be interpreted as an evidence for cooperative processes taking place.

In order to gain more information about the supramolecular structures of the polymers, the aggregates were visualized by TEM experiments, demonstrating the presence of fiber-like structures, with dimensions comparable to those observed for similar copolymers. The tapes in **figures 3.3.5** and **3.3.6** are 7 nm in width and around 500 nm in length. The width of the aggregates corresponds to the molecular dimensions of the oligoaramide (the low contrast of the PEG-block in TEM makes difficult to visualize the corona).

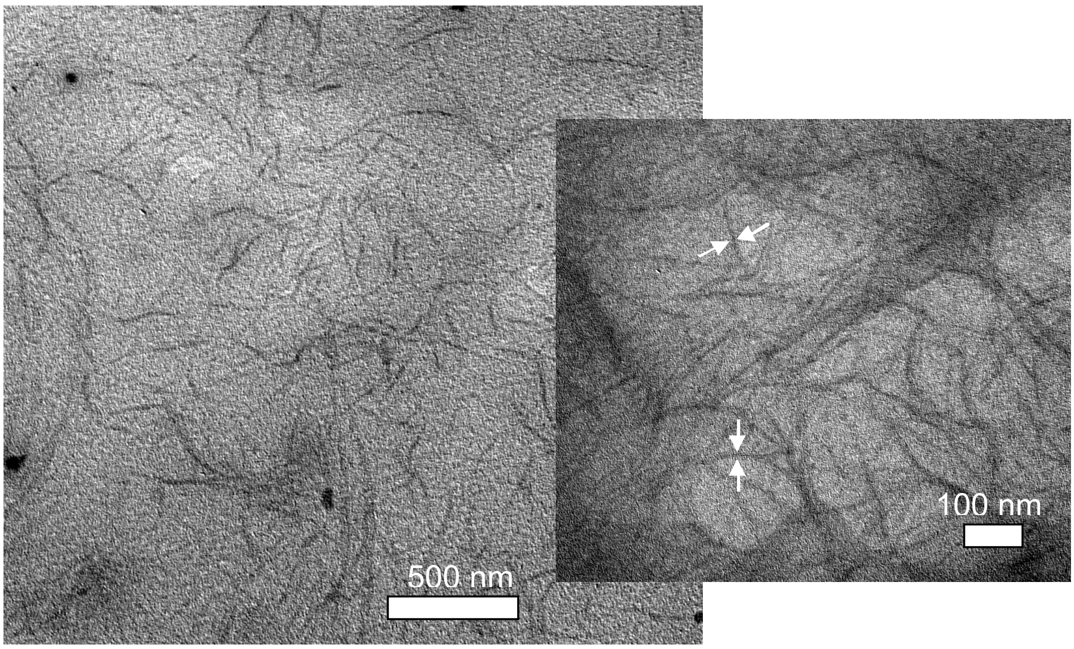

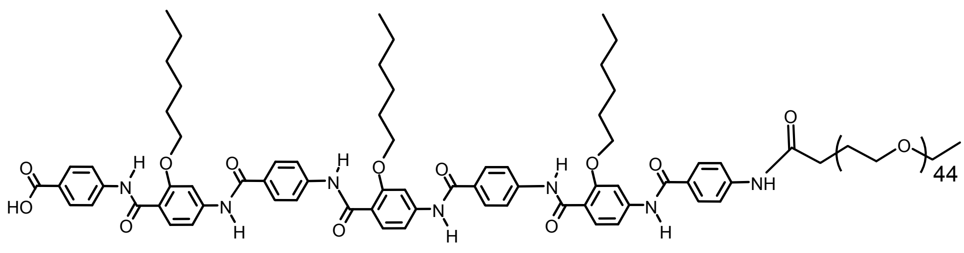

19

Figure 3.3.5. Representative molecular structure and transmission electron micrographs of the supramolecular nanofibres (7 nm in width) formed by self-organization of **19**. Solution concentration: 1.6 mg / ml. Solvent: 36 vol % DMSO in TCM.

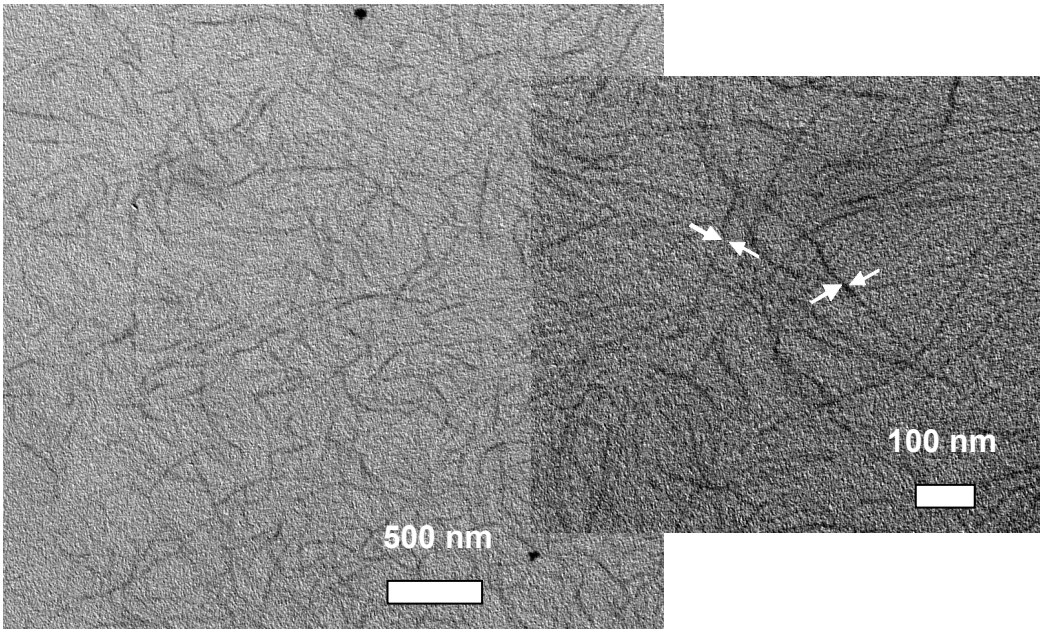

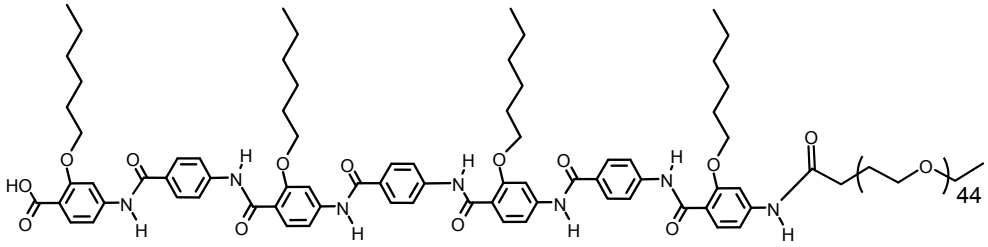

20

Figure 3.3.6. Chemical structure and transmission electron micrographs of the supramolecular nanofibres (7 nm in width) formed by self-organization of **20**. Solution concentration: 1.6 mg / ml. Solvent: 36 vol % DMSO in TCM.

The main difference to the prior published structures[14a,18] concerns their rigidity. The aggregates shown here present a less rod-like form, while unsubstituted aramide copolymers align into exceptionally linear rigid aggregates mainly due to directional hydrogen bond formation and in less intent due to π-stacking. Both interactions are present in the new system, but also additional forces between the highly nonpolar hydrocarbon chains may play a relevant role. These hydrophobic interactions act as flexible junction points, enabling the rods to shift with respect to each other because of the less directional forces. π-Interactions contribute importantly to the formation of these

nanotapes, as the introduction of the hydrogen bond acceptor induces a more planar alignment of the aromatic rings, thus favoring strand stacking.

Comparing the nanofibers of **19** and **20** it can be determined, that the aramide sequence does not show any remarkable influence on the fibril morphology. The supramolecular fiber formation can then be described by the self-assembly model proposed in **figure 3.3.7**. One edge of the rods is capable of forming hydrogen bonds to the next building block. Matching of multiple H-bond sites generates the maximum driving force for their alignment into supramolecular structures. Further interactions between the alkyl chains to the next hydrogen bonded dimer define the inner structure of the fiber. The H-bond interactions between two rods are only maximal for a parallel arrangement, although no preferential direction is dictated by the entanglement of the hydrophobic chains, so that forward fiber growth at this junction points can occur in an anti-parallel or parallel way.

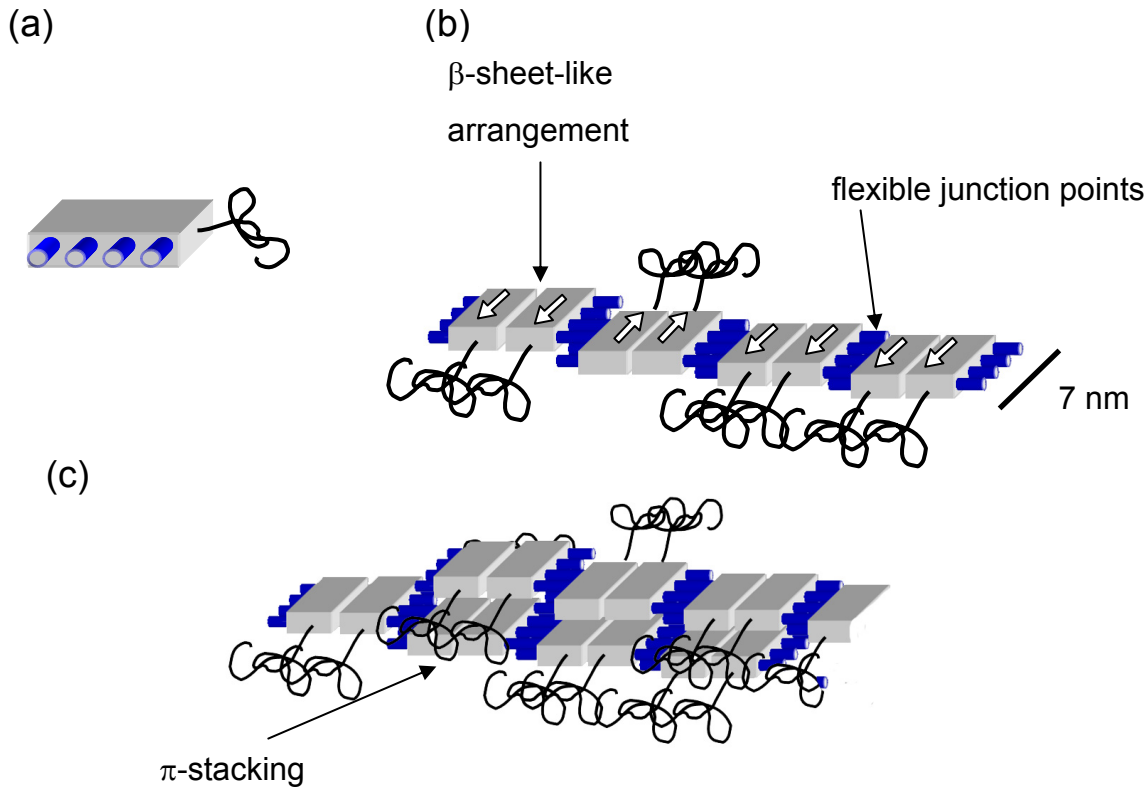

Figure 3.3.7. (a) Schematic representation of the comb-like OPBA-heptamer Proposed model for the self-assembly into tape-like structures. The interplay of (b) strong directional hydrogen bonding, hydrophobic interactions and (c) π-stacking favor the fiber formation with an aromatic inner and the PEG-polymer on the outer sides.

3.3.3. Conclusions

In summary, defined sequences of comb-like aramides decorated with hexyloxy side chains (three and four pendant groups) were attached to PEG-polymers with 2000 g/mol average molecular weight. The substitution of every second aromatic unit and the stabilization of the rotamers by intramolecular hydrogen bond formation to the ether functionality, leads to a hydrophobic molecule edge of the rod block. The other molecule side is functionalized with an array of H-bonding acceptors and donors. The aggregation of the rod-coil copolymer in TCM and TCM / DMSO mixtures was analyzed by GPC and TEM-techniques. The molecular self-assembly into fibrous monolayer structures involves most probably several processes: H-bonding, π-stacking and hydrophobic interactions. This synthetic strategy was shown to be useful for the preparation of fibers with monodisperse width and of great potential for the design and creation of novel nanomaterials with well defined structures in the nanometer scale.

3.3.4. Experimental Section

General.

Poly(ethylene oxide) with molecular mass of about 2000 g/mol was obtained from Sigma Aldrich Chemie GmbH. DCM and NMP were dried over P_2O_5 and CaH_2 respectively. Both solvents were freshly distilled prior to use. All other reagents were used as received. Deuterated solvents (DMSO-d_6 and $CDCl_3$) were purchased from Deutero GmbH. The heterosequences were synthesized as described in chapter **3.1**.

Methods.

Preparation of TEM samples. The polymer was dissolved in 36 vol % DMSO in TCM and the solution was equilibrated for 48 h, drop-casted (4 x) onto hydrophilized carbon coated copper grids and dried in vacuum over night.

Instruments

Standard proton nuclear magnetic resonance spectra were recorded on a Bruker AC (300 MHz) or on a Bruker AMX 400 (400 MHz). Infrared spectra were recorded on a Nicolet 5 DXC FT-IR spectrometer. Matrix-assisted laser desorption and ionization time-of-flight (MALDI-TOF) measurements were performed on a Shimadzu Axima CFR MALDI-TOF mass spectrometer equipped with a nitrogen laser delivering 3 ns laser pulses at 337 nm. Dithranol was used as matrix and potassium cations were added. A Philips EM 420 transmission electron microscope using a LaB_6 cathode at an acceleration voltage of 120 kV was used to obtain TEM-images. TEM grids (carbon film on copper, 300 mesh) were obtained from Electron Microscopy Sciences, Hatfield, PA, USA. The synthesis of the oligomers was performed on an Applied Biosystems ABI 431a automated peptide synthesizer using standard Fmoc chemistry protocols.
Gel permeation chromatography with TCM was carried out on an instrument consisting of a Waters 717 plus auto sampler, a TSP Spectra Series P 100 pump and a set of three PSS SDV columns ($10^6/10^5/10^4$ g/mol). Signal detection was performed with a TSP Spectra System UV 2000 (UV 254 nm) and a Wyatt Optilab DSP (refractive index). Measurements in DMF (containing 1 g/L of lithium bromide) were performed on an Agilent 1100 Series was used as an integrated instrument including a PSS Gral column ($10^4/10^3/10^2$ g/mol), a UV (254 nm) and RI detector. Calibration was done using poly(styrene) standards provided by Polymer Standards Service.

PEG-carboxylic acid **(17)**: CrO_3 (3.2 g, 32 mmol) was dissolved in 35 ml water and added to a solution of PEG_{2000} monomethyl ether (20 g) in 170 ml water and 56 ml sulfuric acid. During the addition, the reaction mixture was cooled with an external ice bath. The solution was then stirred 48 hrs at rt and extracted with DCM (3 x 150 ml). The organic layers were combined, washed with water (2 x 50 ml) and brine (2 x 50 ml), dried over $MgSO_4$, concentrated under reduced pressure and the product precipitated in diethyl ether. The PEG-COOH was filtered off and dried in vacuum (16.6 g, 83 %).

^{1}H-NMR: δ (300 MHz, $CDCl_3$) 3.38 (s, 3H); 3.54-3.73 (m, 176 H); 4.15 (s, 2 H).
IR ν (cm^{-1}): 2881, 1753, 1466, 1340, 1278, 1239, 1145, 1103, 1059, 947, 841.
M (ESI): *m/z* (%) = 1693.03 ($[PEG\text{-}COONa+K]^+$, calc.= 1693.02).

*General method for the attachment of the PEG-block to the hepta(benzamide) on the solid support (***GM 1***):*

PEG 2000 was dissolved in dry DCM and oxalyl chloride under an inert atmosphere and stirred for 3.5 hours at room temperature. The residual oxalyl chloride was removed under reduced pressure by the addition of fresh dry DCM (3 times). The solid residue was dissolved in a minimum amount of dry NMP.
Wang resin functionalized with the hepta(benzamide) was swollen in NMP for 30 min. The PEG-acid chloride solution in NMP was added to the resin. The reaction mixture was shaken for 12 hours and the resin was then rinsed several times with NMP and DCM. The procedure was repeated with fresh prepared PEG-acid chloride.
The aramide-functionalized polymer was cleaved from the solid support by shaking 2 h in a solution of DCM / TFA (2:3). The product was precipitated in diethyl ether and purified by preparative GPC in DMF.

Compound **(19)**: was prepared as described in **GM 1** using 489 mg of functionalized resin **8*** (0.181 mmol), 1.81 g PEG-COOH **17**, 10 ml oxalyl chloride, 10 ml DCM to obtain 214 mg (38 %) of crude product. A portion (50 mg) was purified by preparative GPC to afford 10 mg pure **19**.

^{1}H-NMR: δ (400 MHz, DMSO-d_6) 0.79-0.87 (m, 9 H); 1.20-1.50 (m, 18 H); 1.76-1.90 (m, 6 H); 3.23 (s, 3 H); 3.28-3.80 (m, 119 H); 4.13-4.16 (m, 6 H); 7.21-8.05 (m, 25 H); 10.0 (s, 1 H); 10.28-10.43 (m, 5 H).

Compound **(20)**: was prepared as described in **GM 1** using 230 mg functionalized resin **9*** (0.08 mmol), 0.8 g PEG-COOH **17**, 4.6 ml oxalyl chloride and 4.6 ml DCM to obtain 120 mg (46 %) of crude product. A portion (50 mg) was purified by preparative GPC to afford 8 mg of pure **20**.

^{1}H-NMR: δ (400 MHz, DMSO-d_6) 0.83-0.90 (m, 12 H); 1.24-1.33 (m, 16 H); 1.45-1.48 (m, 8 H); 1.72-1.92 (m, 8 H); 3.24 (s, 3 H); 3.50 (br. s, 177 H); 4.00-4.19 (m, 8 H); 7.19-8.06 (m, 24 H); 9.88 (s, 1 H); 10.27-10.38 (m, 6 H).
M (MALDi-TOF): *m/z* = 3036.5 ($[M+K]^+$, calc. = 3036.4).

3.3.5. References

[1] (a) Lehn, J.-M. *Science* **2002**, *295*, 2400; (b) Withesides, G. M.; Grzybowski, B. *Science* **2002**, *295*, 2418.

[2] (a) Fuhrhop, J. H.; Helfrich, W. *Chem. Rev.* **1993**, *93*, 1565. (b) Okahata, Y.; Kunitake, T. *J. Am. Chem. Soc.* **1979**, *101*, 5231; (c) Kunitake, T.; Okahata, Y.; Shimomura, M.; Yasunami,S.; Takarabe, K. *J. Am. Chem. Soc.* **1981**, *103*, 5401; (d) Nakamura, H.; Matsui, Y. *J. Am. Chem. Soc.* **1995**, *117*, 2651; (e) Frankel, D. A.; O'Brien, D. F. *J. Am. Chem. Soc.* **1994**, *116*, 10057-10069; (f) Schoonbeek, F. S.; van Esch, J. H.; Wegewijs, B.; Rep, D. B. A.; de Haas, M. P.; Klapwijk, T. M.; Kellogg, R. M.; Feringa, B. L. *Angew. Chem. Int. Ed.* **1999**, *38*, 1393; (g) van Esch, J.; Kellogg, R. M.; Feringa, B. L. *Tetrahedron Lett.* **1997**, *38*, 281; (h) de Loos, M.; Feringa, B. L.; van Esch, J. H. *Eur. J. Org. Chem.* **2005**, 365; (i) Schoonbeek, F. S.; van Esch, J. H.; Hulst, R.; Kellogg, R. M.; Feringa, B. L. *Chem. Eur. J.* **2000**, *6*, 2633; (j) Claussen, R. C.; Rabatic, B. M.; Stupp, S. I. *J. Am. Chem. Soc.* **2003**, *125*, 12680-12681; (k) Behanna, H. A.; Donners, J. J. J. M.; Gordon, A. C.; Stupp, S. I. *J. Am. Chem. Soc.* **2005**, *127*, 1193; (l) Ryu, J. H.; Lee, M. *J. Am. Chem. Soc.* **2005**, *127*, 14170; (m) Paramonov, S. E.; Jun, H. W.; Hartgerink, J. D. *Biomacromolecules* **2006**, *7*, 24; (n) Liu, G.; Qiao, L.; Guo, A. *Macromolecules* **1996**, *29*, 5508; (o) Genson, K. L.; Holzmueller, J.; Ornatska, M.; Yoo, Y. S.; Par, M. H.; Lee, M.; Tsukruk, V. V. *Nano Lett.* **2006**, *6*, 435; (p) Liu, D.; De Feyter, S.; Cotlet, M.; Wiesler, U. M.; Weil, T.; Herrmann, A.; Muellen, K.; De Schryver, F. C. *Macromolecules* **2003**, *36*, 8489; (q) Jang, W. D.; Aida, T. *Macromolecules* **2004**, *37*, 7325; (r) Yan, P.; Chowdhury, A.; Holman, M. W.; Adams, D. M. *J. Phys. Chem. B* **2005**, *109*, 724.

[3] (a) Lenhert, S.; Zhang, L.; Mueller, J.; Wiesmann, H. P.; Erker, G.; Fuchs, H.; Chi, L. *Adv. Mater.* **2004**, *16*, 619; (b) Candau, S. J.; Hirsch, E.; Zana, R.; Adam, M. *J. Colloid Interface Sci.* **1988**, *122*, 430; (c) Ringsdorf, H.; Schlarb, B.; Venzmer, J. *Angew. Chem. Int. Ed. Engl.* **1988**, *27*, 113; (d) Ahlers, M.; Mueller, W.; Reichert, A.; Ringsdorf, H.; Venzmer, J. *Angew. Chem. Int. Ed. Engl.* **1990**, *29*, 1269; (e) Lehn, J. M. *Supramolecular Chemistry, Concepts and Perspectives*, VCH, Weinheim **1995**.

[4] (a) Menger, F. M.; Yamasaki, Y.; Catlin, K. K.; Nishimi, T. *Angew. Chem. Int. Ed. Engl.* **1995**, *34*, 585; (b) Yanagawa, H.; Ogawa, Y.; Furuta, H.; Tsuno, K. *J. Am. Chem.*

Soc. **1989**, *111*, 4567; (c) Song, B.; Wei, H.; Wang, Z.; Zhang, X.; Smet, M.; Dehaen, W. *Adv. Mater.* **2007**, *19*, 416-420.

[5] Hamley, I. W. *Angew. Chem. Int. Ed.* **2007**, *46*, 8128 – 8147.

[6] Zutshi, R.; Franciskovich, J.; Shultz, M.; Barbara Schweitzer, B.; Bishop, P.; Wilson, M.; Chmielewski, J. *J. Am. Chem. Soc.* **1997**, *119,* 4841-4845; (b) Brik, A.; Wong, C.-H. *Org. Biomol. Chem.* **2003**, *1*, 5-14.

[7] Nowick, J. S. *Acc. Chem. Res*. **1999,** *32*, 287-296.

[8] Lashuel, H. A.; LaBrenz, S. R.; Woo, L.; Serpell, L. C.; Kelly, J. W. *J. Am. Chem. Soc.* **2000**, *122*, 5262.

[9] Schlaad, H. *Adv. Polym. Sci*. **2006**, *202*, 53.

[10] (a) Rathore, O.; Sogah, D. Y. *J. Am. Chem. Soc.* **2001**, *123*, 5231; (b) Rathore, O.; Sogah, D. Y. *Macromolecules* **2001**, *34*, 1477; (c) Yao, J.; Xiao, D.; Chen, X.; Zhou, P.; Yu, T.; Shao, Z. *Macromolecules* **2003**, *36*, 7508.

[11] Scheibel, T.; Parthasarathy, G.; Sawicki, G.; Lin, X.-M.; Jaeger, H.; Lindquist, S. L. *Proc. Natl. Acad. Sci. USA* **2003**, *100*, 4527.

[12] (a) Vandermeulen, G. W. M.; Tziatzios, C.; Klok, H.-A. *Macromolecules* **2003**, *36*, 4107; (b) Vandermeulen, G. W. M.; Klok, H.-A. *Macromol. Biosci.* **2004**, *4*, 383; (c) Hamley, I. W. *Block Copolymers in Solution*, Wiley, Chichester, **2005**.

[13] Koenig, H. M.; Kilbinger, A. F. M. *Angew. Chem. Int. Ed.* **2007**, *46*, 8334 – 8340.

[14] (a) Koenig, H. M.; Kilbinger, A.F.M. *Macromol. Rapid Commun.* **2008,** *29*, 1721; (b) Koenig, H. M.; Gorelik, T.; Kolb, U.; Kilbinger, A. F. M. *J. Am. Chem. Soc.* ***2007,*** *129, 704; (c)* Koenig, H. M.; Abbel, R.; Schollmeyer, D.; Kilbinger, A. F. M. *Org. Lett.* **2006**, *8*, 1819; (d) Seyler, H.; Storz, C.; Abbel, R.; Kilbinger, A.F.M. *Soft Matter* **2009**, DOI: 10.1039/b903488a.

[15] Schleuss, T. W.; Abbel, R.; Gross, M.; Schollmeyer, D.; Frey, H.; Maskos, M.; Berger, R.; Kilbinger, A. F. M. *Angew. Chem. Int. Ed.* **2006**, *45,* 2969-2975.

[16] Seyler, H.; Kilbinger, A.F.M. "Tuning Oligo(*p*-benzamide) Aggregation via Heterosequences", *in preparation*.

[17] Fishman, A.; Acton, A.; Lee-Ruff, E. *Synthetic Commum.* **2004**, *34* (12), 2309-2312.

[18] Klos, J.; Wurm, F.; Koenig, H. M.; Kilbinger, A.F. M. *Macromolecules* **2007***, 40, 7827*.

3.3.6. Supporting Information for ”Comb-like Rod-Coil Copolymers”

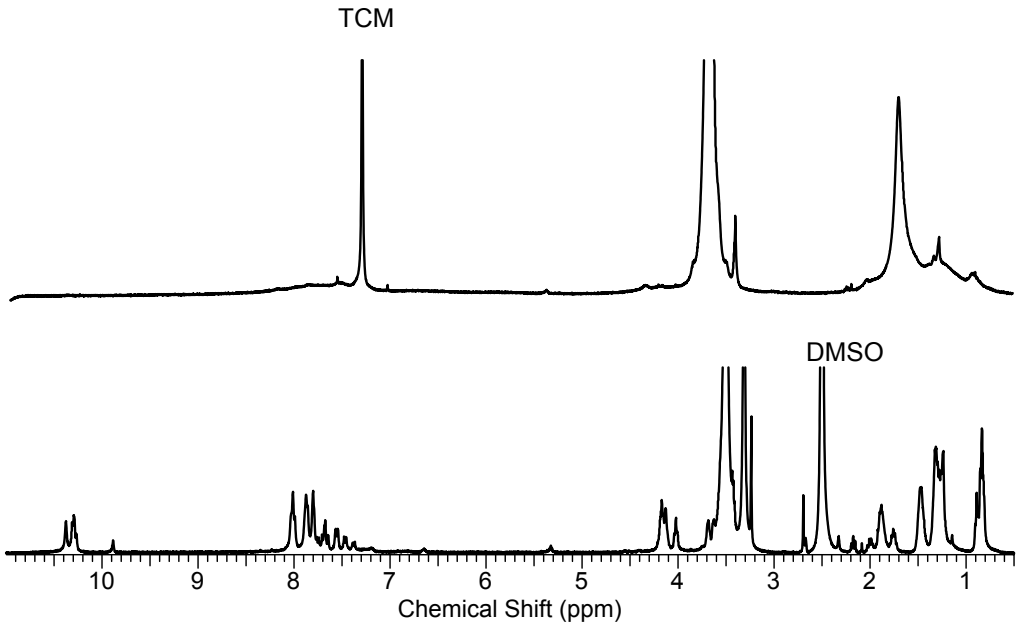

Figure SI-3.3.1. ^{1}H-NMR spectra (400 MHz) of **20** in $CDCl_3$ (*top*) and DMSO-d_6 (*bottom*). The aromatic proton signals in unpolar solvents can not be resolved due to the aggregation of the rod block.

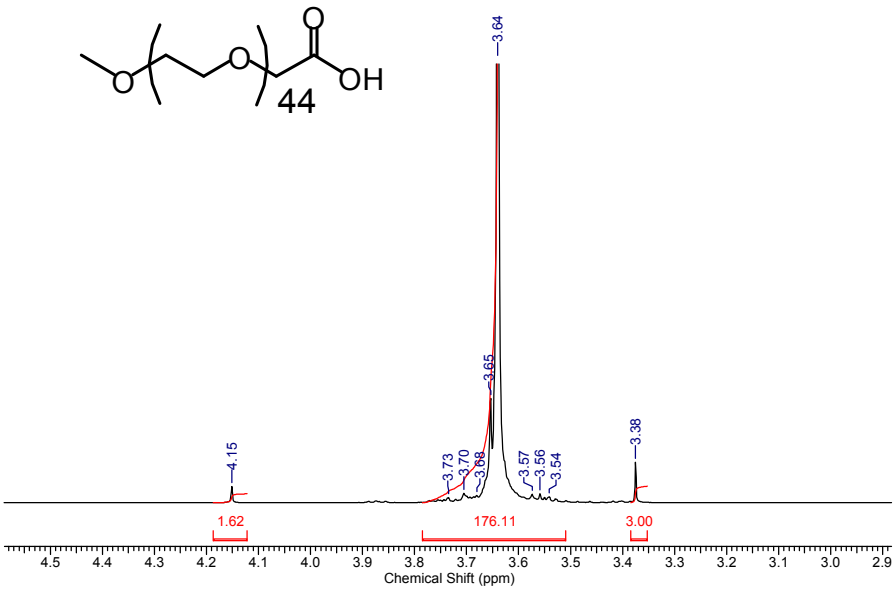

Figure SI-3.3.2. ^{1}H-NMR spectrum of PEG-carboxylic acid **17** in $CDCl_3$.

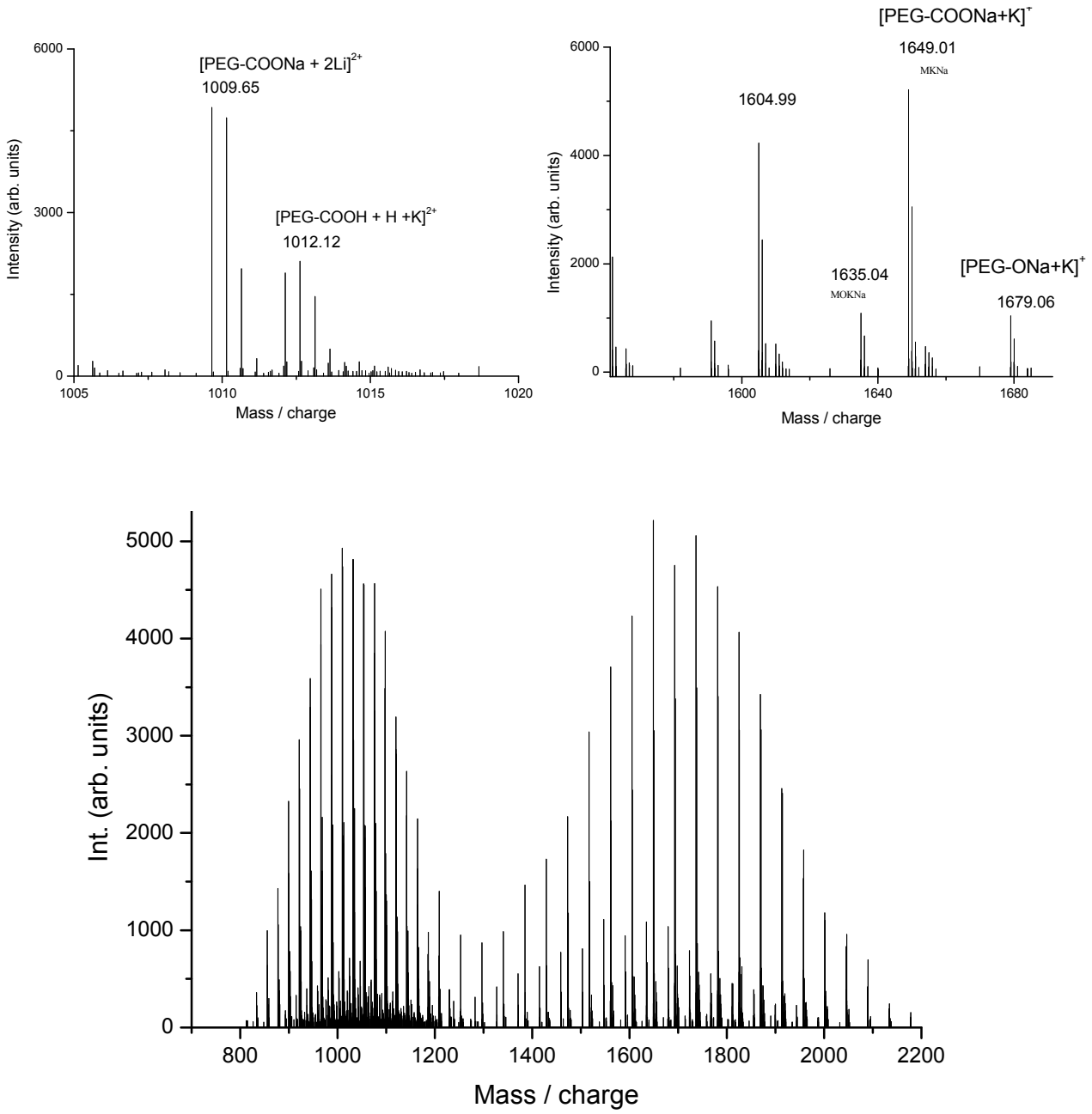

Figure SI-3.3.3. ESI mass spectrum of PEG-carboxylic acid **17**. *Bottom*: distributions of the single and double charged products are observed. *Top-left*: enlargement of the double charged distribution shows only the desired product. *Top-right*: enlargement of the single charged distribution shows the presence of PEG-COOH and impurities of reactant PEG-OH.

Chapter 4

Hairy Rod-like Macromolecules

4.1 Linear soluble Poly(*p*-Benzamide)

*Helga Seyler, Andreas F. M. Kilbinger **

Abstract

Organo soluble, shape persistent oligo- and poly(*p*-benzamide)s are synthesized and characterized. Triethylene glycol (TEG) substituents are introduced as solubilizing side chains on the benzene rings of the polyamide backbone. The new monomer was polymerized by the facile polycondensation of the corresponding *N*-sulfinylamino benzoyl chloride. A well defined heptamer was prepared as a model compound on a peptide synthesizer. The TEG-grafted products show good solubility in common organic solvents, yet high aggregation tendency in polar and nonpolar media. The self-organization of the poly(2-TEG-*p*-benzamide) was examined by GPC, NMR- and UV- spectroscopy. Transmission electron microscopy (TEM) allowed the visualization of the supramolecular assemblies, showing the formation of micrometer-sized rigid structures.

Kurzfassung

Formtreue lösliche Oligo- and Poly(*p*-benzamide) wurden hergestellt und charakterisiert. Die Einführung von Triethylenglykol-Substituenten (TEG) am aromatischen Rückgrad führte zu einer erhöhten Löslichkeit der Makromoleküle. Das neu entwickelte Monomer wurde durch Polykondensation des entsprechenden *N*-Sulfinylaminobenzoesäurechlorids polymerisiert. Die Herstellung von monodispersen Modellverbindungen erfolgte an der Festphase mittels eines Peptid-Syntheseautomaten. Die „TEG-*grafted*“ Makromoleküle weisen gute Löslichkeit in gewöhnlichen organischen Lösungsmitteln auf. Gleichzeitig zeigen sie eine hohe Aggregationstendenz in sowohl polaren als auch unpolaren Lösungsmitteln. Die Selbstorganisation der Poly(2-TEG-*p*-benzamide) wurde mittels GPC, NMR- und UV-Spektroskopie untersucht. Untersuchungen am Transmissionselektronenmikroskop (TEM) erlaubten die direkte Abbildung der mikrometergroßen supramolekularen Objekte.

4.1.1. Introduction

Aromatic polyamides such as Kevlar® and poly(*p*-benzamide) have attracted a great deal of attention due to their inherently extended rigid chain structure. This is caused by the interplay of *para*-linked benzene rings and the partial double bond character of the *trans*-amide linkages.[1] In addition to their chemical structure, the hydrogen bonding network in aromatic polyamides plays an important role for their thermomechanical properties.[2] The combination of the high persistence length and inter-chain attraction leads to materials with high mechanical strength and excellent temperature resistance.[3] As a consequence of these features, such polymers are only soluble in a few special solvents like DMAc / LiCl and sulfuric acid, from which fibers can be spin-processed.[4,3a]

Approaches to improve the solubility, while maintaining novel material properties of the polyaramides include the introduction of *N*-protective groups[5] or the synthesis of block copolymers.[6] Another usual strategy to improve solubility in rigid rod-like molecules is the attachment of flexible side chains to the stiff oligomer/polymer backbone.[7]

Here, we report the facile synthesis of a soluble poly(*p*-benzamide) carrying TEG-side chains on the benzene rings. The TEG-grafted polymer and oligomer are highly interesting materials, as they combine good solubility in common organic solvents like TCM in addition to shape persistence and the ability to organize into supramolecular structures.

4.1.2. Results and Discussion

Synthesis. The new monomers were synthesized from 4-amino salicylic acid as outlined in **scheme 4.1.1**. 4-Aminosalicylic acid **1** was *N*-acetylated using one equivalent of acetyl chloride to give **2** in 85 % yield. The subsequent reaction with 2-[(methoxyethoxy)ethoxy]ethyl bromide (TEG-bromide) or hexyl bromide, produced the corresponding ethers and esters **4a** and **4b** in 75 % and 82 % yield, respectively. Cleavage of the amide and ester of the TEG- and hexyl-substituted monomers was performed under alkaline conditions to afford **5a** (70 %) and **5b** (85 %). *N*-Fluorenylmethoxycarbonyl (Fmoc) protection of **5a** and **5b** was achieved using 9-fluorenylmethyl chloroformate (Fmoc-Cl) to give **8a** and **8b** in moderate to quantitative yields (70-89 %).

Activation as an acid chloride for solid phase synthesis was carried out *in situ* using $SOCl_2$ and *N*-methylpyrrolidone (NMP).[8]

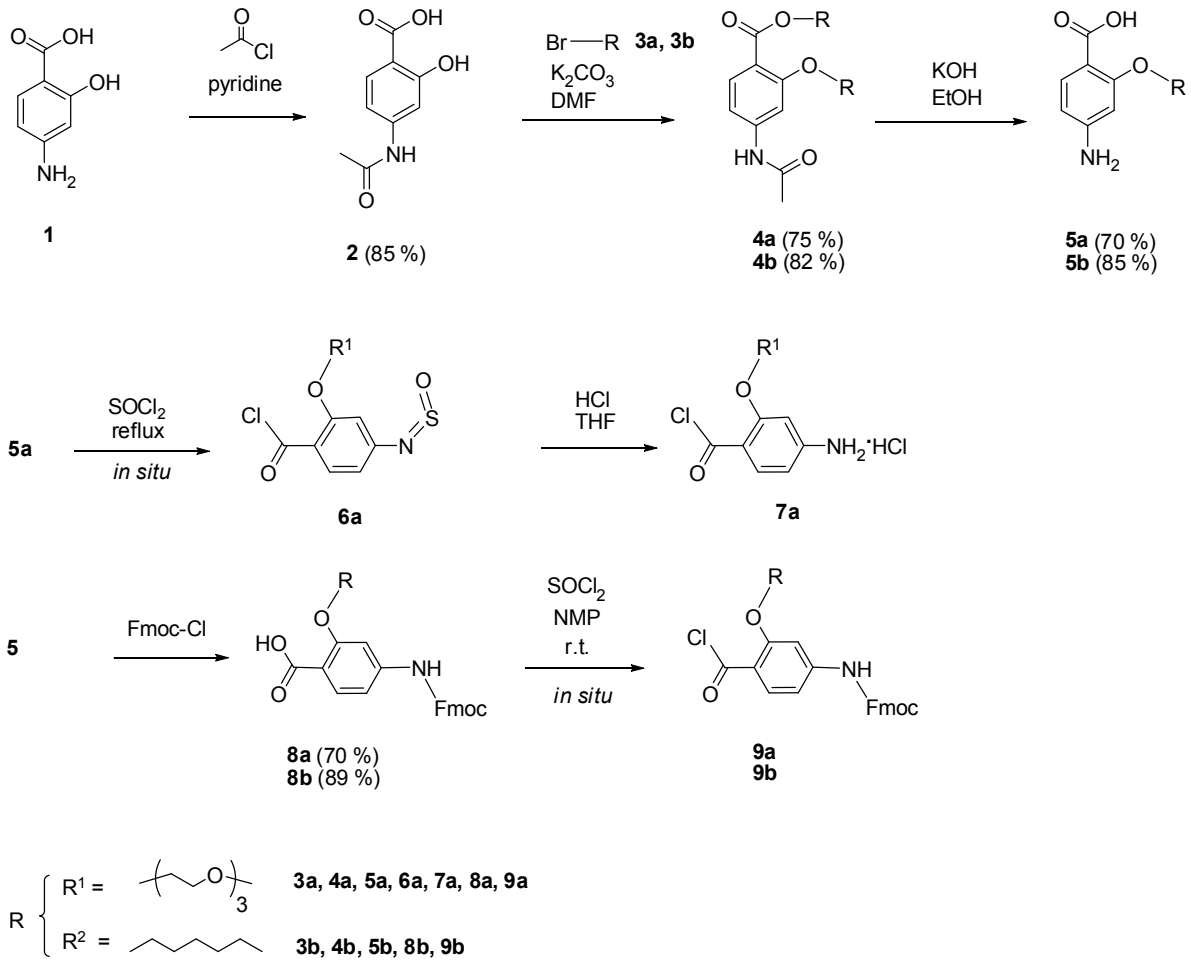

Scheme 4.1.1. Synthesis of the monomers

For the polycondensation, we chose the activation of the monomer into the corresponding *N*-sulfinylamino benzoyl chloride **6a**.[1] The later compound was converted into the 2-TEG-4-amino benzoyl chloride hydrochloride salt **7a** and further dissolved in dry NMP to afford poly(2-TEG-1,4-benzamide) **11aii** (**scheme 4.1.2**, *path* **ii**). Amino acid **5a** was also polymerized in a typical direct condensation reaction using triphenyl phosphite and pyridine in NMP (**scheme 4.1.2**, *path* **i**).[9] During the polycondensation of the 2-TEG-4-amino benzoyl chloride hydrochloride salt **7a**, the polymer **11ai** remained soluble without the need of salt addition. The NMP assisted polycondensation of the ammonium salts achieved higher molecular weight polymers with higher polydispersities compared to the activation promoted by phosphites (see supporting information, **figure SI-4.1.8**). Attempts using the analogous hexyloxy substituted monomer **5b**, afforded

11bi, which precipitated from NMP during the polymerization and was only soluble in sulfuric acid (see supporting information, **figure SI-4.1.4**). Thermogravimetric analysis (TGA) showed the thermal resistance of the grafted poly(*p*-benzamide)s. The insoluble polymer **11bi** shows a higher stability than the TEG-grafted one. The onset decomposition temperatures (T_D) are high for both materials: 394 °C for the insoluble hexyl-grafted polymer and 378 °C for the soluble TEG-grafted polymer (see supporting information, **figure SI-4.1.11**).

Monodisperse hepta(2-TEG-1,4-benzamide) and hepta(2-hexyloxy-1,4-benzamide) were synthesized on the solid support in a peptide synthesizer in a analogous procedure as described in previous chapters. Hereby, repeated alternating cycles of *N*-Fmoc deprotection and coupling of **9** are sequentially programmed into the peptide synthesizer.[10] The final product is then cleaved under acidic conditions from the solid support (**scheme 4.1.2**, *path* **iii**).

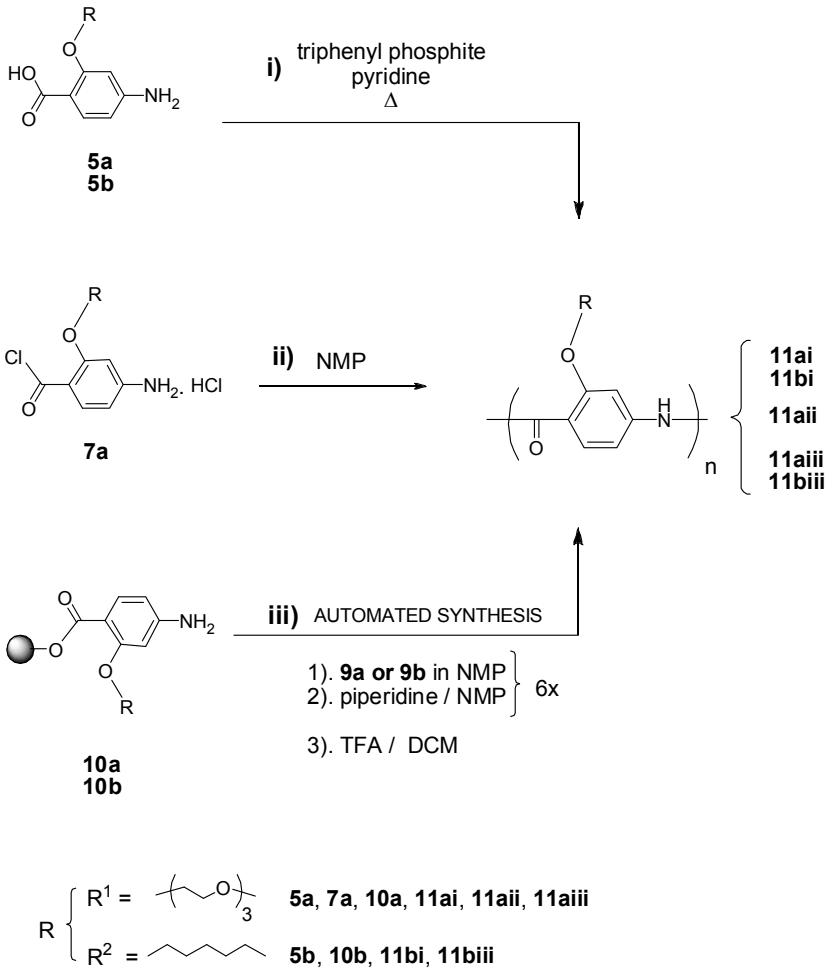

Scheme 4.1.2. Synthesis of the polydisperse and monodisperse grafted poly- and oligo-(*p*-benzamides).

Characterization. Gel permeation chromatography of polymer **11aii** in TCM shows a broad UV-signal over the whole elution volume, with highest intensity modes at low and high molar masses (see supporting information, **figure SI-4.1.8**). This fact can be explained by the formation of supramolecular structures induced by strong interactions of the aramide backbone due to π-stacking as well as selective solvent driven aggregation. The stability of those structures is shown to be high enough not to be disrupted during the elution through the GPC column. Nuclear magnetic resonance experiments of the polymer in aprotic polar solvents (DMSO and DMF/LiBr) also revealed the formation of aggregates, observed by the broadening of the signals (see supporting information, **figure SI-4.1.9** for spectra in DMSO). However, the stability of these supramolecular structures is lower compare to those formed in nonpolar solvents. Their molecular weights (determined by GPC) in DMF/LiBr are noticeably smaller compared to those observed in TCM (see supporting information, **table SI-4.1.1** and **figure SI-4.1.8**). The photophysical properties of the supramolecular assemblies were further investigated via UV-vis spectroscopy. **Figure 4.1.1** shows the absorption spectra of **11aii** compared to the model heptamer **11aiii** in TCM. The absorption spectra of **11aii** in TCM shows a hypsochromic shift of the absorption maxima compared to the model compound **11aiii** ($\Delta\lambda_{max}$ = 10 nm), attributed to the formation of H-aggregates of the OPBA chromophores.

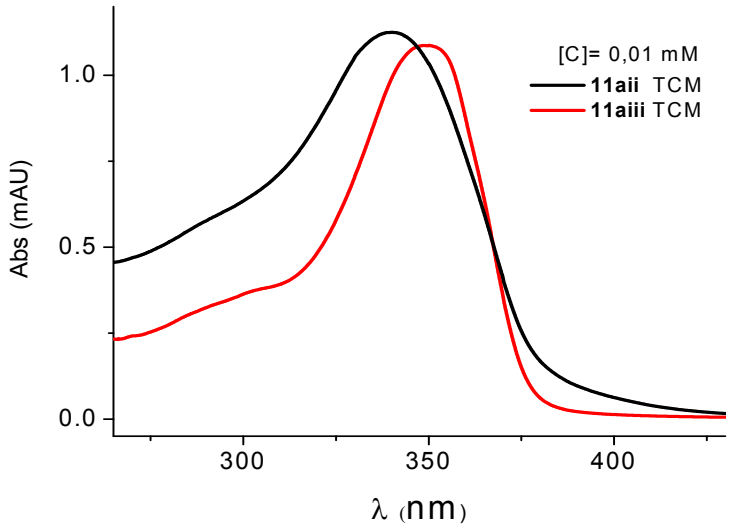

Figure 4.1.1. UV-absortion spectra of polymer **11aii** and heptamer **11aiii** in TCM.

Transmission electron microscope studies of **11aii** in TCM elucidate the stained stiff structures with nano- to micrometer lengths, built form individual fibers of 38 nm in width.

Many *p*-linked aromatic polyamides form an anisotropic phase in selected solvents at defined concentrations,[11] usually in fully substituted amides.[3a] The TEG-grafted poly(*p*-benzamide) forms also an anisotropic phase at room temperature in high concentrated solutions, like DMF. **Figure 4.1.2** (*bottom, left*) shows the birefringence of the anisotropic phase by viewing a thin layer of a concentrated solution under the microscope and under crossed polarizers.

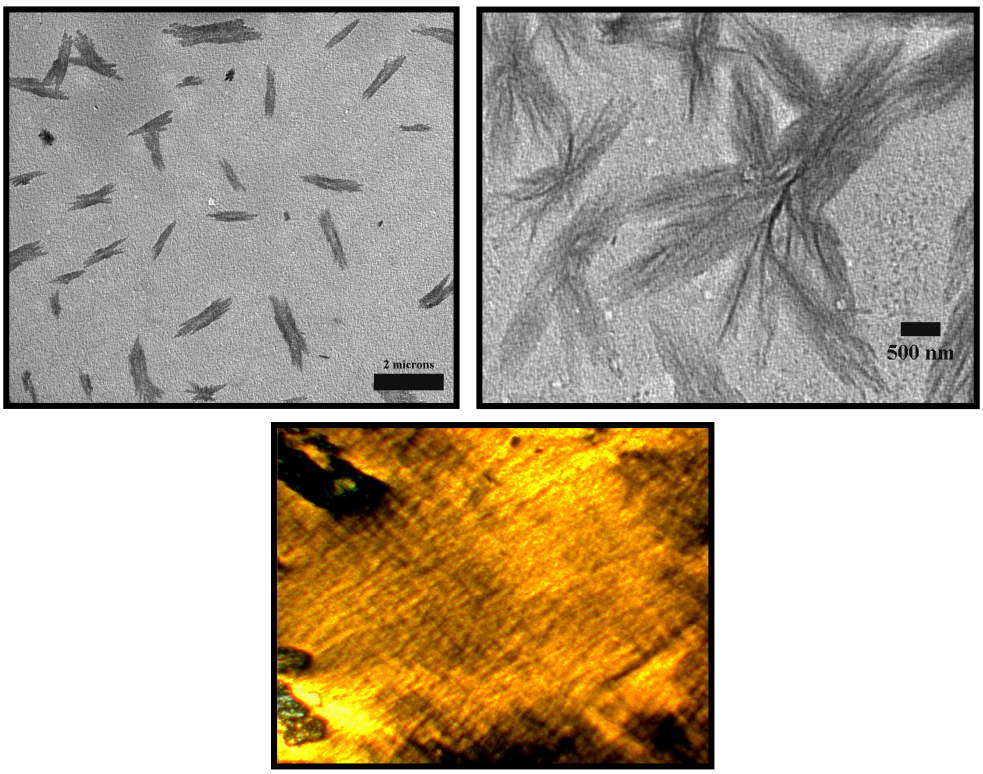

Figure 4.1.2. *Top*: TEM micrographs of **11aii** from TCM (drop cast, stained with OsO_4). *Bottom:* micrograph under crossed polarizers of the anisotropic phase of a thin layer from a highly concentrated solution of **11aii** (*right*) ([c] = 87 wt% in DMF).

The synthesis of polymers derived from the amino salicylic acid monomer with different side chains showed an enormous solubility difference depending on the polarity and length of the side groups. Hexyl-substituted polymers exhibit no solubility in organic media. On the other hand, polymers with TEG-side chains showed excellent solubility even in nonpolar solvents. Model compounds **11aiii** and **11biii** were synthesized in order to evaluate the influence of molecular weight and polydispersity on the solubility

properties of the polymers. Monodisperse heptamers show identical solubility behavior as their counterpart polymeric compounds. It is known from the literature, that the introduction of a hydrogen bond acceptor (for example an ether oxygen) in *ortho*-position to the carbonyl group of an amide bond, induced the restriction of the amide-aryl bond rotation.[12] The *anti*-conformation of the Ar-CO-NH linkages is stabilized by the six-membered hydrogen bonded ring (see **figure 4.1.3(a)**). Because of the conjugation between the amide and aromatic groups, a coplanar or close to coplanar conformation is usually adopted.[12,13] This conformational restriction and coplanarity alignment of the phenyl rings induces a stiff molecule backbone and promotes its intermolecular π-stacking. The high concentration of nonpolar side chains on the periphery enhances their mutual attraction by simultaneous alkyl chain extension due to repulsion from the aramide backbone. The result is lower solvatization and therefore lower solubility of the polymer.

The more polar TEG-side chains expert both attractive interactions to the also polar aramide backbone as well as to the organic solvents, acting as solubility-enhancing groups. The longer, flexible TEG-chains may also assume a larger number of conformations in solution. Hence, dissolution of the polymer is accompanied by a higher gain in entropy compared to the hexylated macromolecules.

Figure 4.1.3 (a) shows the *anti*-conformation of the aryl-amide bonds stabilized by hydrogen bond formation and the possible aggregation mechanisms for the fiber formation: **(b)** π-stacking and **(c)** entanglements of the TEG-side chains.

4.1.3. Conclusions

A new soluble poly(*p*-benzamide) with triethylene glycol side chains was developed. The high solubility in organic solvents in addition to the shape persistence and thermal stability, show great promise for this material, where tedious processing using sulphuric acid could be replaced by an ordinary solvent. Intermolecular interactions (π-stacking, H-bonding, etc.) even in solvents with high polarity, resulted in supramolecular assemblies in the micrometer scale. The rigidity of the structures resulted in anisotropic solutions, as expected for polybenzamides in high concentrated solutions.

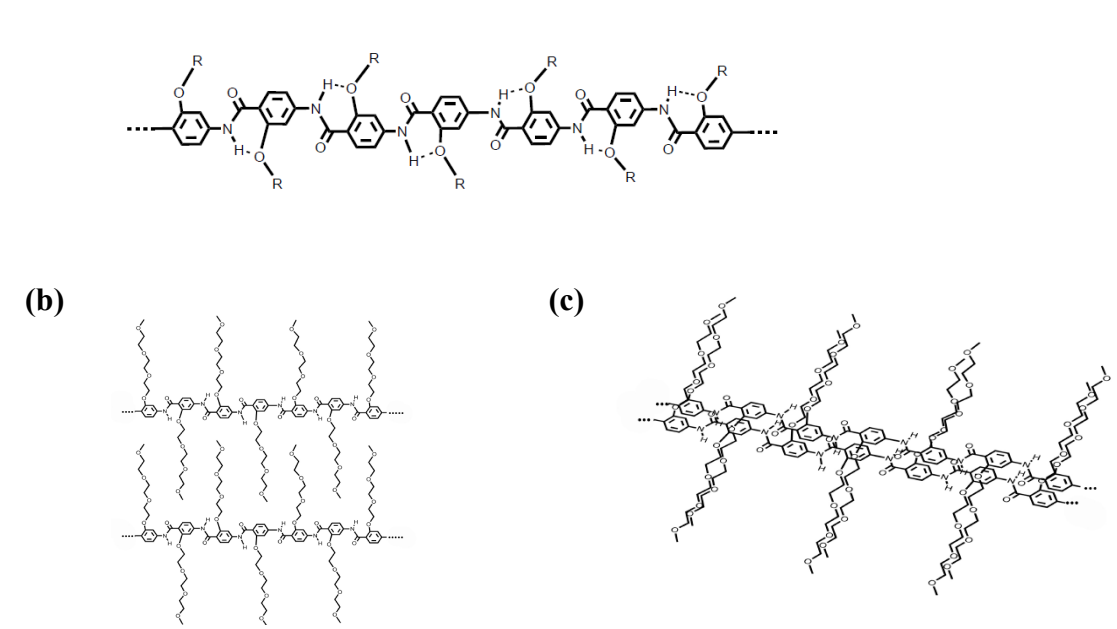

Figure 4.1.3. (a) Preferred *anti*-conformation of the aryl-amide bond due to hydrogen bonded stabilized six membered ring. Proposed aggregation mechanisms for the fiber formation: **(b)** TEG-chain entanglements and **(c)** π-stacking.

4.1.4 Experimental Details

Materials.

NMP was stored over molecular sieves. THF was dried over sodium and distilled under nitrogen prior to use. The other reagents and solvents were obtained commercially and used as received. TEG-bromide **3a** was prepared as described in the literature.[14]

Methods.

Nuclear magnetic resonance spectra were recorded on a Bruker AC (300 MHz) or on a Bruker AMX 400 (400 MHz). Infrared spectra were recorded on a Nicolet 5 DXC FT-IR spectrometer. RP-HPLC analysis was performed on a Hewlett Packard HP 1090 Liquid Chromatograph equipped with PerfectSil column (MZ Analysentechnik, Mainz, Germany, 250 x 4.0 mm; 120 ODS-2 5 μm). The samples were eluted with an acetonitrile/water gradient (buffered with 0.1 % TFA), starting from 10 % acetonitrile, rising to 90 % over a period of 35 min and maintained constant for additional 10 min.

UV-detection was performed at 254 nm. Melting points were recorded on a FP 62 Mettler Toledo in a capillary tube and are uncorrected. Field desorption mass spectra were measured on a Finnigan MAT 95 and ESI mass spectra on a Micromass Q-TOF Ultima 3. Matrix-assisted laser desorption and ionization time-of-flight (MALDI-TOF) measurements were performed on a Shimadzu Axima CFR MALDI-TOF mass spectrometer equipped with a nitrogen laser delivering 3 ns laser pulses at 337 nm. 2-(4-hydroxyphenylazo) benzoic acid (HABA) was used as matrix. UV-vis measurements were accomplished on a V-630 UV-VIS Spectrophotometer. A Philips EM 420 transmission electron microscope using a LaB_6 cathode at an acceleration voltage of 120 kV was used to obtain TEM-images. The synthesis of the monodisperse heptamer was performed on an Applied Biosystems ABI 431a automated peptide synthesizer using standard Fmoc chemistry protocols, similar to the synthesis described before.[15]

Monomer Synthesis.

4-Acetamidosalicylic acid **(2)***:* Acetyl chloride (23.2 ml, 1 eq.) was added dropwise into a cold solution of 4-aminosalicylic acid **1** (50 g, 0.33 mol, 1 eq.) in pyridine (250 ml) under an inert atmosphere. The solution was further refluxed for 2 hrs. The cold reaction mixture was poured into a mixture of 800 ml ice and 400 ml 6N hydrochloric acid. The solid was filtered, washed with water and dried to give **2** (54 g, 85%).

mp: 222 ºC.

^{1}H-NMR: δ (300 MHz, DMSO-d_6) 2.06 (s, 3 H); 7.04 (d, ^3J = 8.46 Hz, 1 H); 7.34 (s, 1 H); 7.70 (d, ^3J = 8.46 Hz, 1H); 10.21 (s, 1H).

^{13}C-NMR and DEPT: δ (300 MHz, DMSO-d_6) 24.29 (+); 105.77 (+); 107.48; 110.11 (+); 131.05 (+); 145.7; 162.21; 169.2; 171.69.

IR ν (cm^{-1}): 3350, 2872, 1676, 1599, 1535, 1383, 1282, 1222, 1162.

RP-HPLC (min.): 9.9.

M (FD): *m/z* (%) = 195.6 (100); 196.6 (9.3); 197.6 (0.49); calc.[$C_9H_9NO_4$] = 195.1

4-Acetamido-2-TEG-benzoic acid TEG-ester **(4a)***:* **2** (20 g, 0.1 mol), dry DMF (320 ml), TEG-Br **3** (46.4 g, 0.2 mol), 18-crown-6 (0.82 g), anhydrous K_2CO_3 (120 g) and KI were heated for 30 hrs under reflux and inert atmosphere. The solvent was removed under reduced pressure; water was added to the residue, the resulting solution extracted with

dichloromethane, dried over magnesium sulfate and the solvent removed on a rotary evaporator to give **4a** as brown oil (37.3 g, 75 %).

^{1}H-NMR: δ (300 MHz, $CDCl_3$) 2.16 (s, 3 H); 3.33 (s, 6 H); 3.49-3.83 (m, 20 H); 4.10 (t, 2 H, J = 4.8 Hz); 4.36 (t, 2 H, J = 4.9 Hz); 7.08 (dd, 1 H, ^{4}J = 1.84 Hz, ^{3}J = 8.46 Hz); 7.44 (d, 1 H, ^{4}J = 1.47 Hz); 7.73 (d, 1 H, ^{3}J = 8.46 Hz).
^{13}C-NMR and DEPT: δ (300 MHz, DMSO-d_6) 24.37 (+); 58.65 (+); 58.76 (+); 63.36 (-); 68.45 (-); 69.02 (-); 69.21 (-); 69.80 (-); 70.17 (-); 70.32 (-); 70.38 (-); 70.41 (-); 70.57 (-); 71.62 (-); 71.65 (-); 104.27 (+); 110.77 (+); 114.37; 132.54 (+); 143.67; 159.47; 165.14; 169.25.
IR ν (cm^{-1}): 3319, 2873, 1693, 1591, 1529, 1406, 1241, 1081, 1025, 847, 776.
RP-HPLC (min.): 13.6.
M (FD): *m/z* (%) = 526.2 (100); 527.2 (22); 528.2 (5.6); calc.[$C_{23}H_{37}NO_{10}K$] = 526.2

4-Acetamido-2-hexyloxy-benzoic acid hexyl ester **(4b)**: The reaction was performed as described for **4a**. 2 (37.1 g, 0.19 mol), dry DMF (700 ml), 1-bromohexane (153 ml, 1.1 mol), 18-crown-6 (1,5 g), anhydrous K_2CO_3 (229,8 g). and KI were heated for 50 hrs under reflux and inert atmosphere. After removal of the dichloromethane, the residue was cooled over night at -18 ºC, the precipitate was collected by suction filtration, washed with cold petroleum and dried in vacuum to give **4b** as a beige solid (56.7 g, 82 %).

mp: 66 ºC.
^{1}H-NMR: δ (300 MHz, DMSO-d_6) 0.84-0.89 (m, 6 H); 1.25-1.49 (m, 12 H); 1.59-1.76 (m, 4 H); 2.06 (s, 3H); 3.94 (t, ^{3}J = 6.25 Hz, 2 H); 4.15 (t, ^{3}J = 6.4 Hz, 2 H); 7.16 (dd, ^{4}J = 1.7 Hz, ^{3}J = 8.6 Hz, 1 H); 7.47 (d, ^{4}J = 1.47 Hz, 1 H); 7.64 (d, ^{3}J = 8.46 Hz, 1 H); 10.18 (s, 1 H).
^{13}C-NMR and DEPT: δ (300 MHz, DMSO-d_6) 13.87 (+); 22.08 (+); 22.14 (+); 24.2 (+); 25.21 (-); 25.3 (-); 28.31 (-); 28.68 (-); 31.03 (-); 31.08 (-).
IR ν (cm^{-1}): 3306, 3272, 2955, 2932, 2856, 1679, 1662, 1595, 1543, 1409, 1274, 1261, 1191, 1138, 831.
RP-HPLC (min.): 35.6.
M (FD): *m/z* (%) = 363.4 (100); 364.4 (19); calc.[$C_{21}H_{33}NO_4$] = 363.2

4-Amino-2-TEG-benzoic acid **5a***:* A solution of **4a** (14.17 g, 0.029 mol), KOH (6.8 g) and ethanol (100 ml) were heated under reflux for 50 hrs. The solvent was then removed under reduced pressure, the residue dissolved in water and extracted with chloroform. The aqueous phase was then neutralized and the product isolated by concentration of the organic phase after extraction of the later aqueous phase. Chromatographic purification (eluent TCM:MeOH 15:1) afforded the pure product **5a** (6 g, 70 %).

^{1}H-NMR: δ (300 MHz, DMSO-d_6) 3.36 (s, 3 H); 3.52-3.55 (m, 2 H); 3.63-3.73 (m, 6 H); 3.88 (t, ^{3}J = 4.6 Hz, 2 H); 4.27 (t, ^{3}J = 4.6 Hz, 2 H); 6.22 (d, ^{4}J = 1.84 Hz, 1 H); 6.35 (dd, ^{3}J = 8.46 Hz, ^{4}J = 2.21 Hz, 1 H); 7.91 (d, ^{3}J = 8.46 Hz, 1 H).
^{13}C-NMR and DEPT: δ (300 MHz, DMSO-d_6): 58.74; 68.48 (-); 68.54 (-); 70.29 (-); 70.33 (-); 70.45 (-); 71.64 (-); 97.82 (+); 106.64; 108.4 (+); 134.9 (+); 153.5; 159.15; 166.15.
IR ν (cm^{-1}): 3446, 3354, 3235, 2877, 1701, 1600, 1449, 1336, 1268, 1196, 1095, 1035, 832.
RP-HPLC (min.): 9.1.
M (FD): *m/z* (%) = 322.12 (100); 323.13 (4); calc.[$C_{14}H_{21}NO_6Na$] = 322.1

4-Amino-2-hexyloxy-benzoic acid **(5b)**: A solution of **4b** (55.3 g, 0.15 mol), KOH (35 g) and ethanol (550 ml) was heated under reflux for 50 hrs. The solvent was then removed under reduced pressure, the residue dissolved in water (550 ml) and neutralized with 6N HCl. The precipitate was collected, washed well with water and dried under vacuum at 60 ºC to give **5b** (30.3 g, 85%).

mp: 122 ºC.
^{1}H-NMR: δ (300 MHz, DMSO-d_6) 0.87 (t, ^{3}J = 6.99 Hz, 3 H); 1.26-1.31 (m, 4 H); 1.43 (m, 2 H); 1.71 (tt, 2 H); 3.93 (t, ^{3}J = 6.4 Hz, 2 H); 5.86 (s, 2H); 6.14 (dd, ^{4}J = 1.84 Hz, ^{3}J = 8.46 Hz, 1 H); 6.2 (d, ^{4}J = 2.21 Hz, 1 H); 7.50 (d, ^{3}J = 8.82 Hz, 1 H); 11.31 (s, 1 H).
^{13}C-NMR and DEPT: δ (300 MHz, DMSO-d_6) 13.88 (+); 22.08 (-); 25.09 (-); 28.58 (-); 30.94 (-); 67.98 (-); 97.22 (+); 105.82 (+); 106.06; 133.79 (+); 154.49; 160.42; 166.34.
IR ν (cm^{-1}): 3428, 3345, 3232, 2930, 1685, 1586, 1456, 1401, 1339, 1267, 1191, 998, 831.
RP-HPLC (min.): 21.9
M (FD): *m/z* (%) = 237.8 (100); 238.8 (17); 239.8 (1.4); calc.[$C_{13}H_{19}NO_3$] = 237.1

N-Fmoc-4-amino-2-TEG benzoic acid **(8a): 5a** (5.67 g, 19 mmol) was dissolved in dry NMP (30 ml) under an inert atmosphere followed by the dropwise addition of Fmoc-Cl (5.39 g, 21 mmol) in dry NMP (15 ml). After 24 hrs, the reaction mixture was poured slowly into 300 ml water. The beige precipitate was collected by filtration, washed with water and recrystallized twice from toluene to afford **8a** (6.7 g, 13 mmol, 70 %).

mp: 126 ºC.

^{1}H-NMR: δ (300 MHz, DMSO-d_6) 3.28 (s, 3 H); 3.43-3.46 (m, 2 H); 3.51-3.64 (m, 6 H); 3.81 (t, ^{3}J = 4.41 Hz, 2 H); 4.22-4.29 (m, 3 H); 4.63 (d, ^{3}J = 6.25 Hz, 2 H); 6.83 (dd, ^{3}J = 8.6 Hz, ^{4}J = 1.7 Hz, 1 H); 7.33 (t, ^{3}J = 7.35 Hz, 2 H); 7.42 (t, ^{3}J = 7.2 Hz, 2 H); 7.5 (s, 1 H); 7.56 (s, 1 H); 7.64 (d, ^{3}J = 6.99 Hz, 2 H); 7.79 (d, ^{3}J = 7.35 Hz, 2 H); 8.03 (d, ^{3}J = 8.82 Hz, 2 H).

^{13}C-NMR and DEPT: δ (300 MHz, DMSO-d_6) 46.56 (+); 58.02 (+); 65.83 (-); 68.39 (-); 68.6 (-); 69.59 (-); 69.85 (-); 70.11 (-); 71.26 (-); 103.05 (+); 109.83 (+); 114.49; 120.22 (+); 125.12 (+); 127.16 (+); 127.74 (+); 132.46 (+); 140.83; 143.69; 143.96; 153.24; 158.72; 166.37.

IR ν (cm^{-1}): 3270, 2900, 1728, 1593, 1536, 1428, 1218, 1193, 1132, 1084, 1063, 1045, 1002, 858, 842, 745.

RP-HPLC (min.): 25.9.

M (FD): *m/z* (%) = 544.2 (100); 545.2 (24.9); 546.2 (1.4); calc.[$C_{29}H_{31}NO_8Na$] = 544.2

N-Fmoc-4-amino-2-hexyloxy benzoic acid **(8b). 5b** (19.9 g, 84 mmol) was dissolved in dry NMP (140 ml) under an inert atmosphere followed by the dropwise addition of Fmoc-Cl (21.67 g, 83.8 mmol) in dry NMP (55 ml). After 24 hrs, the reaction mixture was poured slowly into 280 ml water. The beige precipitate was collected by filtration, washed with water, petroleum ether and recrystallized from toluene to afford **8b** (38.6 g, 89%).

mp: 159 ºC.

^{1}H-NMR: δ (300 MHz, DMSO-d_6) 0.86 (t, ^{3}J = 6.62 Hz, 3 H); 1.27-1.30 (m, 4 H); 1.43 (m, 2 H); 1.71 (tt, 2 H); 3.95 (t, ^{3}J = 6.25 Hz, 2 H); 4.32 (t, ^{3}J = 6.62 Hz, 1 H); 4.52 (d, ^{3}J = 6.62 Hz, 2 H); 7.08 (d, ^{3}J = 8.09 Hz, 1H); 7.33-7.45 (m, 5 H); 7.65 (d, ^{3}J = 8.46 Hz, 1H); 7.76 (d, ^{3}J = 6.99 Hz, 2 H); 7.91 (d, ^{3}J = 7.35 Hz, 2 H), 9.98 (s, 1H).

^{13}C-NMR and DEPT: δ (300 MHz, DMSO-d_6) 13.87 (+); 22.06 (-); 25.01 (-); 28.5 (-); 30.9 (-); 46.56 (+); 65.8 (-); 68.15 (-); 102.63 (+); 109.34 (+); 114.43; 120.19 (+); 125.11 (+); 127.13 (+); 127.71 (+); 132.34 (+); 140.82; 143.69; 143.87; 153.24; 158.94; 166.57.
IR ν (cm^{-1}): 3302, 3218, 2952, 2932, 2856, 1738, 1710, 1608, 1528, 1414, 1309, 1196, 1103, 736.
RP-HPLC (min.): 34.9
M (FD): *m/z* (%) = 459.5 (100); 460.6 (16.7); calc.[$C_{28}H_{29}NO_5$] = 459.2

Polycondensation. *Polycondensation method **(i)** using triphenyl phosphite:* A mixture of monomer (**5a**, **5b**) (3.3 mmol), triphenyl phosphite (3.3 mmol), NMP or dichlorobenzene (DCB) (6.6 ml) and pyridine (1.65 ml) was heated under argon at 100 ºC (for NMP) or at 80 ºC (for DCB). After 6 hrs. methanol was added, the precipitate was filtered, washed well with methanol, water, again methanol and then with diethylether. Polymer (**11ai**, **11bi)** precipitated from the reaction mixture after 3 hrs. , affording a product insoluble in methanol, TCM, DMSO, DMF, DMF/LiBr, NMP or hexafluorobenzol.

11ai: ^{1}H-NMR: δ (400 MHz, D_2SO_4) 3.77-4.7 (m, 15 H); 7.31-8.62 (m, 3 H).
IR ν (cm^{-1}): 3334, 2922, 2871, 1668, 1582, 1502, 1454, 1411, 1230, 1095, 848.

11bi: ^{1}H-NMR: δ (400 MHz, D_2SO_4) 0.42 (br. s, 3 H), 0.89-1.03 (m, 6 H), 1.55 (br. s, 2 H), 4.05 (br. s, 2 H), 6.67-7.91 (m, 3 H).
IR ν (cm^{-1}): 3339, 2928, 2857, 1669, 1581, 1517, 1409, 1236, 1191, 1121, 1018, 760.

*Polycondensation method **(ii)** of N-sulfinylamino-2-TEG benzoyl chloride* **(6a)**:[1] 4-Amino-2-TEG-benzoic acid **5a** (1.36 g, 4.5 mmol) was refluxed in thionyl chloride (30 ml). After 3 hrs., the excess of thionyl chloride was removed over night under vacuum to afford *p*-(*N*-sulfinylamino)-2-TEG benzoyl chloride **6**. After dissolution in dry THF (60 ml), the solution was cooled with an external ice bath and HCl was passed through for 2.5 hrs. The solvent was removed under reduced pressure; dry NMP (20 ml) was added and stirring was continued at rt. After 3 days the product was precipitated in MeOH, centrifugated and washed with water (2x) to obtain **11aii** (0.63 g, 46%).

Heptamer synthesis. *Resin functionalization*. Wang resin (417 mg, 0.25 mmol, loading: 0.6 mmol/g) was swollen in a minimum amount of dry NMP. Fmoc-protected amino acid **8a** or **8b** (2 mmol) was dissolved in NMP (2 ml) and thionyl chloride (0.22 ml, 3 mmol) was added. After 2 hrs, the solution was evacuated for 30 min. and poured into the flask containing the wang resin. After 24 hrs the resin was drained and washed 4 times with NMP. Unreacted functional groups on the resin were capped with a solution of 4-nitrobenzoyl chloride (0.46 g, 2.5 mmol) in NMP (1.5 ml).

Preparation of the acid chloride **9a** and **9b** *for the automated solid phase synthesis.* **8a** or **8b** (13 mmol) was dissolved in thionyl chloride (30 ml) and a catalytic amount of dry NMP was added. After stirring for 2.5 hrs, thionyl chloride was removed under reduced pressure, the acid chloride was redissolved in dry DCM and the solvent removed again under vacuum. Dry NMP (23.5 ml) was added and the solution filtered through a 400 micron syringe filter into the cartridges of the peptide synthesizer (1 mmol per cartridge). *Automated heptamer **(11iii)** synthesis on a peptide synthesizer.* The functionalized resin was *N*-deprotected, reacted with 4 eq. acid chloride **9a** or **9b** (2x), followed by the reaction with 4 eq. 4-nitrobenzoyl chloride as capping reagent (0.54 mmol/ml, 2 ml). This sequence was repeated 6 times to afford the heptamer **11aiii** or **11biii**. The efficiency of the monomer coupling steps was monitored during the synthesis by UV-detection of the deprotected Fmoc groups. The oligomer was cleaved off the solid support by stirring in TFA-DCM (50 %) solution for 12 hrs.

11aiii: The solvent was concentrated, the crude product precipitated in ether and centrifugated (0.39 g, 0.2 mmol, 80 %). Purification by column chromatography (1 / 0.1 TCM / MeOH) afforded 180 mg of pure product.
^{1}H-NMR: δ (400 MHz, DMSO-d_6) 3.15-3.23 (m, 21 H); 3.3-4.1 (m, 70 H); 4.13-4.4 (m, 14 H); 6.27 (m, 2 H); 7.20-7.42 (m, 6 H); 7.6-7.97 (m, 13 H); 10.18-10.41 (m, 6 H). M (MALDI-TOF): *m/z* = 2038.2 $[M(K\text{-salt}) + 2Li]^+$; calc.$[C_{98}H_{134}N_7O_{36}KLi_2]^+$ = 2038.8.

11biii: The solvent was concentrated, poured into ether and centrifugated to afford a product insoluble in organic solvents.

4.1.5. References

[1] Kowlek, S. L.; Morgan, P. W.; Schaefgen, J. R.; Gulrich, L. W. *Macromolecules* **1977**, *10*, 1390-1396.

[2] Herlinger, H.; Knoell, H.; Menzel, H.; Schlaefer, J. *Appl. Polym. Symp.* **1973**, *21*, 215-224.

[3] (a) Panar, M.; Beste, L. F. *Macromolecules* **1977**, *10*, 1401-1406; (b) Takahashi, Y.; Ozaki, Y.; Takase, M.; Krigbaum, W. R. *J. Polym. Sci. Part B* **1993**, *31*, 1135-1143.

[4] Herlinger, H., Knoell, H.; Menzel, H.; Schlaefer, J.; *Appl. Polym. Symp.* **1974**, *21*, 212-221.

[5] Yokozawa, T.; Ogawa, M.; Sekino, A.; Sugi, R.; Yokoyama, A. *J. Am. Chem. Soc.* **2002**, *124*, 15158-15159; Seyler, H.; Berger-Nicoletti, E.; Kilbinger, A. F. M. *J. Mater. Chem.* **2007**, *17*, 1954-1957; Abbel, R.; Frey, H.; Schollmeyer, D.; Kilbinger, A. F. M. *Chem. Eur. J.* **2005**, *11*, 2170-2176.

[6] (a) Rivas, B. L.; Canessa, M. L.; Rabagliati, F. M.; Novi, M.; Preston, J.; *Macromol. Chem. Phys.* **2001**, *202*, 1053-1059; (b) Cavalleri, P.; Ciferri, A.; Dell'Erba, C.; Gabellini, A.; Novi, M.; *Macromol. Chem. Phys.* **1998**, *199*, 2087-2094; (c) Abbel, R.; Schleuss, T. W.; Frey, H.; Kilbinger, A. F. M.; *Macromol. Chem. Phys.* **2005**, *206*, 2067-2074; (d) Yokozawa, T.; Ogawa, M.; Sekino, A.; Sugi, R.; Yokoyama, A. *Macromol. Symp.* **2003**, *199*, 187-195; (e) Gabellini, A.; Novi, M.; Ciferri, A.; Dell'Erba, C. *Acta Polym.* **1999**, *50*, 127-134; (f) Rabagliati, F. M.; Aravena, M.; Lillo, I.; Ayal, H. A.; Rivas, B. L.; Canessa, G. S.; *Polym. Bull.* **1996**, *37*, 345-351; (g) Chavan, N.; Ciferri, A.; Dell'Erba, C.; Novi, M.; Renamayor, C. S.; *Macromol. Chem. Phys.* **1996**, *197*, 2415-2428; (h) Rivas, B. L.; Barria, B.; Canessa, G. S.; Rabagliati, F. M.; Preston, J. *Macromolecules* **1996**, *29*, 4449-4452; (i) Marsano, E.; Bianchi, E.; Conio, G.; Mariani, A.; Russo, S. *Polym. Commun.* **1991**, *32*, 45-46; (j) Klos, J.; Wurm, F.; König, H. M.; Kilbinger, A. F. M. *Macromolecules* **2007**, *40*, 7827-7833; (k) Schleuss, T. W.; Abbel, R.; Gross, M.; Schollmeyer, D.; Frey, H.; Maskos, M.; Berger, R.; Kilbinger, A. F. M. *Angew. Chem. Int. Ed.* **2006**, *45*, 2969-2975.

[7] (a) Ballauff, M. *Makromol. Chem., Rapid. Commun*. **1986**, *7*, 407-414; (b) Ballauff, M. *Makromol. Chem., Rapid. Commun*. **1987**, *8*, 93-97; (c) Wenzel, M.; Ballauff, M.; Wegner, G. *Makromol. Chem*. **1987**, *188*, 2865-2873; (d) Herrmann-Schönherr, O.; Wendorff, J. H.; Ringsdorf, H.; Tschirner, P. *Makromol. Chem., Rapid Commun*. **1986**,

7, 791-796; (e) Ballauff, M. *Angew. Chem. Int. Ed*. **1989**, *28*, 253-267, (f) Kricheldorf, H. R.; Bürger, R. *J. Polym. Sci. Pol. Chem.* **1994**, *32*, 355-362.

[8] Bosshard, H. H.; Mory, R.; Schmid, M.; Zollinger, H. *Helv. Chim. Acta* **1959**, *176*, 1653-1658.

[9] Yamazaki, N.; Matsumoto, M.; Higashi, F. *J. Polym. Sci. Part A* **1975**, *13*, 1373-1380.

[10] W. C. Chan, P. D. White, *Fmoc Solid Phase Peptide Synthesis, A.Practical Approach*, W. C., Oxford University Press, Oxford, UK **2000**.

[11] Bair, T. I.; Morgan, P. W.; Killian, F. L. *Macromolecules* **1977**, *10*, 1396-1400.

[12] (a) Huc, I.; *Eur. J. Org. Chem.* **2004**, 17-29; (b) Parra, R.D.; Zeng, H.; Zhu, J.; Zheng, C.; Zeng, X.C.; Gong, B. *Chem. Eur. J*. **2001**, *7*, 4352-4357; (c) Gong, B.; Zeng, H.; Zhu, J.; Yuan, L.; Han, Y.; Cheng, S.; Furukawa, M.; Parra, R.D.; Kovalevsky, A.Y.; Mills, J.L.; Skrzypczak-Jankun, E.; Matrinovic, S.; Smith, R.D.; Zheng, C.; Szyperski, T.; Zeng, X.C. *Proc. Nat. Acad. Sci*. **2002**, *99*, 11583-11588.

[13] Malone, J. F.; Murray, C. M.; Dolan, G. M.; Docherty, R.; Lavery, A. *J. Chem. Mater.* **1997**, *9*, 2983-2989.

[14] Brockmann, T. W.; Tour, J. M. *J. Am. Chem. Soc.* **1995**, *117*, 4437-4447.

[15] (a) Koenig, M. H.; Gorelik, T.; Kolb, U.; Kilbinger, A. F. M. *J. Am. Chem. Soc.* **2007**, *129*, 704-708; (b) Koenig, M. H.; Kilbinger, A. F. M. *Macromol. Rapid Commun.* **2008**, *29*, 1721-1725.

4.1.6. Supporting Information for "Linear soluble Poly(*p*-benzamide)s"

Experimental

Materials

Technical- and *p.a.* quality solvents were purchased from Acros Organics. Dichloromethane and DMSO were purchased from Fisher Scientific. 9-Fluorenylmethyl chloroformate (Fmoc-Cl) and Wang resin were obtained from Iris Biotech GmbH, all other chemical reagents were purchased from Acros Organics and used without further purification. Deuterated solvents (DMSO-d_6 and $CDCl_3$) were purchased from Deutero GmbH.

Thermogravimetric analyses were performed on a Pyris 6 TGA Perkin Elmer.

Automated heptamer 11aiii / 11biii synthesis on a peptide synthesizer

STEP	Rpt.	Name	Modules
1	6	Middle cycle with capping	GgBdefffGgdefffGgeff
7	1	Deprotection and NMP wash	gBd

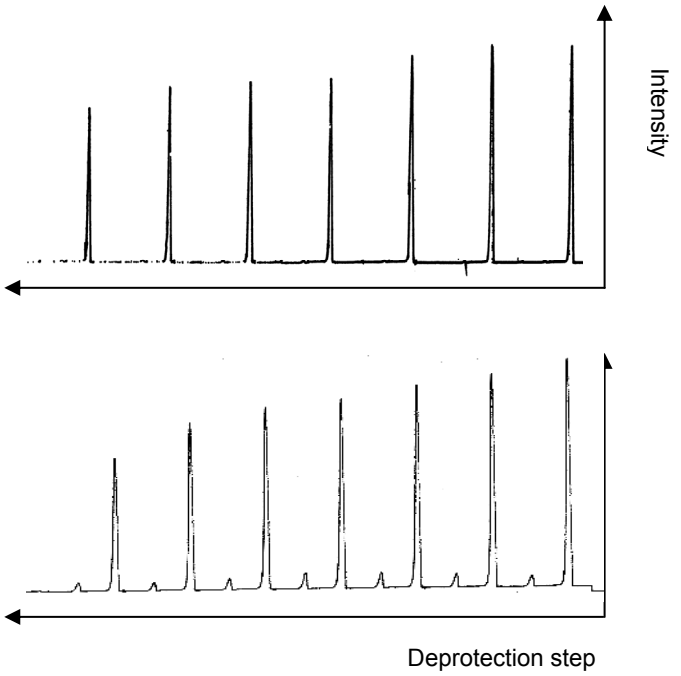

Figure SI-4.1.1. UV-monitoring profile (λ= 301 nm) obtained during the solid phase synthesis of **11aiii** *(top)* and **11biii** (*bottom*).

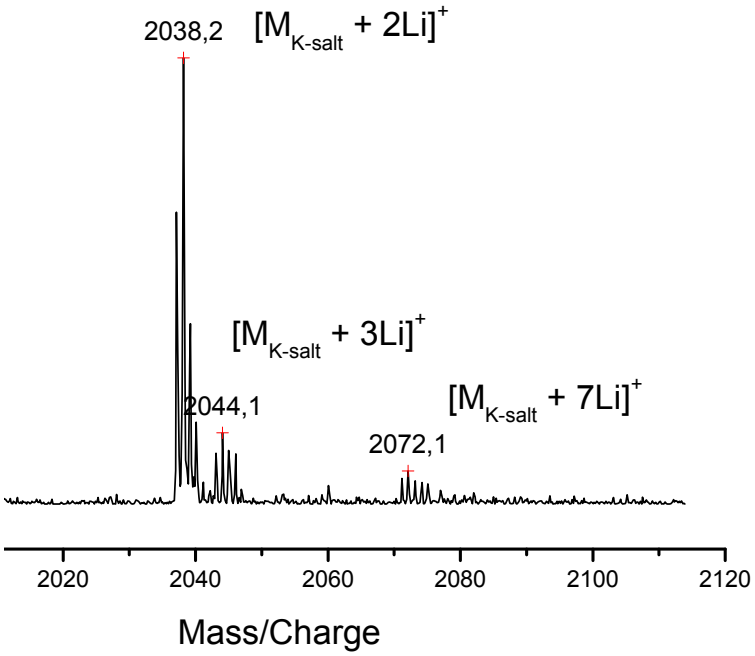

Figure SI-4.1.2. MALDI-TOF spectrum of **11aiii**.

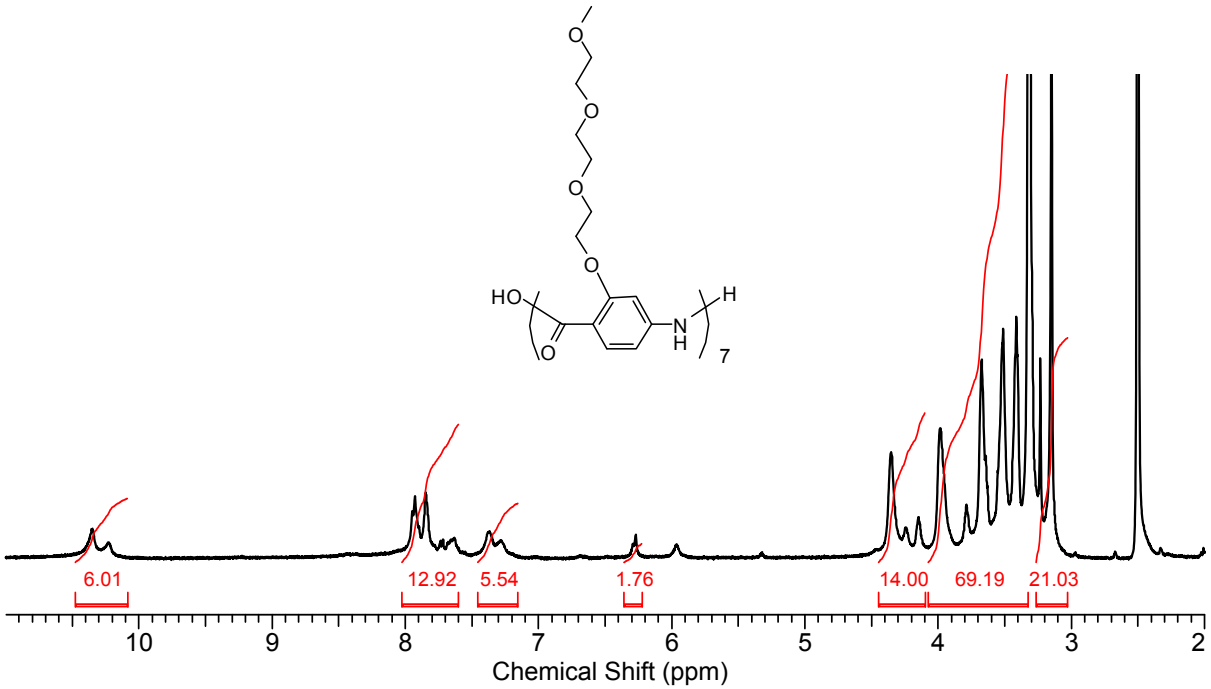

Figure SI-4.1.3. ^{1}H-NMR spectrum (400 MHz) of **11aiii** in DMSO-d_6.

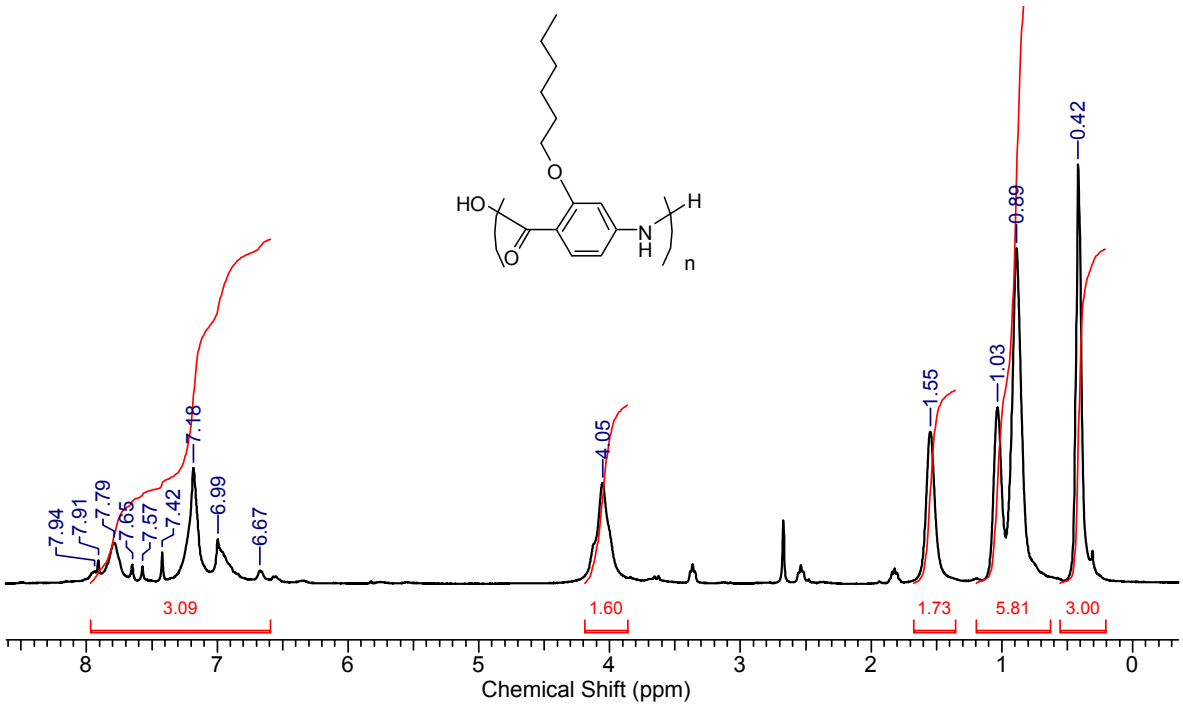

Figure SI-4.1.4. ^{1}H-NMR spectrum (400 MHz) of **11bi** in D_2SO_4.

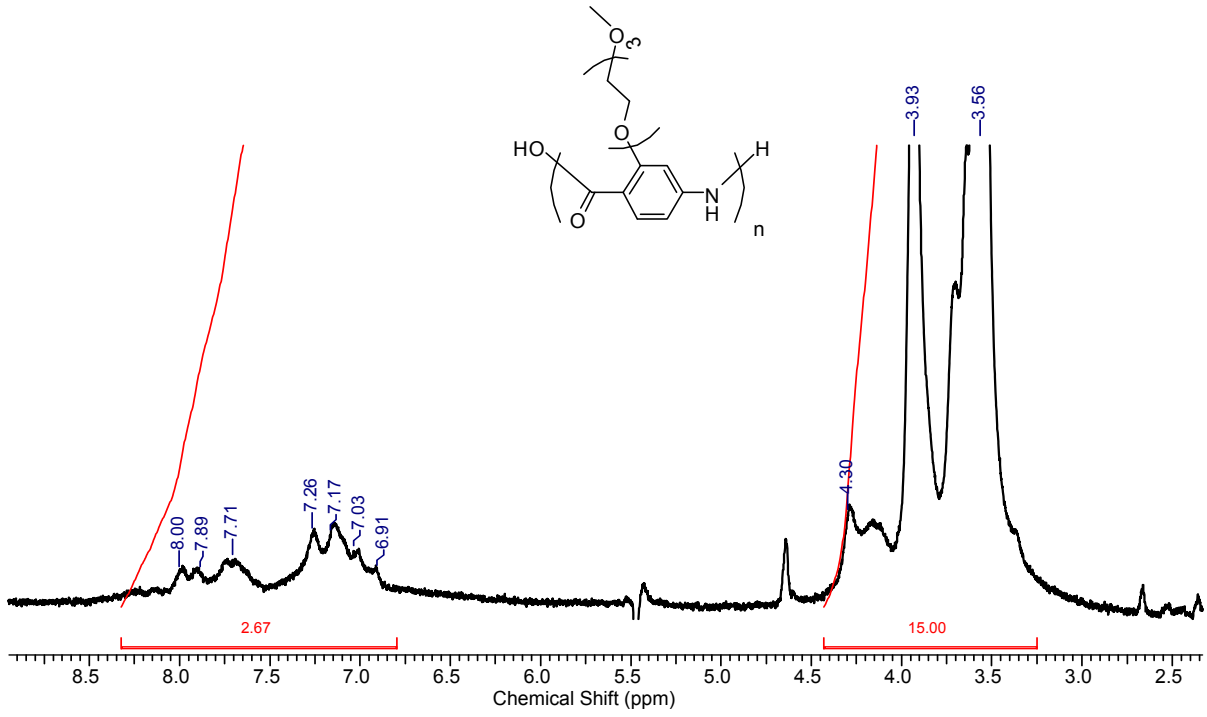

Figure SI-4.1.5. ^{1}H-NMR spectrum (400 MHz) of **11aii** D_2SO_4.

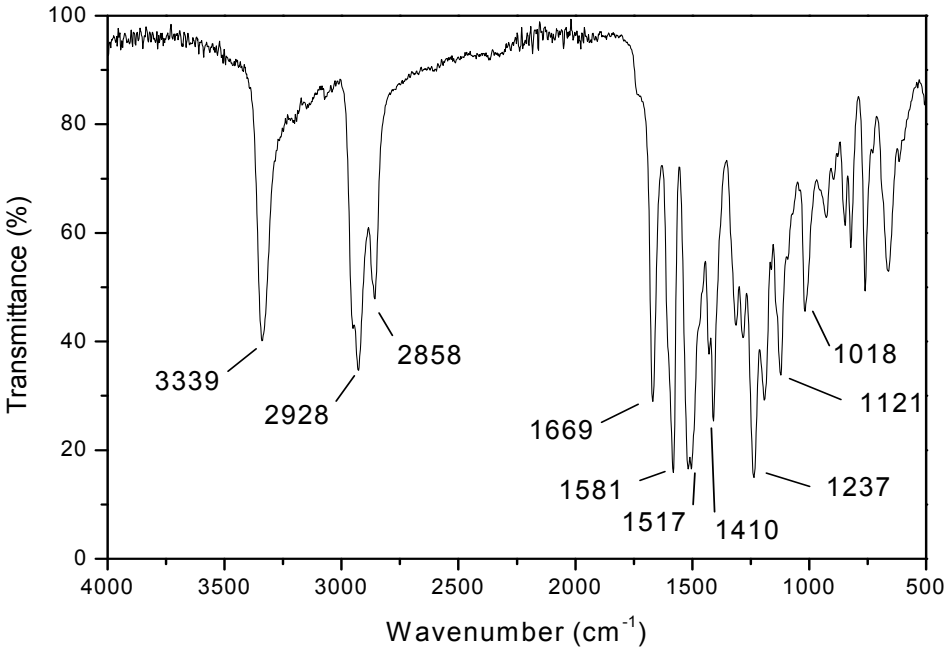

Figure SI-4.1.6. FT-IR spectrum of **11bi**. Absorption bands: 3339 (NH amide), 2928 and 2858 (C-H aliph.), 1669 (C=O amide), 1581 and 1517 (C=C arom.), 1410 (C-H aliph.) 1237-1018 (C-O-C).

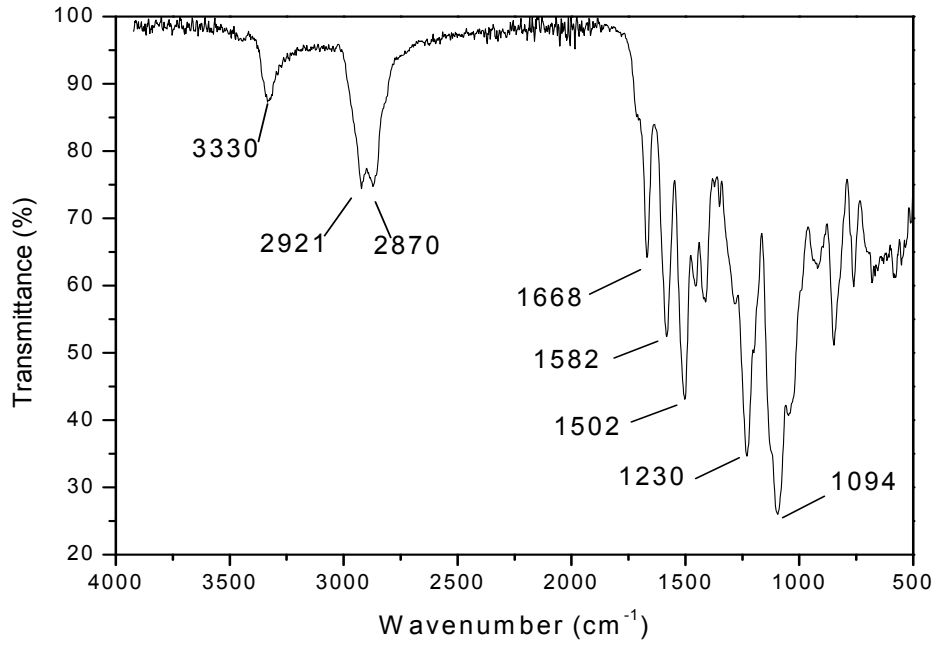

Figure SI-4.1.7. FT-IR spectrum of **11aii**. Absorption bands: 3330 (NH amide), 2921 and 2870 (C-H aliph.), 1668 (C=O amide), 1582 and 1502 (C=C arom.), 1230 and 1094 (C-O-C).

Tab. SI-4.1.1. Molecular weights (determined by GPC in DMF) of the TEG-grafted poly(*p*-benzamide) products afforded by different polymerization methods. **SPS**: Solid Phase Synthesis; **TPP** (NMP/DCB): Triphenylphosphite method (solvent: N-methylpyrrolidone or dichlorobenzene); **NSO**: *N*-sulfinylamino benzoyl chloride method. (* = theoretical values).

	Synthetic strategy	M_n (g/mol)	M_w (g/mol)	PDI
11aiii	**SPS**	390 (1985*)	1150 (1985*)	2.9 (1.0*)
11ai	**TPP** NMP DCB	1370 1590	2090 2150	1.5 1.4
11aii	**NSO**	3070	2470	8

It has to be considered, that the values in **tab. SI-4.1.1** can only be qualitatively interpreted. The monodisperse model compound **11aiii** reveals the underestimation of the molecular weight of the synthesized benzamides determined by this method. The second mode at higher mol masses (outside the calibration limit) provides the indication of the aggregation taking place in TCM. The high polydispersity value observed for the heptamer in DMF (PDI = 2.9, see **tab. SI-4.1.1**) may indicate the formation of noncovalent superstructures in polar solvents.

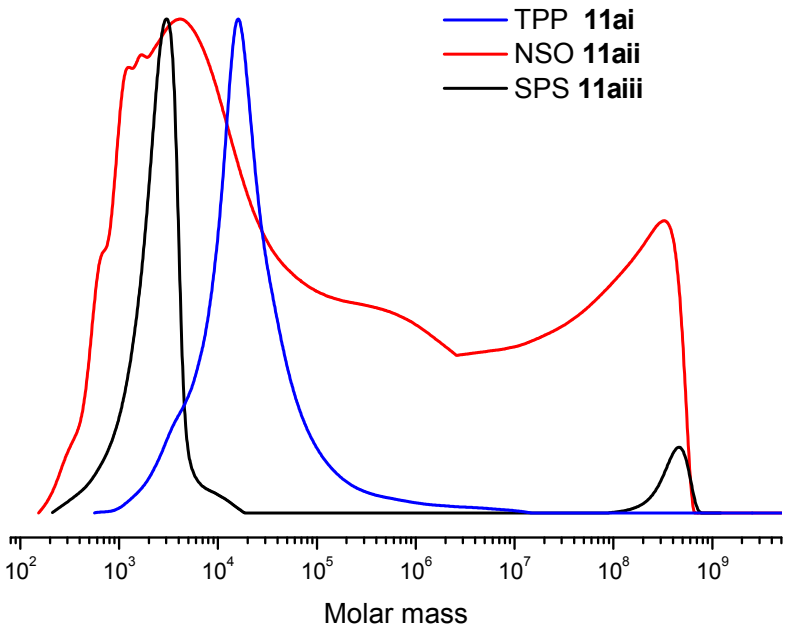

Figure SI-4.1.8. GPC-traces of the monodisperse heptamer **11aiii** and polydisperse products **11ai** and **11aii**.

Comparison of the molecular weights from the GPC measurements in DMF (see **tab. SI-4.1.1**) with the elugrams in TCM (see **figure SI-4.1.8**) elucidates the increment of aggregation tendency and aggregate stability when increasing molecular weight.
The increase of the molecular weight of the aggregates in DMF correlates with the observed stability tendency of the supramolecular structures in TCM.

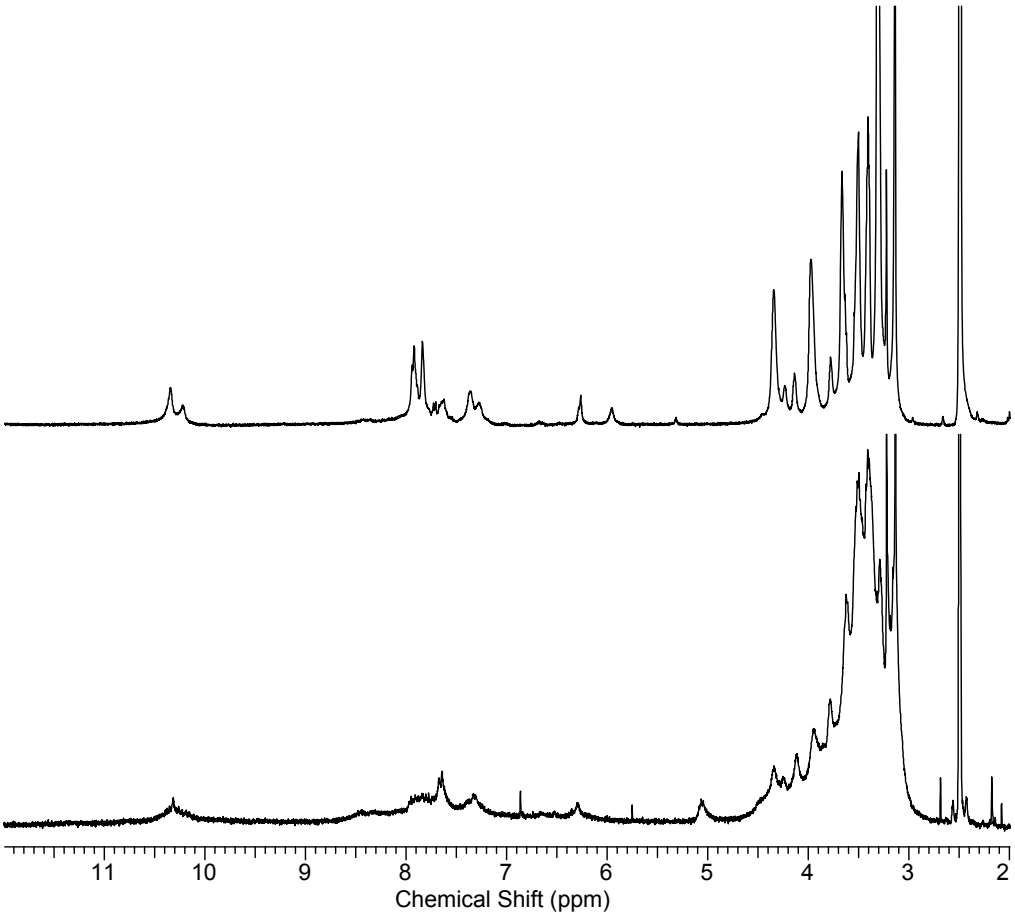

Figure SI-4.1.9. ^{1}H-NMR spectrum (400 MHz) of polymer **11aii** (*bottom*) and heptamer **11aiii** (*top*) in DMSO-d_6. Significant broadening of the aromatic proton signals of the higher molecular weight polymer with respect to the oligomer.

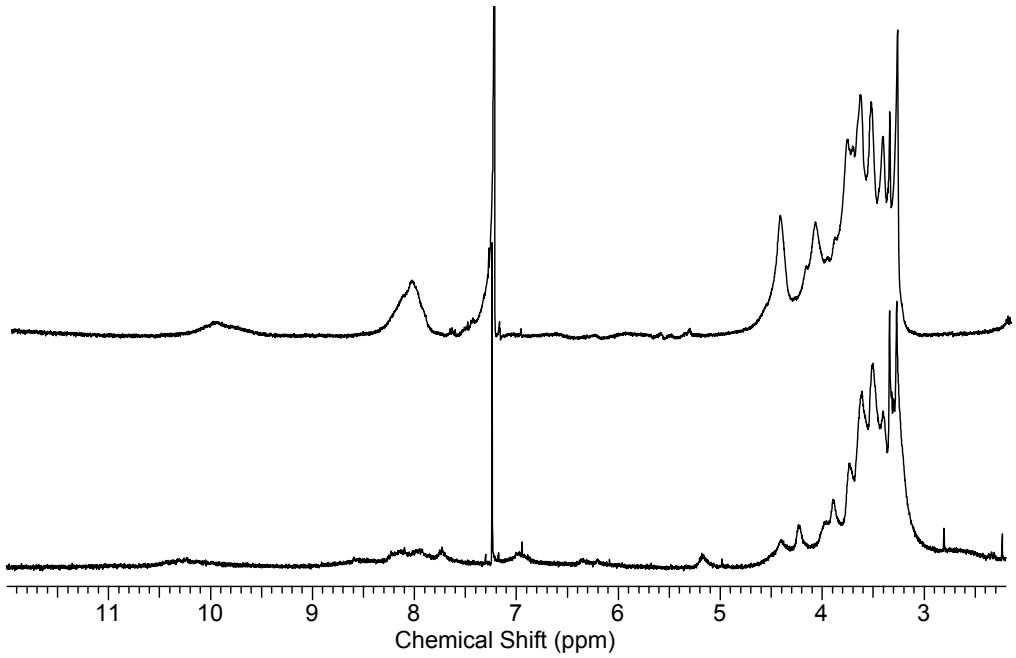

Figure SI-4.1.10. ^{1}H-NMR spectrum (400 MHz) of polymer **11aii** (*bottom*) and heptamer **11aiii** (*top*) in $CDCl_3$. Significant broadening of the aromatic proton signals of the higher molecular weight polymer with respect to the oligomer.

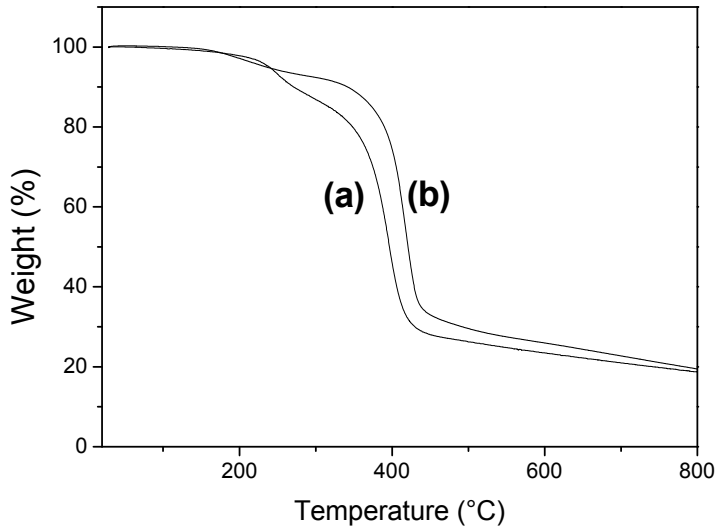

Figure SI-4.1.11. Thermograms (in nitrogen; heating rate 20°C/min) of homopolymers: **(a)** poly(2-TEG-*p*-benzamide) **11aii** and **(b)** poly(2-hexyl-*p*-benzamide) **11bi**.

The initial weight loss (4.4 % for **(a)** and 4.2 % for **(b)**) is negligible and probably caused by residual amounts of NMP (high boiling point and noncovalent interactions to the polymer made the complete removal of the solvent unfeasible). The onset temperatures, at which a rapid weight loss is observed are 378 °C and 394 °C for **(a)** and **(b)** respectively.

4.2. Hairy Rod-Coil Copolymers

Abstract

Monodisperse hairy rod oligomers involving oligo(*p*-benzamide)s carrying alkyl side chains are presented. The hairy nanorods, ranging from 4 to 7 benzamide units, were synthesized automatically and end-chain functionalized with PEG-polymers to improve solubility and control aggregation. The self-organization in solution was investigated by dynamic light scattering and transmission electron microscopy as a function of solvent, equilibration time and property of aggregate deposition surface.

Kurzfassung

Monodisperse "*Hairy Rods*" aus Oligo(*p*-benzamid)en mit direkt am aromatischen Rückgrad kovalent-gebundenen Alkylseitenketten wurden synthetisiert und an PEG Polymere gebunden, um eine höhere Löslichkeit und Kontrolle über das Aggregationsverhalten zu erlangen. Die Selbstorganisation in Lösung von Copolymeren mit alkyl-substituiertem Tetramer und Heptamer wurde mittels dynamischer Lichtstreuung und Transmissionselektronenmikroskopie untersucht, wobei der Einfluss von Lösungsmittel, Äquilibrierungszeit und Substratoberflächen-eigenschaften bei der Trockenpräparation der Proben analysiert wurde.

4.2.1. Introduction

‘‘Hairy rods’’[1] (HR) are stiff insoluble macromolecules with flexible short or long side chains attached to their backbones. These “liquid-like” substituents act like a polymer bound solvent shell, disguise the backbone, and help to achieve higher solubility and easier processability.[2] This new class of polymers have a high tendency to self-assemble into interesting supramolecular structures and materials (**figure 4.2.1**),[3,4] both in bulk and solution. Thin films prepared from hairy rods often exhibit high dimensional stability since the rigid backbones act as reinforcing elements in an amorphous matrix of side chains,[5] overcoming compatibility limitations in some composite materials.[4] Hairy rods show also liquid crystalline properties, if anisotropic nanoparticles are used.[6] They have also received a lot of attention in the context of electrically conductive architectures, when the main chains consist of conjugated rigid polymers.[7]

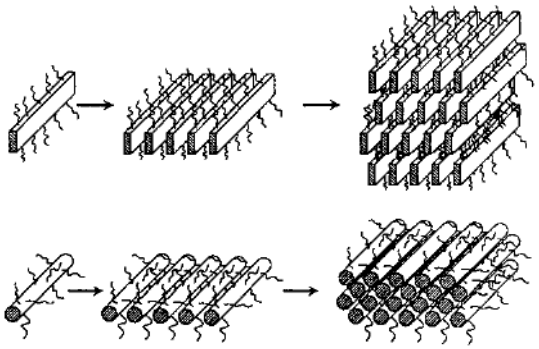

Figure 4.2.1. Supramolecular architectures of HR macromolecules.[2]

Typical polymers and oligomers that belong to these type of materials are substituted glutamates,[1,8] alkylthiophenes,[9,10] substituted *p*-phenylenes[4,11] and fluorenes[10,12].

Applying the concept of ‘‘hairy rods’’ to aromatic amides seemed very promising to us. The synthesis of short ethylene oxide side chains on stiff poly(*p*-benzamide)s (OPBA) was recently described (see **chapter 4.1**) and lead to highly processable materials.[13] On the other hand, a high density of hexyloxy substituents attached to the rod, was shown to induce the opposite property, i.e. insolubility. In order to ‘‘solubilize’’ these hairy nanoobjects with hexyloxy side chains, we approached their functionalization with a soluble PEG-corona.

4.2.2. Results and Discussion

The synthesis of a hairy rod material **1** with a stiff *p*-benzamide backbone and short hexyl side chains was briefly described in **chapter 4.1**. The insolubility of the homopolymer and the oligomers (up to the tetramer) was first counterintuitive to us. *Ab inito* calculations of model compounds revealed that the formation of intramolecular hydrogen bonds to the hexylether resulted in a perfectly flat oligomer with almost no rotational freedom, leading to a highly insoluble material. In order to overcome this solubility problem, the next approach was based on the synthesis of block-copolymers composed of monodisperse hairy rod blocks and a highly soluble polymeric segment.

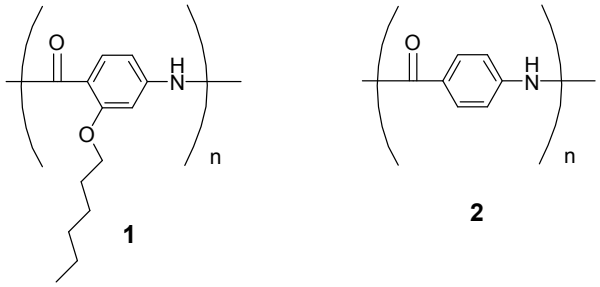

Figure 4.2.2. Chemical structure of HR- **(1)** and plain poly(*p*-benzamide)s **(2)**.

First, hairy rods of different oligomerization degrees were prepared on the solid support in order to systematically study their solubility characteristics (see **scheme 4.2.1**). Similarly to the properties of plain oligo(*p*-benzamide)s **2**, the trimeric compound **4a** could be fully characterized, but only in limited solvents and concentrations. The tri(2-hexyloxy-*p*-benzamide) **4a** was moderately soluble in TCM / MeOH mixtures and fairly soluble in highly polar aprotic solvents like DMSO. Oligomers up to the tetramer **4b** were insoluble in organic media.

As the short hairs with angstroms dimensions (approx. 6 Å) are not long enough to solubilize the stiff aramide backbone, polymer chains were attached to the *N*-terminus of the rods. The same synthetic strategy described in chapter **4.3** for comb-like oligomers, was applied for the hairy *p*-benzamides, in order to synthesize soluble copolymers with PEG blocks (see scheme **4.2.2**). The long polymer chains with nanometer dimensions (approx. 20 nm for the extended chain) and larger free volume (compared to the short alkyl chains) can interact better with the solvent. This large interaction volume between solvent and functionalized rods leads to a good solubility of the material in good solvents for the polymer.[14]

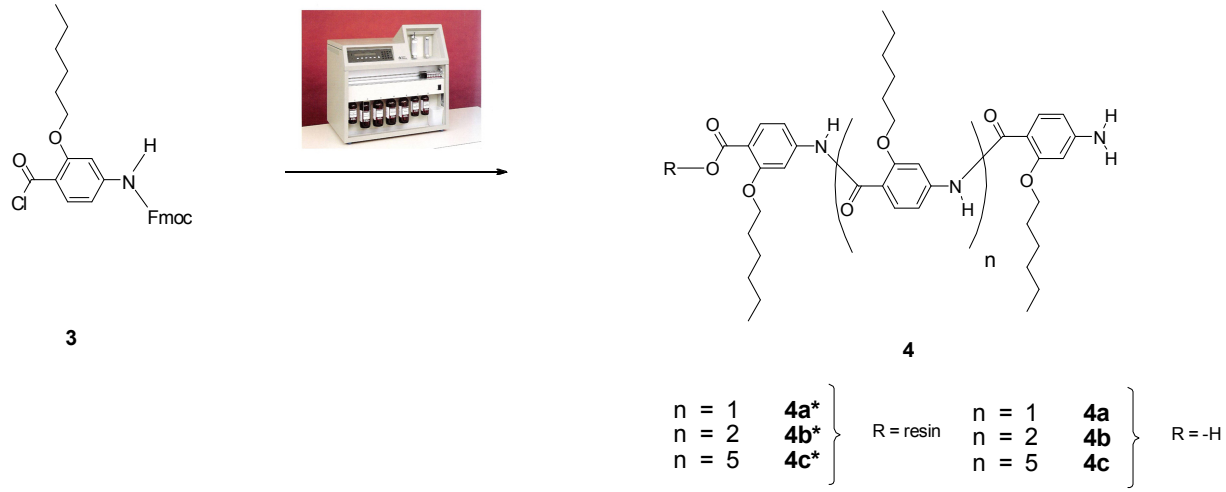

Scheme 4.2.1. Chemical structure of the hairy rod oligomers prepared automatically on a peptide synthesizer.

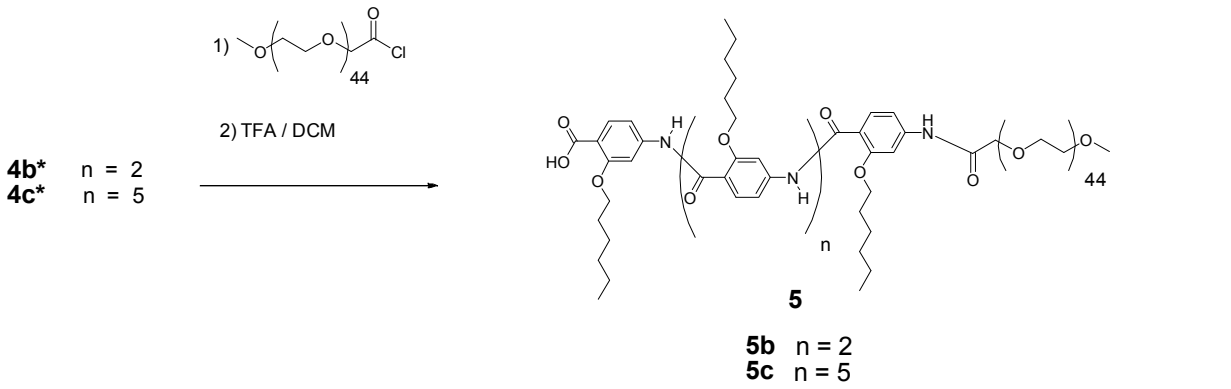

Scheme 4.2.2. Synthetic strategy for the preparation of the hairy rod block copolymers consisting of stiff oligomeric benzamide segments with pedant alkyl groups and a soluble PEG block attached to the *N*-terminus.

Both functionalized PEG blocks **5b** and **5c** with four and seven aramide units showed good solubility in nonpolar organic solvents. Product **5b** could be easily isolated and characterized, as the polymer was long enough to prevent the formation of aggregates. GPC (see **figure 4.2.3**) and NMR experiments (see **figure SI-4.2.3**) showed only the presence of unimers.

On the other hand, characterization of the heptameric rod-PEG conjugate turned out to be more complicated than expected. Homogenous solutions were only achieved for the solvents TCM and 1,1,1,3,3,3-hexafluoro-2-propanol (HFIP). The GPC trace of the TCM solution did not show any UV-absorbance nor refractive index signals. Attempts to

characterize the product by NMR techniques failed as well. This solution behavior might be attributed to the strong aggregation tendency of the copolymer with longer aramide blocks. This trend correlates with previously reported results based on plain aramide-PEG copolymers, where the pentamer was detected as the critical aramide length for aggregates formation in TCM.[15]

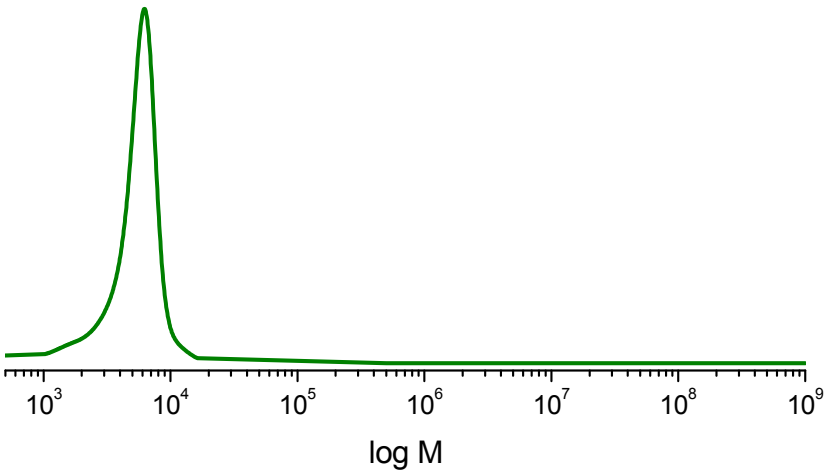

Figure 4.2.3. The GPC-trace of **5b** in TCM shows only the monomodal distribution of the unimers, without evidence for supramolecular aggregate formation.

Due to the limited variety of compatible solvents and the strong aggregation of compound **5c,** solution characterization methods (NMR and GPC) were not decisive for the determination of the reaction success. The product was therefore additionally characterized qualitatively by IR-spectroscopy in the solid state. **Figure 4.2.4** shows sections of the IR- transmission spectra of PEG_{2000}-COOH, of model compound poly(2-hexyloxy-*p*-benzamide) **1** and copolymer **5c**. The PEG_{2000}-COOH spectrum is dominated by the C-H aliphatic stretch signal at 2881 cm^{-1} and by the C-O stretch signal at 1103 cm^{-1}. The influence of the PEG-attachment on the aramide to the product spectrum can be observed by the intensity increase of the C-H vibronic band at 2881 cm^{-1} compared to the next neighboring signal at higher wavenumbers (see **figure 4.2.4**, *top*). Comparison of the transmittance ratio $T\nu_{N\text{-}H}$ / $T\nu_{C\text{-}H}$ of **1** and **5c** showed a higher value for the copolymer, confirming the overlap of the C-H (PEG) and C-H (alkyl) absorption bands and thereby, the product formation. The signal at 1103 cm^{-1} appears also in the copolymer spectrum as a new band arising from the PEG-block in the rod-coil polymer (see **figure 4.2.4**, *bottom*).

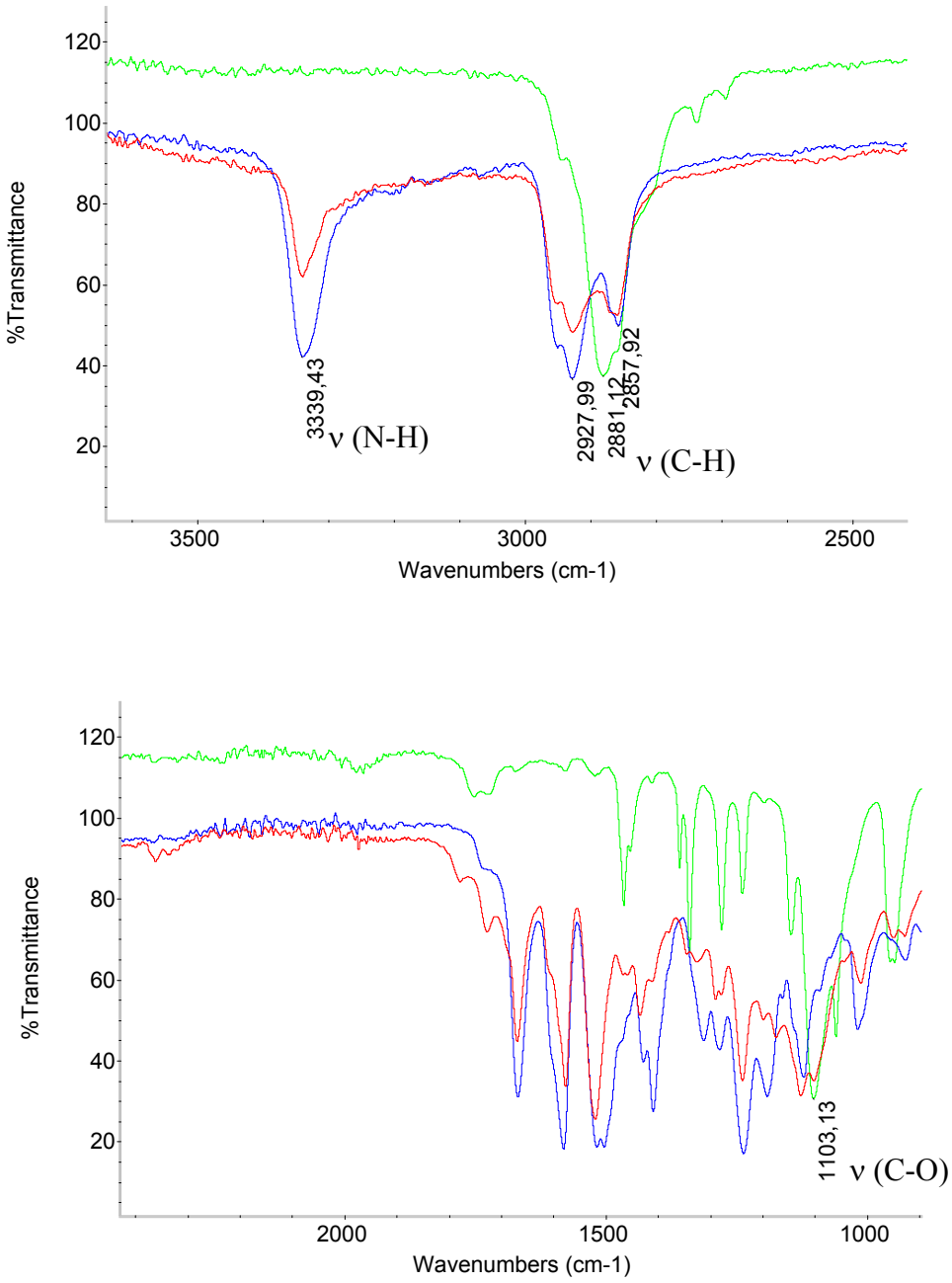

Figure 4.2.4. Lower (*top*) and higher (*bottom*) energy part spectra of PEG-COOH (*green*), PEG-*co*-oligo(2-hexyl-*p*-benzamide) conjugate **5c** (*red*) and poly(2-hexyl-*p*-benzamide) **1** (*blue*).

The presence of the PEG-absorption bands in the IR-spectrum of the copolymer, together with the fact, that the product showed good solubility in nonpolar solvents, confirmed the successful attachment of the polymer block to the otherwise insoluble rods. The strong intermolecular interactions in a variety of solvents impeded its detailed characterization and purification. Therefore the purity level of the crude product could not be determined.

Light scattering allows the determination of the size, shape and mobility of polymers since the scattered intensity depends from the particle properties. Dynamic light scattering experiments yield a quantitative measure for the fluctuation of scattering particles in solution as characterized by their self-diffusion coefficient and thus their hydrodynamic radius. Therefore, DLS measurements were performed to obtain additional proof for the aggregation and solvent influence on the self-assembly in solution.

Monitoring the scattered intensity during the dynamic light scattering experiment at different angles, allows the calculation of the amplitude correlation factor F_s (q,τ) (also called dynamic structure factor) using the appropriate software.[i] A cumulant analysis of the obtained data yields an average diffusion coefficient (first cumulant). For polydisperse samples, the average self-diffusion coefficient determined from the correlation function Fs(q,τ) depends of the scattering vector q and therefore also called the apparent diffusion coefficient $D_{app}(q)$. The "true" average diffusion coefficient $< D_s >_z$, which is a z-average, is determined by extrapolation of the apparent diffusion coefficient $D_{app}(q)$ towards zero scattering vector q. Plotting $D_{app}(q)$ vs. q^2 in experimental practice, may result in a linearly increasing function, whose intercept with the q = 0 axis yields the z-average diffusion coefficient $< D_s >_z$.[ii] Thus, the hydrodynamic radius can be then calculated by applying the Stokes-Einstein relationship **(4.1)**:

$$R_h = \left\langle \frac{1}{R_h} \right\rangle_z^{-1} = \frac{k_B T}{6\pi\eta D_z} \qquad \textbf{(4.1)}$$

The self-diffusion coefficient, and thus the hydrodynamic radius of the scattering particles, can be calculated by dynamic light scattering only in case of very dilute solutions. Solution concentrations in the range between 0.1 and 8 g/L were measured in polar and nonpolar solvents. Additionally, influence of sample equilibration time dependence was examine in order to confirm the intermolecular origin of the strong aggregation taking place in solution. Linear fits of the D_z vs. q^2 data for the different solvents and the calculated hydrodynamic radii are displayed below.

DLS measurements of compound **5c** at low concentrations in the nonpolar solvent confirmed the presence of particles with a large hydrodynamic radius of 279 nm after 1

[i] Fs(q,t) contains the information concerning the motion of the scattering solute particle.

[ii] For small particles (10 nm < particle radius R_H < 100 nm) following equation can be applied:

$$D_{app}(q) = < D_s >_z (1 + K < R_g^2 >_z q^2)$$

day equilibration time. Increasing the equilibration time to 1 week, the hydrodynamic radius obtained for the aggregates was 363 nm. Doubling the concentration, afforded supramolecular particles with R_h values of 235 nm within 1 hour (see **figures 4.2.5** and **4.2.6**).

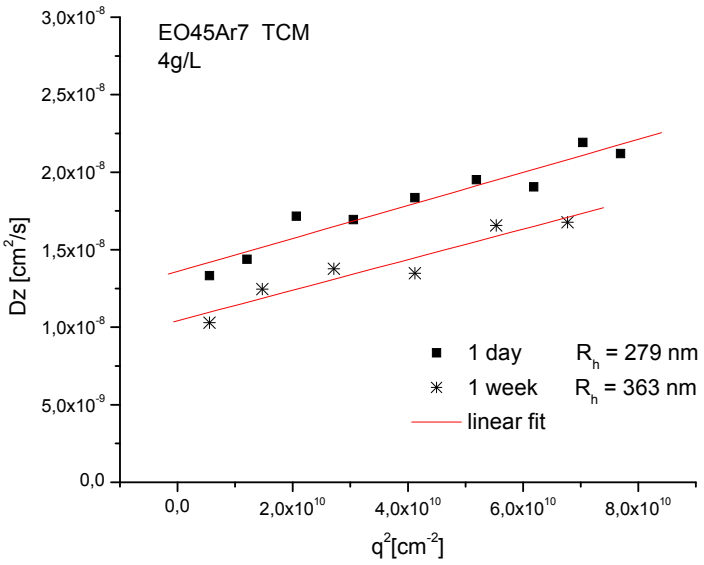

Figure 4.2.5. Apparent diffusion coefficient vs. scattering angle for compound **5c** in TCM after 1 day and 1 week equilibration time ([c] = 4 g/l).

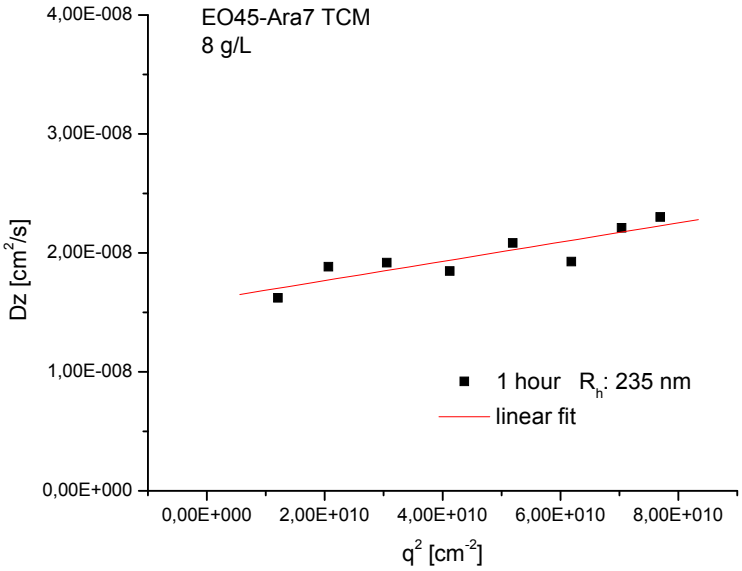

Figure 4.2.6. Apparent diffusion coefficient vs. scattering angle for compound **5c** in TCM after 1 hour equilibration time ([c] = 8 g/l).

5c was shown to form high molecular weight aggregates even in HFIP, after 1 hour equilibration time. Although the high polarity and the ability of HFIP to break hydrogen bonds,[16] the later particles reached a hydrodynamic radius of the 94 nm in this solvent.

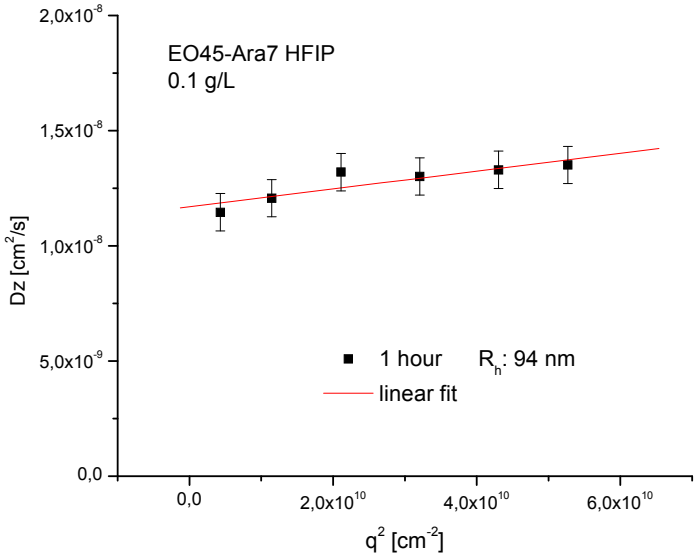

Figure 4.2.7. Apparent diffusion coefficient vs. scattering angle for compound **5c** in HFIP after 1 hour equilibration time ([c] = 0.1 g/l).

The aggregates were further visualized by TEM measurements. The TCM solution was drop cast onto untreated (hydrophobic) and hydrophilized grid surfaces. While the larger PEG-block is more likely to be attracted to the polar surface, individual tapes with an approximate width of 8 nm are observed, when the grid was treated with oxygen plasma (see **figure 4.2.8**, *top*). Deposition of the dissolved aggregates onto the untreated (nonpolar) surface area results in the repulsion of the mesogen-stabilizing polymer block and the particles agglomerate further to higher dimensional bundles of individual tapes (see **figure 4.2.8,** *bottom*).

Dissolution in the fluorinated solvent HFIP, promotes at some extent the disruption of these large aggregates. Shorter and wider noncovalent supramolecular structures (17 nm in width and approx. 170 nm long) were visualized via the transmission electron microscope (see **figure 4.2.9**).

Although GPC and DLS measurements of **5b** solutions in TCM demonstrated the absence of aggregates, DLS analysis of low concentrated HFIP solutions revealed the solvent promoted aggregation for the shorter oligomeric block as well. The TEM-micrograph illustrates the stable and extremely rigid morphology of the polymer with a tetramer benzamide block (see **figures 4.2.10** and **4.2.11**).

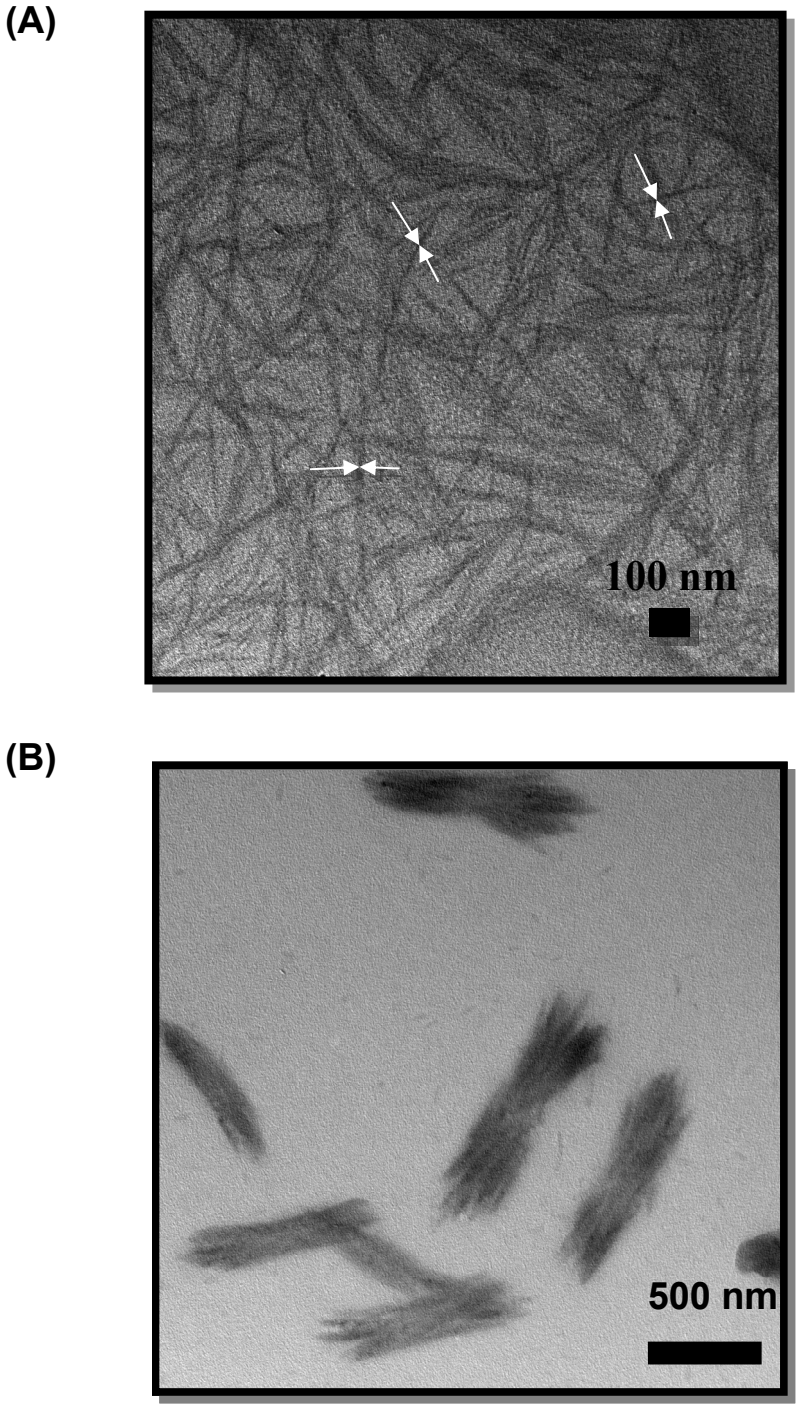

Figure 4.2.8. TEM-micrographs of **5c**. Drop cast (3 times) from TCM solution (5 g/l) onto **(A)** hydrophilized and **(B)** untreated carbon coated copper grids.

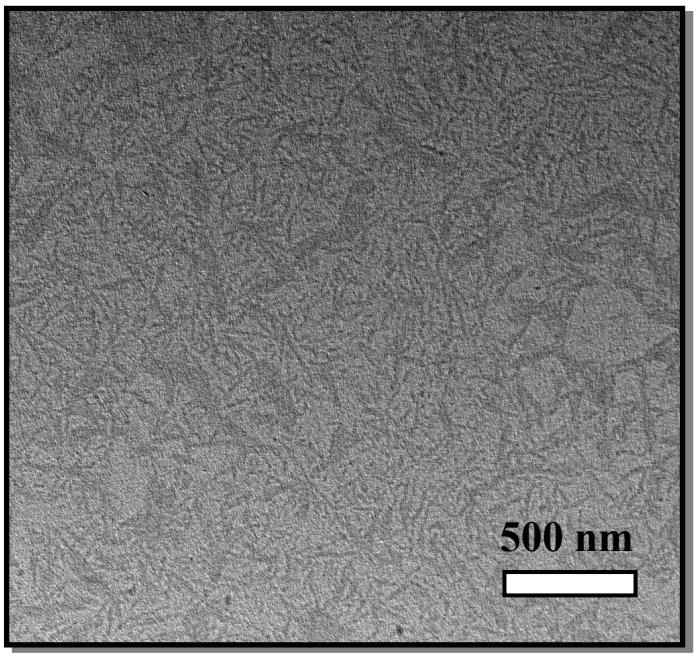

Figure 4.2.9. TEM-micrograph of **5c**. Drop cast (3 times) from HFIP solution (3 g/l) onto a hydrophilized carbon coated copper grid. Hydrophilization was performed to avoid agglomeration of the aggregates (as observed in TCM solution) and for a better adhesion of the solvent on the grid. The rods have monodisperse widths of 17 nm and are approx.170 nm long.

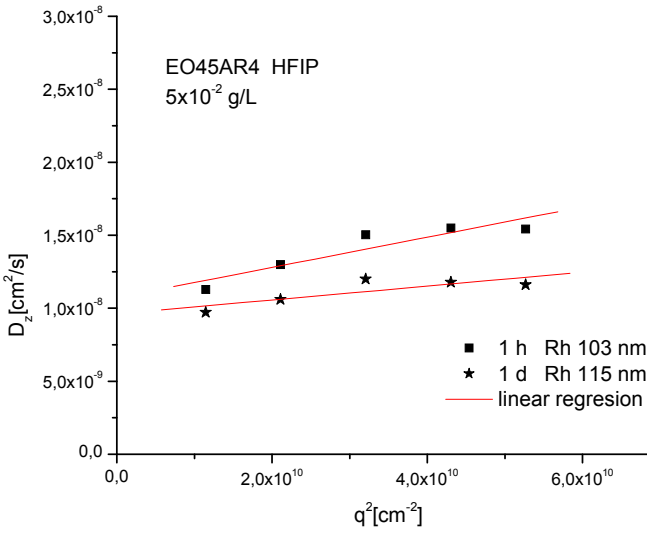

Figure 4.2.10. Apparent diffusion coefficient vs. scattering angle for compound **5b** in HFIP after 1 hour and 1 day of equilibration time ([c] = $5x10^{-2}$g/l).

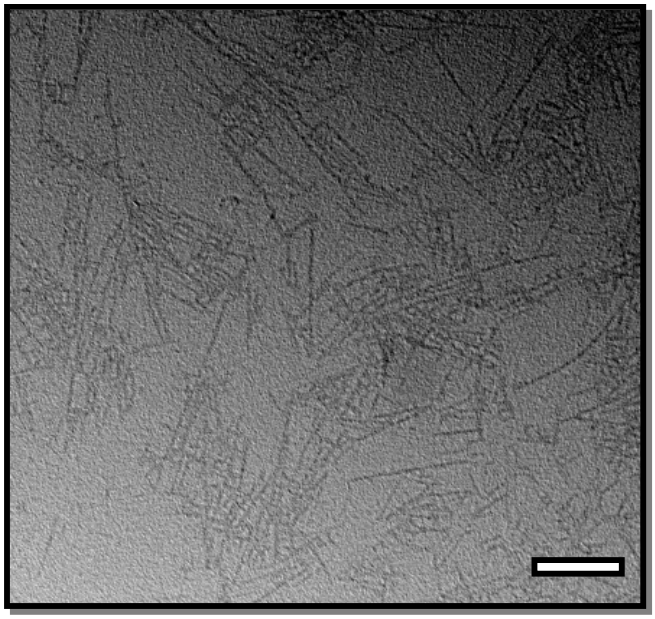

Figure 4.2.11. TEM image of **5b**. Drop cast (3 times) from HFIP ([c]= $5x10^{-2}$ g/l). The nanorods are monodisperse in width (17 nm) and 240 nm to 1 μm in length.

As described before, DLS experiments of **5c** solutions in TCM indicate the formation of supramolecular aggregates, proved by the high R_h. The concentration and equilibration time dependence of the hydrodynamic radius indicates the intermolecular origin of the interactions.

The aggregation of the plain-aramide copolymers in water into nanorods, was previously demonstrated for a hepta- and octa(*p*-benzamide) block.[17] HFIP was shown here to induce similar aggregate formation of hairy rod-PEG copolymers, even for samples with shorter aramide-blocks. Although HFIP is applied usually as a hydrogen bond breaking solvent, it is also well known for its ability to stabilize local hydrogen bonds between close residues in amino-acid sequences, particularly in those forming α-helices,[18] but also in some cases facilitating β-sheet formation.[18d] This observation was attributed to the unique properties of HFIP, combining the polar alcoholic and the hydrophobic trifuoromethyl functionalities.[19]

In the case presented above, the hydrophobic interactions between alkyl chains in the tetramer are probably too weak and can be easily be broken when dissolving the copolymer in nonpolar TCM.

Otherwise, solvophobic interactions between the hexyl side chains are stabilized in the more polar solvent HFIP. The stiffer supramolecular architecture may rely on the unfeasibility of the chains to shift dramatically along the aramide edge, namely due to the shortness of the block and the few pendant groups to interact with.

The copolymer with the heptameric hairy rod showed an increased aggregation tendency compared to the tetrameric analog, making its complete characterization impracticable. Here, higher extent of the rod allows multiple cooperative interaction sites along its edge, the aggregates being stable even in nonpolar solvents. This results in the formation of flexible fiber-like aggregates, in which the rods are able to shift freely in space with respect to each other. Furthermore, it has to be noticed, that the characterization was carried out with the crude product and the presence of impurities may strongly influence the shape of the supramolecular assemblies.

The deposition of the fiber-like aggregates from nonpolar solutions showed their agglomeration into bundles on the hydrophobic surface, probably due to the repulsion of the PEG-block and simultaneously attractive interactions of the alkyl chains to the surface.

4.2.3. Conclusion

This project focused on the functionalization of insoluble hairy nanorods of oligo(*p*-benzamide)s with soluble PEG-polymer. The copolymers were soluble and self-assembled in nonpolar (TCM) and polar (HFIP) solvents. PEG-aramide conjugates with short aramid blocks could easily purified and characterized. Additionally, the spatial restriction for the solvophobic interactions between the alkyl chains, resulted in well defined aggregates in polar solvents. The PEG blocks functionalized with longer anisotropic rods present stronger intermolecular interaction in polar and nonpolar solvents as observed in the DLS- and TEM-measurements. They self-assemble into flexible fiber-like aggregates, easily to recognize, when deposited on a hydrophilic surface.

4.2.4. Experimental Section

Methods.

Standard ^{1}H nuclear magnetic resonance spectra were recorded on a Bruker AMX 400 (400 MHz). Infrared spectra were recorded on a Nicolet 5 DXC FT-IR spectrometer. ESI mass spectra were measured on a Micromass Q-TOF Ultima 3.

Dynamic light scattering (DLS) experiments were performed at 293 K utilizing equipment consisting of a He/Ne laser (λ = 632.8 nm), an ALV 3000 correlator and an ALV-SP86 goniometer. Measurements were performed at different angles (for most samples between 30-120°, 15° steps). Diffusion coefficients were determined by non linear fitting (Simplex algorithm) of the field autocorrelation function applying biexponential fit functions. Hydrodynamic radii were calculated by applying the Stokes-Einstein equation. All solutions were passed through syringe filters (anotop, 20 nm) into dust free cylindrical cuvettes.

A Philips EM 420 transmission electron microscope using a LaB_6 cathode at an acceleration voltage of 120 kV was used to obtain TEM-images. Hydrophilization of the TEM grids (carbon film on copper, 300 mesh) was carried out for 30 s on a plasma cleaner. The samples were prepared by the drop cast method and air dried.

Gel permeation chromatography with TCM was carried out on an instrument consisting of a Waters 717 plus auto sampler, a TSP Spectra Series P 100 pump and a set of three PSS SDV columns ($10^6/10^5/10^4$ g/mol). Signal detection was performed with a TSP Spectra System UV 2000 (UV 254 nm) and a Wyatt Optilab DSP (refractive index).

Characterization.

The hairy rod oligomers were synthesized on an ABI 431a Peptide Synthesizer as described in **chapter 4.1**. The monomer was activated by its conversion into the corresponding acid chloride using thionyl chloride.

The conversion of the PEG monomethyl ether into the PEG carboxylic acid as well as the attachment of the PEG-blocks to the oligoamides on the solid support were accomplished as described in **chapter 3.3.4**.

*Compound **4a**:*

Monomer activation (*in situ*): 2.3 g (5 mmol) *N-Fmoc-4-amino-2-hexyloxy benzoic acid*, 12.5 ml $SOCl_2$ (catalytic amount of dry NMP), 2 hrs at rt.

Coupling solution: **3** in 9.4 ml dry NMP.

Capping solution: 0.69 g (3 mmol) 4-nitro benzoic acid chloride in 5.5 ml dry NMP.
Cleavage from the resin: TFA / TCM (1:1) 6 ml, 2 hrs.
Precipitation solvent: diethyl ether
Purification: the product can be purified in hot methanol / TCM mixtures.
Yield: 120 mg (71 %).
^{1}H-NMR: δ (400 MHz, $CDCl_3$/MeOD (20 vol. % MeOD in $CDCl_3$)) 0.83 (t, 9 H, ^3J = 6.52 Hz); 1.23-1.49 (m, 18 H); 1.82-1.95 (m, 6 H); 4.06 (t, 2 H, ^3J = 6.36 Hz); 4.21 (t, 4 H, ^3J = 6.52 Hz); 6.17 (d, 1 H, ^4J = 1.27 Hz); 6.30 (dd, 1 H, ^4J = 1.91 Hz, ^3J = 8.58 Hz); 6.68 (dd, 1 H, ^4J = 1.59 Hz, ^3J = 8.58 Hz); 6.72 (dd, 1 H, ^4J = 1.59 Hz, ^3J = 8.58 Hz); 7.91 (d, 1 H, ^3J = 8.58 Hz); 7.96 (d, 1 H, ^3J = 8.58 Hz); 8.01-8.07 (m, 3 H).
^{1}H-NMR: δ (300 MHz, DMSO-d_6): 0.80-0.90 (m, 9 H); 1.23-1.46 (m, 18 H); 1.71-1.93 (m, 6 H); 4.0 (t, 2 H, ^3J = 6.36 Hz); 4.10 (m, 4 H); 6.27 (dd, 1 H); 6.29 (d, 1 H); 7.24 (dd, 1 H, ^4J = 1.27 Hz, ^3J = 8.58 Hz); 7.29 (dd, 1 H, ^4J = 1.27 Hz, ^3J = 8.58 Hz); 7.54 (s, 1 H); 7.65-7.75 (m, 4 H); 10.07 (s, 1 H); 10.16 (s, 1 H).
MS (ESI): *m/z* (%) = 698.39 (100); 699.41 (3.7); calc.$(M+Na)^+$ $[C_{39}H_{53}N_3O_7Na]^+$ = 698.38

*Compound **4b**:*

Monomer activation (*in situ*): 3.59 g (7.8 mmol) *N-Fmoc-4-amino-2-hexyloxy benzoic acid*, 19.5 ml $SOCl_2$ (catalytic amount of dry NMP), 2hrs at rt.
Coupling solution: **3** in 10 ml dry NMP.
Capping solution: 0.97 g (5.2 mmol) 4-nitro benzoic acid chloride in 7 ml dry NMP.

*Compound **5b**:*

Activation of the polymer: 2.5 g PEG-COOH, 10 ml oxalyl chloride, 10 ml dry DCM.
Coupling: PEG-COCl (*in situ*) dissolved in minimum amount of dry NMP, functionalized resin **4b*** (0.25 mmol), 24 hrs at rt. The coupling step was repeated once.
Cleavage of **5b** from the resin: DCM / TFA (1:1), 2 hrs.
Yield: 253 mg (crude product).
Purification: crude product (50 mg) was purified by preparative GPC in TCM, affording 37 mg of pure **5b**.
GPC (TCM): M_n = 4850 g/mol; M_w = 5440 g/mol; PDI = 1.12
^{1}H-NMR: δ (300 MHz, $CDCl_3$): 0.92-0.95 (m, 12 H); 1.38-1.59 (m, 24 H); 1.85-2.01 (m, 8 H); 3.37 (s, 3 H); 3.65 (br. s, 151 H); 4.29 (br. s, 8 H); 5.05 (br s; 4 H); 6.54-7.01 (m, 3 H); 7.75-9.89 (m, 9 H); 9.84-10.36 (m, 3 H).

*Compound **4c**:*

Activation of the monomer (*in situ*): 5.98 g (13 mmol) *N-Fmoc-4-amino-2-hexyloxy benzoic acid*, 32.5 ml $SOCl_2$ (catalytic amount of dry NMP), 2 hrs at rt.

Coupling solution: **3** in 24.4 ml dry NMP.

Capping solution: 1.6 g (8.6 mmol) 4-nitro benzoic acid chloride in 13 ml dry NMP.

*Compound **5c**:*

Activation of the polymer: 2.5 g PEG-COOH, 5 ml oxalyl chloride, 5 ml dry DCM, 3-4 hrs at rt.

Coupling: PEG-COCl (*in situ*) dissolved in minimum amount of dry NMP (approx. 5 ml), functionalized resin **4c*** (0.25 mmol), 24 hrs at rt. The coupling step was repeated once.

Cleavage of **5c** from the resin (108 mg): DCM / TFA (1:1), 2 hrs.

Yield: 55 mg (75 %) of a brown product.

IR: 3340, 2928, 2860, 1670, 1578, 1521, 1239, 1127, 1103.

Purification / Characterization: It was impossible to purify the product with standard chromatographic methods or precipitation due to its high aggregation tendency. The characterization by NMR, GPC, HPLC and mass spectrometry techniques failed, making it impossible to estimate the purity level of the afforded product. Solubility of crude **5c**: good soluble in TCM and HFIP; bad soluble in DMSO and DMF; insoluble in acetonitrile, methanol and water.

4.2.5. References

[1] Ballauff, M. *Angew. Chem. Int. Ed. Engl.* **1989**, *28*, 253.

[2] Wegner, G. *Macromol. Symp.* **2003**, *201,* 1-9.

[3] Vanhee, S; Rulkens, R; Lehmann, U.; Rosenauer, C.; Schulze, M.; Kohler, W.; Wegner, G. *Macromolecules* **1996**, *29*, 5136.

[4] Lauter, U.; Meyer, W. H.; Wegner, G. *Macromolecules* **1997**, *30*, 2092-2101.

[5] (a) Wegner, G. *Thin Solid Films* **1992**, *216*, 105; (b) Wegner, G. *Mol. Cryst. Liq. Cryst.* **1993**, *235*, 1; (c) Helmer-Metzmann, F.; Ballauff, M.; Schulz, R. C.; Wegner, G. *Makromol. Chem.* **1989**, *190*, 985.

[6] (a) Zorn, M.; Meuer, S.; Tahir, M. N.; Khalavka, Y.; Sönnichsen, C.; Tremel, W.; Zentel, R. *J. Mater. Chem.* **2008**, *18*, 3050-3058; (b) Dass, N. N.; Date, R. W.; Fawcett, A. H.; McLaughlin, J. D.; Sosanwo, O. A. *Macromolecules* **1993**, *26*, 4192-4195; (c)

Yim, K. S.; Fuller, G. G.; Datko, A.; Eisenbach, C. D. *Macromolecules* **2001,** *34,* 6972-6977.

[7] Ikkala, O.; ten Brinke, G. Self-Organized Supramolecular Polymer Structures to Control Electrical Conductivity, *Handbook of Advance Electronic and Photonic Materials and Devices,* Part 8 Conducting Polymers; Nalwa, H. S., Ed.; Academic Press: San Diego, **2000**.

[8] (a) Uematsu, I.; Uematsu, Y. *Adv. Polym. Sci.* **1984**, *59*, 37; (b) Hanabusa, H.; Sato, M.; Shirai, H.; Takemoto, K.; Iizuka, E. *J. Polym. Sci. Polym. Lett.* **1984**, *22*, 559; (c) Duda, G.; Schouten, A. J.; Arndt, T.; Lieser, G.; Schmidt, G. F.; Bubeck, C.; Wegner, G. *Thin Solid Films* **1988**, *159*, 221; (d) Duda, G.; Wegner, G. *Makromol. Chem. Rapid Commun.* **1988**, *9*, 495; (e) Mabuchi, M.; Kobata, S.; Ito, S.; Yamamoto, M.; Albert Schmidt, A.; Knoll, W. *Langmuir*, **1998**, *14* (25), 7260-7266.

[9] (a) Jen, K.-Y.; Miller, G. G.; Elsenbaumer, R. L. *J. Chem. Soc., Chem. Commun.* **1986**, 1346; (b) Roncali, J. *Chem. Rev.* **1992**, *92* (4), 711-738; (c) Perepichka, I. F.; Perepichka, D. F.; Meng, H.; Wudl, F. *Adv. Mater.* **2005**, *17*, 2281.

[10] See: Schwab, P. F. H.; Smith, J. R.; Michl, J. *Chem. Rev.* **2005**, *105* (4), 1197-1280 and references in it.

[11] (a) McCarthy, T. F.; Witteler, H.; Pakula, T.; Wegner, G. *Macromolecules* **1995**, *28*, 8350; (b) Vahlenkamp, T.; Wegner, G. *Macromol. Chem. Phys.* **1994**, *195*, 1933; (c) Rehan, M.; Schlüter, A.-D.; Wegner, G. *Polymer* **1989**, *30*, 1060; (d) Schlüter, A.-D.; Wegner, G. *Acta Polym*. **1993**, *44*, 59.

[12] (a) Neher, D. *Macromol. Rapid Commun.* **2001**, *22*, 1365; (b) Scherf, U.; List, E. J. W. *Adv. Mater.* **2002**, *14*, 477; (c) Grell, M.; Bradley, D. D. C.; Ungar, G.; Hill, J.; Whitehead, K. S. *Macromolecules* **1999**, *32*, 5810, (d) Lieser, G.; Oda, M.; Miteva, T.; Meisel, A.; Nothofer, H.-G.; Scherf, U.; Neher, D. *Macromolecules* **2000**, *33*, 4490.

[13] Seyler, H.; Kilbinger, A. F. M. "*Linear soluble Poly(p-benzamide)*", *in preparation*.

[14] Flory, P. J. *Principles of Polymer Science*, Cornell University Press, Ithaca, New York, **1953**.

[15] Abbel, R.; Schleuss, T. W.; Frey, H.; Kilbinger, A. F. M. *Macromol. Chem. Phys.* **2005**, *206*, 2067–2074.

[16] Abraham, M. H. *Chem. Soc. Rev.* **1993**, *22*, 73–83.

[17] (a) Koenig, H. M.; Gorelik, T.; Kolb, U.; Kilbinger, A. F. M. *J. Am. Chem. Soc.*, **2007**, *129* (3), 704-708; (b) Klos, J.; Wurm, F.; Koenig, H. M.; Kilbinger, A. F. M. *Macromolecules*, **2007**, *40* (22), 7827-7833.

[18] (a) Buck, M. *Q. Rev. Biophys.* **1998**, *31*, 297-355; (b) Vieira, E. P.; Hermel, H.; Mohwald, M. *Biochim. Biophys. Acta* **2003**, *1645*, 6-14; (c) Nichols, M. R.; Moss, M. A.; Reed, D. K.; Cratic-McDaniel, S.; Hoh, J. H.; Rosenberry, T. L. *J. Biol. Chem.* **2005**, *280* (4), 2471–2480, (d) Juszczyk, P.; Kołodziejczyk, A. S.; Grzonka, Z. *Acta Biochim. Pol.* **2005**, *52* (2), 425–431.

[19] Ennaceur, S. M.; Sanderson, J. M. *Langmuir* **2005**, *21* (2), 552-561.

4.2.6. Supporting Information for ”Hairy Rod-Coil Copolymers”

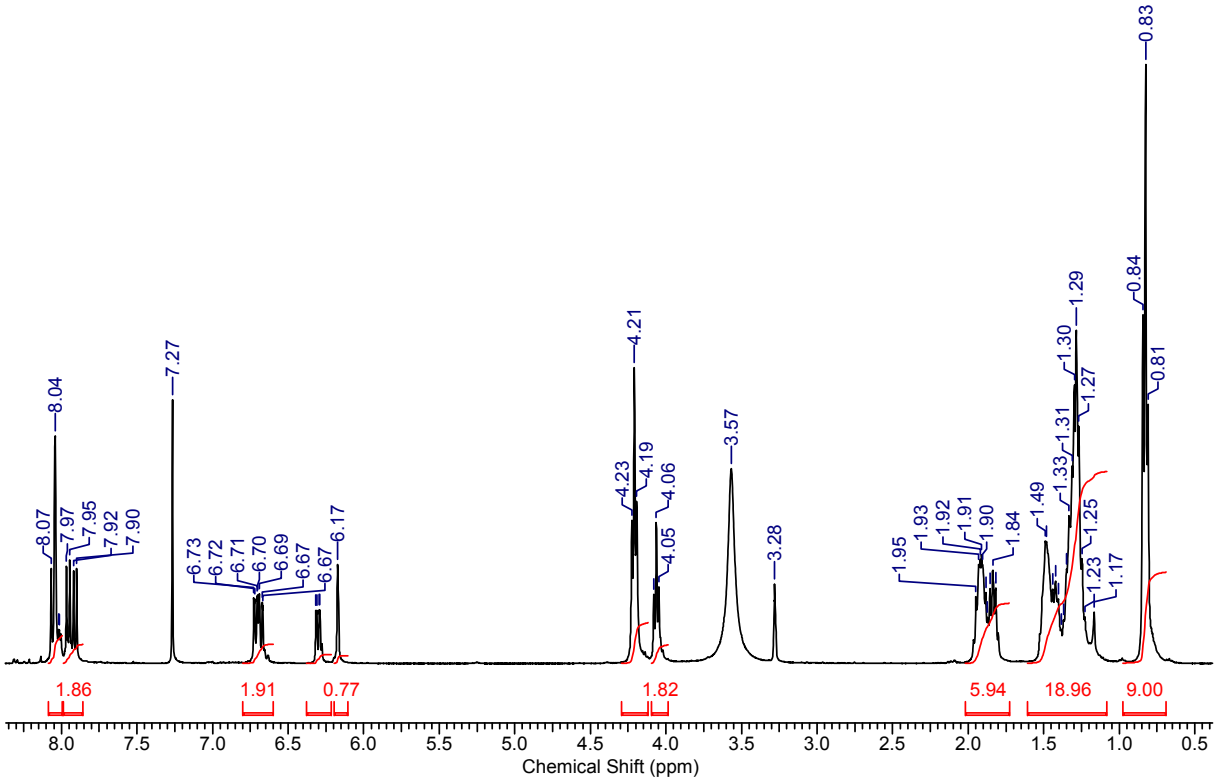

Figure SI-4.2.1. ^{1}H-NMR spectrum (400 MHz) of **4a** in 20 vol % MeOD in $CDCl_3$.

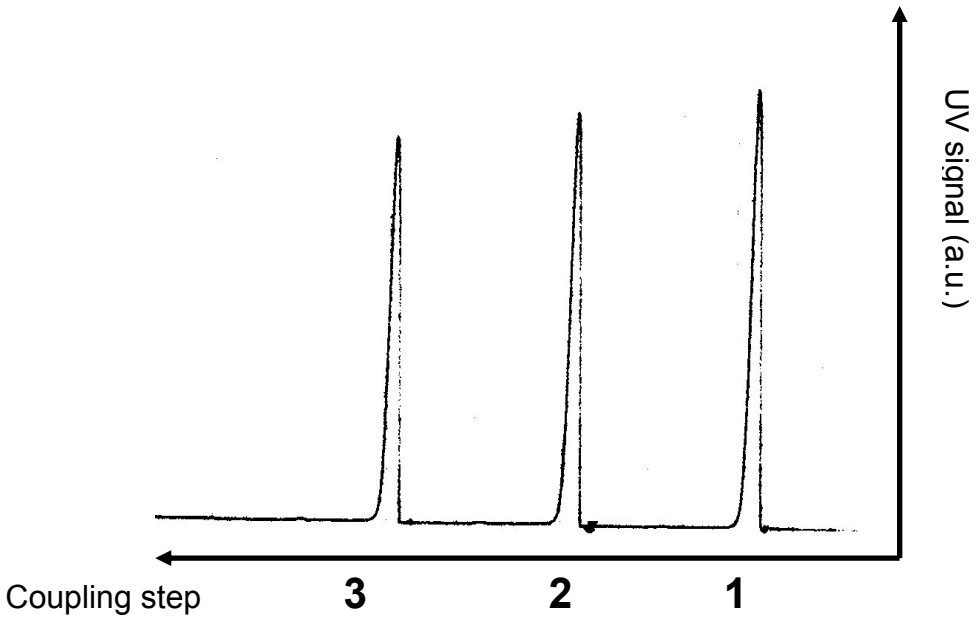

Figure SI-4.2.2. UV-detection of the Fmoc-piperidine adduct at 301 nm after the deprotection of the N-terminus after each coupling cycle during the automated synthesis of **4a**.

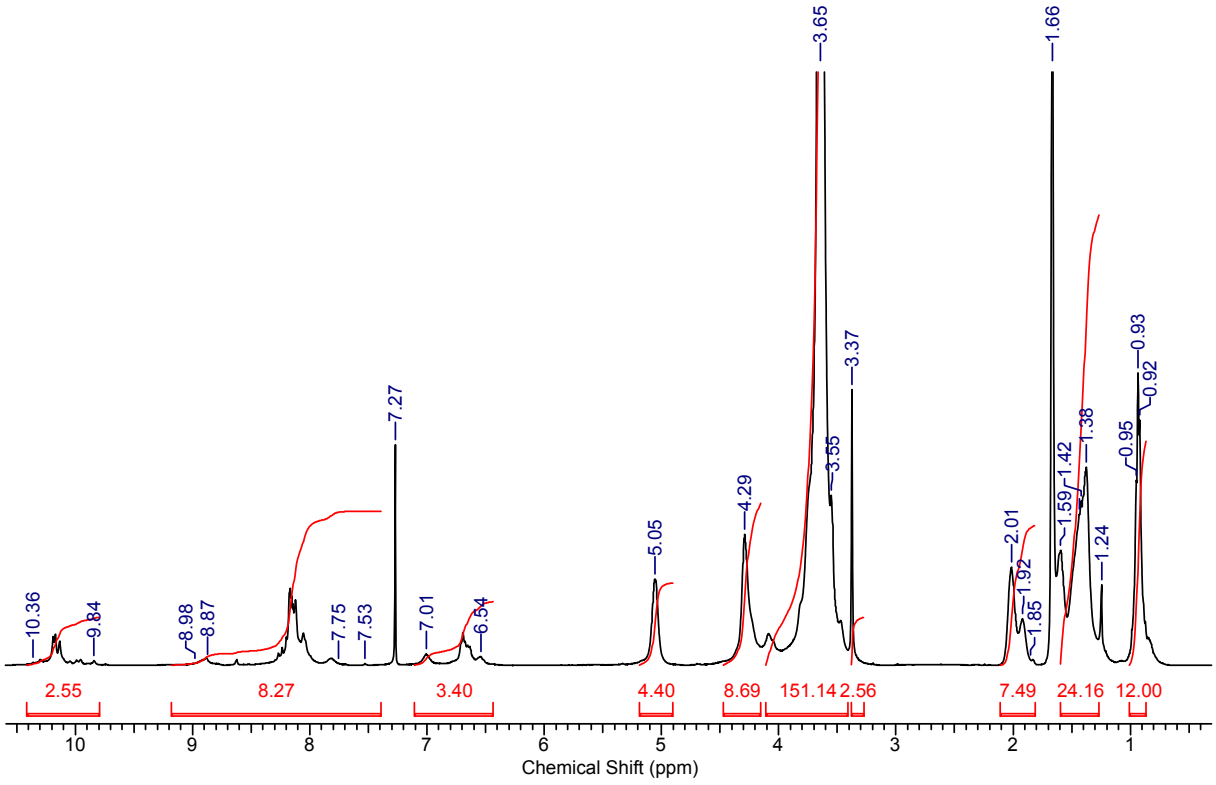

Figure SI-4.1.3. ^{1}H-NMR spectrum (400 MHz) of the PEG-aramide conjugate **5b** in $CDCl_3$.

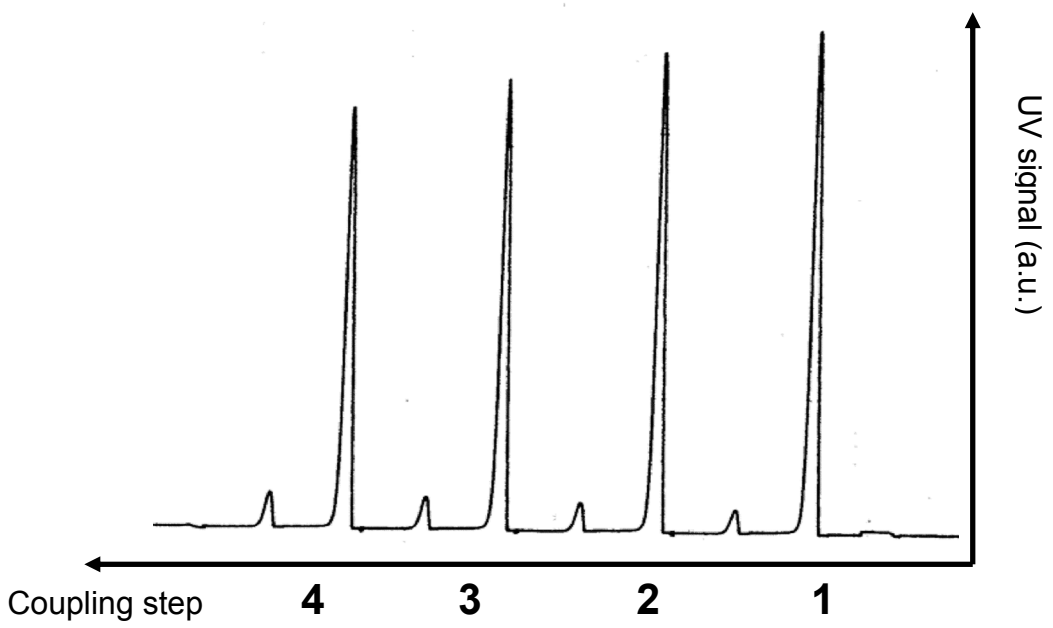

Figure SI-4.2.4. UV-detection of the Fmoc-piperidine adduct at 301 nm after the deprotection of the N-terminus after each coupling cycle during the automated synthesis of **4b**.

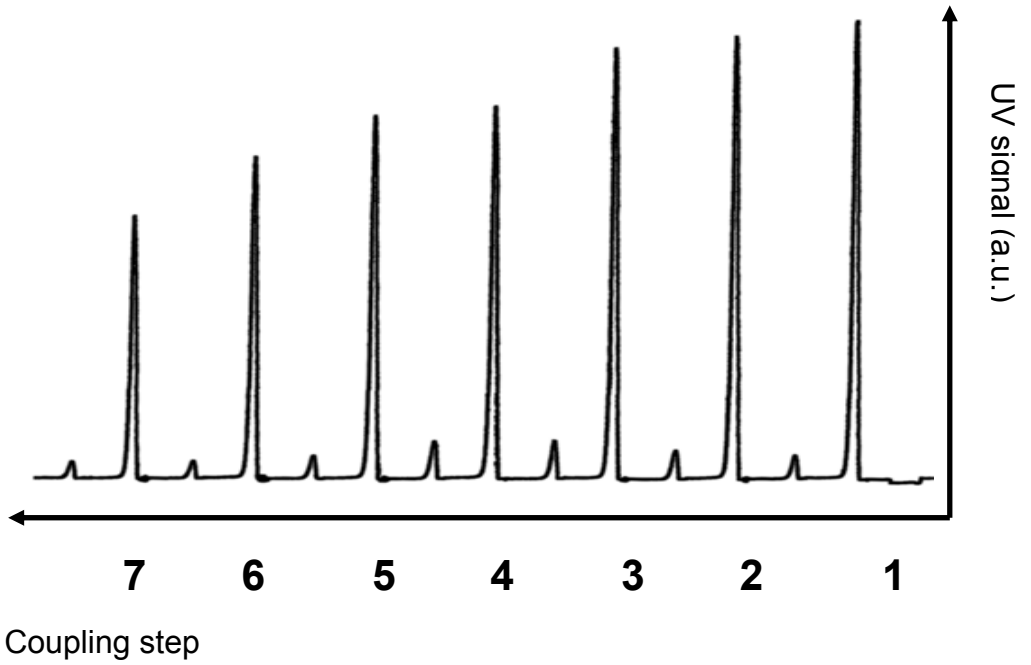

Figure SI-4.2.5. UV-detection of the Fmoc-piperidine adduct at 301 nm after the deprotection of the N-terminus after each coupling cycle during the automated synthesis of **4c**.

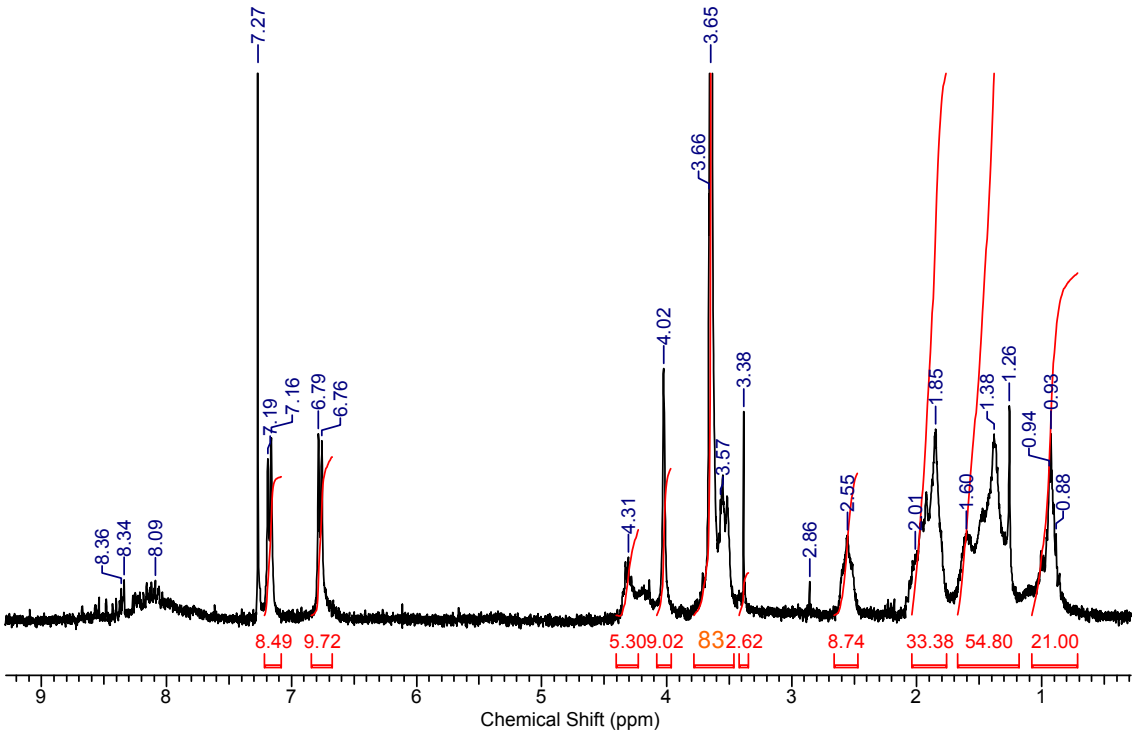

Figure SI-4.2.6. ^{1}H-NMR spectrum (400 MHz) of the PEG-aramide conjugate **5c** in $CDCl_3$. The good product solubility in TCM is attributed the successful PEG-attachment. Signals corresponding to the hexyl-, PEG- and aromatic protons are distinguished. However, from the relative integration, the broad aromatic signal at 8 ppm and the low signal-to-noise ratio can be inferred that aggregation processes are taking place.

Chapter 5

Amphiphilic Rod-like Macromolecules

5.1. Janus Nanorods

Helga Seyler and Andreas F. M. Kilbinger

Abstract

This study presents a simple and novel automated synthetic method for the preparation of monodisperse Janus nanorods (JNR) consisting of an oligo(*p*-benzamide) core with amphiphilic edges. One edge of the stiff rod segment is functionalized with hydrophobic alkyl chains and the other edge with hydrophilic oligoethylene oxide groups. This amphiphilic rod was observed to self-assemble in DMSO solutions into nanoscopic supramolecular aggregates, as characterized by TEM-experiments. This synthetic approach was further developed to automatically recover the monomer excess after each coupling step and allows the facile access to a variety of Janus rods, by systematic modification of the monomer units and sequence variation.

Kurzfassung

Ein konventioneller Peptidsyntheseautomat wurde zur automatisierten Synthese von neuartigen nanoskopischen Janus Architekturen eingesetzt. Dabei wurde ein Rückgrad aus Benzamiden mit hydrophoben Alkyl- und hydrophilen Oligo(ethylenoxid)ketten an den gegenüberliegenden Kanten des Moleküls verknüpft.
Untersuchungen der Selbstorganisation der amphiphilen Janus-Stäbchen in DMSO-Lösungen zeigten die Bildung von supramolekularen Aggregaten, wobei TEM-Aufnahmen die stark anisotrope Natur der Strukturen veranschaulichten.
Diese Methode wurde darüber hinaus für das Recyling von Monomeren weiterentwickelt und stellt einen einfachen und schnellen synthetischen Zugang zu einer großen Vielfalt von Janus-artigen Molekülen dar, die mittels systematischer Modifikation weniger Monomereinheiten und deren Sequenzabfolgen erreicht werden kann.

5.1.1. Introduction

Inspired by nature, the study of materials that self-assemble into supramolecular structures with desirable functionality and physical properties at nano- and mesoscopic length scales became an exciting area of intense research for the design and synthesis of functional materials. For example, the defined primary compositions of amino acids in proteins induce specific secondary and tertiary structures with essential functionality and selectivity.[1] Particularly intriguing is the understanding of molecular recognition processes in materials, for example in those of diversely functionalized faces or sides of molecules, where the selective recognition of top from bottom or right from left is encountered.[2] These kinds of particles, with surfaces / sides differing in polarity / chemistry are denominated as Janus particles, in relation to the two faced Roman god Janus. In general Janus particles can be divided into several classes according to their architecture and dimensionality: spherical, cylindrical and disc-like particles. Additionally, other architectures have been reported, e.g. dumbbell-, acorn-, snowman- and half raspberry-like particles. Concerning monodisperse rod-like Janus-oligomers, the literature is very limited and is mainly focused in the application as spacer in dumbbell-shaped Janus particles[3] or laterally grafted amphiphilic rods[4].

The major challenging aspect in the preparation is the characteristic lack of centro-symmetry.[5,6] There are several reported methods for the construction of Janus particles, for example: the break up of two-layered wax jets generated from a spinning disc edge, metal deposition, microfluidic photopolymerization, immobilization at water and wax / oil interfaces, electrospinning, self-assembly via crosslinking and templates, partial contact with reactive media and controlled surface nucleation.[5,6] Additionally, stepwise solution synthesis of amphiphilic dendritic macromolecules,[7] self-organization of block copolymers[8] and shape persistent macromolecules[9] have been reported for the preparation of Janus-like materials. Although these methods are useful in synthesizing Janus particles, particular efforts have been made in the development of preparation methods to control shape and monodispersity of these particles, allowing an increase of the structural variety of Janus particles, while retaining productivity. Herein, we present a simple method using a conventional peptide synthesizer for the automated synthesis of novel rod-like monodisperse Janus particles. Specification of the monomer sequence allows the precise arrangement of the monomeric units, the position of the functional groups and thus the control of the Janus architecture.

5.1.2 Results and discussion

A new synthetic approach to rod-like Janus particles with a polar oligoethylene oxide- and an nonpolar alkyl- functionalized surface of an oligo(*p*-benzamide) backbone is discussed. Depending on the opted monomer sequence, two different Janus motifs can be designed, when starting with two single monomers. Their structural differentiation concerns the parallel or perpendicular non-centrosymmetry with respect to the longitudinal axis. This chapter comprises only the preparation and characterization of Janus - type **A** oligomers (see **figure 5.1.1**).

This novel procedure not only allows the creation of Janus rod-like architectures, but also the facile preparation of other new structures. For example, helical or rather tubular structures with well defined cavity diameters and different inner /outer polarities can be designed by introducing “turn-inducing” units (*e.g. meta*-substituted phenyl amino acids) and exploiting specific solute / solvent interactions (*e.g.* solvophobic effects).

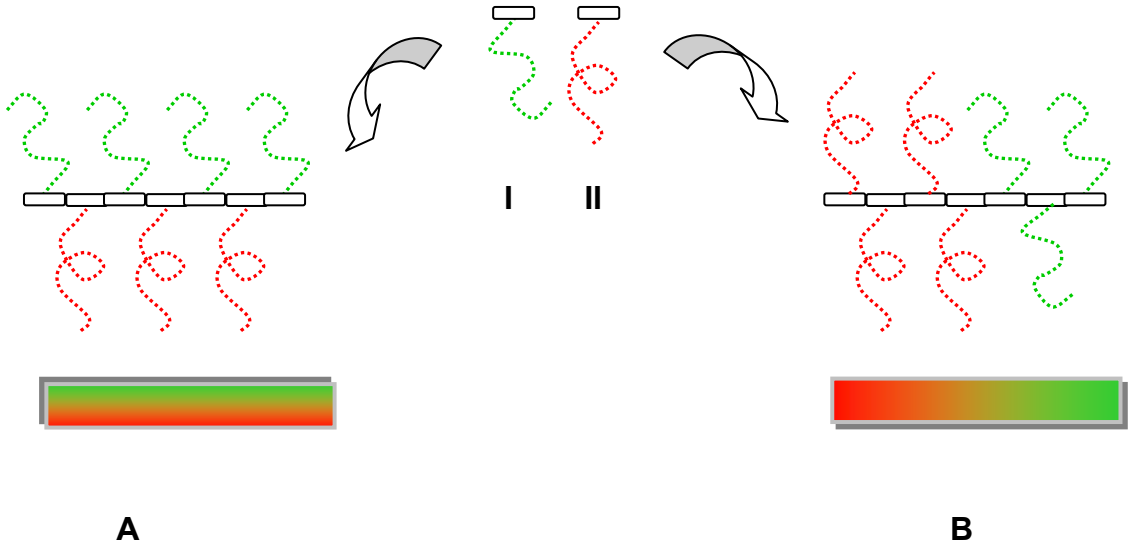

Figure 5.1.1. Schematic representation of the two accessible types of Janus rods **A** and **B** through automated synthesis using two different monomers **I** and **II**.

The synthesis of JNR **4** was performed automatically on a peptide synthesizer in an analogous approach according to the procedures previously described in **chapter 4.1** and is outlined in **scheme 5.1.1**. The intramolecular hydrogen bonds between ether oxygens and amide protons induce a perfectly flat molecule (see **chapter 3**), whereas

the alternating orientation of the carbonyl groups aligns every second chain to the same molecule edge. Therefore, choosing an alternating amino acid sequence of monomer **2** and **3**, the molecule thus carries polar TEG chains on one side and nonpolar hydrocarbon groups on the opposite side (see **scheme 5.1.1**).

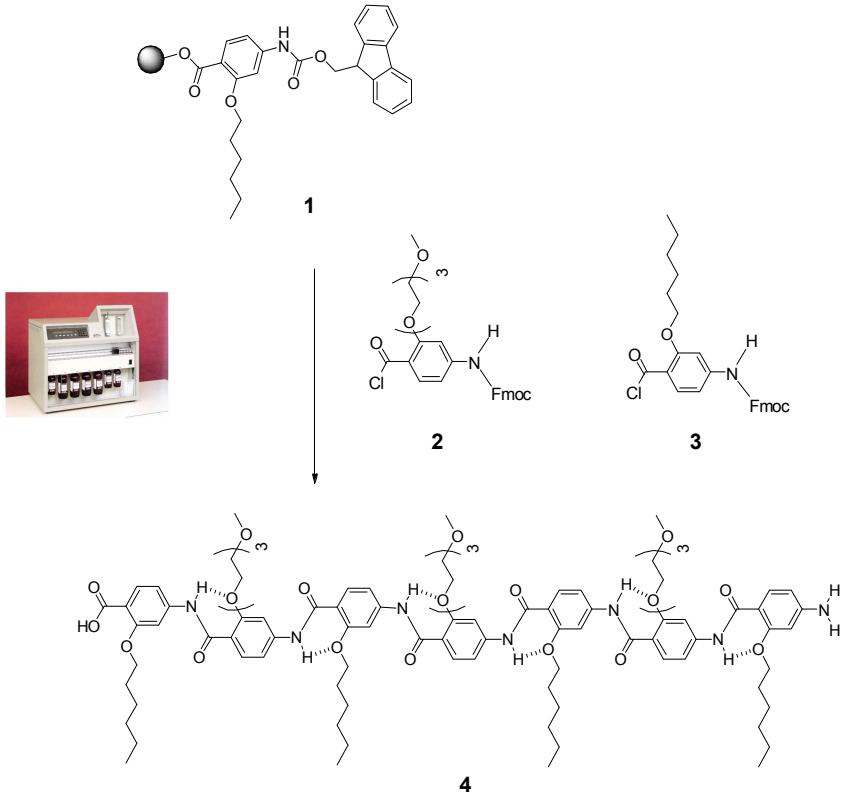

Scheme 5.1.1. Simplified reaction scheme for the automated, solid supported synthesis of **4**.

Regarding the UV-absorption monitoring of the solutions containing the cleaved Fmoc groups (see **figure SI-5.1.1**), a slight intensity decrease up to the third coupling step is observed and implies the presence of failure sequences. The purification and characterization of the heptamer **4** could only be performed in DMSO at 100 °C due to its poor solubility in other organic solvents. Concentrations of around 10 mg/ml of JNR **4** in hot DMSO form gels on cooling to room temperature.

Figure 5.1.2 shows the ^{1}H-NMR spectrum of the product before and after washing with hot solvent. The top spectrum clearly shows the presence of impurities, as the integration of the signals does not match with the expected values. As an example, the mismatching of the integration of amide protons with respect to the hexyl- and TEG-methyl groups is highlighted (*top spectrum*). After rinsing the product with hot DMSO, the integration of the signals mentioned before fit well, although the intensity of the 2 doublets at 8.2 and 8.4 ppm decreased remarkably. The splitting into doublets could

suggest the presence of *N*-capped failure sequences with a terminal 4-nitrobenzoic acid unit. Alternatively, these signals could also correspond to the aromatic group at the electron poor C-terminus (see **figure 5.1.2**).

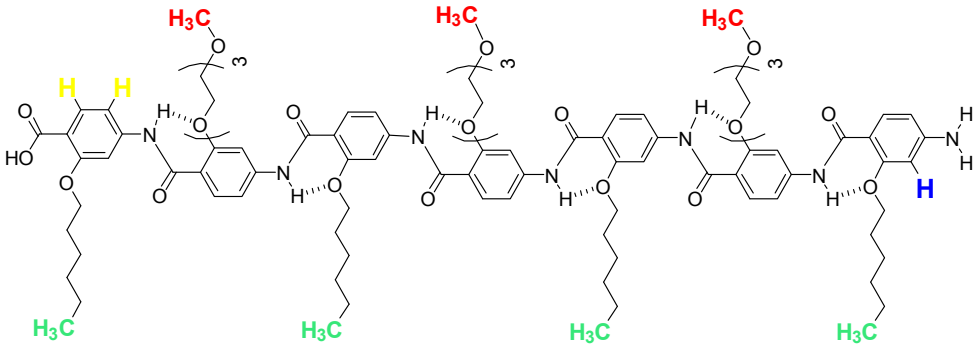

4

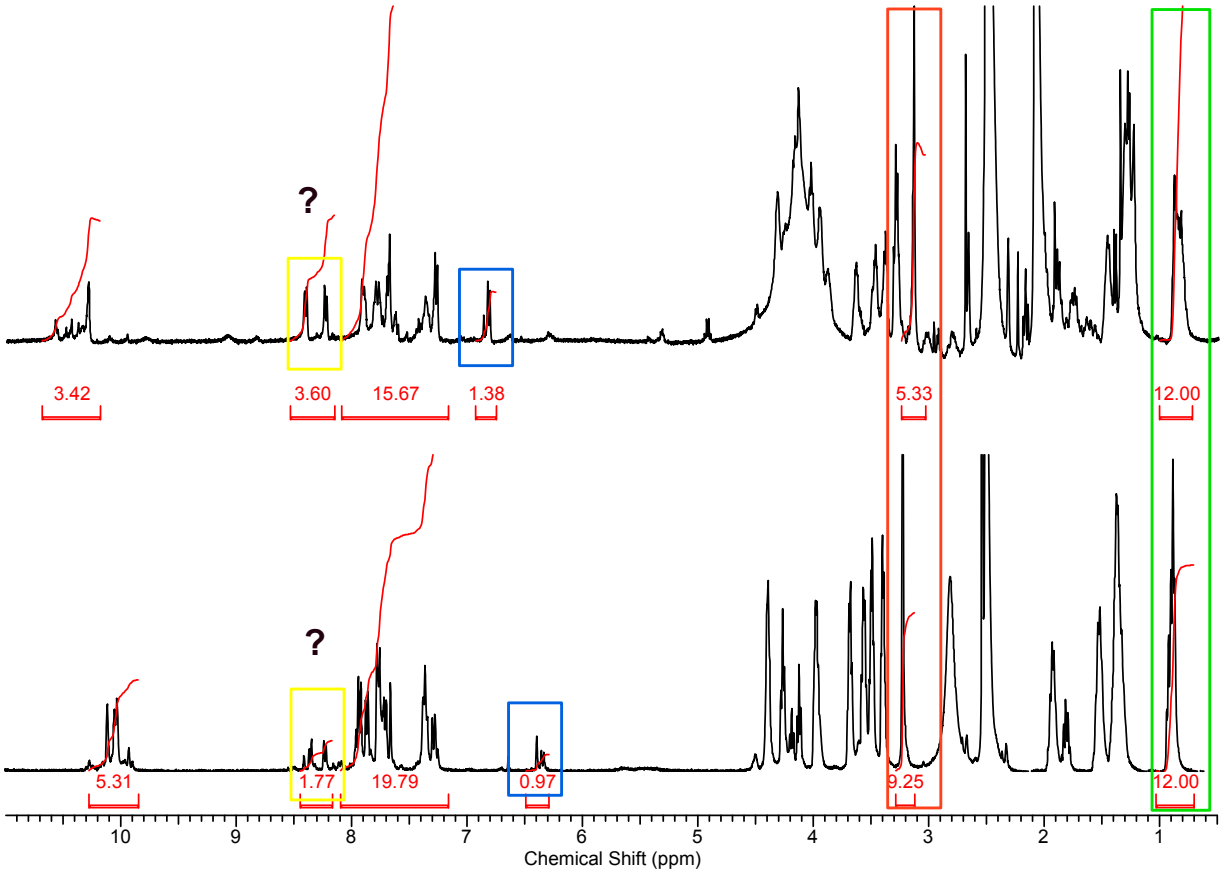

Figure 5.1.2. ^{1}H-NMR spectra of crude (*top*) and rinsed (*bottom*) **4**. The intensity and thus the integration value of the two doublets at 8.2 and 8.4 ppm decreased after rinsing with hot DMSO. It is additionally relevant to notice, that the integration of the oligoether- and alkyl chain signals match very well with the expected values. For clarity, only the values for the methyl groups are displayed in the figure.

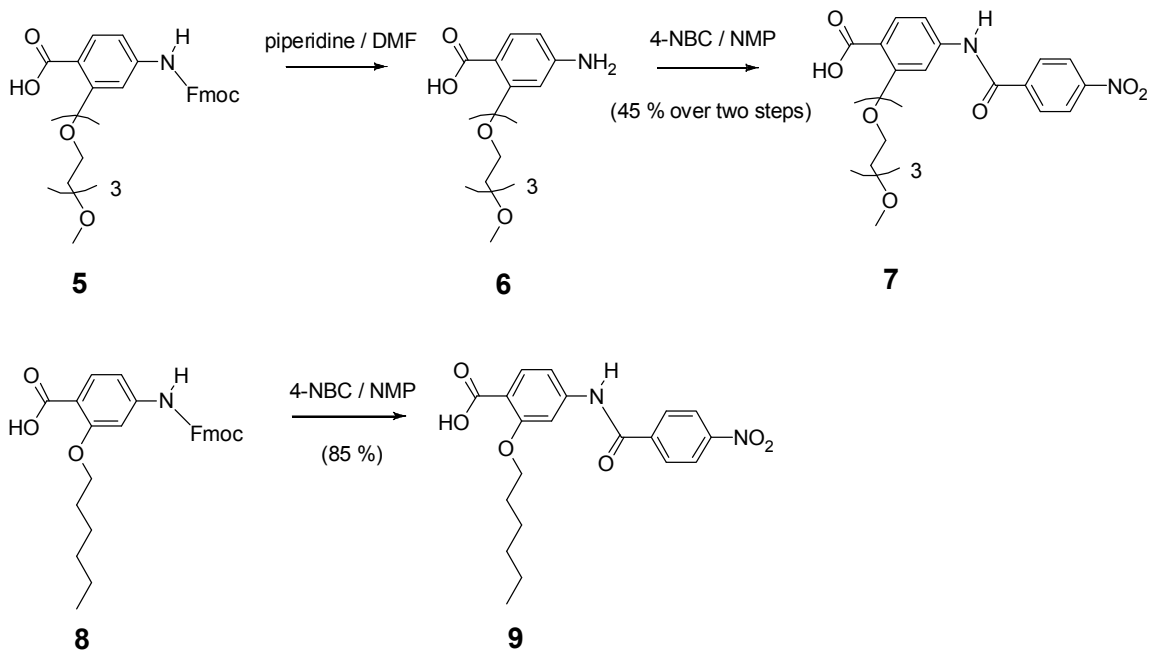

Scheme 5.1.2. Solution synthesis of the dimeric model compounds **7** and **9**.

Model compounds **7** and **9** were manually synthesized in order to corroborate the origin of these downfield-shifted signals. Monomer **5** was primarily *N*-deprotected; **6** and **8** were subsequently reacted with 4-nitro benzoic acid chloride in NMP at rt. The NMR characterization is detailed in the supporting information. The aromatic regions of the spectra of **4**, **7** and **9** are compared in **figure 5.1.3**. The chemical shifts of the capping aromatic units in the dimers are very similar to those of the unknown signal in the spectrum of the JNR **4**. Interpreting the integration values of the purified product **4**, one would deduce a 2:1 ratio of capped to clean product as the integration value of each unassignable doublet corresponds to one proton. On the other hand, there is a big discrepancy between this assumed purity level and the well-matching integration values of the TEG- and hexyl methyl signals. The low solubility of the compound impeded its further characterization and the self assembly of the JNR in DMSO-gels was examined by TEM without additional work up.

Figure 5.1.4 shows the images obtained after drop deposition of the hot solution of the gelated solvent on the carbon coated cupper grids after returning to rt and drying at 60 °C in vacuum. The pictures revealed the presence of large aggregates with strongly oriented tape-like rods with lengths ranging from 100 nm to 0.5 µm and widths of 9 nm.

These tapes assemble further to spatially dispersed agglomerates and form a non-covalent network of fibers, resulting in a macroscopic gelation of the solvent.

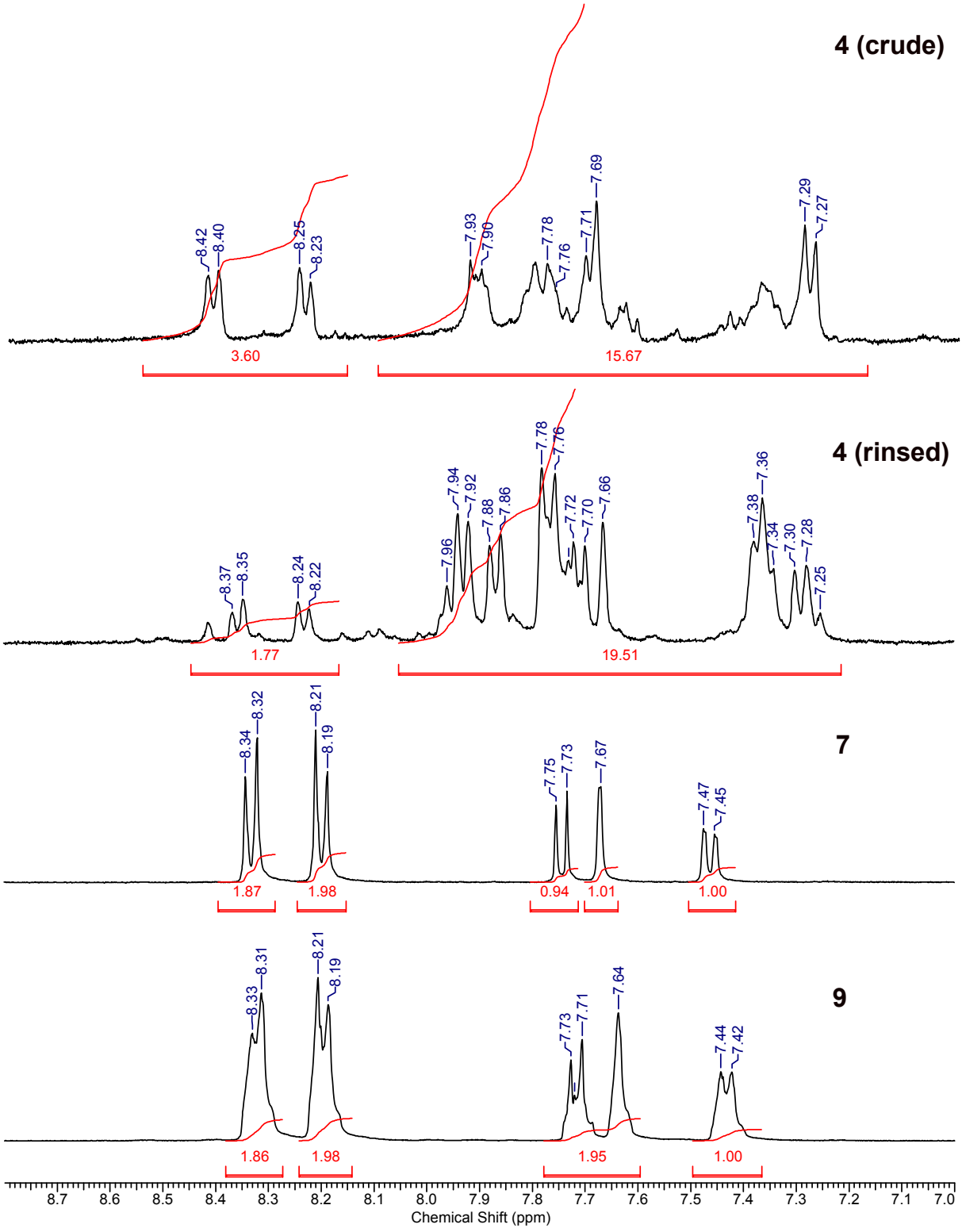

Figure 5.1.3. Comparison of the aromatic part of the ^{1}H-NMR (400 MHz) spectra of the crude and purified heptamer **4** as well as for the model compounds **7** and **9** in DMSO-d_6 at 100 °C.

Unfortunately, verifying the chemical dis-symmetry of these nanorods is impossible with common imaging techniques like TEM, as the Janus-like character occurs in domains at the molecular level. The formation of bilayers can be proposed from the width of the tapes, while the interaction between chains of the same polarity induces their length. The noncovalent networks could result from the partial shift of the rods and π-π stacking interactions. **Figure 5.1.5** serves as a cartoon of the proposed aggregation processes leading to rod-like architectures in nanometer dimensions.

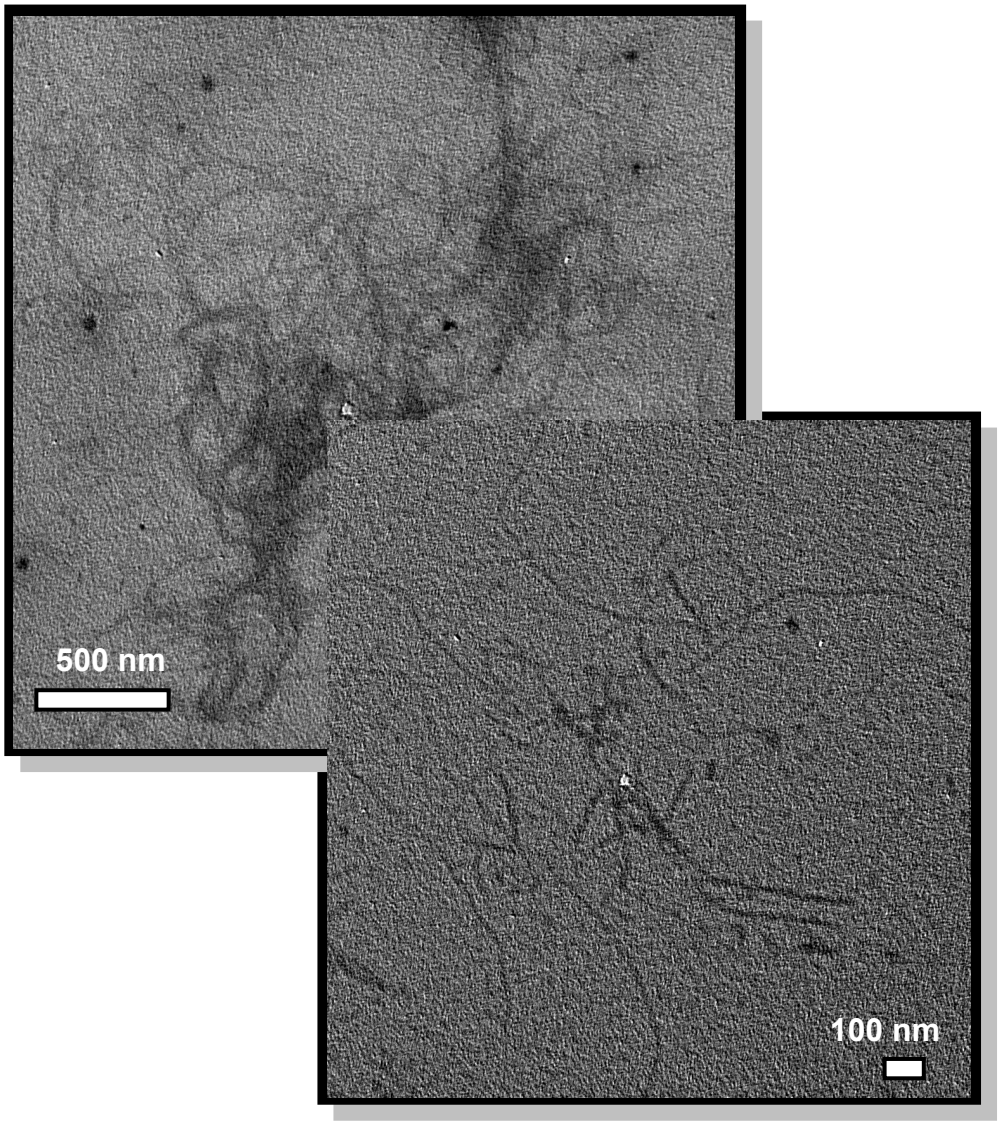

Figure 5.1.4. TEM images of the supramolecular structures of the JNR **4** from DMSO-gels.

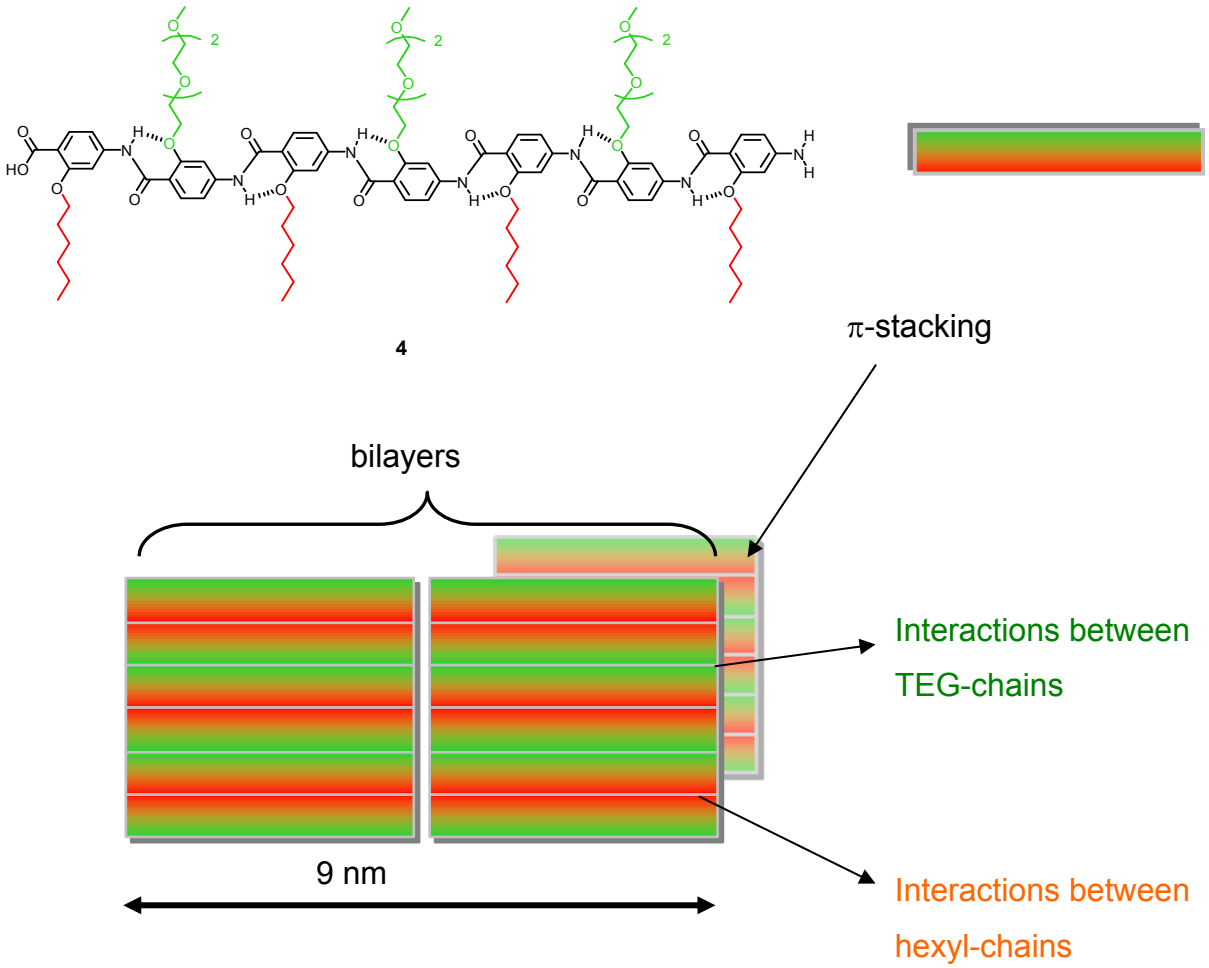

Figure 5.1.5. Schematic representation of compound **4** (*top*) and proposed aggregation mechanisms for the formation of tapes and networks (*bottom*).

The synthesis of an almost insoluble molecule on the solid support shows multiple advantages: the reagents can be easily removed by filtration and washing, multiple step synthesis can be automatized and physical losses of product can be minimized as it remains attached to the support throughout the synthesis.[10] This method is also useful for the sequence / shape and monodispersity control of the oligomers, although one of its limitations is the wasting of large amounts of the designed monomers, as solid phase synthesis requires large excess of building blocks (typically 2-10 times the resin functionality) and high reagent concentrations. This aspect becomes even more disadvantageous when difficult sequences[11] are synthesized and multiple repetitions of the coupling cycles have to be performed.

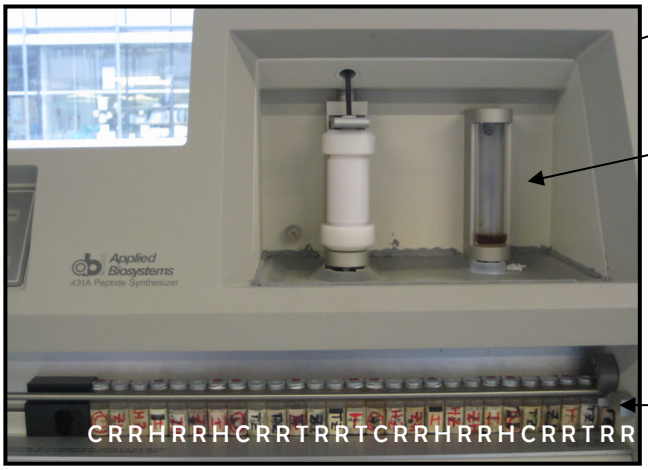

Figure 5.1.5. Photographs of the ABI 431A Peptide Synthesizer. The letters indicate the monomer / cartridge sequence: **R** = empty cartridge for monomer recycling; **T** = cartridge with **2**; **H** = cartridge with **3**; **C** = cartridge with capping agent. Each monomer coupling step is repeated once after recovering of the coupling solution and before the subsequent capping step. Hence, two empty vessels for the monomer recycling steps were placed between the two filled monomer cartridges (double coupling). The sequence continues with the capping step, followed by the coupling of the next monomer.

This problem was minimized in the synthesis of JNR **4** by programming a new module for conventional peptide synthesizers, which permits the recovery and recycling of monomers. Thereby the reaction mixture is transferred into a new cartridge after the coupling step, the resin rinsed with fresh solvent and the solution pumped again into the next empty cartridge (see **figure 5.1.5**, **appendix A** and **B** for detailed module H and system description).

Additionally, the synthetic protocols were reprogrammed for solvent economization. The protocols used in our prior works were based on standard Fmoc-chemistry protocols, in which the subsequent monomer is transferred in the activator until the end of the coupling run (see **figure 5.1.5**, *bottom figure*). Within the new protocol, the monomer remains in the cartridge until the running reaction is completed and the resin rinsed. Thereafter it is directly delivered into the reaction vessel, without the need of any activator washing steps (see **appendix C**).

5.1.3. Conclusions.

In conclusion, the automated synthesis of a new type of JNR was described, whereby artificial peptides based on monodisperse oligo(*p*-benzamide)s with hydrophobic and hydrophilic side chains were prepared. The particular property of oligomer **4** compared with other known Janus particles, is its linear, shape persistent and monodispese rod-like architecture with nanometer dimensions. The ability to control the precise location of functional groups and their spatial position within the molecule may enable the application as building blocks for supramolecular assemblies.

One major limitation in the synthesis of aramide based Janus particles is the low solubility in organic solvents, mainly when hexyloxy substituents are introduced. This new synthetic procedure allows the fast and easy preparation, which otherwise would be impossible to carry out in solution. Regardless of this progress, the purification and characterization still is the main challenge, due to their strong aggregation behavior.

This synthetic approach can be easily applied for the preparation of a variety of new oligomers with different monomer arrays. The influence of substituent sort and arrays, as well as oligomer length can be easily analyzed, regarding the final solubility and self-assembly properties. Concomitantly, this synthetic technique for the preparation of non-

spherical particles contributes to the study and understanding of the geometry effect in Janus particles aggregate formation.

The introduction of *turn-inducing* building blocks to these shape persistent JRN oligomers will be further investigated in the preparation of helices with different inner and outer functionalities. The presented approach to nanorods is also very promising for the synthesis of hybrid organic-inorganic Janus particles, for example by the precise positioning of anchor groups for the complexation of inorganic materials as iron- or manganese oxide particles (*e.g.* catechol moieties). This approach will serve to easily distinguish the different chemical hemispheres of the particle and to enhance their contrast for TEM-characterization.

5.1.4. Experimental Section

Methods.

Standard ^{1}H nuclear magnetic resonance spectra were recorded on a Bruker AMX 400 (400 MHz) at 100 °C.

The heptamer **4** was synthesized automatically on an ABI 431a Peptide Synthesizer as described in **chapter 5.1**. The wang resin was previously functionalized with the *N*-Fmoc-4-amino-2-hexyloxy benzoic acid chloride **3**. The monomers were activated by its conversion into the corresponding acid chlorides using thionyl chloride.

RP-HPLC analysis was performed on a Hewlett Packard HP 1090 Liquid Chromatograph equipped with PerfectSil column (MZ Analysentechnik, Mainz, Germany, 250 x 4.0 mm; 120 ODS-2 5 μm). The samples were eluted with an acetonitrile / water gradient that started from 10 % acetonitrile rising to 90 % over a period of 35 min and maintained constant for additional 10 min. Both solvents were buffered with 0.1 % TFA. UV-detection was performed at 254 nm.

Materials.

Dry NMP (over molecual sieves) and 4-nitro benzoic acid chloride were purchased from Aldrich and used as received. Wang resin loading was 0.6 mmol/g (Iris Biotech) and its

functionalization was accomplished following the synthetic description in **chapter 4.1**. DMSO-d_6 was purchased from Deutero GmbH and stored over molecular sieves.

Compound **6**.

N-Fmoc-4-amino-2-TEG benzoic acid **5** (495 mg, 1 mmol) was dissolved in 6 ml piperidine in DMF (20 vol. %) under an inert atmosphere. After 2 hrs, the reaction mixture was filtered, the solvent removed at 80 °C under reduced pressure to afford **6** as an oil. The product was used without further purification. The characterization was performed by HPLC (9 min) and TLC (TCM : MeOH = 6:1; R_f = 0.3).

Compound **7**.

4-Nitro-benzoic acid chloride (38 mg, 0.23 mmol) was dissolved in a minimum amount of dry NMP and added dropwise under an inert atmosphere to a concentrated solution of 4-amino-2-TEG benzoic acid **6** (47 mg, 0.18 mmol) in the same solvent. After 24 hrs the product was precipitated in demin. water, filtrated and washed with diethyl ether (40 mg, 45 %).

^{1}H-NMR: δ (400 MHz, 100 °C, DMSO-d_6): 3.27 (s, 3 H); 3.46 (t, 2 H); 3.55-3.6 (m, 2 H); 3.67 (t, 2 H); 3.84 (t, 2 H); 4.24 (t, 2 H); 6.46 (dd, 1 H); 6.67 (d, 1 H); 7.74 (d, 1 H); 8.2 (d, 2 H); 8.33 (d, 2 H); 10.37 (s, 1 H).

Compound **9**.

4-Nitro-benzoic acid chloride (0.437 g, 2.3 mmol) was dissolved in a minimum amount of dry NMP and added dropwise under an inert atmosphere to a concentrated solution of 4-amino-2-hexyloxy benzoic acid **8** (0.5 g, 2.1 mmol) in the same solvent. After 24 hrs the product was precipitated in demin water, filtrated and washed with diethyl ether (770 mg, 85 %).

^{1}H-NMR: δ (400 MHz, 100 °C, DMSO-d_6): 0.91 (t, 3 H); 1.35-1.52 (m, 6 H); 1.77-1.84 (m, 2H); 4.11 (t, 2 H); 7.43 (d, 1 H); 7.64 (s, 1 H); 7.72 (d, 1 H); 8.20 (d, 2 H); 8.32 (d, 2 H); 10.31 (s, 1 H).

*Compound **4**.*

In situ activation of monomer **(5)**: 3.65 g (12 mmol) *N*-Fmoc-4-amino-2-TEG benzoic acid **5**, 17.5 ml $SOCl_2$ (with catalytic amount of dry NMP), 2-3 hrs at RT.

Coupling solution of monomer **(2)**: **2** was dissolved in 13 ml dry NMP.

Activation of monomer *N*-Fmoc-4-amino-2-hexyloxy benzoic acid (*in situ*): 3.22 g (13.5 mmol) *N*-Fmoc-4-amino-2-hexyloxy benzoic acid, 17.5 ml $SOCl_2$ (catalytic amount of dry NMP), 2-3 hrs at rt.

Coupling solution of monomer **(3)**: **3** was dissolved in 13 ml dry NMP.

Capping solution: 1.61 g (7 mmol) 4-nitro benzoic acid chloride in 12.5 ml dry NMP.

Cleavage from the resin: TFA / TCM (1:1) 6 ml, 2 hrs.

Precipitation solvent: diethyl ether

Purification: the product was rinsed twice with hot DMSO (100 °C), washed with diethyl ether and centrifugated.

Yield: 26 mg of a slight yellow powder.

5.1.5. References

[1] Lehn, J.-M. *Supramolecular Chemistry: Concepts and Perspectives*, VCH, Weinheim, **1995.**

[2] de Gennes, P.-G. *Angew. Chem. Int. Ed. Engl.* **1992**, *31* (7), 842.

[3] (a) Kim, J.-K.; Lee, E.; Lim, Y.-B, Lee, M. *Angew. Chem. Int. Ed.* **2008**, *47*, 4662-4666; (b) Lee, E.; Jeong, Y.-H.; Kim, J.-K.; Lee, M. *Macromolecules* **2007**, *40* (23) 8355-8360.

[4] Lee, E.; Kim, J.-K.; Lee, M. *Angew. Chem. Int. Ed*. **2009**, *48*, 3657-3660.

[5] Walther, A.; Müller, A. H. E. *Soft Matter* **2008**, *4*, 663-668.

[6] Perro, A.; Reculusa, S.; Ravaine, S.; Bourgeat-Lami, E.; Duguet, E. *J. Mater. Chem*. **2005**, *15*, 3745-3760.

[7] (a) Feng, Y.; He, Y. M.; Zhao, L. W.; Fan, Q. H.; *Org. Lett.* **2007**, *9*, 2261-2264; (b) Grayson, S. M.; Frechet, J. M. J. *J. Am. Chem. Soc.* **2000**, *122*, 10335-10344; (c) Maraval, V.; Laurent, R.; Donnadieu, B.; Mauzac, M.; Caminade, A. M.; Majoral, J. P. *J. Am. Chem. Soc.* **2000**, *122*, 2499-2511; (d) Fuchs, S. Pla-Quintana, A.; Mazères, S.; Caminade, A.-M. Majoral, J.-P. *Org. Lett*. **2008**,*10* (21) 4751-4754; (e) Saez, I. M.; Goodby, J. W. *Chem. Comm*. **2003**, 1726-1727; (f) Feng, X.; Taton, D.; Ibarboure, E.;

Chaikof, E. L.; Gnanou, Y. *J. Am. Chem. Soc.* **2008**, *130* (35), 11662-11676; (g) Wooley, K. L., Hawker, C. J.; Frechet J. M. J. *J. Am. Chem. Soc* **1993**, *115* (24), 11496-11505; (h) Hawker, C. J.; Wooley, K. L.,; Frechet J. M. J. *J. Chem. Soc. Perkin Trans. 1* **1993**, 1287-1297; (i) Percec, V.; Imam, R. M.; Bera, T. K.; Balagurusamy, V. S. K.; Peterca, M.; Heiney, P. A. *Angew. Chem. Int. Ed.* **2005**, *44*, 4739-4745; (j) Yang, M.; Wang, W., Lieberwirth, I.; Wegner, G. *J. Am. Chem. Soc.* **2009**, *131* (17), 6283-6292.

[8] (a) Erhardt, R.; Böker, A.; Zetl, H.; Kaya, H.; Pyckhout-Hintzen, W.; Krausch, G.; Abetz, C.; Müller, A. H. E. *Macromolecules* **2001**, *34*, 1069; (b) Erhardt, R.; Zhang, M; Böker, A.; Zetl, H.; Abetz, C.; Müller, A. H. E. *J. Am. Chem. Soc.* **2003**, *125*, 3260; (c) Xu, H.; Rehardt, R.; Abetz, V.; Müller, A. H. E.; Goedel, W. *Langmuir* **2001**, *17*, 6787; (d) Hamelin, B.; Jullien, L.; Laschewsky, A.; Hervé du Penhoat, C. *Chem. Eur. J.* **1999**, *5*, 546.

[9] Zhao, D.; Moore, J. S. *Chem. Comm*. **2003**, 807.

[10] Chang, W. C.; White, D. P. *Fmoc solid phase peptide synthesis – A practical approach*, Oxford University Press, Ed. Hames, B. D., **2000**.

[11] (a) Kent, S. B. H. *Peptides, structure and function; Proceedings of the 9th American Peptide Symposium;* Ed. Deber., C. M.*;* Hruby, V. J.; Kopple, K. D., 407, Pierce Chemical Co., Rockford, IL, **1985**.; (b) Atherton, E.; Sheppard, R. C.. *Peptides, structure and function; Proceedings of the 9th American Peptide Symposium,* Ed. Deber., C. M.*;* Hruby, V. J.; Kopple, K. D., 415, Pierce Chemical Co., Rockford, TL., **1985**.

5.1.6. Supporting Information for “Janus Nanorods“

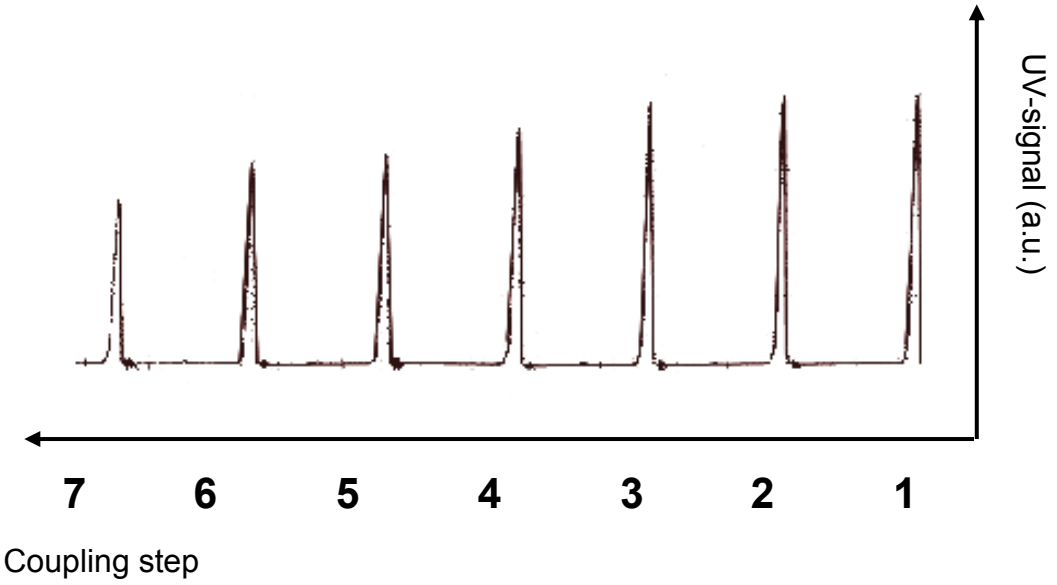

Figure SI-5.1.1. UV-detection of Fmoc groups at 301 nm after each deprotection step during the automated synthesis of **4**.

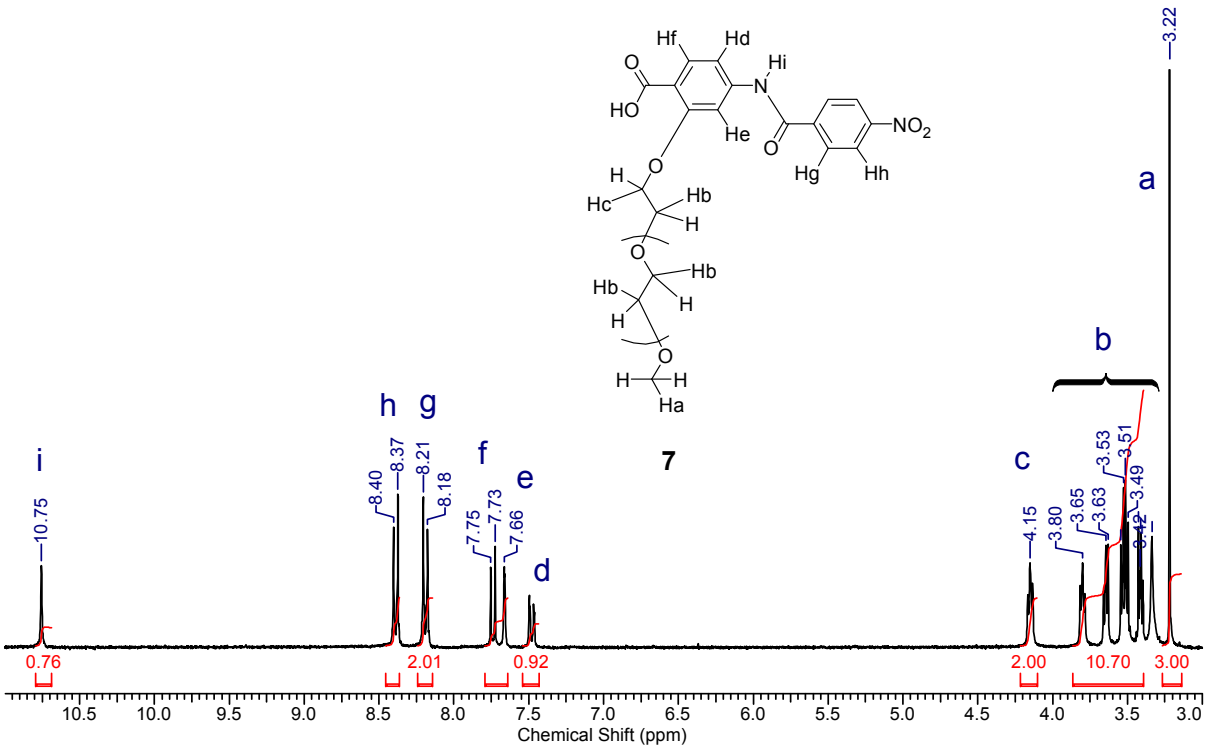

Figure SI-5.1.2. ^{1}H-NMR spectrum (300 MHz) of **7** in DMSO-d_6 at rt and signal assignment.

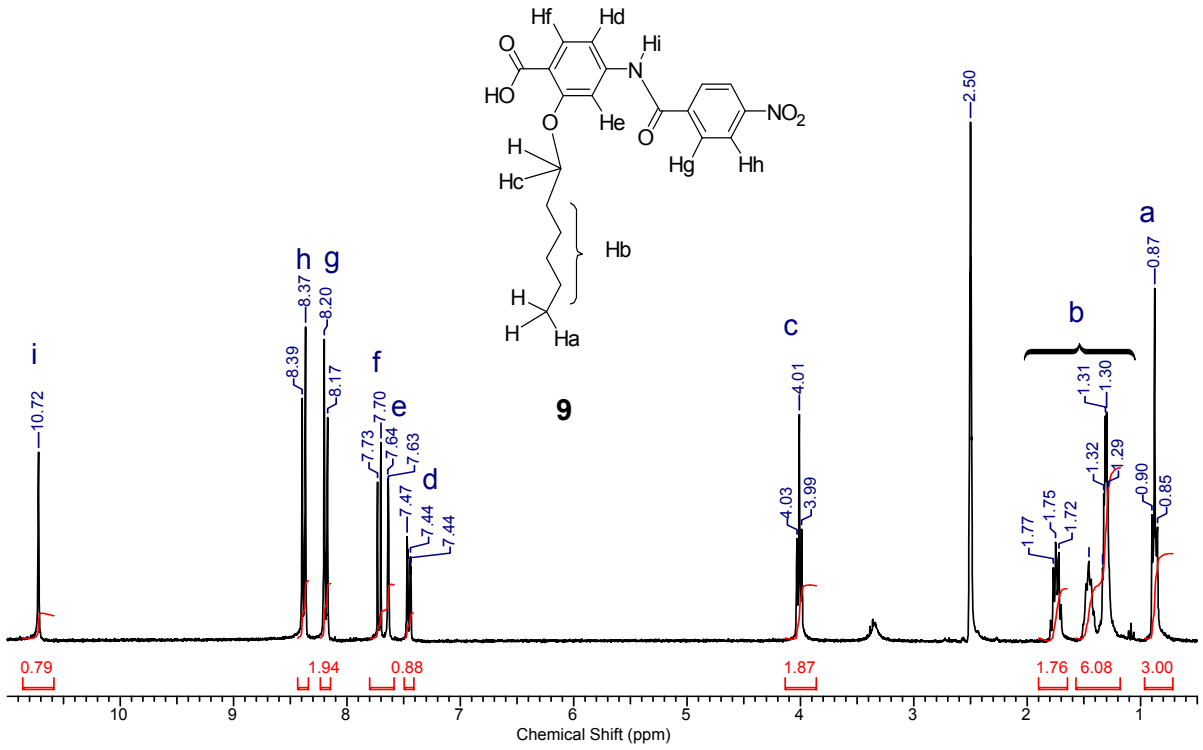

Figure SI-5.1.3. ^{1}H-NMR spectrum (300 MHz) of **9** in DMSO-d_6 at rt and signal assignment.

5.2. “A facile synthesis of aramide-peptide amphiphiles”

*Helga Seyler, Christof Storz, Robert Abbel and Andreas F.M. Kilbinger**

Published in *Soft Matter* **2009, DOI:** 10.1039/b903488a

Abstract

A new peptide amphiphile, consisting of a natural and an artificial peptide oligomer, where the hydrophobic character is provided by oligo(*p*-benzamide)s has been accomplished. A combination of aramide and peptide automated solid-phase chemistry was developed as a new strategy for preparing well defined amphiphilic oligoamide conjugates. UV absorption, ^{1}H-NMR spectra and TEM investigations revealed the aggregation of the amphiphile in water as worm-like structures, driven entirely by the combination of solvophobic effects and strong hydrogen bonds between the oligo(*p*-benzamide) strands.

Kurzfassung

Ein neues Block-Oligomer bestehend aus einem natürlichen und einem synthetischen Peptide Block mit amphiphilen Eigenschaften wurde hergestellt und dessen Aggregationsverhalten in Wasser untersucht. Die Synthese wurde auf automatisierte Weise an der Festphase neu entwickelt, durch die Kombination aus Aramid- und Peptid-Festphasenchemie. UV-Absorption, ^{1}H-NMR und TEM-Untersuchungen ermöglichten die Charakterisierung der wurmartigen supramolekularen Strukturen, die durch das Zusammenspiel von solvophoben Effekten und Wasserstoffbrückenbindungen enstehen.

5.2.1. Introduction

In recent years, increasing attention has been drawn to low molecular weight compounds that self-organize into supramolecular structures in solution. An important class of self-assembling oligomers is represented by peptide amphiphiles (PA). They often consist of a hydrophilic charged peptide segment covalently linked to a hydrophobic moiety. The supramolecular nanostructures built from PAs are particularly interesting, as they can be induced by chain-selective solvents or variations in pH, finding application in *e.g.* tissue engineering, biomineralization,[1] as surfactants and detergents,[2] as mimics of different cellular phenomena or as drug-delivery carriers.[3] In addition to low molecular peptides only and lipidated peptides amphiphiles,[4] semi-rigid segments from *p*-amino benzoic acid-β-alanine,[5] π-conjugated oligomeric blocks such as oligo(thiophene)[6] and oligo(*p*-phenylene vinylene)[7] have also been used as hydrophobic blocks in the synthesis of PAs. For these, spatial orientation and packing of the supramolecular nanostructures are mainly dictated by the peptide sequence.

Oligo(*p*-benzamide)s (OPBAs) are particularly interesting in this context as they form shape-persistent linear rigid rods with hydrogen-bond acceptors and donors pointing towards the edges of the flat oligomer, thereby mimicking peptide strands in β-sheets.[8] In addition, both OPBA and peptides offer the great advantage of automated synthesis on a solid support (SPS) using commercial peptide synthesizers.[9] Here, we present the first synthesis of a peptide amphiphile based on an aramide–peptide conjugate, prepared entirely on a solid support. We chose a polyanionic water-soluble L-aspartic acid pentamer as the oligopeptide block. In addition to providing excellent solubility in an aqueous environment due to its ionomer properties, oligo(L-aspartic acid)s have received interest as models for plastocyanine–cytochrome interactions[10] and in biomineralization processes.[11] The well defined amphiphilic tetra(PBA)–benzylamine–penta(Asp) oligomer **15** (PBA_4–BA–Asp_5) was synthesized in a fully automated fashion on a modified peptide synthesizer.This allowed full control over the molecular weight of both blocks and amino acid sequence.

5.2.2. Results and discussion.

The solid supported hydrophobic block **14** (see **figure 5.2.1**) carrying a benzylamine functional end group was sequentially constructed from four Fmoc-protected *p*-amino benzoyl chlorides **11a**[9b,12] and one Fmoc-protected 4-(aminomethyl) benzoyl chloride **11b**.[13] The more nucleophilic benzylic amine serves as a linker for subsequent attachment of the peptide segment as oxybenzotriazole esters (OBt) of α-amino acids cannot directly be coupled to the less nucleophilic aromatic amines.

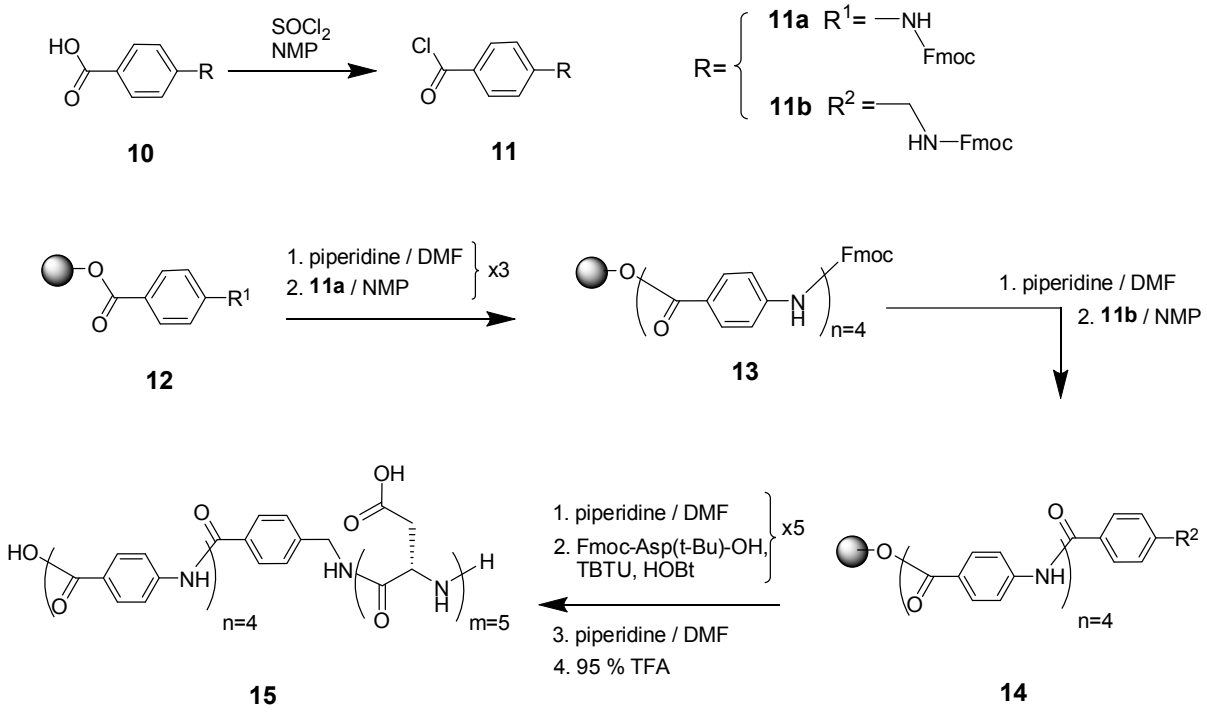

Figure 5.2.1. Automated synthesis of (*p*-benzamide)-*block*-(L-aspartic acid) conjugate.

The *t*-butyl-protected penta(aspartate) was built by conventional Fmoc chemistry (Fastmoc).[14] We evaluated different coupling reagents and cleavage conditions for the *N*-protective group. *In situ* activation with 2-(1*H*-benzotriazole-1-yl)-1,1,3,3-tetramethyluronium tetrafluoroborate–1-hydroxybenzotriazol (TBTU–HOBt) (see **figure 5.2.1**) and short Fmoc cleavage times (2.5 min) with piperidine (20% in *N*-methylpyrrolidone, NMP) afforded the pentamer without detection of aspartimide formation. Treatment of the resin with trifluoroacetic acid (90%) afforded **15**, as

confirmed by MALDI-TOF mass spectrometry and ^{1}H-NMR spectroscopy measurements (see **figure SI-5.2.1**).

As expected for amphiphilic molecules, dissolution in basic ($NaHCO_3$ or NaOH) water, which acts as a selective solvent for the peptide block, resulted in supramolecular aggregation, leading to broadening of the ^{1}H-NMR signals. Solution characterization of **15** in a good solvent for both blocks like DMSO-d_6 resulted in the molecularly dissolved oligomer (see **figure SI-5.2.3**).

A TEM examination of basic (NaOH) aqueous solutions of **15** (see **figure 5.2.2**) revealed long worm-like as well as more rigid shorter aggregates. Among these, monodisperse widths (*ca.* 7 nm) and lengths up to 400 nm (see **SI**) are observed. The formation of longer and smaller aggregates could be a direct result of present impurities (see **SI**, **figure SI-5.2.10**). We believe that the aggregates are formed as a result of the hydrophobic effect and hydrogen bonds between the β-strand-like OPBA rods (see **figure 5.2.3**). The linear aggregates are surrounded by penta(aspartate)s, similar to the supramolecular structures observed for poly(ethylene oxide)–OPBA amphiphiles.[12,15]

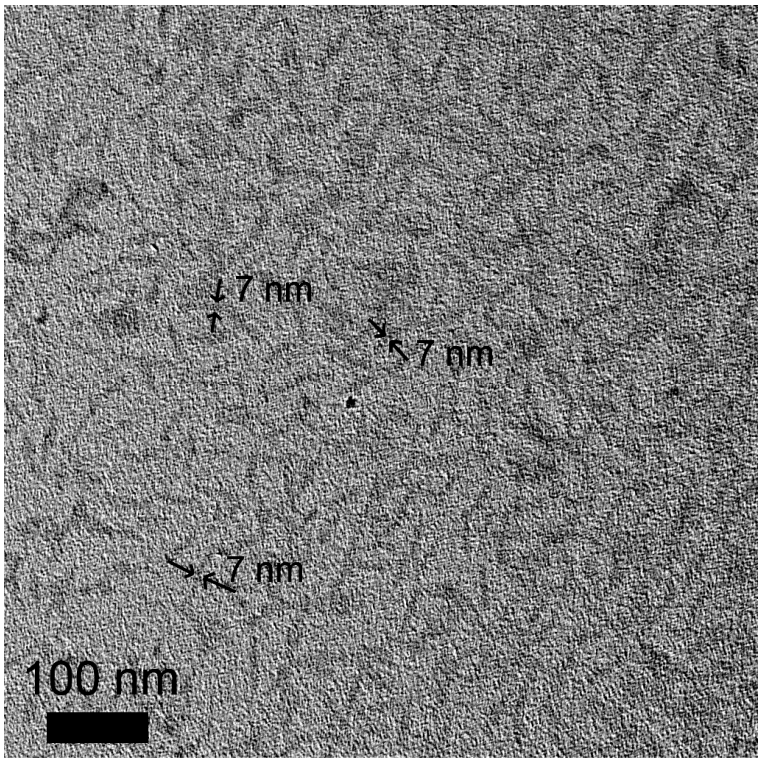

Figure 5.2.2. TEM micrograph of the rod-like nanostructures observed from H_2O solution of **15** (6 eq. NaOH). The arrows drawn on the TEM micrograph show a width of the peptide amphiphile fibers of *ca.* 7 nm.

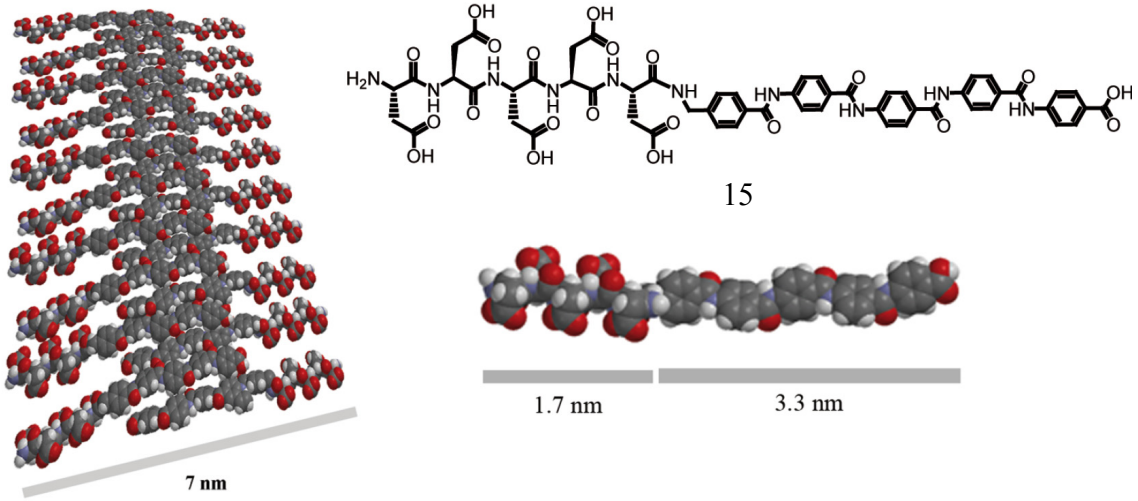

Figure 5.2.3. *Left*: Schematic representation of the proposed aggregation mechanism showing H-bonded nano-rods. *Right*: Structure and molecular model of the peptide amphiphile **15**. The model proposes a slightly overlapping interdigitated assembly of the aromatic oligoamides (3.3 nm in length). This would lead to self-assembled tapes of 7 nm in width (assuming stretched out Asp_5 blocks (1.7 nm in length)). The lengths of the oligomers were obtained from molecular mechanics models of **15**.

UV-vis experiments show a hypsochromic shift of the absorption maximum ($\Delta\lambda_{max}$ = 19 nm) in basic (NaOH) water (λ_{max} = 301 nm) compared to the DMSO (λ_{max} = 320 nm) absorption spectrum (see **figure 5.2.4**). This effect is indicative of H-aggregate formation and attributed to the stacking of the OPBA chromophores in the core of the worm-like superstructures (see also **SI**, **figure SI-5.2.6**).[16] This observation supports our model of the OPBA block being responsible for supramolecular fiber formation in aqueous solution. We believe that the hydrophobic benzene rings are the driving force for aggregation and the hydrogen bonds reinforce and direct the resulting aggregates, aligning them perfectly even in the presence of competing amides (of the peptide) and water.

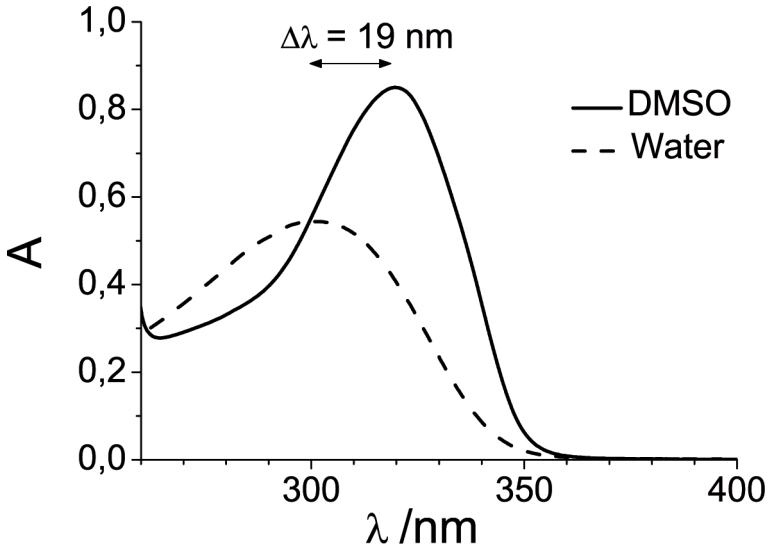

Figure 5.2.4. UV-vis spectra of **15** in water (with 6 eq. NaOH) and DMSO (*c* = 0.01 mM).

UV-vis measurements of basic (NaOH) aqueous solutions of **15** as a function of temperature (up to 80 °C) show no significant shift of the absorption maximum, proving the thermal stability of the supramolecular structures formed. Circular dichroism studies reveal an absence of chiral supramolecular aggregation (see **figure SI-5.2.7**). We believe that this is a direct result of the strong directional linear aggregation of individual OPBA rods. In order for the fibers to exhibit supramolecular chirality, a slight deviation from perfect co-planarity of the interacting OPBAs would be necessary. Only in the latter case could a chiral superstructure be formed. We believe that the OPBA stacks are locked into a perfectly *anti*-parallel stack by multiple hydrogen bonds. A small deviation from this arrangement would lead to the loss of several hydrogen-bond interactions and therefore to an energetically less favored assembly.

We therefore propose the packing of the amphiphilic molecules into tapes, with the perfectly aligned OPBA blocks inside of the fiber-like micelle surrounded by the oligopeptide segments (see **figure 5.2.3**, *left*).

This model results in fibers or tapes with a width of *ca.* 7 nm (see **figure 5.2.2**), corresponding well to the structures observed in the TEM measurements. The dimensions of the fibers can be estimated from both of the previous crystal structure studies on oligo(*p*-benzamide)s[15a] and from molecular mechanics molecular modeling (Spartan 08) of an extended individual molecule. The extended conformation of the

oligo(peptide) block is induced by ionic repulsion of the densely packed carboxylates (due to the addition of sodium hydroxide).

It is important to emphasize that the peptide amphiphiles presented here form particularly strong aggregates that are stable even up to 80 °C in water. One could therefore envisage such OPBA-based amphiphiles as molecular scaffolds for peptide epitope presentation, as shape-anisotropic templates for biomineralization studies or as synthetic polypeptide mimics.

5.2.3. Conclusions

In summary, a new peptide amphiphile, consisting of a natural and an artificial peptide oligomer, where the hydrophobic character is provided by oligo(*p*-benzamide)s has been accomplished. A combination of aramide and peptide automated solid-phase chemistry was developed as a new strategy for preparing amphiphilic well defined oligoamide conjugates. Penta(L-aspartic acid) was chosen as the peptide block due to its high solubility and lack of preferential secondary organization in water. UV absorption, ^{1}H-NMR spectra and TEM investigations revealed the aggregation of the amphiphile in water as worm-like structures. An aggregation model was proposed in which aggregation is driven entirely by the combination of solvophobic effects and strong hydrogen bonds between the oligo(*p*-benzamide) strands.

Ease of synthesis and compatibility with existing peptide synthesizer protocols makes this class of peptide amphiphiles particularly attractive. Potential applications for the presentation of peptides on a rigid supramolecular backbone could be epitope presentation, supramolecular nucleation sites for biomineralization or the mimicking of polypeptides.

5.2.4. Experimental Part

Materials.

Technical- and most of the p. a. quality solvents were purchased from Acros Organics. DCM and DMSO were purchased from Fisher Scientific. *N*-Methylpyrrolidone (NMP)

was kindly donated by BASF and stored over molecular sieve (4 Å).9-Fluorenylmethyl chloroformate (Fmoc-Cl), N-(9-Fluorenylmethyloxycarbonyl)-L-aspartic acid β-*t*-butyl ester (Fmoc-L-Asp(t-Bu)OH), trifluoroacetic acid and Wang resin were obtained by Iris Biotech GmbH, all other chemical reagents were purchased from Acros Organics and were used without further purification. Deuterated solvents (D_2O, DMSO-d_6) were purchased from Deutero GmbH.

Techniques.

Standard ^{1}H and ^{13}C nuclear magnetic resonance spectra were recorded on a Bruker AC (300 MHz) or on a Bruker AMX 400 (400 MHz). Infrared spectra were recorded on a Nicolet 5 DXC FT-IR spectrometer. RP-HPLC analysis was performed on a Hewlett Packard HP 1090 Liquid Chromatograph equipped with PerfectSil column (MZ Analysentechnik, Mainz, Germany, 250 x 4.0 mm; 120 ODS-2 5 μm). The samples were eluted with an acetonitrile/water gradient that started from 10 % acetonitrile rising to 90 % over a period of 35 min and maintained constant for additional 10 min. Both solvents were buffered with 0.1 % TFA. UV-detection was performed at 254 nm. Melting points were recorded on a FP 62 Mettler Toledo in a capillary tube and are uncorrected. Field desorption mass spectra were measured on a Finnigan MAT 95 and ESI mass spectra on a Micromass Q-TOF Ultima 3. Matrix-assisted laser desorption and ionization time-of-flight (MALDI-TOF) measurements were performed on a Shimadzu Axima CFR MALDI-TOF mass spectrometer equipped with a nitrogen laser delivering 3 ns laser pulses at 337 nm. Sinapinic acid was used as matrix. UV-vis measurements were accomplished on a V-630 UV-VIS Spectrophotometer and CD-spectra recorded on a JASCO J-815 CD Spectrometer. A Philips EM 420 transmission electron microscope using a LaB_6 cathode at an acceleration voltage of 120 kV was used to obtain TEM-images. TEM grids (carbon film on copper, 300 mesh) were obtained from Electron Microscopy Sciences, Hatfield, PA, USA. The synthesis of the oligomers was performed on an Applied Biosystems ABI 431a automated peptide synthesizer using standard Fmoc chemistry protocols. Modules A, G and E were modified for the aramide synthesis as described in detail before.[i]

[i] Koenig, M. H.; Gorelik, T.; Kolb, U.; Kilbinger, A.F.M *J. Am. Chem. Soc.* **2007**, *129*, 704.

Sample preparation for the TEM experiments.

The peptide amphiphile **15** was dissolved in water by the addition of 6 eq. sodium hydroxide to afford a solution concentration of 1 mg/ml. The sample for TEM analysis was prepared by the drop cast method after a solution equilibration period of one week. One drop of the solution was deposited onto the carbon-coated grid, after hydrophilization of the grids for 30 s with a plasma cleaner. The samples were dried in air over night.

Synthesis of N-Fmoc-4-(aminomethyl) benzoic acid (N-Fmoc-PAMBA) (**11b**).

Aminomethylbenzoic acid (5 g, 33 mmol) and sodium bicarbonate (10.5 g, 99 mmol) were dissolved in a mixture of dioxane/water (1:1, 420 ml) and cooled to 0 °C with vigorous stirring. 9-fluorenylmethylchloroformate (8.54 g, 33 mmol) was dissolved in dioxane (14 ml) added dropwise over 15 min. The ice bath was removed and the suspension was allowed to stir at rt. After 24 h 856 ml water was added and the mixture was extracted with ether (3 x 150 mL). The aqueous layer was acidified carefully at 0 °C and with concentrated hydrochloric acid to pH 3. The resulting white precipitate was extracted into ethyl acetate. The combined organic layers were washed with water (3 x 150 ml), dried over Na_2SO_4 and concentrated in vacuo to yield a white solid (12.3 g, 65 %).

mp: 220 °C

^{1}H-NMR: δ (300 MHz, DMSO-d_6): 7.90 (m, 5 H), 7.71 (d, J=7.4 Hz, 2 H), 7.42 (t, J=7.72 Hz, 2 H), 7.34 (t, J=6.25 Hz, 4 H), 4.41 (d, J=7 Hz, 2 H), 4.26 (m 3 H).

^{13}C-NMR and DEPT: δ (300 MHz, DMSO-d_6): 167.3, 156.5, 144.9, 143.9, 140.8, 129.4 (+), 129.3, 128.2 (+), 127.6 (+), 127.1 (+), 126.9 (+), 125.2 (+), 120.2 (+), 65.3 (-), 46.9 (+), 43.6 (-).

RP-HPLC (min.): 24.1

IR: 3311, 3066, 2884, 2673, 2543, 1685, 1535, 1425, 1291, 1253, 757, 736.

M (FD): *m/z* (%) = 396.1 (100); 397.1 (10.7); 769.2 (5.6); 770.2 (1.6); calc.[$C_{23}H_{19}NO_4$] = 373.1

Synthesis of (p-benzamide)-block-(L-aspartic acid) conjugate (**15**).

Resin functionalization and PBA_5 were accomplished as described before.[i]

The aspartic acid block was prepared by TBTU/HOBt activation.

The reaction time for each Fmoc-deprotection step was 2.5 min. Cleavage from the resin was performed using 90 % TFA for 1.5 h. Azeotropic distillation of the TFA/H_2O solution with toluene afforded the product as a white solid (76 mg, 25%)

^{1}H-NMR: δ (300 MHz, DMSO-d_6): 10.53-10.46 (m, 4 H); 8.79 (s, 1 H); 8.29-7.94 (m, 22 H); 7.41 (d, J = 8.5 Hz, 2 H); 4.57-4.49 (m, 3 H); 4.36 (s, 2 H), 4.01 (m, 1 H); 2.69 (m, 10 H).
^{13}C-NMR and DEPT: δ (300 MHz, DMSO-d_6): 35.99 (-), 36.07 (-), 36.16 (-), 36.47 (-), 50.05 (+), 50.13 (+), 119.42 (+), 125.36, 126.78 (+), 127.79 (+), 128.65 (+), 130.22 (+), 132.95, 142.66, 143.46, 165.25, 165.33, 165.75, 166.99, 170.47, 170.47, 65, 171.76, 171.95, 172.05, 172.08.
M (MALDI-TOF): *m/z* = 1203 $[M + H]^+$; 1225 $[M + Na]^+$; 1247 $[M_{Na\text{-}salt} + Na]^+$; calc.$[C_{56}H_{54}N_{10}O_{21}]$ = 1202.

5.2.5. References

[1] Hartgerink, J. D.; Beniash, E.; Stupp, S. I. *Science* **2001**, *294*, 1684–1688.

[2] (*a*) Vauthey, S.; Santoso, S.; Gong, H.; Watson, N.; Zhang, S. *Proc. Natl. Acad. Sci. U. S. A.* **2002**, *99*, 5355–5360; (*b*) Santoso, S.; Hwang, W.; Hartman H.; Zhang, S. *Nano Lett.*, **2002**, *2*, 687–691; (*c*) Von Maltzahn, G.; Vauthey, S.; Santoso, S.; Zhang, S. *Langmuir*, **2003**, *19*, 4332–4337.

[3] (*a*) Guler, M. O.; Claussena, R. C.; Samuel, I.; Stupp, S. I. *J. Mater. Chem.*, **2005**, *15*, 4507–4512; (*b*) Kokkoli, E.; Mardilovich, A.; Wedekind, A.; Rexeisen, E. L.: Garg, A.; Craig, J. A. *Soft Matter*, **2006**, *2*, 1015–1024; (*c*) Hentschel, J.; ten Cate, M. G. J.; Börner, H. G. *Macromolecules*, **2007**, *40*, 9224–9232.

[4] Loewik, D. W. P. M.; van Hest, J. C. M. *Chem. Soc. Rev.* **2004**, *33*, 234–245.

[5] Claussen, R. C.; Rabatic, B. M.; Stupp, S. I. *J. Am. Chem. Soc.* **2003**, *125*, 12680–12681.

[6] Klok, H. A.; Rösler, A.; Götz, G.; Mena-Osteritz, E.; Bäuerle, P. *Org. Biomol. Chem.* **2004**, *2*, 3541–3544.

[7] (*a*) Harrington, D. A.; Behanna, H. A.; Tew, N. G.; Claussen, R. C.; Stupp, S. I. *Chem. Biol.*, **2005**, *12*, 1085–1091; (*b*) Matmour, R.; De Cat, I.; George, S. J.; Adriaens,

W.; Leclére, P.; Bomans, P. H. H.; Sommerdijk, N. A. J. M.; Gielen, J. C.; Christianen, P. C. M.; Heldens, J. T.; van Hest, J. C. M.; Loewik, D. W. P. M.; De Feyter, S.; Meijer E. W.; Schenning, A. P. H. J. *J. Am. Chem. Soc.* **2008**, *130*, 14576–14583.

[8] Koenig, H. M.; Gorelik, T.; Kolb, U.; Kilbinger, A. F. M. *J. Am. Chem. Soc.* **2007**, *129*, 704–708.

[9] (*a*) Merrifield, R. B.; Stewart, J. M. *Nature* **1965**, *207*, 522–523; (*b*) Koenig, H. M.; Kilbinger, A. F. M. *Macromol. Rapid Commun.* **2008**, *29*, 1721–1725.

[10] (*a*) Hirota, S.; Endo, M.; Tsukazaki, T.; Takabe, T.; Yamauchi, O. *JBIC, J. Biol. Inorg. Chem.* **1998**, *3*, 563–569; (*b*) Hirota, S.; Endo, M.; Hayamizu, K.; Tsukazaki, T.; Takabe, T.; Kohzuma, T.; Yamauchi., O. *J. Am. Chem. Soc.* **1999**, *121*, 849–855.

[11] Loges, N.; Graf, K.; Nasdala, L.; Tremel, W. *Langmuir* **2006**, *22*, 3073–3080.

[12] Bosshard, H. H.; Mory, R.; Schmid, M.; Zollinger, H. *Helv. Chim. Acta* **1959**, *42*, 1653–1658.

[13] Schneider, S. E.; Patricia, A.; Bishop, P. A.; Salazar, M. A.; Bishop, O. A.; Anslyn, E. V. *Tetrahedron* **1998**, *54*, 15063–15086.

[14] Atherton, E.; Logan, C. J.; Sheppard, R. C. *J. Chem. Soc., Perkin Trans. 1* **1981**, 538–546.

[15] (*a*) Schleuss, T. W.; Abbel, R.; Gross, M.; Schollmeyer, D.; Frey, H.; Maskos, M.; Berger, R.; Kilbinger, A. F. M. *Angew. Chem. Int. Ed.* **2006**, *45*, 2969–2975; (*b*) Seyler, H.; Berger-Nicoletti, E.; Kilbinger, A. F. M. *J. Mater. Chem.* **2007**, *17*, 1954–1957; (*c*) Klos, J.; Wurm, F.; Koenig, H. M.; Kilbinger, A. F. M. *Macromolecules* **2007**, *40*, 7827–7833.

[16] Abbel, R.; Schleuss, T. W.; Frey, H.; Kilbinger, A. F. M. *Macromol. Chem. Phys.* **2005**, *206*, 2067–2074.

5.2.6. Supporting Information for "A facile synthesis of aramide-peptide amphiphiles"

Activation protocol for the aspartic acid block:

Cycle #	Repetition	Cycle description
1	4	BADEFG
5	1	BfDc

Module description for Fastmoc-protocols in automated solid phase synthesis (Applied Biosystems Peptide Synthesizer ABI 431A).

B = Fmoc-deprotection step
A = Dissolution and activation of the amino acid
D/G = Resin wash with NMP
E = Amino acid transfer
F/f = Coupling of the amino acid to the resin
c = Resin wash with DCM

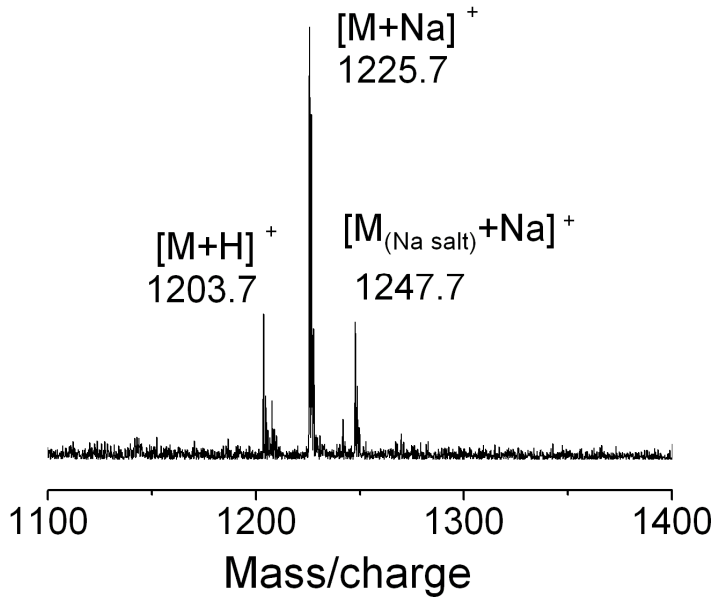

Figure SI-5.2.1. MALDI-TOF-spectrum of peptide-benzamide conjugate **15**.

Monitoring profile.

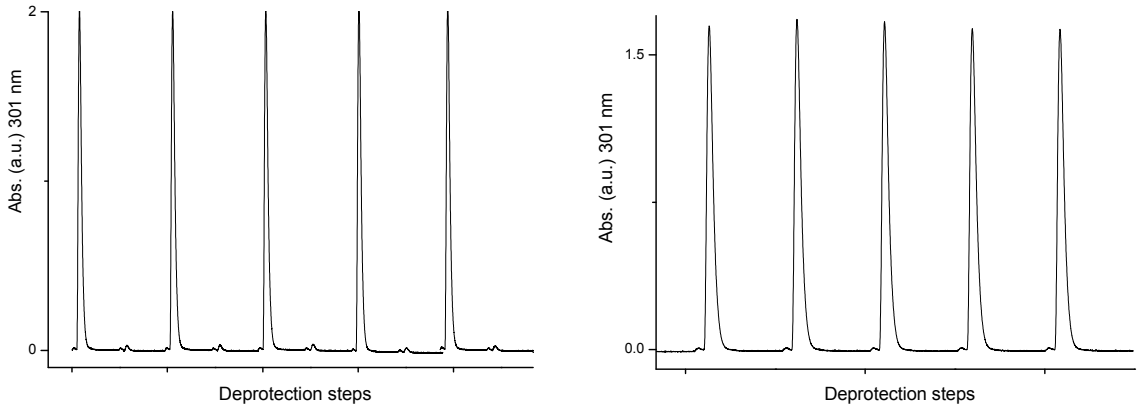

Figure SI-5.2.2. UV-monitoring profile (λ= 301 nm) obtained for the synthesis of the aramide-(*left*) and peptide-(Asp(t-Bu)) (*right*) blocks.

Solution characterization of the aramide-peptide amphiphile.

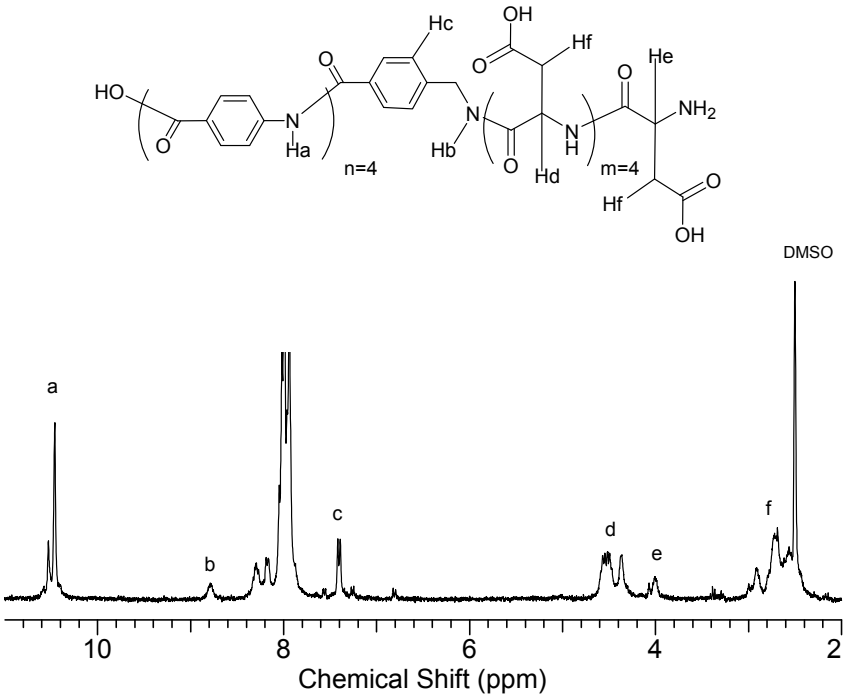

Figure SI-5.2.3. ^{1}H-NMR spectrum of **15** in DMSO-d_6 (at least 90 % purity determined by NMR).

The integral of signal c is 1.8, the integral of the doublet at δ=6.8 is 0.18. To get a lower estimate for the purity of **5** we assumed that the molecular weight of the impurity was identical to that of **15** and that the doublet at δ=6.8 corresponded to 2 aromatic protons in a *para*-substituted benzene. This gave a lower estimate of the purity of ca. 90%.

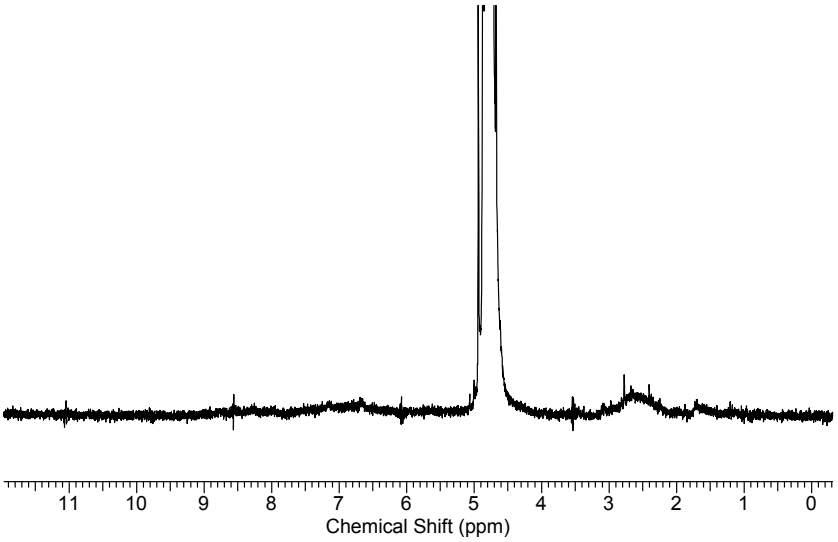

Figure SI-5.2.4. ^{1}H-NMR spectrum of **15** in D_2O (27.7 mM in 0.17 M $D_2O/NaHCO_3$ solution).

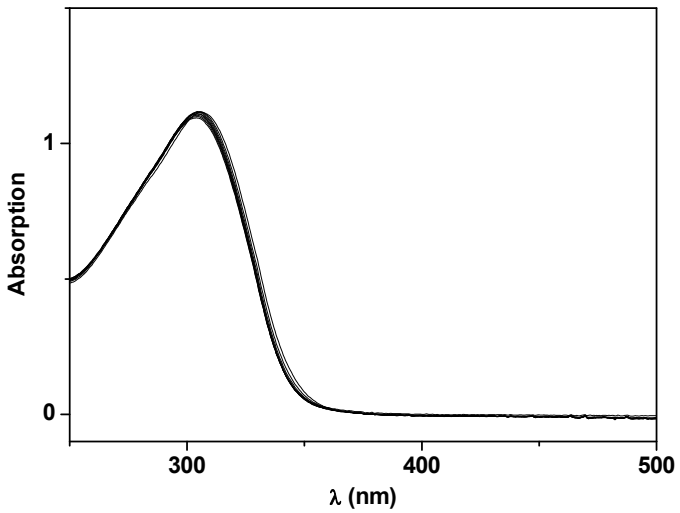

Figure SI-5.2.5. UV-vis absorption measurements of **15** as a function of the temperature (21 uM in 6.5 mM aq. NaOH solution). Sample cooled from 80 °C to 0 °C at a rate of 20 °C/h.

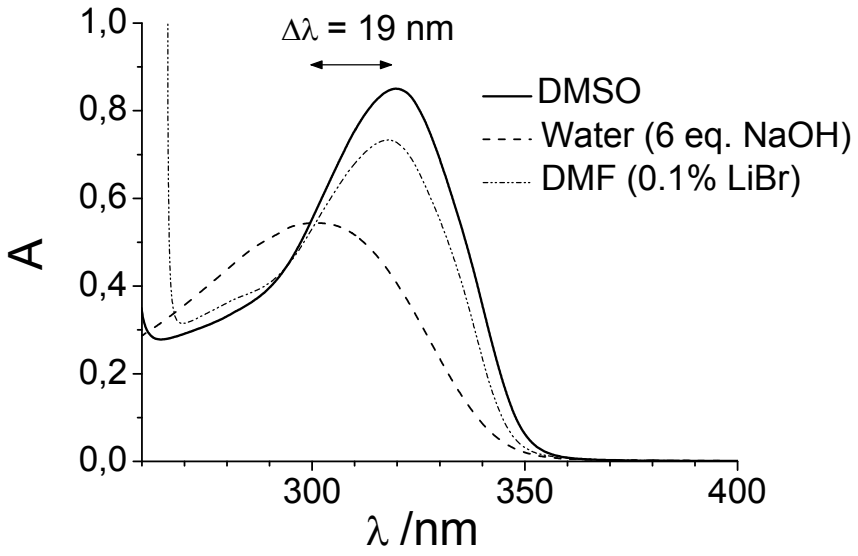

Figure SI-5.2.6. Comparison of the UV-vis absorption spectra of compound **15** in different solvents. The spectrum in water exhibit an hypsochromic shift of the absorption maxima compared to the DMSO absorption spectrum due to aggregation. The spectrum in DMF serves as evidence, that no influences in the spectra are observed due to solvatochromic effects, as no bathochromic shift of the spectral band in DMF [i] is observed when compared to the DMSO spectrum. DMF with 0.1 % LiBr was added to enhance the solubility of **15** in this solvent.

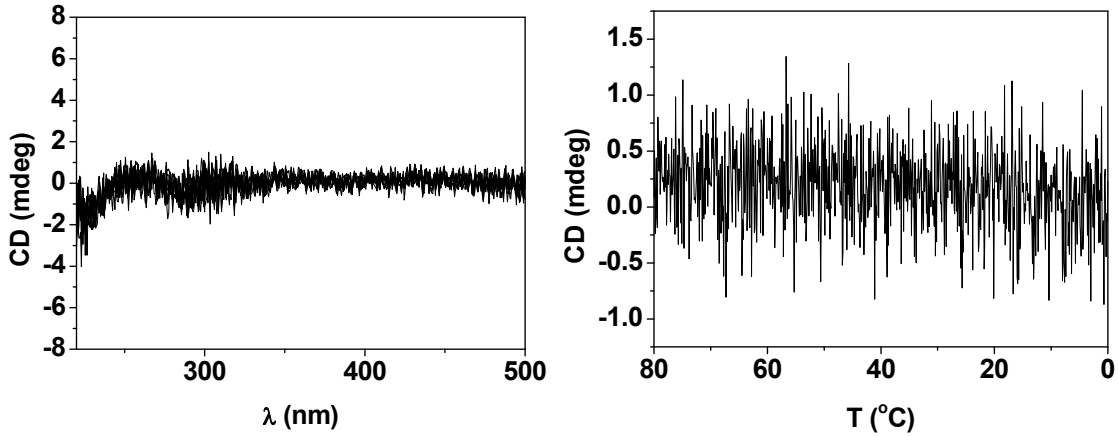

Figure SI-5.2.7. *Left*: CD-spectrum of **15** (21 μM in 6.5 mM aq. NaOH solution). *Right*: CD-temperature scan (300 nm).

[i] The dielectric constants of the solvent were taken as a polarity parameter.

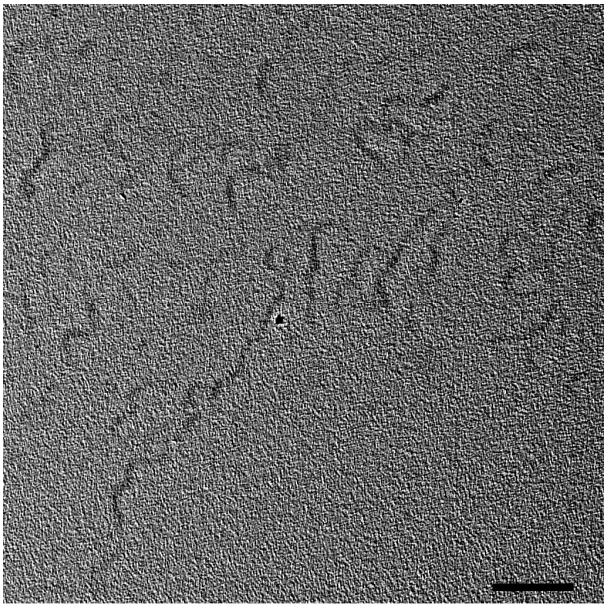

Figure SI-5.2.8. TEM micrograph of **15** showing long worm-like nano-structures obtained from H_2O solution (6 eq. NaOH, scale bar = 100 nm). The image was not stained. Image **figure SI-5.2.8** and **figure 5.2.2** in the manuscript were both recorded from the same TEM grid.

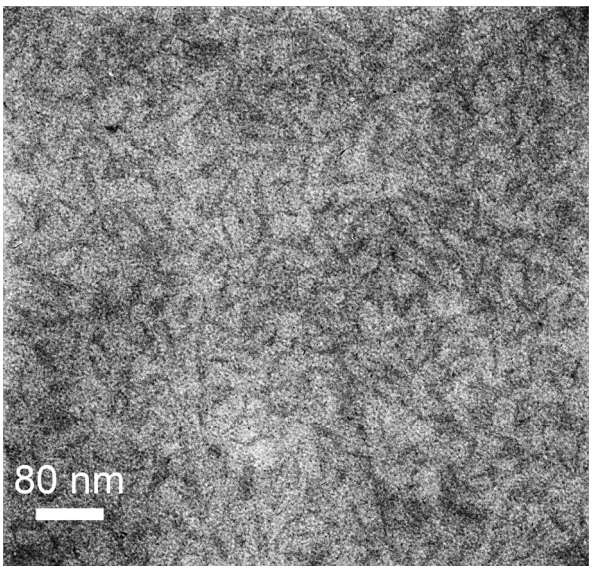

Figure SI-5.2.9. TEM micrograph of **15** showing shorter tape-like nano-structures obtained from H_2O solution (6 eq. NaOH, scale bar = 100 nm). The image was stained with OsO_4. Image **figure SI-9** and **figure SI-10** were both recorded from the same TEM grid.

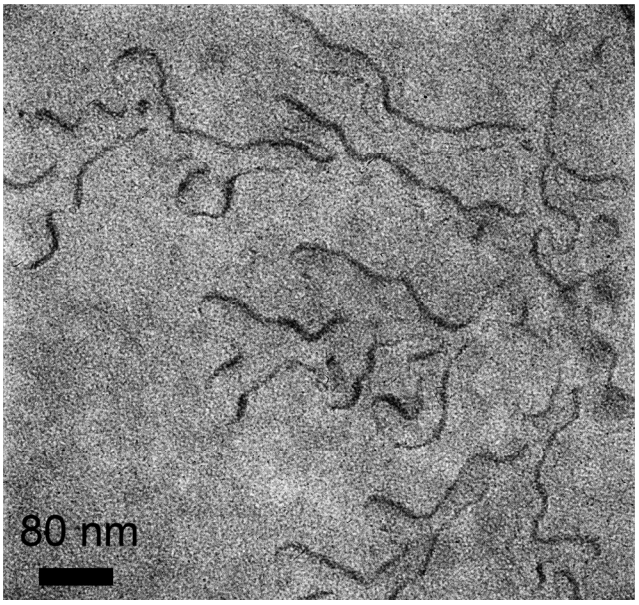

Figure SI-5.2.10. TEM micrograph of **15** showing longer tape-like nano-structures obtained from H_2O solution (6 eq. NaOH, scale bar = 100 nm). The image was stained with OsO_4. Image of **figure SI-5.2.9** and **figure SI-5.2.10** were both recorded from the same TEM grid.

Short and long tape-like structures are observed (**figure SI-5.2.9** and **5.2.10**). Yet, there should be a significant energy penalty at the ends of the micelles/tapes. This could be indicative of impurities in the system leading to a lower energy for the ends (see **figure SI-5.2.3** for an estimate of the purity of **15**).

Chapter 6

Summary and Outlook

6. Summary and Outlook

Stiff-chain macromolecules exhibit particular properties from their chemical and thermomechanical point of view and play therefore an important role at industrial level today. Particularly polyamides, polyesters, π-conjugated systems and fully aromatic materials find miscellaneous uses and are therefore intensively investigated.

In nature also innumerable examples can be found, in which rod-like architectures, evolved from superstructures (α-helices, β-sheets) play a decisive role for the life. The supramolecular approach to the noncovalent assembly of systems based on principles found in nature is applied by numerous research groups, not only for the mimicry of biological systems, but also for the assimilation in the preparation of intelligent materials.

The combination of chain-stiffness, ability of hydrogen bond formation, hydrophobicity, partial double bond character of the *trans*-amide bonds and π-interactions in aromatic backbones present in *p*-benzamides result in highly interesting multifunctional systems. This class of aryl amides is also characterized by excellent thermomechanical stability, anisotropy and their low solubility in organic solvents, as expected for structurally stiff materials. The later disadvantage is often overcome by the modification of the insoluble rod-like molecules with flexible chains, thus leading to solvation. Another approach is the reduction of intermolecular interactions. This is, in the case of amides, often achieved via reduction of hydrogen bond donors or acceptors, hence facilitating their synthesis and handling.

Aromatic oligoamides are an important class of materials for the preparation of supramolecular objects, as they are shape persistent and allow the design of multiple hydrogen bond patterns. This work focused on the synthesis of novel monomers for the design of a series of oligo(*p*-benzamide)s (OPBA) following two approaches: iterative solution synthesis and automated solid phase protocols. The challenge in the synthesis of such materials was their modification, while maintaining the characteristic properties (shape persistence, physical-chemical properties, shape anisotropy). The strategy for the preparation of predictable superstructures was devote to the selective control of the noncovalent interactions, monodispersity and monomer sequence. In addition to this, the structure-properties correlation of the prepared rod-like soluble materials was pointed out within this work.

Practically, the monomer functionalities were properly protected, activated to the corresponding acid chlorides and employed for the preparation of monodisperse OPBAs.

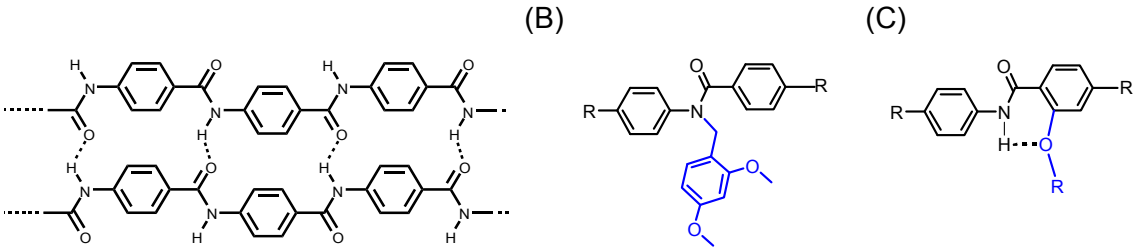

Figure 6.1. (A) Chemical structure of the OPBAs and molecular scaffolds prepared by the introduction (B) of the DMB-*N*-amide protecting group for solution synthesis and (C) of the salicylic acid framework for the preparation of oligomers on the solid phase.

The first approach involved the solution-based aramide synthesis via introduction of 2,4-dimethoxybenzyl (DMB) *N*-amide protective group (see **figure 6.1**, **B**). Therefore an iterative synthetic strategy based on previous works was further developed, in which protection of every second *N*-amide and the folding of the oligomers arising from the conformational preferences of the amide bonds were exploited. The conformation of the secondary and tertiary amide linkages were investigated in solution via 2D-NMR spectroscopy and in the solid state via X-ray crystallographic analysis. An alkyne derivatized octa(*p*-benzamide) was linked to a PEG-polymer chain. The cleavage of the DMB-groups induces the structural change of the copolymer by changing from a coil-coil like to a rod-coil like morphology, capable of aggregate formation.

The second approach combined the established group experience in the field of aramide chemistry and solid-phase-supported peptide synthesis. It focused on the implementation of the salicylic acid scaffold to introduce substituents on the aromatic backbone for the stabilization of the OPBA-rotamers (intramolecular interactions between the ether oxygens and the amide protons of adjacent units; see **figure 6.1 C**). The prepared oligomers were analyzed regarding their solubility and aggregation properties by systematically changing the degree of rotational freedom of the amide bonds, side chain polarity, monomer sequence and degree of oligomerization. The syntheses were performed on a modified commercial peptide synthesizer using a combination of fluorenylmethoxycarbonyl (Fmoc) and aramide chemistry.

Homo- and hetero-oligomers up to the heptamer with hexyloxy-, triethylene glycol and non-functionalized monomeric units were prepared by this route. The automatized system allowed the preparation of a small substance library of aramides with potential applications as nanoscaffolds in supramolecular chemistry, *e.g*. comb-like- , hairy- and Janus rods as well as peptide amphiphiles.

The heterosequences (comb-like rods) carrying hexyloxy side chains self-assembled in DMSO at low concentrations (1.2 wt %) to noncovalent networks, resulting in a microscopic gel formation. The thermal stability (70-82 °C) of the DMSO-gels was analyzed by DSC- and "*dropping ball"* methods. The nanofibrous structure and the subsequent aggregation into bundles could further be visualized using TEM-techniques.

The investigation on the hexyl- and glycol-functionalized *hairy* rods was of fundamental relevance, regarding the influence of the nature, length and polarity of the side chains on the solubility properties of the final homo-oligomer.

Comb-like and hairy-rods were conjugated to highly soluble PEG-polymers in order to diminish their aggregation tendencies and simultaneously to further enhance the solubility of the products and extend the variety of characterization techniques of choice.

Additionally, the synthesis of OPBA-based peptide amphiphiles was presented and the aggregation properties in water were discussed. Therefore, the sequential attachment of amino acids onto the OPBA *N*-terminus was accomplished in order to achieve water solubility via an oligoelectrolyte (penta(L-aspartic acid)). UV absorption, ^{1}H-NMR spectra and TEM investigations revealed the aggregation of the amphiphiles in water as worm-like structures, driven entirely by the combination of solvophobic effects and strong hydrogen bonds between the oligo(*p*-benzamide) strands.

Finally, polydisperse homopolymers derived from the hexyl- and glycol-functionalized monomers were prepared via polycondensation through triphenyl phosphite- and *N*-sulfinylaminobenzoyl chloride activation. Solubility, thermal stability as well as the liquid crystalline properties of the polymers were analyzed.

This novel approach to sequence controlled synthesis of side-chain and main-chain functionalized oligomers in a fully automated fashion, presents a useful method for the preparation of an immense variety of nanoscaffolds based on oligo(*p*-benzamide)s. Polarity and chain length of the substituent were analysed within this work, achieving materials with high aggregation tendency. The preparation of aramides carrying bulky side chains is another promising parameter to be investigated in future projects in order

to reduce the aggregation tendency and thus to facilitate the prediction of supramolecular structures.

The synthesis of linear functional oligomers of variable length in combination with the introduction of bent units will allow the synthesis of novel architectures, for example giant helices with chemically different inner and outer sides, tubular structures for host-guest systems or nanoreactors.

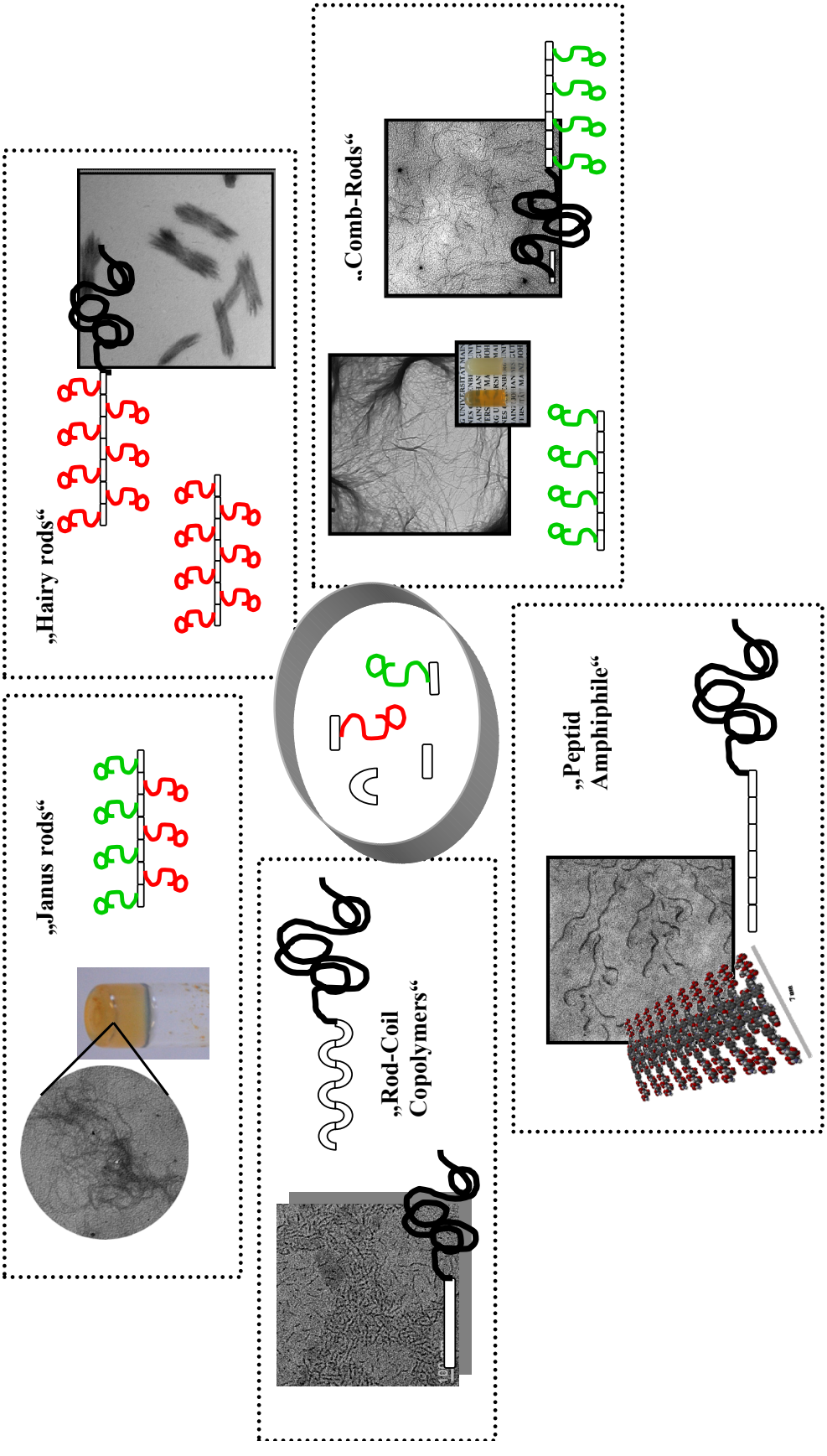

Figure 6.2. Diverse molecular architectures assembled via iterative solution- and solid phase synthesis.

6. Zusammenfassung und Ausblick

Formtreue Moleküle spielen heutzutage für die Synthese chemisch- und thermomechanisch-stabiler Materialien auf industrieller Ebene eine sehr wichtige Rolle. Polyamide, Polyester, π-konjugierte Systeme und voll aromatische Materialien werden vielseitig eingesetzt und intensiv erforscht. Auch in der Natur findet man eine große Anzahl an Beispielen für kettensteife Polymere, in denen die Stäbchengestalt durch Überstrukturbildung (α-Helices, β-Faltblatt) eine wesentliche Rolle für deren Funktionalität spielen. Das Zusammenspiel von Wasserstoffbrückenbindungen, elektrostatischen Wechselwirkungen und hydrophobem Effekt inspiriert viele wissenschaftliche Arbeiten nicht nur zur Nachahmung von biologischen Systemen, sondern auch für die Entwicklung intelligenter Materialien.

Die Kombination von Kettensteifigkeit, der Fähigkeit Wasserstoffbrücken ausbilden zu können, Hydrophobizität und π-Wechselwirkungen im aromatischen Molekülrückgrad machen aus den *p*-Benzamiden sehr interessante Stoffe. So zeichnen sie sich außerdem durch ihre hervorragende thermomechanische Stabilität, ihre Anisotropie und geringe Löslichkeit in organischen Medien aus. Viele Ansätze, die Löslichkeit solcher Materialen zu erhöhen, beruhen auf der Einführung von Substituenten, die als Löslichkeitsvermittler dienen. Dies können z.B. Polymere sein, die üblicherweise am Ende des Moleküls kovalent gebunden werden oder niedermolekulare Verbindungen, die am Molekülrückgrad eingeführt werden. Besonders bei aromatischen Oligoamiden dient die Einführung von Amidschutzgruppen als eine weitere Methode, die Synthese, Aufarbeitung und Handhabung dieser Materialien zu erleichtern.

Die Eigenschaften von aromatischen Oligoamiden zur Bildung von multiplen Wasserstoffbindungen spielen eine große Rolle in dem Design von supramolekularen Objekten. Hierfür sind Selektivität der nicht kovalenten Bindungen und definierte Molgewichte von besonderer Wichtigkeit, um Kontrolle über das Aggregationsverhalten zu erzielen. Im Rahmen dieser Arbeit wurden neue Monomere hergestellt und zur Darstellung einer Serie von löslichen Oligo(*p*-benzamid)en (OPBA) nach zwei Syntheserouten eingesetzt: der iterativen Lösungssynthese und der Festphasensynthese. Die besondere Herausforderung bei der Herstellung solcher Moleküle bestand darin, ihre interessante Eigenschaften

(Formtreue, Stabilität, Anisotropie) auch nach der Modifizierung zu erhalten. Zusätzlich wurde die Korrelation zwischen Struktur und Eigenschaften der löslichen benzamid-basierten Materialien aufgezeigt. Die Monomere wurden entsprechend geschützt, zu reaktiven Säurechloriden umgesetzt und für den Aufbau von monodispersen Molekülen eingesetzt.

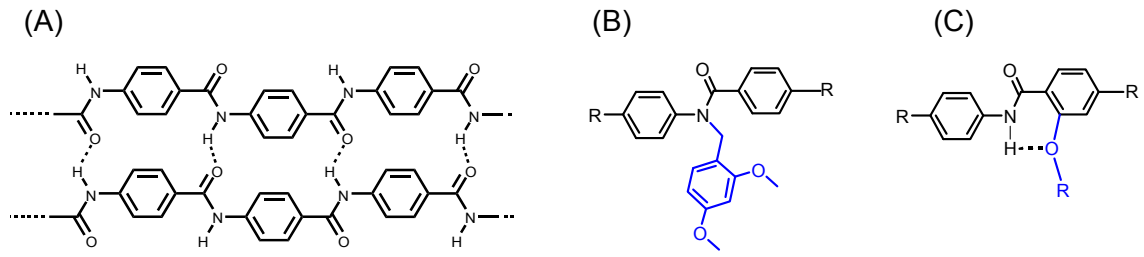

Abb. 6.1. (A) Chemische Struktur der OPBA. Molekulare "*Gerüste*" für die Synthese von löslichen OPBA: Einführung (B) der DMB-Schutzgruppe für die Lösungssynthese und (C) des Salicylsäuremotivs für die Festphasensynthese.

Ein Ansatz beruhte auf der lösungsbasierten Aramidsynthese mittels Einführung der Dimethoxybenzyl (DMB)-*N*-Amidschutzgruppe (siehe **Abb. 6.1 B**). Hierfür wurde eine iterative Syntheseroute, die über Dimer- und Tetramervorstufen verlief, bis zum löslichen Octa(*p*-benzamid) entwickelt. Durch partiellen *N*-Amidschutz nehmen die Amidbindungen alternierend *cis*- und *trans*-Konformationen ein, welche zu einer räumlich „gefalteten" Struktur führen. Die bevorzugte Konformation der sekundären und tertiären Amidbindungen wurde am Beispiel eines Tetramers mittels 2D-NMR-Spektroskopie in Lösung untersucht und durch Röntgenstrukturanalyse an Einkristallen im Festkörper bestätigt.

Das *N*-geschützte Octa(*p*-benzamid) wurde mit einem terminalen Alkin an der Carbonylfunktion funktionalisiert und in einer Huisgen 1,3-dipolaren Cycloaddition an Monomethyl-PEG-azid gebunden. Nach Abspaltung der säurelabilen DMB-Schutzgruppen, wurde die supramolekulare Strukturbildung des Blockcopolymers untersucht.

Der zweite Ansatz beruhte auf der trägerbasierten Synthese von Oligo(*p*-benzamid)en mit löslichen niedermolekularen Substituenten am aromatischen Oligomerrückgrad.

Das Salicylsäure-Gerüst ermöglicht somit zum einen die Einführung von Substituenten, die das steife Molekülrückgrad „solvatisieren“ und zum anderen, die Stabilisierung von Rotameren über die Ether-Funktionalisierung (intramolekulare Wechselwirkung zwischen dem H-Brückenakzeptor in *ortho*-Position zur Carbonylfunktion und dem Amid-Wasserstoff, siehe **Abb. 6.1 C**). Durch die gezielte Auswahl der H-Brückenakzeptor-Positionen innerhalb des Oligomers sollten die H-Brückendonoren (Amid-Wasserstoffe) selektiv gesättigt, die Löslichkeit erhöht und Kontrolle über die supramolekulare Architekturbildung erzielt werden. Die Durchführung erfolgte in automatisierter Form an einem Peptidsynthesizer unter Verwendung der Fluorenylmethoxycarbonyl (Fmoc) Amin-Schutzgruppe. Darüber hinaus wurde eine systematische Variation von Seitenketten, Monomersequenz und Oligomerisierungsgrad durchgeführt, um weitere Informationen über Struktur und Aggregationsverhalten der Oligomere zu gewinnen.

Homo- und alternierende Hetero-Oligomere von Hexyloxy-, Triethylenglykol substituierten und unsubstituierten Monomereinheiten, wurden dargestellt, wobei die Sequenzkontrolle durch den Einsatz des Peptidsynthesizers erreicht wurde. Die Automatisierung erlaubte es, mittels kombinatorischer Chemie, eine kleine Substanzbibliothek basierend auf drei Monomere, aufzubauen. Dabei konnten unterschiedliche Molekülarchitekturen dargestellt werden wie z. B. „comb-like rods“, „hairy rods“, „Janus rods“ und „Peptid Amphiphile“. Zusätzlich wurden Polymer-Aramid Konjugate durch die Anbindung von Polyethylenoxid am Amin-Terminus der Aminosäuresequenzen synthetisiert und deren Eigenschaften auf supramolekularer Ebene untersucht.

Die Heterosequenzen (comb-like rods) mit Hexyloxy-Seitenketten organisieren sich in DMSO bei geringen Konzentrationen (1,2 Gew. %) zu nicht kovalenten Netzwerken, wodurch eine makroskopische Gelbildung resultiert. DSC- und „*dropping ball*“- Untersuchungen der Gele in DMSO zeigten deren hohe thermische Stabilität (70-82°C). Die nano- und mikroskopische Gelstruktur wurde mittels Transmissionselektronmikroskopie analysiert. Hierbei wurden lange, anisotrope Fasern visualisiert, die sich zu räumlich-ausgedehnten (pseudo)kristallinen Bündeln zusammenlagerten.

Die Untersuchung der Eigenschaften der Homo-Oligomere mit Triethylenglykol- und Hexyl-Substituenten („hairy rods“) zeigt die besondere Bedeutung, die die Natur und Länge der Seitenketten auf das Löslichkeitsverhalten der Oligo(*p*-benzamid)e

ausüben. So wiesen Triethylenglykolreste die geeignete Polarität und Kettenlänge auf, um das steife Molekül zu solvatisieren. Die Synthese von kammartigen (comb-like) und haarigen (hairy) Oligoaramid-PEG Konjugaten verbesserte die Löslichkeitseigenschaften bei gleichzeitiger Verringerung der Aggregationstendenz, wodurch auch eine vollständige Charakterisierung ermöglicht wurde.

Im Rahmen dieser Arbeit konnten auch OPBA-Peptid Amphiphile komplett automatisiert dargestellt werden. Hierfür wurde durch sequenzielle Anbindung von Aminosäuren an den OPBA-Block, ein Oligoelektrolyt (Penta(L-Asparaginsäure))am N-Terminus angehängt, um die supramolekulare Aggregation in Wasser zu untersuchen. Diese Strukturen unterscheiden sich von den üblichen Peptid Amphiphilen dadurch, dass die Überstrukturbildung allein durch die selbst-organisierenden Eigenschaften der hydrophoben OPBA-Stäbchen hervorgerufen werden. Polydisperse Homopolymere der Hexyl- und Triethylenglykol-substituierten Monomere wurden durch Polykondensation nach der Triphenylphosphit-Methode und über *N*-Sulfinylaminobenzoylchlorid-Aktivierung hergestellt. Löslichkeit, thermische Stabilität und flüssigkristalline Eigenschaften der Materialien wurden im Rahmen der Arbeit ebenfalls analysiert.

Der vorgestellte Ansatz für die automatisierte und sequenzkontrollierte Synthese von funktionalisierten Oligomeren, stellt eine brauchbare Methode zur Herstellung von einer großen Vielfalt an Nanostrukturen auf Aramid-Basis dar. Den Einfluss von Polarität, Kettenlänge und der Anzahl der Substituenten, wurde in dieser Arbeit untersucht, wobei Materialien mit einer hohen Aggregationstendenz erhalten wurden. Unter diesen Aspekten stellt die Synthese von Aramiden mit sterisch-anspruchsvolle Resten, als eine interessante Ansatzmöglichkeit für zukünftige Arbeiten dar.

Die Synthese funktionalisierter Oligomere mit unterschiedlichen Blocklängen in Kombination mit gewinkelten Monomereinheiten bietet darüber hinaus auch die Möglichkeit zur Herstellung von Riesenhelices mit chemisch-unterschiedlichen Innen- und Aussenseiten, tubulären Strukturen für *host-guest* Systemen oder zur Anwendung als Nanoreaktoren.

Appendix

Appendix A

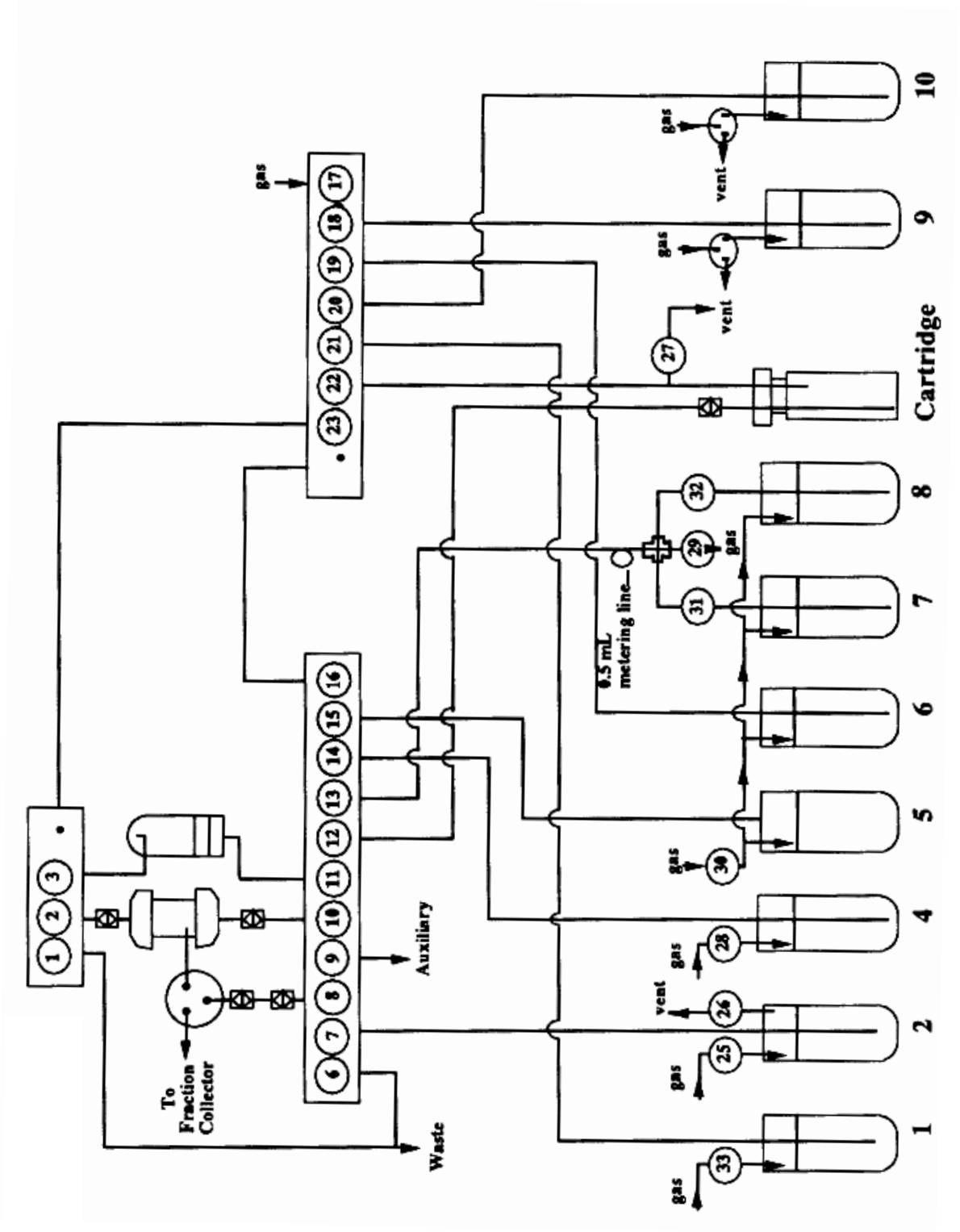

Figure SI-6.1.3. Schematic system description of 431A peptide synthesizer.

Appendix B

Modules and cycles created for the synthesis with monomer recovering programm using standard Fmoc-chemistry

```
431A Chemistry 02
Fmoc (Standard) [0.25 mmol]
```

Cycle #	Repetition #	Cycle description	Modules
1	1	cap with p-nitrobenzoyl Cl	GgeFF
2	3	erste lsg capp ZuGew	GgBdeFFHGgeFFHGgeFF
5	1	deprotect	gBdc

Module: B -> Deprotection mit Monitoring

Sept #	Function #	Function Name	Time	add. Time
1	110	begin loop	2	0
2	42	Drain Reaction Vessel	20	2
3	98	BEGIN LOOP	3	0
4	56	#10 to Reaction Vessel	14	1
5	88	RS switch to RV	1	0
6	91	#10 to resin sample	3	0
7	89	RS switch to fraction collecto	1	0
8	40	Mix Reaction Vessel	2	0
9	2	Vortex On	3	0
10	40	Mix Reaction Vessel	3	0
11	3	Vortex Off	1	0
12	42	Drain Reaction Vessel	15	1
13	50	#10 to top of RV with drain	4	0
14	42	Drain Reaction Vessel	10	1
15	99	END LOOP	1	0
16	56	#10 to Reaction Vessel	13	2
17	79	Pressurize bottle #1	10	0
18	51	#1 to Reaction Vessel	8	1
19	56	#10 to Reaction Vessel	2	0
20	40	Mix Reaction Vessel	2	0
21	98	BEGIN LOOP	5	0
22	2	Vortex On	15	0
23	3	Vortex Off	15	0
24	99	END LOOP	1	0
25	2	Vortex On	1	0
26	14	#10 thru bottom valve block	2	0
27	118	#10 to auxiliary waste	15	0
28	3	Vortex Off	1	0
29	118	#10 to auxiliary waste	15	0
30	116	Relay 1 on	1	0
31	42	Drain Reaction Vessel	2	0
32	13	#10 thru top valve block	2	0
33	118	#10 to auxiliary waste	120	0
34	117	Relay 1 off	1	0
35	111	end loop	1	0
36	10	Gas thru bottom valve block	4	0

37	40	Mix Reaction Vessel	2	0
38	41	Vent Reaction Vessel at top	1	0
39	88	RS switch to RV	1	0
40	93	Gas to resin sampler	3	0
41	41	Vent Reaction Vessel at top	2	0
42	89	RS switch to fraction collecto	1	0
43	2	Vortex On	1	0
44	98	BEGIN LOOP	2	0
45	13	#10 thru top valve block	1	0
46	14	#10 thru bottom valve block	3	0
47	9	Gas thru top valve block	3	0
48	10	Gas thru bottom valve block	5	0
49	99	END LOOP	1	0
50	3	Vortex Off	1	0

Module: F -> coupling

Sept #	Function #	Function Name	Time	add. Time
1	14	#10 thru bottom valve block	1	0
2	13	#10 thru top valve block	1	0
3	10	Gas thru bottom valve block	5	0
4	9	Gas thru top valve block	5	0
5	98	BEGIN LOOP	18	0
6	2	Vortex On	13	0
7	10	Gas thru bottom valve block	3	0
8	20	Mix Activator	1	0
9	3	Vortex Off	15	0
10	99	END LOOP	1	0
11	91	#10 to resin sample	1	0
12	93	Gas to resin sampler	2	0
13	41	Vent Reaction Vessel at top	2	0
14	88	RS switch to RV	1	0
15	93	Gas to resin sampler	2	0
16	41	Vent Reaction Vessel at top	1	0
17	89	RS switch to fraction collecto	1	0
18	98	BEGIN LOOP	36	0
19	2	Vortex On	13	0
20	10	Gas thru bottom valve block	3	0
21	20	Mix Activator	1	0
22	3	Vortex Off	15	0
23	99	END LOOP	1	0
24	9	Gas thru top valve block	2	0
25	13	#10 thru top valve block	1	0
26	9	Gas thru top valve block	5	0
27	14	#10 thru bottom valve block	1	0
28	10	Gas thru bottom valve block	5	0

Module: G -> Aktivierung aus Lsg

Sept #	Function #	Function Name	Time	add. Time
1	5	Needle Down	10	0
2	61	Vent amino acid cartridge	10	0
3	6	Needle Up	10	0
4	7	Eject Cartridge	10	0
5	8	Advance Cartridge	10	0
6	5	Needle Down	10	0

7	20	Mix Activator	5	0
8	22	Drain Activator	10	0
9	11	#9 thru top valve block	1	0
10	29	#9 to top of ACT with drain	4	0
11	22	Drain Activator	40	0
12	14	#10 thru bottom valve block	1	0
13	10	Gas thru bottom valve block	6	0
14	60	Mix amino acid cartridge	5	0
15	24	Cartridge to Activator	30	0
16	98	BEGIN LOOP	4	0
17	24	Cartridge to Activator	5	0
18	1	Wait	5	0
19	99	END LOOP	1	0
20	65	#10 to amino acid cartridge	2	0
21	10	Gas thru bottom valve block	6	0
22	20	Mix Activator	1	0
23	14	#10 thru bottom valve block	1	0
24	10	Gas thru bottom valve block	3	0
25	14	#10 thru bottom valve block	1	0
26	1	Wait	5	0
27	10	Gas thru bottom valve block	6	0
28	20	Mix Activator	1	0
29	12	#9 thru bottom valve block	1	0
30	1	Wait	5	0
31	10	Gas thru bottom valve block	2	0
32	14	#10 thru bottom valve block	1	0
33	9	Gas thru top valve block	10	0
34	10	Gas thru bottom valve block	10	0
35	61	Vent amino acid cartridge	10	0
36	62	Drain amino acid cartridge	10	0

Module: H -> Zurückgewinnung

Sept #	Function #	Function Name	Time	add. Time
1	100	User function A	8	0
2	61	Vent amino acid cartridge	3	0
3	6	Needle Up	10	0
4	7	Eject Cartridge	10	0
5	8	Advance Cartridge	10	0
6	5	Needle Down	10	0
7	10	Gas thru bottom valve block	2	0
8	56	#10 to Reaction Vessel	5	0
9	40	Mix Reaction Vessel	3	0
10	2	Vortex On	15	0
11	3	Vortex Off	1	0
12	100	User function A	8	0
13	61	Vent amino acid cartridge	3	0
14	6	Needle Up	10	0
15	7	Eject Cartridge	10	0
16	8	Advance Cartridge	10	0
17	5	Needle Down	10	0
18	10	Gas thru bottom valve block	2	0
19	56	#10 to Reaction Vessel	5	0
20	40	Mix Reaction Vessel	3	0
21	2	Vortex On	15	0
22	3	Vortex Off	1	0
23	100	User function A	8	0
24	61	Vent amino acid cartridge	3	0
25	6	Needle Up	10	0

Module: c -> DCM Wash

Sept #	Function #	Function Name	Time	add. Time
1	10	Gas thru bottom valve block	2	0
2	9	Gas thru top valve block	2	0
3	12	#9 thru bottom valve block	1	0
4	11	#9 thru top valve block	1	0
5	55	#9 to Reaction Vessel	10	1
6	2	Vortex On	1	0
7	40	Mix Reaction Vessel	2	0
8	90	#9 to resin sampler	1	0
9	93	Gas to resin sampler	3	0
10	41	Vent Reaction Vessel at top	2	0
11	88	RS switch to RV	1	0
12	90	#9 to resin sampler	2	0
13	93	Gas to resin sampler	2	0
14	90	#9 to resin sampler	5	0
15	89	RS switch to fraction collecto	1	0
16	40	Mix Reaction Vessel	2	0
17	3	Vortex Off	1	0
18	42	Drain Reaction Vessel	10	0
19	49	#9 to top of RV with drain	5	0
20	42	Drain Reaction Vessel	8	1
21	98	BEGIN LOOP	6	0
22	55	#9 to Reaction Vessel	8	1
23	2	Vortex On	1	0
24	55	#9 to Reaction Vessel	4	0
25	40	Mix Reaction Vessel	4	0
26	3	Vortex Off	1	0
27	42	Drain Reaction Vessel	10	0
28	49	#9 to top of RV with drain	4	0
29	42	Drain Reaction Vessel	10	1
30	99	END LOOP	1	0
31	55	#9 to Reaction Vessel	10	1
32	2	Vortex On	1	0
33	40	Mix Reaction Vessel	2	0
34	41	Vent Reaction Vessel at top	2	0
35	88	RS switch to RV	1	0
36	90	#9 to resin sampler	2	0
37	93	Gas to resin sampler	2	0
38	90	#9 to resin sampler	5	0
39	89	RS switch to fraction collecto	1	0
40	40	Mix Reaction Vessel	2	0
41	3	Vortex Off	1	0
42	42	Drain Reaction Vessel	10	0
43	49	#9 to top of RV with drain	5	0
44	42	Drain Reaction Vessel	20	1
45	41	Vent Reaction Vessel at top	2	0
46	12	#9 thru bottom valve block	1	0
47	10	Gas thru bottom valve block	10	0
48	93	Gas to resin sampler	10	0
49	9	Gas thru top valve block	10	0

Module: d -> NMP Wash

Sept #	Function #	Function Name	Time	add. Time
1	14	#10 thru bottom valve block	1	0
2	56	#10 to Reaction Vessel	12	1
3	2	Vortex On	1	0

4	40	Mix Reaction Vessel	2	0
5	41	Vent Reaction Vessel at top	1	0
6	88	RS switch to RV	1	0
7	93	Gas to resin sampler	3	0
8	91	#10 to resin sample	5	0
9	89	RS switch to fraction collecto	1	0
10	40	Mix Reaction Vessel	2	0
11	10	Gas thru bottom valve block	6	0
12	20	Mix Activator	1	0
13	3	Vortex Off	1	0
14	42	Drain Reaction Vessel	10	1
15	50	#10 to top of RV with drain	5	0
16	42	Drain Reaction Vessel	10	0
17	98	BEGIN LOOP	4	0
18	56	#10 to Reaction Vessel	13	1
19	2	Vortex On	1	0
20	40	Mix Reaction Vessel	3	0
21	10	Gas thru bottom valve block	6	0
22	20	Mix Activator	1	0
23	3	Vortex Off	1	0
24	42	Drain Reaction Vessel	10	1
25	50	#10 to top of RV with drain	5	0
26	42	Drain Reaction Vessel	10	0
27	99	END LOOP	1	0
28	56	#10 to Reaction Vessel	12	1
29	2	Vortex On	1	0
30	41	Vent Reaction Vessel at top	1	0
31	88	RS switch to RV	1	0
32	93	Gas to resin sampler	3	0
33	91	#10 to resin sample	5	0
34	89	RS switch to fraction collecto	1	0
35	40	Mix Reaction Vessel	2	0
36	10	Gas thru bottom valve block	6	0
37	98	BEGIN LOOP	3	0
38	20	Mix Activator	1	0
39	1	Wait	2	0
40	99	END LOOP	1	0
41	3	Vortex Off	1	0
42	42	Drain Reaction Vessel	10	1
43	50	#10 to top of RV with drain	5	0
44	42	Drain Reaction Vessel	15	0
45	9	Gas thru top valve block	3	0
46	10	Gas thru bottom valve block	3	0
47	93	Gas to resin sampler	2	0

Module: e -> Transfer

Sept #	Function #	Function Name	Time	add. Time
1	14	#10 thru bottom valve block	1	0
2	5	Needle Down	10	0
3	60	Mix amino acid cartridge	2	0
4	10	Gas thru bottom valve block	3	0
5	20	Mix Activator	1	0
6	2	Vortex On	1	0
7	98	BEGIN LOOP	2	0
8	28	Gas to top of Activator	3	0
9	8	ACT to RV (Top RV open)	4	0
10	99	END LOOP	1	0
11	3	Vortex Off	1	0
12	98	BEGIN LOOP	3	0
13	28	Gas to top of Activator	2	0
14	38	ACT to RV (Top RV open)	3	0

15	99	END LOOP	1	0
16	21	Vent Activator	2	0
17	26	#10 to top of Activator	2	0
18	28	Gas to top of Activator	3	0
19	21	Vent Activator	2	0
20	36	#10 ACT thru bottom valve bloc	2	0
21	20	Mix Activator	5	0
22	28	Gas to top of Activator	3	0
23	38	ACT to RV (Top RV open)	6	0
24	40	Mix Reaction Vessel	2	0
25	93	Gas to resin sampler	2	0
26	41	Vent Reaction Vessel at top	2	0
27	88	RS switch to RV	1	0
28	93	Gas to resin sampler	3	0
29	41	Vent Reaction Vessel at top	2	0
30	89	RS switch to fraction collecto	1	0
31	2	Vortex On	1	0
32	11	#9 thru top valve block	1	0
33	21	Vent Activator	2	0
34	29	#9 to top of ACT with drain	5	0
35	62	Drain amino acid cartridge	5	0
36	3	Vortex Off	1	0
37	34	#6 to Activator	16	0
38	20	Mix Activator	3	0
39	67	#10 to small cartridge needle	2	0
40	66	#9 to small cartridge needle	2	0
41	62	Drain amino acid cartridge	15	0
42	12	#9 thru bottom valve block	1	0
43	98	BEGIN LOOP	2	0
44	64	#9 to amino acid cartridge	20	0
45	2	Vortex On	1	0
46	1	Wait	3	0
47	60	Mix amino acid cartridge	5	0
48	3	Vortex Off	1	0
49	24	Cartridge to Activator	20	0
50	99	END LOOP	1	0
51	2	Vortex On	1	0
52	62	Drain amino acid cartridge	10	0
53	60	Mix amino acid cartridge	15	0
54	61	Vent amino acid cartridge	5	0
55	3	Vortex Off	1	0
56	98	BEGIN LOOP	7	0
57	20	Mix Activator	5	0
58	1	Wait	5	0
59	99	END LOOP	1	0
60	22	Drain Activator	20	0
61	2	Vortex On	1	0
62	22	Drain Activator	10	0
63	3	Vortex Off	1	0
64	98	BEGIN LOOP	3	0
65	29	#9 to top of ACT with drain	3	0
66	22	Drain Activator	5	0
67	99	END LOOP	1	0
68	2	Vortex On	1	0
69	12	#9 thru bottom valve block	1	0
70	35	#9 to Activator	2	0
71	20	Mix Activator	3	0
72	3	Vortex Off	1	0
73	22	Drain Activator	30	0
74	9	Gas thru top valve block	5	0
75	10	Gas thru bottom valve block	5	0

Module: g -> Wash & R.S.

Sept #	Function #	Function Name	Time	add. Time
1	13	#10 thru top valve block	1	0
2	91	#10 to resin sample	2	0
3	41	Vent Reaction Vessel at top	2	0
4	88	RS switch to RV	1	0
5	93	Gas to resin sampler	3	0
6	91	#10 to resin sample	5	0
7	89	RS switch to fraction collecto	1	0
8	98	BEGIN LOOP	3	0
9	14	#10 thru bottom valve block	1	0
10	40	Mix Reaction Vessel	4	0
11	9	END LOOP	1	0
12	2	Vortex On	5	0
13	40	Mix Reaction Vessel	4	0
14	3	Vortex Off	1	0
15	40	Mix Reaction Vessel	4	0
16	10	Gas thru bottom valve block	6	0
17	20	Mix Activator	1	0
18	42	Drain Reaction Vessel	20	2
19	56	#10 to Reaction Vessel	14	1
20	41	Vent Reaction Vessel at top	1	0
21	88	RS switch to RV	1	0
22	91	#10 to resin sample	5	0
23	89	RS switch to fraction collecto	1	0
24	2	Vortex On	3	0
25	40	Mix Reaction Vessel	3	0
26	3	Vortex Off	1	0
27	42	Drain Reaction Vessel	15	1
28	50	#10 to top of RV with drain	4	0
29	42	Drain Reaction Vessel	10	0
30	98	BEGIN LOOP	4	0
31	56	#10 to Reaction Vessel	14	1
32	2	Vortex On	1	0
33	40	Mix Reaction Vessel	3	0
34	3	Vortex Off	1	0
35	42	Drain Reaction Vessel	10	1
36	50	#10 to top of RV with drain	4	0
37	42	Drain Reaction Vessel	10	0
38	99	END LOOP	1	0
39	56	#10 to Reaction Vessel	14	1
40	41	Vent Reaction Vessel at top	1	0
41	88	RS switch to RV	1	0
42	91	#10 to resin sample	5	0
43	89	RS switch to fraction collecto	1	0
44	2	Vortex On	1	0
45	40	Mix Reaction Vessel	3	0
46	10	Gas thru bottom valve block	6	0
47	20	Mix Activator	1	0
48	3	Vortex Off	1	0
49	42	Drain Reaction Vessel	15	1
50	14	#10 thru bottom valve block	1	0
51	56	#10 to Reaction Vessel	14	1
52	2	Vortex On	1	0
53	40	Mix Reaction Vessel	1	0
54	91	#10 to resin sample	2	0
55	93	Gas to resin sampler	2	0
56	90	#9 to resin sampler	2	0
57	93	Gas to resin sampler	1	0
58	91	#10 to resin sample	2	0
59	93	Gas to resin sampler	2	0

60	98	BEGIN LOOP	1	0
61	39	Momentarily close Relay 0	1	0
62	13	#10 thru top valve block	1	0
63	41	Vent Reaction Vessel at top	2	0
64	88	RS switch to RV	1	0
65	91	#10 to resin sample	2	0
66	93	Gas to resin sampler	1	0
67	91	#10 to resin sample	2	0
68	41	Vent Reaction Vessel at top	1	0
69	48	Gas to top of Reaction Vessel	1	0
70	87	Take resin sample	2	0
71	89	RS switch to fraction collecto	1	0
72	90	#9 to resin sampler	2	0
73	93	Gas to resin sampler	2	0
74	90	#9 to resin sampler	2	0
75	93	Gas to resin sampler	2	0
76	90	#9 to resin sampler	4	0
77	93	Gas to resin sampler	4	0
78	41	Vent Reaction Vessel at top	2	0
79	88	RS switch to RV	1	0
80	91	#10 to resin sample	3	0
81	93	Gas to resin sampler	3	0
82	91	#10 to resin sample	5	0
83	89	RS switch to fraction collecto	1	0
84	39	Momentarily close Relay 0	1	0
85	99	END LOOP	1	0
86	3	Vortex Off	1	0
87	42	Drain Reaction Vessel	20	2

User Function A,Valve 02,Valve 10,Valve 12,Valve 17,Valve 23,Valve 27

Appendix C

Modules and cycles created for the synthesis for solvent saving using standard Fmoc-chemistry

```
431A Chemistry 02
Fmoc (Standard) [0.25 mmol]

  1   1 wash                          g
  2   1 coupling                      BdCfffgCfffgCffg
  3   1 deprotect                     gBd


Module: B -> Deprotection mit Monitoring

Sept #    Function #  Function Name                   Time    add. Time

  1         110         begin loop                     2         0
  2         42          Drain Reaction Vessel         20         2
  3         98          BEGIN LOOP                     3         0
  4         56          #10 to Reaction Vessel        14         1
  5         88          RS switch to RV                1         0
  6         91          #10 to resin sample            3         0
  7         89          RS switch to fraction collecto 1         0
  8         40          Mix  Reaction Vessel           2         0
  9         2           Vortex On                      3         0
 10         40          Mix  Reaction Vessel           3         0
 11         3           Vortex Off                     1         0
 12         42          Drain Reaction Vessel         15         1
 13         50          #10 to top of RV with drain    4         0
 14         42          Drain Reaction Vessel         10         1
 15         99          END LOOP                       1         0
 16         56          #10 to Reaction Vessel        13         2
 17         79          Pressurize bottle #1          10         0
 18         51          #1 to Reaction Vessel          8         1
 19         56          #10 to Reaction Vessel         2         0
 20         40          Mix  Reaction Vessel           2         0
 21         98          BEGIN LOOP                     5         0
 22         2           Vortex On                     15         0
 23         3           Vortex Off                    15         0
 24         99          END LOOP                       1         0
 25         2           Vortex On                      1         0
 26         14          #10 thru bottom valve block    2         0
 27         118         #10 to auxiliary waste        15         0
 28         3           Vortex Off                     1         0
 29         118         #10 to auxiliary waste        15         0
 30         116         Relay 1 on                     1         0
 31         42          Drain Reaction Vessel          2         0
 32         13          #10 thru top valve block       2         0
 33         118         #10 to auxiliary waste       120         0
 34         117         Relay 1 off                    1         0
 35         111         end loop                       1         0
 36         10          Gas thru bottom valve block    4         0
 37         40          Mix  Reaction Vessel           2         0
 38         41          Vent Reaction Vessel at top    1         0
 39         88          RS switch to RV                1         0
 40         93          Gas to resin sampler           3         0
 41         41          Vent Reaction Vessel at top    2         0
 42         89          RS switch to fraction collecto 1         0
```

43	2	Vortex On	1	0
44	98	BEGIN LOOP	2	0
45	13	#10 thru top valve block	1	0
46	14	#10 thru bottom valve block	3	0
47	9	Gas thru top valve block	3	0
48	10	Gas thru bottom valve block	5	0
49	99	END LOOP	1	0
50	3	Vortex Off	1	0

Module: C -> akt lsg transfer wash cart

Sept #	Function #	Function Name	Time	add. Time
1	6	Needle Up	10	0
2	7	Eject Cartridge	10	0
3	8	Advance Cartridge	10	0
4	5	Needle Down	10	0
5	60	Mix amino acid cartridge	5	0
6	98	BEGIN LOOP	1	0
7	2	Vortex On	1	0
8	60	Mix amino acid cartridge	30	0
9	3	Vortex Off	1	0
10	60	Mix amino acid cartridge	30	0
11	99	END LOOP	1	0
12	14	#10 thru bottom valve block	1	0
13	10	Gas thru bottom valve block	3	0
14	98	BEGIN LOOP	5	0
15	44	Cartridge to RV	6	0
16	2	Vortex On	3	0
17	3	Vortex Off	2	0
18	99	END LOOP	1	0
19	40	Mix Reaction Vessel	2	0
20	10	Gas thru bottom valve block	5	0
21	65	#10 to amino acid cartridge	2	0
22	60	Mix amino acid cartridge	3	0
23	44	Cartridge to RV	8	0
24	1	Wait	2	0
25	40	Mix Reaction Vessel	2	0
26	2	Vortex On	1	0
27	62	Drain amino acid cartridge	5	0
28	3	Vortex Off	1	0
29	67	#10 to small cartridge needle	2	0
30	66	#9 to small cartridge needle	2	0
31	62	Drain amino acid cartridge	15	0
32	12	#9 thru bottom valve block	1	0
33	98	BEGIN LOOP	2	0
34	64	#9 to amino acid cartridge	20	0
35	2	Vortex On	1	0
36	1	Wait	3	0
37	60	Mix amino acid cartridge	5	0
38	3	Vortex Off	1	0
39	62	Drain amino acid cartridge	20	0
40	99	END LOOP	1	0
41	2	Vortex On	1	0
42	62	Drain amino acid cartridge	10	0
43	60	Mix amino acid cartridge	15	0
44	61	Vent amino acid cartridge	5	0
45	3	Vortex Off	1	0
46	9	Gas thru top valve block	5	0
47	10	Gas thru bottom valve block	5	0

Module: d -> NMP Wash

Sept #	Function #	Function Name	Time	add. Time
1	14	#10 thru bottom valve block	1	0
2	56	#10 to Reaction Vessel	12	1
3	2	Vortex On	1	0
4	40	Mix Reaction Vessel	2	0
5	41	Vent Reaction Vessel at top	1	0
6	88	RS switch to RV	1	0
7	93	Gas to resin sampler	3	0
8	91	#10 to resin sample	5	0
9	89	RS switch to fraction collecto	1	0
10	40	Mix Reaction Vessel	2	0
11	10	Gas thru bottom valve block	6	0
12	20	Mix Activator	1	0
13	3	Vortex Off	1	0
14	42	Drain Reaction Vessel	10	1
15	50	#10 to top of RV with drain	5	0
16	42	Drain Reaction Vessel	10	0
17	98	BEGIN LOOP	4	0
18	56	#10 to Reaction Vessel	13	1
19	2	Vortex On	1	0
20	40	Mix Reaction Vessel	3	0
21	10	Gas thru bottom valve block	6	0
22	20	Mix Activator	1	0
23	3	Vortex Off	1	0
24	42	Drain Reaction Vessel	10	1
25	50	#10 to top of RV with drain	5	0
26	42	Drain Reaction Vessel	10	0
27	99	END LOOP	1	0
28	56	#10 to Reaction Vessel	12	1
29	2	Vortex On	1	0
30	41	Vent Reaction Vessel at top	1	0
31	88	RS switch to RV	1	0
32	93	Gas to resin sampler	3	0
33	91	#10 to resin sample	5	0
34	89	RS switch to fraction collecto	1	0
35	40	Mix Reaction Vessel	2	0
36	10	Gas thru bottom valve block	6	0
37	98	BEGIN LOOP	3	0
38	20	Mix Activator	1	0
39	1	Wait	2	0
40	99	END LOOP	1	0
41	3	Vortex Off	1	0
42	42	Drain Reaction Vessel	10	1
43	50	#10 to top of RV with drain	5	0
44	42	Drain Reaction Vessel	15	0
45	9	Gas thru top valve block	3	0
46	10	Gas thru bottom valve block	3	0
47	93	Gas to resin sampler	2	0

Module: e -> Transfer

Sept #	Function #	Function Name	Time	add. Time
1	14	#10 thru bottom valve block	1	0
2	5	Needle Down	10	0
3	60	Mix amino acid cartridge	2	0
4	10	Gas thru bottom valve block	3	0
5	20	Mix Activator	1	0
6	2	Vortex On	1	0
7	98	BEGIN LOOP	2	0

8	28	Gas to top of Activator	3	0
9	38	ACT to RV (Top RV open)	4	0
10	99	END LOOP	1	0
11	3	Vortex Off	1	0
12	98	BEGIN LOOP	3	0
13	28	Gas to top of Activator	2	0
14	38	ACT to RV (Top RV open)	3	0
15	99	END LOOP	1	0
16	21	Vent Activator	2	0
17	26	#10 to top of Activator	2	0
18	28	Gas to top of Activator	3	0
19	21	Vent Activator	2	0
20	36	#10 ACT thru bottom valve bloc	2	0
21	20	Mix Activator	5	0
22	28	Gas to top of Activator	3	0
23	38	ACT to RV (Top RV open)	6	0
24	40	Mix Reaction Vessel	2	0
25	93	Gas to resin sampler	2	0
26	41	Vent Reaction Vessel at top	2	0
27	88	RS switch to RV	1	0
28	93	Gas to resin sampler	3	0
29	41	Vent Reaction Vessel at top	2	0
30	89	RS switch to fraction collecto	1	0
31	2	Vortex On	1	0
32	11	#9 thru top valve block	1	0
33	21	Vent Activator	2	0
34	29	#9 to top of ACT with drain	5	0
35	62	Drain amino acid cartridge	5	0
36	3	Vortex Off	1	0
37	34	#6 to Activator	16	0
38	20	Mix Activator	3	0
39	67	#10 to small cartridge needle	2	0
40	66	#9 to small cartridge needle	2	0
41	62	Drain amino acid cartridge	15	0
42	12	#9 thru bottom valve block	1	0
43	98	BEGIN LOOP	2	0
44	64	#9 to amino acid cartridge	20	0
45	2	Vortex On	1	0
46	1	Wait	3	0
47	60	Mix amino acid cartridge	5	0
48	3	Vortex Off	1	0
49	24	Cartridge to Activator	20	0
50	99	END LOOP	1	0
51	2	Vortex On	1	0
52	62	Drain amino acid cartridge	10	0
53	60	Mix amino acid cartridge	15	0
54	61	Vent amino acid cartridge	5	0
55	3	Vortex Off	1	0
56	98	BEGIN LOOP	7	0
57	20	Mix Activator	5	0
58	1	Wait	5	0
59	99	END LOOP	1	0
60	22	Drain Activator	20	0
61	2	Vortex On	1	0
62	22	Drain Activator	10	0
63	3	Vortex Off	1	0
64	98	BEGIN LOOP	3	0
65	29	#9 to top of ACT with drain	3	0
66	22	Drain Activator	5	0
67	99	END LOOP	1	0
68	2	Vortex On	1	0
69	12	#9 thru bottom valve block	1	0
70	35	#9 to Activator	2	0

71	20	Mix Activator	3	0
72	3	Vortex Off	1	0
73	22	Drain Activator	30	0
74	9	Gas thru top valve block	5	0
75	10	Gas thru bottom valve block	5	0 ¦

Module: f -> Coupling [20mn]

Sept #	Function #	Function Name	Time	add. Time
1	14	#10 thru bottom valve block	1	0
2	13	#10 thru top valve block	1	0
3	10	Gas thru bottom valve block	5	0
4	9	Gas thru top valve block	5	0
5	98	BEGIN LOOP	18	0
6	2	Vortex On	13	0
7	10	Gas thru bottom valve block	3	0
8	20	Mix Activator	1	0
9	3	Vortex Off	15	0
10	99	END LOOP	1	0
11	91	#10 to resin sample	1	0
12	93	Gas to resin sampler	2	0
13	41	Vent Reaction Vessel at top	2	0
14	88	RS switch to RV	1	0
15	93	Gas to resin sampler	2	0
16	41	Vent Reaction Vessel at top	1	0
17	89	RS switch to fraction collecto	1	0
18	98	BEGIN LOOP	18	0
19	2	Vortex On	13	0
20	10	Gas thru bottom valve block	3	0
21	20	Mix Activator	1	0
22	3	Vortex Off	15	0
23	99	END LOOP	1	0
24	9	Gas thru top valve block	2	0
25	13	#10 thru top valve block	1	0
26	9	Gas thru top valve block	5	0
27	14	#10 thru bottom valve block	1	0
28	10	Gas thru bottom valve block	5	0 ¦

Module: g -> Wash & R.S.

Sept #	Function #	Function Name	Time	add. Time
1	13	#10 thru top valve block	1	0
2	91	#10 to resin sample	2	0
3	41	Vent Reaction Vessel at top	2	0
4	88	RS switch to RV	1	0
5	93	Gas to resin sampler	3	0
6	91	#10 to resin sample	5	0
7	89	RS switch to fraction collecto	1	0
8	98	BEGIN LOOP	3	0
9	14	#10 thru bottom valve block	1	0
10	40	Mix Reaction Vessel	4	0
11	99	END LOOP	1	0
12	2	Vortex On	5	0
13	40	Mix Reaction Vessel	4	0
14	3	Vortex Off	1	0
15	40	Mix Reaction Vessel	4	0
16	10	Gas thru bottom valve block	6	0
17	20	Mix Activator	1	0
18	42	Drain Reaction Vessel	20	2
19	56	#10 to Reaction Vessel	14	1
20	41	Vent Reaction Vessel at top	1	0

21	88	RS switch to RV	1	0
22	91	#10 to resin sample	5	0
23	89	RS switch to fraction collecto	1	0
24	2	Vortex On	3	0
25	40	Mix Reaction Vessel	3	0
26	3	Vortex Off	1	0
27	42	Drain Reaction Vessel	15	1
28	50	#10 to top of RV with drain	4	0
29	42	Drain Reaction Vessel	10	0
30	98	BEGIN LOOP	4	0
31	56	#10 to Reaction Vessel	14	1
32	2	Vortex On	1	0
33	40	Mix Reaction Vessel	3	0
34	3	Vortex Off	1	0
35	42	Drain Reaction Vessel	10	1
36	50	#10 to top of RV with drain	4	0
37	42	Drain Reaction Vessel	10	0
38	99	END LOOP	1	0
39	56	#10 to Reaction Vessel	14	1
40	41	Vent Reaction Vessel at top	1	0
41	88	RS switch to RV	1	0
42	91	#10 to resin sample	5	0
43	89	RS switch to fraction collecto	1	0
44	2	Vortex On	1	0
45	40	Mix Reaction Vessel	3	0
46	10	Gas thru bottom valve block	6	0
47	20	Mix Activator	1	0
48	3	Vortex Off	1	0
49	42	Drain Reaction Vessel	15	1
50	14	#10 thru bottom valve block	1	0
51	56	#10 to Reaction Vessel	14	1
52	2	Vortex On	1	0
53	40	Mix Reaction Vessel	1	0
54	91	#10 to resin sample	2	0
55	93	Gas to resin sampler	2	0
56	90	#9 to resin sampler	2	0
57	93	Gas to resin sampler	1	0
58	91	#10 to resin sample	2	0
59	93	Gas to resin sampler	2	0
60	98	BEGIN LOOP	1	0
61	39	Momentarily close Relay 0	1	0
62	13	#10 thru top valve block	1	0
63	41	Vent Reaction Vessel at top	2	0
64	88	RS switch to RV	1	0
65	91	#10 to resin sample	2	0
66	93	Gas to resin sampler	1	0
67	91	#10 to resin sample	2	0
68	41	Vent Reaction Vessel at top	1	0
69	48	Gas to top of Reaction Vessel	1	0
70	87	Take resin sample	2	0
71	89	RS switch to fraction collecto	1	0
72	90	#9 to resin sampler	2	0
73	93	Gas to resin sampler	2	0
74	90	#9 to resin sampler	2	0
75	93	Gas to resin sampler	2	0
76	90	#9 to resin sampler	4	0
77	93	Gas to resin sampler	4	0
78	41	Vent Reaction Vessel at top	2	0
79	88	RS switch to RV	1	0
80	91	#10 to resin sample	3	0
81	93	Gas to resin sampler	3	0
82	91	#10 to resin sample	5	0
83	89	RS switch to fraction collecto	1	0

84	39	Momentarily close Relay 0	1	0
85	99	END LOOP	1	0
86	3	Vortex Off	1	0
87	42	Drain Reaction Vessel	20	2